Specialised Architecture and Dynamics of Immune Synapses in B Cell Populations

Carla Rose Nowosad

The Francis Crick Institute,
Mill Hill Laboratory

PhD Supervisor: Dr. Pavel Tolar

A thesis submitted for the degree of
Doctor of Philosophy
University College London
September 2016

Declaration

I Carla Rose Nowosad, confirm that the work presented in this thesis is my own. Where information has been derived from other sources, I confirm that this has been indicated in the thesis.

Publications arising from this thesis

Nowosad, C.R., Spillane, K.M. & Tolar, P., 2016. Germinal center B cells recognize antigen through a specialized immune synapse architecture. *Nature immunology*, 17(7), pp.870–877.

Nowosad, C.R & Tolar, P. 2016. Plasma Membrane Sheets for the study of B cell antigen capture. Methods in Molecular Biology (Chapter 26). In Press

Malinova, D. et al., Fritzsche, M., Nowosad, C.R., Armer, H., Munro, P.M.G., Blundell, M.P., Charras, G., Tolar, P., Bouma, G., Thrasher, A.J. 2016. WASp-dependent actin cytoskeleton stability at the dendritic cell immunological synapse is required for extensive, functional T cell contacts. *Journal of leukocyte biology*, 99(5), pp.699–710.

Abstract

B cells are specialised lymphocytes that are responsible for the production of antibodies during an immune response. When B cells bind membrane-presented antigen they form an immune synapse, which provides the context for coordinated B cell receptor (BCR) signalling and antigen internalisation, both of which are paramount for full B cell activation. Synapse formation has been well characterised in the largest B cell subset- follicular (FO) B cells, although little is known about how synapse formation is altered in less common B subsets, whose activation supports distinct aspects of the antibody response.

Germinal center (GC) B cells develop from follicular B cells after antigen stimulation. They are confined to specialised sites in lymphoid organs, where they undergo somatic hypermutation and affinity improvement of their immunoglobulins. BCR signalling is speculated to be largely inactive in GC B cells, with antigen internalisation, processing and presentation to T cells driving their selection. However, there is limited knowledge of synapse formation, signalling and intracellular antigen trafficking in these cells.

Using a newly developed high-content, large-scale fluorescent imaging platform we uncovered subset specific differences in synapse formation and mechanisms of antigen extraction in B cells of different subsets. Immunisation or infection-induced GC B cells showed the most striking difference, forming unique peripheral synapses where antigen was internalised by a distinct pathway independent of antigen movement to the centre of the contact. These cells still relied on proximal BCR signalling, but had defects in the NF-κB pathway, supporting a role for T-dependent selection of high affinity clones. GC cells produced higher tugging forces on the BCR than FO cells and were more effective at affinity discrimination. We conclude that unique biomechanical patterns control stringency of antigen binding in GC B cells, and propose that resultant effects on antigen presentation and availability of T cell help ultimately dictate GC B cell fate. Understanding requirements for the activation of GC B cells has applications in rational vaccine design, as well as for B cell malignancies. Therefore, these results have important implications for the future development of novel immunotherapies.

Acknowledgements

Firstly, I owe enormous thanks to Dr. Pavel Tolar for a taking a chance on me all those years ago, I am immensely grateful. You have taught me to always aim high and strive to do excellent science. Thanks for your cool head and superhuman intelligence, both without which I am sure I would not have achieved half as much. Similarly, I'd like to thank Professor Victor Tybulewicz, for providing insight, opportunities and encouragement throughout the PhD.

To all the people who trained me: Elizabeth Natkanski, Wing-Yiu Lee, Antonio Casal and many, many others, thanks for always being thorough, patient and helpful- and for always indulging my chit chat. You've truly been great people to work around. Thanks Sophie Roper, you are hilarious and a brilliant, very talented person.

Thanks to all the inspirational women I know: Laura and Lydia Nowosad, Maria Iachetta, Alex Gaze and Helena Aegerter in particular. You are some of the best, kindest, most successful and fantastic people I know, thanks for giving me something to look up to.

Lastly, but most importantly, thanks to my wonderful parents for always standing right behind me supporting everything I chose to do, I love you very much. You had this way of assuring us that we could achieve absolutely anything we dreamed of. Guess what, turns out you were right.

Table of Contents

Table of figures

List of tables

Abbreviations

%	Percent
2D	Two dimensional
3D	Three dimensional
Ab	Antibody
AID	Acitvation-induced cytidine deaminase
APC	Antigen presenting cell
B1-8	B1-8$^{flox/flox}$ Igκ$^{Ctm1Cgn/tm1Cgn}$
BAFF/R	B cell activating factor/ receptor
BCL-2	B cell lymphoma 2
BCL-6	B cell lymphoma 6
BCR	B cell receptor
BiFC	Bimolecular fluorescence complementation
Bl6	C57Bl/6
BLNK	B cell linker
BM	Bone marrow
bnAb	Broadly-neutralising antibody
BSA	Bovine serum albumin
Btk	Bruton's tyrosine kinase
CCP	Clathrin-coated pit
CD	Cluster of differentiation
CD40L	CD40-ligand
CLP	Common lymphoid progenitor
CO_2	Carbon dioxide
CpG	Cytosine-phosphate-guanine
CR	Complement receptor
cSMAC	Central supramolecular activation cluster
CSR	Class-switch recombination
CXCL	Chemokine (C-X-C) ligand
CXCR	Chemokine (C-X-C) receptor
Cy	Cyanine
Da/ kDa	Dalton/ kilodalton
DAPI	4',6-diamidino-2-phenylindole
DC	Dendritic cell
DC-SIGN	Dendritic cell-specific intercellular adhesion molecule-3-grabbing non-integrin
DiD/ DiI	Long-chain dialkylcarbocyanide dyes
DMEM	Dulbecco's Modified Eagle's Medium
DMF	Dimethylformamide
DMSO	Dimethylsulfoxide
DNA	Deoxyribonucleic acid

DOPC	1,2-dioleoyl-*sn*-glycero-3-phosphocholine
DOPE-Cap-biotin	1,2-dioleoyl-*sn*-glycero-3-phosphoethanolamine-N-(cap biotinyl)
dSTORM	Direct stochastic optical reconstruction microscopy
DTT	Dithiothreitol
EDTA	Ethylenediaminetetraacetic acid
Erk	Extracellular signal-regulated kinase
ERM	Ezrin, Radixin, Moesin
F.U.	Fluorescence units
Fab	Antibody binding fragment
FBS	Fetal bovine serum
Fc	Fraction crystallisable
FCγRIIB	Inhibitory low affinity receptor for IgG
FDC	Follicular dendritic cell
FO	Follicular
Foxo1	Forkhead box protein O1
FRC	Fibroblastic reticular cell
FRET	Förster Resonance Energy Transfer
FV	Friend Virus
GC	Germinal centre
GFP	Green fluorescent protein
HBSS	Hank's Buffered Saline Solution
HEL	Hen egg lysozyme
HEK	Human embryonic kidney cell
HEV	High endothelial venule
HIV	Human immunodeficiency virus
hr	Hour
i.p	Intra-peritoneal
i.v	Intra-venous
IC	Immune complex
ICAM-1	Intracellular adhesion molecule-1
Ig	Immunoglobulin
IgH/L	Immunoglobulin heavy/light chain
IKK	Inhibitor of kappa-kinase
IKβ	Inhibitor of kappa-B
IL	Interleukin
IMDM	Iscove's Modified Dulbecco's Medium
iNKT	Invariant natural killer T cell
IS	Immune synapse
ITAM	Immunoreceptor tyrosine-based activation motif
ITIM	Immunoreceptor tyrosine-based inhibition motif
L	Litre
LFA-1	Lymphocyte function-associated antigen-1

LN	Lymph node
LZ	Light zone
MAC-1	Macrophage differentiation antigen-1
mg	Milligram
mIg	Membrane immunoglobulin
min	Minute
ml	Millilitre
mM	Millimolar
MTOC	Microtubule organising centre
MWCO	Molecular weight cut off
MZ	Marginal zone
nAb	Natural antibody
NEAA	Non-essential amino acid
NF-κB	Nuclear factor- kappa- B
NFAT	Nuclear factor of activated T cells
NIP	4-Hydroxy-3-iodo-5-nitrophenylacetic acid
NK	Natural killer cell
nm	Nanometre
nM	Nanomolar
NP	4-Hydroxy-3-nitrophenyl acetyl
p.i	Post-infection
Pax-5	Paired box 5
PBS	Phosphate buffered saline
PC	Plasma cell
PFA	Paraformaldehyde
PI3K	Phosphoinositide-3-OH-kinase
PKC	Protein kinase C
PLB	Planar lipid bilayer
PLCγ	Phospolipase C gamma
pMHCII	Peptide-bound major histocompatibility complex type 2
PMS	Plasma membrane sheet
pN	Piconewton
PP	Peyer's patch
pSMAC	Peripheral supramolecular activation cluster
RAG 1/2	Recombination activating gene
Rpm	Revolutions per minute
RPMI	Roswell Park Memorial Institute medium
s	Second
SCS	Subcapsular sinus
SFFU	Spleen focus forming unit
SHIP1	Phosphatidylinositol-3,4,5-trisphosphate 5-phosphatase 1
SHP1	Src homology region 2 domain-containing phosphatase-1
SIPR1/2	Sphingosine-1-phosphate receptor 1/2

SLC	Surrogate light chain
SLO	Secondary lymphoid organ
SMH	Somatic hypermutation
SRBC	Sheep red blood cell
Syk	Spleen tyrosine kinase
T1/2/3	Transitional 1/2/3 cell
TCR	T cell receptor
TD	T-dependent
TEL	Turkey egg lysozyme
T_{FH}	T follicular helper cell
TI	T-independent
TIRFM	Total internal reflection microscopy
TLR	Toll-like receptor
U	Units
v/v %	Volume per volume percent
VCAM-1	Vascular adhesion protein-1
VLA-4	Very late antigen-4, also known as alpha-4-beta-1 integrin
w/v %	Weight per volume percent
WASP	Wiskott-Aldrich syndrome protein
α	Alpha
β	Beta
γ	Gamma
δ	Delta
κ	Kappa
λ	Lambda
µg	Microgram
µl	Microlitre
µM	Micromolar
µm	Micrometre

Chapter 1. Introduction

The immune system functions as a complex network of cells, tissues and molecular components that rely on communication with each other to recognise, respond to and ultimately clear infections.

The immune system may be categorised into two major arms, the innate and adaptive immune systems, which work synergistically to provide immediate, general immunity as well as potent and precise specific responses with the capacity to form immune 'memory'. Innate immunity is rapid, with cells responding to pathogen-associated or 'non-self' patterns with a limited number of generic germline-encoded surface receptors (Janeway & Medzhitov 2002). These cells can communicate with the adaptive branch, alerting the system to danger by inducing inflammation. Cells of the adaptive immune system must respond to these innate cues and make fate decisions governing their differentiation. Here, we focus on how different kinds of a specific adaptive immune cell, the B cell, sees and responds to invaders during an immune response.

1.1 The Adaptive Immune System

Adaptive immunity is the defence against pathogens conferred by specialised white blood cells known as lymphocytes. Lymphocytes arise from a common lymphoid progenitor cell in the bone marrow and go on to mature in either the thymus or the bone marrow to make two cell types, the T lymphocyte and the B lymphocyte (T cell, B cell). Each lymphocyte has divergent roles in the immune system, but share a commonality, a unique immunoglobulin (Ig)-type surface receptor specific for antigen. When one of these highly specialised surface receptors binds its cognate antigen signals are transduced into the cell to promote proliferation and differentiation into the effector form of the responding lymphocyte. Diversity is generated amongst the lymphocyte receptors during a process of ordered genomic rearrangements of variable, diversity and joining gene segments, known as V(D)J recombination. Survival of lymphocytes is dependent on successful V(D)J recombination and the subsequent surface expression of an intact antigen receptor

(Meffre & Nussenzweig 2002; Reichlin et al. 2001). The resultant receptor diversity is immense, creating an arsenal of lymphocytes displaying millions of individual receptors specific for their own unique antigen (Borst et al. 1996). Further to expressing a surface-bound receptor, B cells play a pivotal role in pathogen clearance as the lymphocyte responsible for producing specific secreted immunoglobulin, or antibody. Antibodies are produced as soluble versions of surface bound B cell receptors and can act directly to neutralize pathogens or indirectly as opsonins, recruiting other defensive molecules and immune cell subsets.

1.2 Development and function of B cell subsets

Whilst B cells are the hallmark of humoral immunity, all B cells are not created equal. B cells exist in a catalogue of distinct subpopulations, providing divergent effector outcomes. Anatomical location, migratory capacity, sensitivity to different pathogens and ability to be activated in the presence or absence of T cells are some of the major factors that define B cell subsets.

B cells begin their development in the embryonic fetal liver, and then following birth and throughout life, in the bone marrow (BM) from common lymphoid progenitor (CLP) cells (Kondo et al. 1997). Commitment to the B cell lineage occurs immediately after the CLP stage, concomitant with expression of B220, a pan-B cell marker (Hardy et al. 2000; Allman et al. 1999). In addition to B220 expression all immature B cell subsets in the bone marrow are identified by upregulation of the target of the monoclonal antibody AA4.1 (Hardy & Hayakawa 2001). Progression to the pro-B cell stage and maintenance of B lineage restriction is controlled by induction of the transcription factor Pax-5 (Barberis et al. 1990; Nutt et al. 1999). The next step in development is the rearrangement of the heavy chain Ig locus and expression of the pre-B cell receptor (pre-BCR) (Figure 1) (Nagata et al. 1997; Nutt et al. 1999). Ig loci are altered from the default germline configuration by the RAG1/RAG2 (recombinase-activating gene 1/2) enzyme complex, which specifically induces double-strand DNA breaks at defined intergenic sequences called recombination signal sequences (Oettinger et al. 1990; Schatz et al. 1989).

This progresses in a stepwise fashion, with D_H and J_H sections rearranging initially, followed by a second wave of rearrangement joining an upstream V_H region to the assembled DJ_H segment. The rearranged heavy chain mu (μ) protein associates with a surrogate light chain (SLC) and the Igα/β signalling heterodimer to form the intact pre-BCR (Melchers 2005; Melchers et al. 1999). Correct pre-BCR expression is an essential checkpoint in B cell development, and without appropriate feedback from signal transduction through the assembled receptor capacity there is a total block of B cell development (Kitamura et al. 1992; Kitamura et al. 1991; Mombaerts et al. 1992; Reichlin et al. 2001; Meffre & Nussenzweig 2002).

Studies on the pre-BCR showed it signals independently of a specific ligand (or antigen), and instead induces signalling by aggregating rapidly upon surface expression due to the highly polyreactive nature of the non-Ig portion of the SLC component λ5 (Ohnishi & Melchers 2003). Pre-BCR signalling is involved in allelic exclusion, a process of IgH chain silencing at one locus to prevent a single B cell expressing receptors of two specificities (Melchers et al. 1999; Grawunder et al. 1995). Signals from the pre-BCR also act to cease λ5 gene expression, initiating the downregulation of the SLC and inducing its replacement with a rearranged conventional κ or λ light chain (Reth et al. 1987), which in combination with the μ heavy chain makes up an IgM BCR whose expression on the B cell surface transitions the pre-B cell to an Immature B cell.

Immature B cells with correctly assembled surface IgM receptors can leave the bone marrow and enter into the periphery as transitional subsets, which they pass through sequentially before reaching full maturity (Chung et al. 2003). Surface characteristics of these cells are detailed in Table 4. During transitional stages BCRs are tested against self-antigens in a bid to eliminate any autoreactivity, a critical step considering 55-75% of newly formed B cells possess some degree of self reactivity (Wardemann et al. 2003). Cells that crosslink their BCR at this stage may be either simply eliminated (known as clonal deletion) or their receptors re-edited. A third tolerance mechanism called anergy also exists, and anergic, selfreactive B cells are said to be enriched in a distinct developmental transitional lineage, the T3 lineage (Merrell et al. 2006). They represent a ‘silenced’

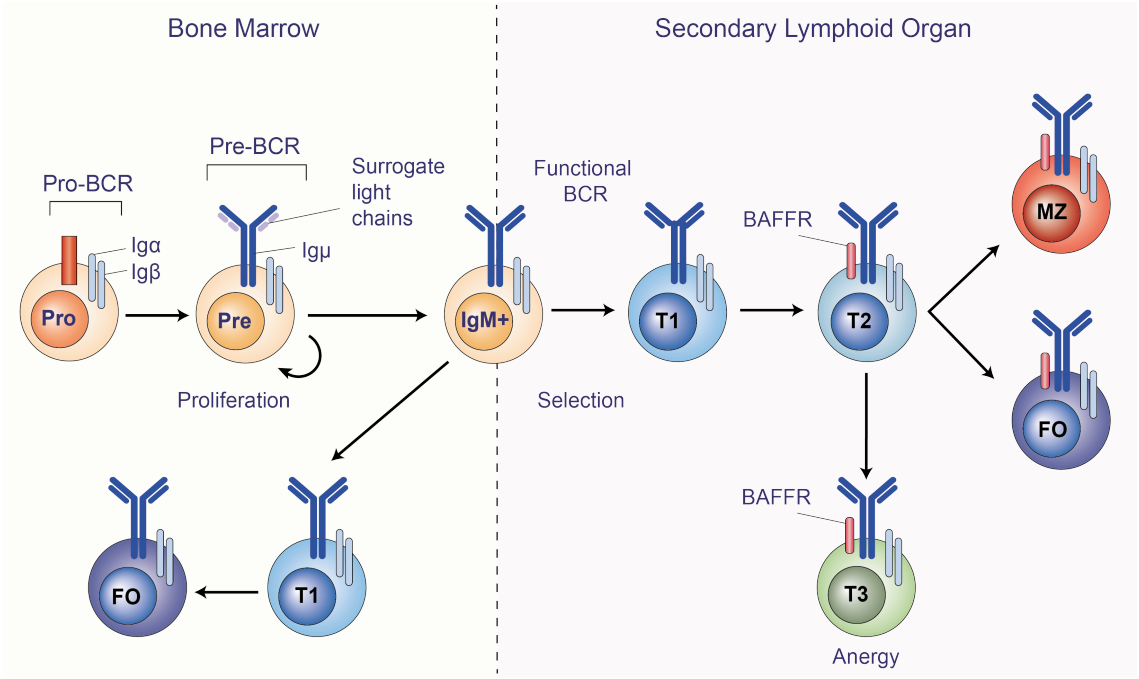

Figure 1 B cell development

B cell development occurs within the bone marrow and in peripheral lymphoid organs like the spleen. Early B cell development in the bone marrow progresses through pro-, pre- and immature B cell stages. The result of this differentiation is the surface expression of a pre-B cell receptor, where the surrogate light chain is eventually replaced to form a mature BCR capable of antigen binding. Immature B cells are tested for absence of autoreactivity and successful antigen binding before being positively selected for exit to the spleen. Splenic B cells progress through separate transitional stages, where the T3 stage is considered to represent anergic cells rather than a true transitional subset. Following T2, B cell survival is dependent on tonic signalling through the BAFF-receptor (BAFFR). After transitional stages B cells finally mature into follicular or marginal zone B cells. Follicular cells may also mature in the bone marrow.
Adapted from (Cambier et al. 2007) with permission from Nature Publishing Group.

subset of B cells that is functionally unresponsive, escaping earlier checkpoints and expressing a dangerously autoreactive BCR in the periphery. Generally, high-affinity BCR interactions result in clonal deletion, whereas lower affinity interactions or interaction with soluble antigens divert cells to receptor editing or anergy (Goodnow et al. 1988; Hartley & Goodnow 1994; Hartley et al. 1991; Benschop et al. 1999; Hartley et al. 1993).

1.3 Mature B cell Fate Decisions: Marginal Zone versus Follicular B cells

After passing through transitional checkpoints around three quarters of B cells leave the BM and home to the spleen to make fate decisions to attain full maturity as a Marginal Zone (MZ) or Follicular (FO) B cell (Cariappa et al. 2007). This decision is important owing to the differential biological responses of the two cells types. MZ B cells are long-lived and self-renewing, making up 5-10% of all splenic B cells with their designation referring primarily to their anatomical location within the marginal zone of the spleen, which forms the interface between the red and white pulp, flanking the marginal sinus. MZ cells express very high levels of CD21 and CD1d and respond robustly to blood-borne pathogens flowing through the red pulp (Martin & Kearney 2000; Pillai & Cariappa 2009; Allman & Pillai 2008). MZ cells are particularly specialised to respond to T-independent antigens using a 'pre-diversified' Ig repertoire whose mutations arose in the absence of antigen (Weller et al. 2004), although they can contribute to T-dependent responses in some circumstances (Phan et al. 2005). MZ B cells have a lower threshold of activation and respond rapidly to produce antibody, mostly of the IgM class, with broad specificity and low affinity. MZ B cells can be activated independently of T-cell help to respond rapidly to innate Toll-like receptor (TLR) stimuli and lipid antigens. High levels of surface CD1d is important in lipid-presentation to invariant natural killer T (iNKT) cells (Leadbetter et al. 2008), and such the splenic MZ is proposed as an important source of lipid-specific antibodies (Barral et al. 2008).

FO B cells make up the vast majority of B cells in the spleen, lymph nodes and other secondary lymphoid organs where they reside in follicles positioned adjacent to T-cell rich zones (Cyster 2010). FO B cells generally participate in T-dependent reactions and therefore must migrate and meet their partner T cells at the border of the two zones to interact. MZ responses are often termed 'innate-like' and act to bridge the time-gap created as FO B cells find their cognate antigen, obtain T-cell help and undergo processes of affinity maturation in the specialised germinal centre reaction (Discussed in section 1.10). Although multiple models have been proposed to interpret the MZ or FO fate decision (Pillai et al. 2004; Cariappa et al.

2001; Wen et al. 2005; Saito et al. 2003), it is thought to depend on a combination of signaling through the BCR, Notch2, the receptor for B cell-activating factor (BAFFR) and the canonical nuclear factor-κB (NF-κB) pathway. Factors affecting chemokine composition or integrin activation may affect the B cell fate by misdirecting cells to defined anatomical locations or affecting retention in their respective zones (Pillai & Cariappa 2009). Increased BCR signal strength is broadly associated with a push to the FO cell fate, shown by loss of FO cells in mice with defects in BCR signalling, and loss of MZ cells in mice with deletions of inhibitory BCR regulators (Hardy et al. 1983; Wen et al. 2003; Bell et al. 2004; Pani et al. 1997; Cariappa et al. 2001; Pillai & Cariappa 2009; Samardzic et al. 2002; Kraus et al. 2001; Loder et al. 1999; Kurosaki 2002). Chronic BCR signalling through high-affinity interactions with self promotes death by apoptosis (Taylor et al. 2015). Signals from the BCR collaborate with a number of pathways mostly converging on Notch2 signalling and the canonical NF-κB pathway- downstream of tonic survival signals from the BAFFR- to continue driving the MZ fate over the FO cell fate, which is Notch2-independent.

1.4 B Cell Antigen Encounter

Because of the high diversity of BCRs, the likelihood of a productive encounter between a B cell and its cognate antigen is low. The architecture and layout of three specialized secondary lymphoid organs (SLOs), the spleen, lymph nodes (LN) and Peyer's patches (PP) create an environment optimised for immune cell communication and antigen access. SLOs, through their excellent connections with both blood and lymph, become depositories for foreign antigen where B cells continuously migrate in response to specialised chemokine environments, scanning sites where antigen is concentrated (Allen et al. 2007; Hauser et al. 2007; Okada et al. 2005; Schwickert et al. 2007; Andrian & Mempel 2003). B cells are always on the move, migrating at rates of up to 6 μm/ minute (Okada et al. 2005) and dwelling in their defined zones in any given SLO for up to 24 hours before egressing to the circulation (Goodnow 1997). Depending on the entry route of the pathogen, the draining SLO, and the characteristics of the antigen, the nature of a B cells encounter with antigen and the resultant activation can vary.

1.4.1 Soluble Antigen Encounter

Although all antigens were initially imagined to be soluble, it is relatively unusual for antigen to enter SLOs free-floating (Figure 2). Soluble antigen may be relevant in immune responses as products generated by protease-mediated cleavage of larger microorganisms, secreted bacterial products or delivered during vaccination (Roozendaal et al. 2009; Catron et al. 2010). Entry of antigen into SLOs like the LN was originally an intriguing topic given that although the LN is supplied with lymphatic fluid through the afferent vessel at all times, antigen does not freely circulate due to a barrier of cells lining the inner surface of the LN at the subcapsular sinus (SCS) very tightly (Gretz et al. 2000; Gretz et al. 1997). This implied antigen supply was a controlled process.

An intricate tubular system of channels constructed from three-dimensional bundles of collagen fibres wrapped around a layer of fibroblastic reticular cells (FRCs) was discovered to run from the high-endothelial venules (HEVs) through to the SCS and was termed the conduit system (Andrian & Mempel 2003; Sixt et al. 2005). Dendritic cells (DCs), a kind of professional antigen presenting cell (APC), interact with these conduit vessels, acquiring antigen and squeezing through the SCS floor before moving through to the T-cell zone for the antigen to be processed and presented on MHC molecules. Therefore conduits were initially described to generally only supply soluble protein antigen to T cell regions in SLOs (Gretz et al. 2000; Okada & Cyster 2006; Sixt et al. 2005). Antigen had been described to flow through small pore-like gaps in the SCS floor for interaction with B cells, as identified by electron microscopy (Pape et al. 2007).

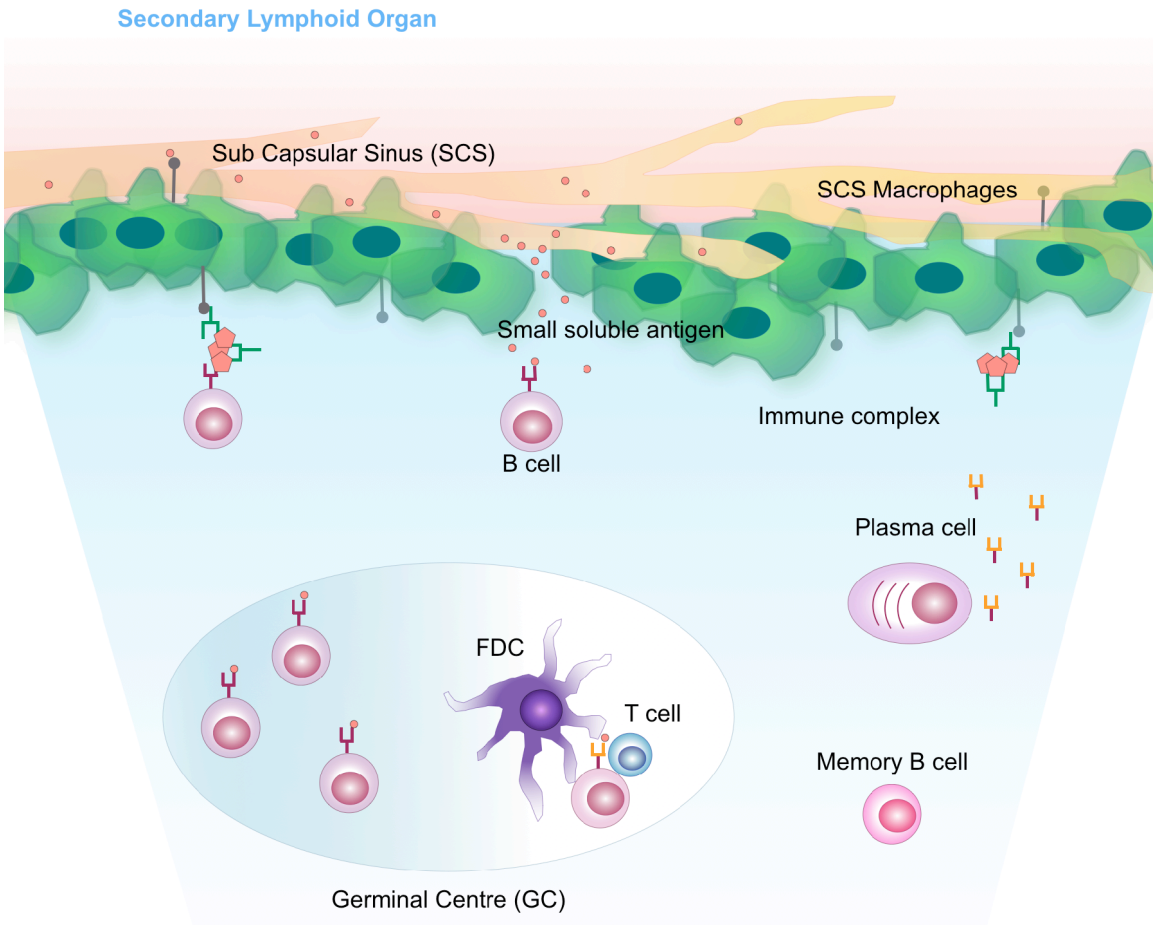

Figure 2 Antigen format in secondary lymphoid organs

B cells may access small, soluble antigen filtering into secondary lymphoid organs through the conduit system. Immune complexes made up of antigen, circulating natural antibody and complement are shuttled via surface receptors on macrophages lining the subcapsular sinus, situated near to incoming lymphatic vessels. B cells must extract antigen from the surface of SCS macrophages in order to become fully activated and enter into germinal centre reactions, differentiate into plasma cells or form memory B cells.
FDC, follicular dendritic cell
Adapted from (Batista & Harwood 2009) with permission from Nature Publishing Group

Two-photon microscopy was later used to track Turkey Egg Lysozyme (TEL), a small protein antigen marked with a fluorescent dye, moving through the conduits in real time. This unveiled a size-exclusion function in SLOs mediating the differential sorting of large antigens onto cell surfaces (as described by others (Junt et al. 2007; Phan et al. 2009; Carrasco & Batista 2007)) and molecules smaller than 70kDa passing through conduit networks, but this time conduits were observed also permeating into follicles for direct sampling by B cells (Roozendaal et al. 2009). B cell pseudopods were seen extending directly into conduit walls and sampling antigen from the core of the vessel (Roozendaal et al. 2009). Interestingly, as well as transporting small, soluble antigens into SLOs, conduits are also implicated in the transport of chemokines, such as CXCL13, a potent chemoattractant implicated in B cell homing in the LNs (Allen & Cyster 2008; Cyster et al. 2000). This may be secreted from the site of infection or from LN stromal cells and could act to localise B cells to sites of high antigen concentration (Roozendaal et al. 2009; Roozendaal et al. 2008; Harwood & Batista 2009).

1.4.2 Membrane-bound antigen encounter

Historically, it was thought that B cells were stimulated only by soluble antigen. This was partly due to the observation of high affinity interactions between soluble antigens and the BCR *in vitro* leading to very efficient B cell activation. However, *in vivo* the story is somewhat different. Although B cells have the capability to respond to soluble antigen, they are predominantly exposed to membrane-bound antigen displayed on a variety of APCs (Carrasco & Batista 2006a; Depoil et al. 2008). These include DCs (Huang et al. 2005; Wykes et al. 1998), FDCs (Chen et al. 1978; Tew et al. 1980) and specialized SCS macrophages (Koppel et al. 2005) (Figure 2). When B cells interact with antigen in presented in the context of a membrane they require a lower threshold for activation (Batista et al. 2001; Batista & Neuberger 1998; Batista & Neuberger 2000) compared to an equivalent soluble antigen (Qi et al. 2006). This is thought to be dependent on a variety of integrin molecules expressed on the surface of APCs which aid the formation of more stable, long-lasting contacts with cognate B cells (Carrasco et al. 2004). ICAM-1/LFA-1 and VLA-4/VCAM-1 interactions have both been shown to be important in

enhancing B cell activation (Carrasco et al. 2004; Carrasco & Batista 2006b)-associated with conformational changes promoting a high affinity state, causing stronger adhesion and therefore increasing the surface available for BCR-antigen engagement. Additionally, antigen becomes clustered on the surface of APCs causing it to concentrate, increasing total avidity (Suzuki et al. 2009). This could play an important role in B cell activation in the face of very low affinity antigens. The outcome of B cell activation centres around two distinct processes: transmembrane signalling and antigen internalisation. Longer lasting contacts could help prolong otherwise transient signals and clustering of receptors and integrins may gather important reciprocal signalling molecules in close proximity for interaction. The co-receptor CD19 was shown to improve signalling through the BCR (Carter & Fearon 1992) and is required in the microcluster for B cell activation (Depoil et al. 2008). CD19 acts in tandem with CD21- a different member of the membrane co-receptor complex that has the ability to interact with antigens tagged with C3d, a component of the complement cascade. It is well known that large amounts of complement become deposited on FDCs during antigen capture and upon binding of C3d-tagged antigens, CD21 causes cross-linking of the BCR with CD19, which here acts as a membrane adaptor recruiting downstream signalling molecules thereby amplifying early B cell activation events (Carter & Fearon 1992). CD19-CD21 complexes were shown to enhance B cell activation during interactions with FDCs (Tew et al. 1997), but are not required in B cell responses to soluble antigen.

1.5 Antigen Presentation and Transport in Secondary Lymphoid Organs

Initial antigen capture is carried out primarily by two kinds of APC: DCs and SCS macrophages. Later, FDCs play a more prominent antigen presentation role in germinal centre reactions (see Section 1.12). Features of the paracortex of the LN make it the perfect environment for B cells to acquire DC-presented antigen. It is an area densely populated with DCs along with both B and T cells (Lindquist et al. 2004), close to the high endothelial venules (HEVs) and so is the first point of contact for migrating lymphocytes and DCs bringing in antigen from peripheral

tissue. DCs are widely regarded as the best professional APC and play an established role in the presentation of peptide-MHCII (pMHCII) complexes to T cells (Dudziak et al. 2007; Itano et al. 2003). Peptide-MHCII complexes are generated by internalisation of antigen followed by intracellular processing and loading of the resultant short peptide antigen onto pre-formed MHCII molecules in endosomal compartments before trafficking of the assembled complex to the membrane for presentation. B cells don't interact with pMHCII, but rather interact with unprocessed, native antigen- implying any antigen presented by DCs to B cells must either just be captured and held at the membrane or partly resists degradation during internalisation and is recycled back to the plasma membrane (Bergtold et al. 2005; Huang et al. 2005). Using intravital microscopy populations of DCs displaying whole antigen have been identified clustered close to HEVs in the paracortex (Wykes et al. 1998; Qi et al. 2006) where they are largely sessile but extend out dendrites into their neighbouring HEV to sample its contents (Qi et al. 2006). The inhibitory low affinity receptor for IgG (FcγRIIB) present on DC surfaces can capture antigen coated in secreted natural antibody (nAbs) produced elsewhere in the immune response by B-1 B cells. Capture through FcγRIIB has been shown to direct antigen through non-degradative internalisation pathways (Bergtold et al. 2005). A similar phenomenon has been observed for a different surface receptor C-type lectin DC-specific ICAM3-grabbing non-integrin (DC-SIGN), where antigen was accumulated in neutral endosomes where it remained unprocessed and simply was recycled to the cell surface. This was illustrated by shuttling of HIV into non-lysosomal intracecullar compartments of the DC and successive detection of fully intact HIV-1 virions in SLOs (Kwon et al. 2002). After surface receptor stripping by protease treatment, DCs retained the ability to activate B cells *in vitro* providing further evidence that unprocessed antigen is recycled through endosomes (Batista & Harwood 2009).

Microscopy studies identified a specific set of SCS macrophages lining the underside of the SCS and extending their processes up into it, sampling lymphatic fluid in a similar manner to DCs at HEVs (Clark 1962; Fossum 1980; Farr et al. 1980; Szakal et al. 1983). SCS macrophages are rather inefficient at phagocytosis (Fossum 1980; Szakal et al. 1983) and have low levels of lysosomal enzymes

(Phan et al. 2007), causing them to retain antigen intact on their cell surfaces and hence rendering them excellent antigen presenters for B cells. These cells can grab hold of antigen via a large range of surface receptors including complement receptors, pattern recognition receptors or carbohydrate-binding scavenger receptors (Taylor et al. 2015; Batista & Harwood 2009). Antigen decorated in the complement component C3 binds macrophages via MAC1 (or αMβ2 integrin) a receptor implicated in antigen retention, which is particularly enhanced for clusters of coated antigens known as immune complexes (ICs) (Fossum 1980) that can be held on SCS cell surfaces for as long as 72 hours (Taylor et al. 2005). Binding by other receptor types- including those described for DCs- might lead to phagocytosis into neutral endosomes and recycling to the cell surface (Batista & Harwood 2009) possibly at the opposite pole of the cell (Phan et al. 2007).

SCS macrophages have been implicated in the rapid accumulation and movement of both complement and antibody coated ICs and 'mopping up' of large quantities of viral particles, making them instrumental in limiting systemic spread of pathogens from lymphatic tissue (Junt et al. 2007; Carrasco & Batista 2007; Phan et al. 2007). From here, a further role for SCS macrophages as transport cells emerged, with SCS macrophages identified in follicles after some types of immunisation (Mueller et al. 2001; Martinez-Pomares et al. 1996). In a vasticular stomatitis virus model deletion of macrophages from the SCS (hence no viral capture or IC relay) resulted in defective initiation of adaptive immune responses and a systemic viral load (Junt et al. 2007). During infection, lymphoid organ architecture can be disrupted, dampening effective responses to secondary infections (Scandella et al. 2008). Architecture of the SCS and distribution of SCS macrophages is severely affected (Gaya et al. 2015), compromising the ability of B cells in that node to respond to a secondary infection. SCS macrophages were therefore described to act as an 'immune sensing valve' triggering the LN to be temporarily refractory to incoming secondary infections to prioritise control of the primary pathogen (Gaya et al. 2015).

The adhesion molecules ICAM-1 and VCAM-1 (Junt et al. 2007) are also highly expressed in the SCS. These integrins may act on B cells both by lowering activation thresholds in addition to allowing them to crawl along the SCS floor internalising antigen before migrating to the T-B boundary to gain T cell help. Alternatively, two-photon microscopy has recently revealed an interesting notion that there is a role for FO B cells themselves as antigen transporting cells. As well as binding cognate antigen, they were able to capture ICs via complement receptors (CRs) completely independently of their BCR (Phan et al. 2007). B cells strip these ICs from SCS macrophages and subsequently deposit them onto FDCs by a possible mechanism involving competition for CRs. MZ cells of the spleen have also been implicated in this follicular IC shuttling role. This IC transport by B cells is important as it means antigen can be available for prolonged periods of time, allowing late arriving B cells into SLOs to continue sampling antigen for up to one week (Suzuki et al. 2009).

1.6 The B cell receptor (BCR)

B cells must be activated appropriately to elicit beneficial responses and this is dependent on the binding of exogenous antigen to the BCR. The BCR is a multiprotein structure made up of the heavy and light chains of the membrane-tethered immunoglobulin (mIg) noncovalently associated with a signalling active Igα/β heterodimer (Reth 1989). The BCR binds antigen through its variable region domains (Lanzavecchia 1987). Crosslinking of this complex of transmembrane proteins triggers a B cell signalling cascade that starts the B cell activation program and initiates a genetic switch towards antibody production (Rajewsky 1996). Igα and Igβ subunits act to transduce binding of antigen into alterations in intracellular signalling, namely through phosphorylation of intracellular tyrosine residues (Rickert 2013; Mowen & David 2014), but also via regulation through ubiquitination (Thome et al. 2010) and other post-translational modifications. Specifically, this includes phosphorylation of immunoreceptor tyrosine activation motifs (ITAMS) on cytoplasmic tails of Igα/β subunits of the BCR by sarcoma (Src) family kinase Lyn which recruits spleen tyrosine kinase (Syk) (Reth & Wienands 1997). This initiating ‘first signal’ is vital for activation, triggering several interconnected signalling

cascades (Dal Porto et al. 2004). These include the Mek/Erk kinase cascade and kinases Akt and Protein kinase C (PKC). These kinases act on a number of transcription factors including NFAT, c-Myc and NF-κB.

1.6.1 BCR signalling following antigen binding

Studies of the cytoplasmic domain of the BCR suggest binding of Src kinases may occur after a conformational change in cytoplasmic regions of Igα/β (Tolar 2011). Lyn (or other Src family kinases expressed in B cells, such as Blk, Fyn or Lck) phosphorylates the N-terminal ITAM tyrosine, leading to additional binding of Lyn to Igα via Lyn's SH2 domain. Subsequently, dual phosphorylation of the ITAM is achieved potentially by the action of both Lyn and Syk. Following dual phosphorylation, Syk forms high affinity interactions via a pair Src-homology domains that dock to the reciprocal pair of phosphotyrosines (Geahlen 2009; Pao et al. 1998). Monophosphorylation of ITAMs can result in unbalanced recruitment of Lyn over Syk causing a shift to inhibitory signalling pathways rather than downstream signal propagation conditional on Syk. This kind of BCR signalling is important in B cell tolerance and has roles in the maintenance of anergy (Cambier et al. 2007; Getahun et al. 2016; Gauld et al. 2005).

Initial Src activation events commences the stepwise formation of the signalosome, a collection of sequentially phosphorylated BCRs and signaling proteins including phospholipase-Cγ2 (PLCγ2), phosphoinositide-3-OH kinase (PI3K), Bruton's tyrosine kinase (Btk), and Vav. These proteins are recruited by adaptor proteins like B cell linker (BLNK) (Kurosaki 2002) and co-receptors such as the aforementioned CD19. Recent mass-spectrometry based proteomics allowed extensive mapping of the BCR signalosome and ubiquitylome, identifying more than 100 proteins which became phosphorylated and many more whose ubiquitinylation profile was altered after BCR crosslinking (Satpathy et al. 2015). After signalosome assembly downstream events such as internalization of antigen, signaling through second messengers (such as calcium and diacylglycerol) and regulation of gene expression may proceed.

BCR signalling is tightly controlled and kept transient by the activity of inhibitory phosphatases, especially SH2-containing tyrosine (SHP1) and phosphatidylinositol-5 (SHIP1) (Blasioli & Goodnow 2002; Nitschke et al. 1997; Nitschke 2005), which are active at phosphorylated immunoreceptor tyrosine-based inhibitory motifs (ITIMs) in inhibitory receptors like CD22 (Nitschke et al. 1997) also recruited to the signalosome by Lyn. The targets of SHP1 are protein phosphotyrosine residues, while SHIP1 converts the active lipid PI(3,4,5)P to PI(3,4)P, thereby removing membrane docking sites for Akt, PLCγ2 and Btk consequently terminating their activity (Leung et al. 2009).

Receptors become clustered after antigen binding and preferentially associate with cholesterol and glycolipid- rich microdomains called lipid rafts (Sohn et al. 2008) which become highly organised in the plasma membrane after BCR crosslinking. Lyn is a raft-resident Src- family kinase and thus membrane reorganisation is implicated as the mechanism Lyn primarily uses to sense BCR occupancy (Sohn et al. 2008; Sohn et al. 2003; Cheng et al. 1999). Perturbation of local lipid environment has even been suggested to be directly linked to bringing about conformational changes in cytoplasmic domains (Liu, Sohn, et al. 2010).

1.6.2 BCR signalling independent of antigen binding

BCR signalling is not only important for antigen-induced activation, but also for ‘tonic’ signalling. Tonic signalling via the PI3 kinase (PI3K) pathway is vital for mature B cell survival (Srinivasan et al. 2009). Deleting the BCR, Igα or even just the ITAM containing portion of Igα results in sudden mature B cell death (Kraus et al. 2004; Lam et al. 1997) highlighting the importance of constitutive signalling through the BCR. Survival signals can also be transduced through the BAFFR, which can work in unison with the BCR (with it functioning as a kind of adaptor protein) to phosphorylate Syk, the kinase responsible for translating survival signals via Erk and the PI3K pathway (Schweighoffer et al. 2013).

1.6.3 BCR organisation in the plasma membrane

Opposing schools of thought exist about how the 120,000 copies of the resting BCR complex exist in the plasma membrane. Total internal reflection fluorescence microscopy (TIRFM) on live cells and fluorescence resonance energy transfer (FRET) provided evidence that, at rest, the BCR exists as a monomer in the membrane. Without antigen, FRET signal was low indicating up to 80% of BCRs in a resting membrane are freely diffusing monomers (Tolar et al. 2005). In the presence of antigen, large increases in fluorescence between FRET donor and acceptor fluorophores indicated that BCR monomers moved into closer proximity forming larger, slower moving oligomers. The signal then decreased coinciding with the recruitment of signalling molecules to the cytoplasmic domains of the BCR complex. These data suggested there was movement from a 'closed' to 'open' conformation of cytoplasmic domains of the Igα/β signalling-active subunits of the BCR upon oligomerisation (Tolar et al. 2005).

This model is consistent with the 'picket fence' plasma membrane model, whereby dynamic compartments exist composed of actin-anchored proteins interspersed though an underlying actin meshwork, and was devised based on the observation that motility of various proteins and lipids was slower in plasma membranes of live cells than in artificial lipid bilayers (Treanor et al. 2010). As monomeric BCR protein complexes oligomerise their increase in size means it is harder for them to diffuse between compartments in the plasma membrane, known as 'oligomerization-induced trapping'. This could play a role in gathering multiple components together on the cell surface (Tolar & Pierce 2010). The cortical actin cytoskeleton is important for BCR organisation and linked to signalling functions, where artificial depolymerisation of actin with drugs caused spontaneous signalling through the BCR independent of antigen (Treanor et al. 2010). The ezrin-radixin-moesin (ERM) family member protein, ezrin, can restrict the movement of the BCR (Treanor et al. 2010). In resting cells, ezrin associates with lipid rafts (Gupta & DeFranco 2007) and could form part of the borders that make up nanoscale confinement zones in the plasma membrane. Upon BCR activation the dephosphorylation of ezrin

detaches it from the cytoskeleton removing imposed constraints on BCR diffusion and receptor clustering.

It has also been suggested that the BCR rests as an inactive oligomer with cytoplasmic domains inhibiting one another. It was proposed that upon antigen binding, multimeric antigen forces these oligomers apart and frees them from auto-inhibition, exposing cytoplasmic tails to participate in signalling (Yang & Reth 2010). Authors used the BiFC method, where fluorescent signals could only be seen if components on two receptors come together as dimers. The authors, however, did not determine the percentage of dimerised (or more highly ordered receptors), which could have been similar to the 20% seen in previous FRET studies.

Using direct stochastic optical reconstruction microscopy (dSTORM) BCRs were observed to rest in nanoclusters of 25-50 IgM molecules or 30-150 IgD molecules (Mattila et al. 2013). This technique can visualize molecules at 20nm resolution compared to 200nm resolution of conventional TIRF microscopy (Pierce et al. 2010). However, quantification of receptor clustering from STORM images is complicated by the fact that each labelled molecule is detected multiple times. It is therefore unclear whether these nanoclusters are true units of signalling or whether they need to aggregate to form active microclusters. A distinct disadvantage of dSTORM is also that it must be carried out on fixed cells. Given the dynamic nature of the BCR, this data still leaves the topic very much open for discussion.

1.7 Immune Synapse formation

B cells are tuned to respond with exquisite sensitivity and specificity to as few as 10 high-affinity antigens (Tolar 2011). Partly responsible is the contact interface formed between a B cell and an APC, termed an Immunological Synapse (IS, synapse). The synapse was first observed in live imaging studies of helper T cells interacting with APCs (Monks et al. 1998) then characterised further using high resolution TIRFM on surrogate planar lipid bilayer (PLB) systems (Grakoui et al. 1999). The synapse as a structure is typified by a central accumulation of T cell receptors (TCRs) surrounded in a bulls-eye configuration by a ring of adhesion

molecules. This receptor patterning was soon recognised in B cells (Batista et al. 2001) and cytotoxic T cells (Stinchcombe et al. 2001) and is now widely regarded as a common feature of all antigen-sensing immunoreceptors (Fooksman & Dustin 2010; Dustin & Groves 2012; Harwood & Batista 2011; Griffiths et al. 2010). Synapses vary in function according to cell type, in helper T cell cells to activate (Dustin 2009), in cytotoxic T cells to potentiate target cell killing (Stinchcombe et al. 2001; Bossi et al. 2002; Huse et al. 2008), in NK cells to integrate activating and inhibitory signals (Carlin et al. 2001) and in B cells to support antigen internalisation (Batista et al. 2001; Huang et al. 2005).

PLBs have served as excellent platforms to precisely elucidate each step making up the two-phase process of B cell synapse formation (Dustin 2009; Kessler et al. 2013; Tolar & Meckel 2009) (Figure 3). During phase one B cells make contact with antigen (via the BCR) through processes extending from their membranes, initiating a spreading response, where they move over the surface of the presenting cell by centripetal flow of filamentous actin at the leading edge of lamellepodia, travelling inwards towards the centre of the contact (Fleire et al. 2006). This dynamic actin flow bears a striking resemblance to the retrograde actin flow known to push lamellepodia forward (Dustin 2005). Spreading responses are said to be sensors of affinity and grow in magnitude with increasing receptor affinity and avidity (Fleire et al. 2006; Treanor et al. 2010; Liu, et al. 2010). The spreading response culminates with the formation of nanoscale aggregations known as microclusters at peripheral lamellepodia.

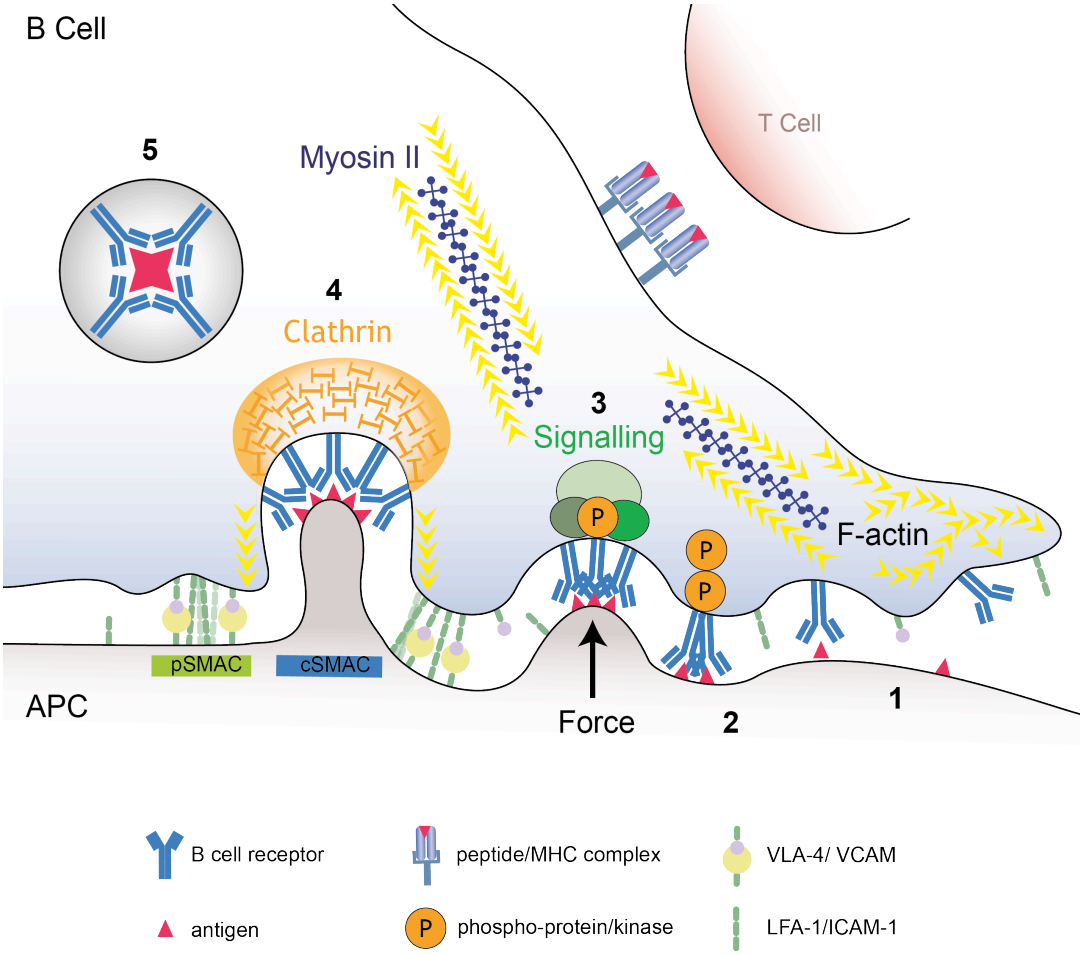

Figure 3 Immune synapse formation proceeds through a number of defined stages

1. Spreading phase. B cells contact antigen through the BCR and initiate a spreading response dependent on F-actin polymerisation
2. Contraction phase. Microclusters of BCRs form, which fuse as they are dragged towards the centre of the contact by actin flow and myosin IIA contractility. These are signalling active, with Src-family kinases recruiting components of the signalosome.
3. Upward pulling. Myosin IIA contractility causes tugging forces and invaginations of the presenting membrane as microclusters move to the cSMAC. This mechanically tests antigen binding. The BCR signalosome has fully formed.
4. Mature synapse formation. Microcluster movement arrests at the cSMAC, which is surrounded by a pSMAC of scaffolding adhesion molecules. Clathrin-coated pits facilitate pinching off of invaginated antigen clusters into endosomes.
5. Antigen is processed and loaded onto MHCII molecules for presentation to T cells.

These start containing just a few BCRs, but rapidly grow to contain hundreds of BCRs with extensive signalling machinery, and in fact are regarded as hotspots for BCR signalling (Fleire et al. 2006; Weber et al. 2008; Depoil et al. 2008). Association and immobilisation of freely diffusing BCRs drives microcluster formation, primarily through antigen binding-induced exposure of cryptic binding sites in the Cμ4 domain of the BCR (Tolar et al. 2009; Tolar et al. 2009), although important contributions from the actin cytoskeleton and physical topology of the membrane are also key in this process (Varma et al. 2006; Choudhuri et al. 2005; Campi et al. 2005; Fleire et al. 2006; Weber et al. 2008). Phase two of the response is a slower contraction phase (Fleire et al. 2006) whereby the mature synapse structure is formed. Here, microclusters are dragged towards the centre of the contact, growing in number over time before eventually fusing into the central supramolecular activation cluster (cSMAC). Early growth might act as a mechanism by which the cell 'counts' how much antigen is bound and may be an important determinant of affinity (Fleire et al. 2006; Dustin 2014b). An actin-rich ring of adhesion molecules called the peripheral supramolecular activation cluster (pSMAC) surrounds BCR complexes in the cSMAC. The integrin LFA-1 is an important molecule in the pSMAC that interacts with ICAM-1 on APCs (Carrasco et al. 2004) providing scaffolds to stabilise the contact.

Cytoskeletal machinery is central in regulating BCR signalling as it directly controls spatial organization (or indeed segregation) of essential components of B cell activation, including the BCR, co-receptors and adhesion molecules. The contraction response is an F-actin dependent mechanism of depolymerisation and repolymerisation relying on signals from activated Vav1, Vav2, PI3K, and Rac2 and eventually WASP (Arana et al. 2008). The tetraspanin network has been implicated in the proper organisation of nanoclusters in membranes (Mattila et al. 2013) along with the ERM proteins and the microtubule motor protein, dynein (Schnyder et al. 2011), which together perform pivotal roles in antigen gathering. Reorientation of the microtubule organising centre (MTOC- the point at which microtubules converge) by the formin family of actin nucleators is an important step in synapse formation in T cells (Gomez et al. 2007) and is absolutely required in cytotoxic T cells for the directed secretion of toxic cargo and docking of lysosomes at the

contact site (Stinchcombe et al. 2011; Ritter et al. 2015; Huse et al. 2013; Quann et al. 2009). The MTOC was shown to rapidly reorient during synapse formation in B cells (Yuseff et al. 2011) along with a general reorientation of organelles to become polarised towards the synapse (Yuseff et al. 2011; Obino & Lennon-Duménil 2014). It is speculated that the repositioning of key organelles such as the golgi apparatus and nucleus might optimise downstream transcription and translation required for effector functions. Studies from T cells show myosinIIA may play a role in TCR microcluster movement along actin filaments (Ilani et al. 2009; Kumari et al. 2012) and is known as an indispensible force-generator in B cells (Natkanski et al. 2013; Obino & Lennon-Duménil 2014), discussed later in the context of antigen extraction.

1.8 Antigen extraction and internalisation

The cSMAC functions as the site of antigen internalisation (Batista et al. 2001; Fleire et al. 2006), where B cells transform themselves from antigen-sensing cells to APCs. Extracted antigen is directed through endocytic processing pathways for loading onto MHCII molecules (Vascotto et al. 2007) and surface presentation to T cells (Siemasko et al. 1999; Siemasko & Clark 2001). Antigen internalisation might perform a secondary role in clearing occupied receptors or removing activated effector molecules, a theory so far only observed in T cells (Purbhoo 2013). In a departure from T cells, where receptor internalisation terminates signalling, the BCR continues signalling well after internalisation. These signals are important for intracellular antigen processing, a practice unique to B cells. Cellular location can modulate signalling rather than extinguish it altogether, with an entirely different set of kinases active inside the cell compared with at the plasma membrane (Chaturvedi et al. 2011; Chatterjee et al. 2012).

Most available data supports the model that antigen internalisation by B cells is driven by the formation of clathrin-coated pits (CCPs) (Figure 3) (Natkanski et al. 2013; Busman-Sahay et al. 2013; Chaturvedi et al. 2011; Stoddart et al. 2005; Stoddart et al. 2002). Although clathrin-independent, lipid raft- and actin-dependent pathways might also be involved (Stoddart et al. 2005), genetic interference with either clathrin or any member of the CCP pathway results in a substantial reduction

of both soluble or membrane-bound antigen-internalisation (Natkanski et al. 2013; Stoddart et al. 2005). Like other cytoskeletal components clathrin has strong links with BCR signalling: clathrin is phosphorylated by Lyn (Stoddart et al. 2002) and number of CCPs and their lifetimes steadily increase with synapse progression- a BCR signalling-dependent process (Natkanski et al. 2013). CCPs form in areas of membrane curvature, after upward pulling of membrane-tethered microclusters. Binding of clathrin to BCRs is proposed to be dependent on either the dephosphorylation of Igα/β to mediate binding of the adaptor AP2 (Hou et al. 2006; Busman-Sahay et al. 2013; Gazumyan et al. 2006) or ubiquitination of Igβ and Syk (Jacob et al. 2008; Dykstra et al. 2003; Zhang et al. 2007). Energy required to form CCPs- particularly when membrane tension is high- is generated mainly by polymerisation of actin (Boulant et al. 2011). B cells seem to generate areas of high membrane tension locally during internalisation even in the case of soluble antigen (Malhotra et al. 2009; Sharma et al. 2009).

Despite the importance of actin-dependent CCP formation these two molecules are not alone sufficient for BCR internalisation. Inhibition of myosin IIA (referred to herein as myosin) blocks internalisation by hindering the formation of the membrane invaginations that precede CCP formation (Natkanski et al. 2013). Myosin is a force-generator important in many aspects of synapse formation as well as being implicated in CCP-mediated internalisation of other molecules, like cadherin (Levayer et al. 2011) and termination of the strikingly similar focal adhesion structure (Kuo et al. 2011; Caswell et al. 2009). Elsewhere in synapse formation myosin contractility plays a role in lateral pulling forces during contraction and lamellepodia retraction (Tolar et al. 2009; Tolar & Spillane 2014). During microcluster movement into the cSMAC myosin exerts strong upwards pulling forces which physically detach antigen from membranes (Natkanski et al. 2013). This detachment does not always separate antigen from its receptor, but instead an upward pull of several hundred nanometers creates nanotubes in the presenting membrane from which clathrin can pinch the entire complex, including small portions of the presenting membrane, in a process resembling transendocytosis. This mechanism has been described in an array of other receptor-ligand systems (Qureshi et al. 2011; Marston et al. 2003) and agrees with *in vivo* B cell

experiments where extracted antigen colocalised with membrane proteins removed from presenting FDCs (Suzuki et al. 2009). Using mechanical force to extract antigen may cause very weak bonds between the BCR and antigen to rupture and consequently read out as less or no internalisation. This represents a seemingly crude but beautifully simple mechanism of early affinity testing or thresholding of BCR interactions. Considering the extensive regulation of the cytoskeleton by BCR signalling (Harwood & Batista 2011; Treanor et al. 2010; Song et al. 2013; Liu et al. 2013; Mattila et al. 2013), the tuning of BCR signalling by binding strength (Harwood & Batista 2011; Carrasco & Batista 2006a), and the idea that myosin IIA may bind directly to actin filaments (Lecuit et al. 2011) to cause contractions of differing magnitude depending on antigen binding (Natkanski et al. 2013), suddenly the concept of force-mediated extraction provides a multi-layered and elegant model of affinity-dependent antigen extraction in the synapse.

T cell synapses are well characterised as sites of secretion, where both cytokines and lytic granules may be delivered to target cells (Stinchcombe et al. 2011; Poo et al. 1988). An exocytic capacity for B cells has been proposed, whereby lysosomes dock at the synapse and release their contents, mainly proteases, into the cleft. These may then act on antigen to release it from presenting membranes by degradation, contributing to its efficient extraction (Yuseff et al. 2011). Lipases have also been speculatively suggested to be released during lysosome export to 'loosen' antigen from the APC membrane (Obino & Lennon-Duménil 2014). It is as yet unknown whether similar constraints exist on this kind of secretion as in T cells, where exocytosis occurs specifically in regions of central actin clearance (Stinchcombe et al. 2006). Degradation might represent an alternative path to extraction when antigen is stuck on unusual or very rigid surfaces like bone or cartilage (Li et al. 2010), or might depend on some other biomechanical or physical property of the antigen. The circumstances under which degradation occur are unclear, and whether it acts as a complimentary mechanism alongside force-mediated extraction or a compensatory mechanism when force-mediated extraction fails is elusive. Degradation may also represent an attractive model to explain dissociation of the synaptic contact, a process that as it stands, is poorly understood in B cells.

1.9 T-dependent (TD) and T-independent (TI) immune responses

The conventional route for antibody production by B cells follows BCR engagement and activation signals leading to proliferation and differentiation of the B cells into plasma cells, a process that may proceed either in the presence or absence of T-cell help. These responses were elucidated from studies in normal mice or athymic mice who lacked T cells (Gershon & Kondo 1970), and were thus termed Thymus-dependent (TD) or Thymus- independent (TI) immune responses. TD responses are usually elicited to protein Ags and involve cognate B cell-T cell interactions that either cause rapid differentiation of the B cells into extrafollicular plasmablasts or generate germinal center responses (MacLennan et al. 2003; MacLennan 1994) (covered at length in the coming sections). Aside from protein Ags, TD responses can also be initiated in response to glycolipids via help delivered by invariant NKT (iNKT) cells- an innate-like, thymus-derived T cell which recognise synthetic, self or microbial glycolipids and self phospholipids presented by the MHC I-like molecule CD1d rather than MHC I and II in conventional T cells (Barral et al. 2008; Chang et al. 2012; Detre et al. 2012; Leadbetter et al. 2008; Venkataswamy & Porcelli 2010). Unconventional CD1d-restricted NKT cell-driven TD responses are called TD type 2 (TD-2) and are able to rapidly induce GC formation; although antibody responses are less extensively affinity matured memory responses are compromised (Chang et al. 2012; King et al. 2012). CD1d is expressed on naive, mature and memory B cells as well as plasma cells and regulatory B cells (Mauri & Bosma 2012; Allan et al. 2011; Chaudhry & Karadimitris 2014).

Table 1 Characteristics and outcomes of antibody responses

Adapted from (Vinuesa & Chang 2013) with permission from Nature Publishing Group. PS = polysaccharide, MZ = marginal zone, FM = family members, GC-I = GC independent, SHM= somatic hypermutation, AM = affinity maturation

Antibody response	Antigen	Respond-ing B cells	Source of help	GCs	Memory B cells	Extra follicular response
TD-1	Protein	Follicular	T_{FH} cells, CD40L, IL-21, SLAM FMs	Yes, SHM, AM	Yes, pre and post-GC memory	Yes, delayed
TD-2	Glycoprotein	CD1d+ (MZ?)	NK cell, T_{FH} cell, IL-21, SLAM FMs	Yes, non productive no SHM or AM	Minimal	Yes, early, robust, SHM
TI-1	LPS, CpG, lipopeptides, RNA	MZ, B-1	B cell TLRs	Possibly	B-1 derived, GC-I	Yes, early
TI-2	Bacterial capsular PS, viral capsids	MZ, B-1	Extensive BCR signalling, Btk	Yes, (not often) non productive	B-1 derived, GC-I	Yes, early

TI responses represent two types of response, TI-1 and TI-2 according their signalling dependence on the kinase Btk (Vinuesa et al. 2016). TI-1 Ags provide B cell signals through Toll-like receptors (TLRs) that act independently of Btk. TLRs are specific for microbial products such as lipopolysaccharide (LPS), CpG DNA, viral RNA, lipopeptides and some viral coat proteins and act synergistically with BCRs for optimal antibody production (Ding & Jego 2009). Multivalent or repeating structures denote antigens in TI-2 responses, which after extensive BCR crosslinking transmit signals via Btk. TI-2 Ags include bacterial capsular

polysaccharides and highly repetitive viral capsid motifs (de Vinuesa et al. 2000). There is a division of labour amongst B cells such that specific subsets tackle their own specific antigen formats (Vinuesa & Chang 2013) (Table 1). MZ B cells are implicated primarily, but not exclusively in the initiation of TI immune responses. In addition, FO B cells participate in TI responses in some cases (Cariappa et al. 2005). MZ cells are the first line of defence against blood-borne Ags. TI responses have little immunological memory, although memory cells in the MZ can respond in a TD-manner in recall responses (Liu et al. 1988). Interestingly, MZ cells were also shown to be capable of germinal center differentiation in response to TD Ags but with altered kinetics (Song & Cerny 2003; Phan et al. 2005).

1.10 The germinal center reaction- an overview

During TD immune responses some activated naive B cells form germinal centers (GCs) (Figure 4). GCs may be thought of as specialised sites within an SLO, where a small fraction of B cells responding to a given pathogen are drawn into close proximity with (a) each other to establish competition between clones and (b) a microenvironment of multiple cells and factors supportive of high-affinity antibody production. After encountering antigen, activated B cells travel to the T-B border to interact with cognate T cells, and then decide whether to enter the GC reaction or become short-lived plasmablasts. This decision is incompletely understood but it is thought that very high affinity BCR crosslinking favours the plasmablast route (Paus et al. 2006; O'Connor et al. 2006). Remaining clones are directed into the GC pathway, where interclonal competition at the T-B border selects the higher affinity clones in the pool to seed the GC through a T-cell mediated checkpoint (Schwickert et al. 2011). Resultant GC B cells, through collaboration with follicular dendritic cells and T cells, generate a slower second-wave of higher quality TD plasma cells.

GCs are highly dynamic, transient areas of intense B cell proliferation. (Victora & Nussenzweig 2012; Allen 2007; Rajewsky 1996; Nieuwenhuis & Opstelten 1984; MacLennan 1994). In addition to B cells, GCs contain various specialised cells types that respond to specific chemical cues

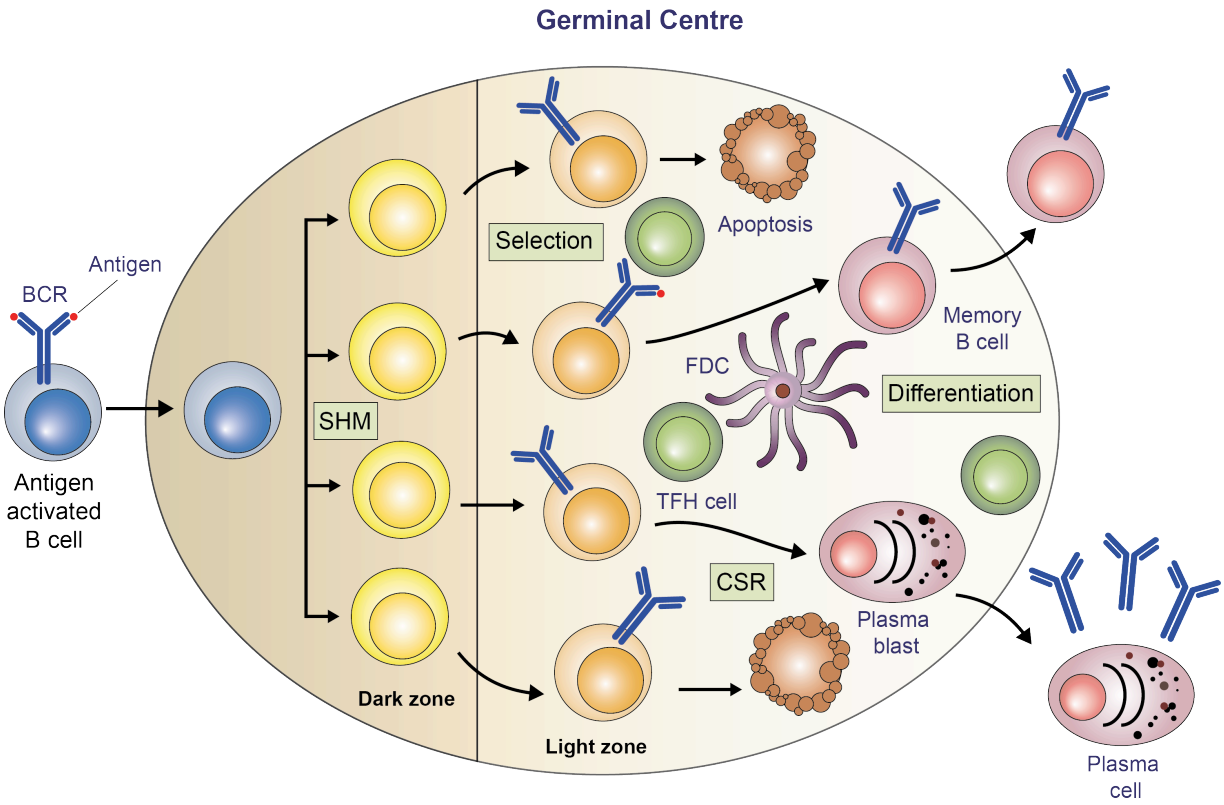

Figure 4 The germinal centre niche

Activated B cells enter into the germinal entre that is divided into two anatomical zones, the light and dark zone, established by chemokine gradients. In the dark zone, B cells proliferate and undergo the process of somatic hypermutation (SHM) where BCRs are diversified by the insertion of base-pair mutations into the V(D)J region of rearranged Ig genes in the variable regions of the light and heavy chains. Cells then migrate to the light zone where new BCRs are tested for productive rearrangements. B cells interact with antigen displayed on the surface of follicular dendritic cells (FDCs) and then based on amounts of antigen extracted, processed and presented, compete for limiting signals from T follicular helper cells. Some B cells change their receptor isotype by class-switch recombination (CSR). Non-productive rearrangements result in cell death by apoptosis. Positive selection of B cells causes cycling between zones and eventual differentiation into plasma cells or memory B cells.
Adapted from (Heesters et al. 2014) with permission from Nature Publishing Group.

controlling their positioning and behaviour (Figure 4) (Pereira et al. 2010). Deficient GC formation severely impairs protective high-affinity antibody responses and is associated with the onset of humoral autoimmunity or malignancies (Vinuesa et al. 2009; Klein & Dalla-Favera 2008); hence the reaction is tightly regulated at multiple levels. Two key genetic processes take place in the GC to alter BCR structure: stochastic point mutations in Ig variable genes called somatic hypermutation (SMH) (Jacob et al. 1991), which causes alteration in the antigen-binding CDR3 region, and class-switching between BCR isotypes, which replaces the heavy chain Fc region of the Ig molecule with different effector variants (Gray 1993). The genetic alterations and the following BCR 'testing' occur in distinct anatomical zones, called the dark and light zones, respectively (LZ, DZ) (Nieuwenhuis & Opstelten 1984). GC cells cycle through these zones numerous times before differentiating into effector antibody-secreting plasma cells or memory B cells and exiting the GC reaction. Receptor changes result in a Darwinian-like evolution of the BCR (and resultant secreted antibody) known as affinity maturation where overall antigen affinity dramatically increases over the lifetime of the reaction (Eisen 2014; Eisen & Siskind 1964). The mechanisms to effectively select and expand improved clones are essential for efficient progression of affinity maturation. These are dependent on competition between B cell clones.

The arrival of multiphoton microscopy has completely revolutionised our understanding of GC B cells (Victora et al. 2010; Schwickert et al. 2007; Hauser et al. 2007; Allen et al. 2007), which were inaccessible by traditional biochemical techniques due to their transient nature, low cell number and propensity for cell death after B cell isolation. The coming sections provide a review of the most up to date view of the GC niche, our current understanding of antigen transport to the GC and the areas where the GC reaction remain poorly understood.

1.11 GC zonal organisation and cellular dynamics

Activated B cells destined to participate in the GC reaction alter their migratory capacity to localise to central regions of the follicle (Pereira et al. 2009; Gatto et al. 2009). GC differentiation begins outside the follicle through the upregulation of the

master regulator B cell lymphoma 6 (BCL-6) (Kitano et al. 2011; Kerfoot et al. 2011). In T cells, this promotes differentiation into the T-follicular helper (T_{FH}) cell phenotype, with the accompanying upregulation of cell surface markers CXC-chemokine receptor 5 (CXCR5), programmed cell death protein 1 (PD1) and activation marker GL7 (Baumjohann et al. 2011). BCL-6 upregulation in B cells controls entry into the inner follicles (Huang et al. 2014; Kitano et al. 2011) and affects other migratory properties of B cells entering the GC programme. This occurs through dynamic regulation of receptors that respond to environmental cues, gleaned from studies using BCL-6 knockout B cells. BCL-6 deficient B cells do not downregulate the G-protein coupled receptor EBI2 (Huang et al. 2014; Kitano et al. 2011), whose expression is normally downregulated by to promote follicle entry (Pereira et al. 2009; Gatto & Brink 2013; Gatto et al. 2009; Cyster et al. 2014) nor do they upregulate the chemokine receptor CXCR4 which is required for GC B cells with the DZ phenotype (Allen et al. 2004). B cells lacking BCL-6 misregulate expression of sphingosine phosphate receptors S1PR1 and S1PR2, failing to downregulate S1PR1 which promotes trafficking out of the follicle rather than retention in the GC by S1PR2 (Cinamon et al. 2004; Green et al. 2011; Huang et al. 2014).

After positioning in the central follicle, activated B cells can enter the GC, which matures over time into a specialized microenvironment polarised into two distinct zones, the light and dark zones (LZ, DZ) (MacLennan 1994; Victora & Nussenzweig 2012) organized by chemokine receptors CXCR5 and CXCR4 respectively (Allen et al. 2004). Establishment of the LZ and DZ is highly conserved across species, highlighting how important proper zonal establishment, and subsequent B cell positioning is in the GC reaction (Yasuda et al. 1998; Victora et al. 2012; Allen et al. 2004). Originally named after observations from histological dye studies the DZ is tightly packed full of proliferating GC B cells named centroblasts making it appear dark, whereas the LZ is more sparsely populated with GC B cells named centrocytes (Röhlich 1930). Although first thought to be completely independent developmental stages defined by cell size and location (MacLennan 1994), LZ and DZ cells were later shown to flux dynamically between compartments and be morphologically indistinguishable from one another (Victora

et al. 2010; Schwickert et al. 2007; Hauser et al. 2007), and hence the terms centroblasts and centrocytes were seen as somewhat confusing and their use diminished. Rather than looking for larger or smaller cells, LZ and DZ cells may be identified phenotypically by expression patterns of CXCR4, CD83 and CD86; with LZ cells identified as $CXCR4^{low}$ $CD83^{hi}$ $CD86^{hi}$ and DZ cells the reverse (Victora et al. 2010). DZ cells rapidly proliferate after rounds of receptor mutation amongst a supportive network of CXC- chemokine ligand 12 (CXCL12)- expressing reticular cells (Bannard et al. 2013). In concurrence with this model, DZ cells express more of the enzyme AID, responsible for introduction of mutations into germline BCRs. Along with B cells, the LZ also contains T_{FH} cells, FDCs and specific macrophages, and serves as the area for GC B cell antigen interaction and T-B communication after receptor editing where GC B cells receive T cell help (Victora & Nussenzweig 2012). GC B cells undergo iterative rounds of DZ BCR mutation and LZ T-dependent selection, cycling between zones multiple times, in a migratory process known as cyclic-reentry (Allen 2007; Victora & Nussenzweig 2012; Schwickert et al. 2007; Hauser et al. 2007). Rather than being defined by location only, each GC B cell state has its own distinct genetic programme, where gene expression varies between LZ and DZ cells; mostly in genes activated following acquisition of T-cell derived signals in LZ cells and cell-cycle regulators in DZ cells (Victora et al. 2010).

Studies from the Cyster Laboratory provided breakthrough insights into the organisation and behaviours of GC B cell phenotypes. They showed that the ligand for CXCR5, CXCL13 is expressed on the surface of LZ FDCs and guides migrating LZ B cells into the compartment for antigen interaction, whereas migration away from CXCL13, and back into the DZ, is mediated by upregulation of CXCR4 on DZ B cells for interaction with its partner ligand CXCL12, produced by DZ stromal cells (Bannard et al. 2013; Allen et al. 2004). CXCR4 upregulation correlated with increased DNA synthesis, confirming its location in the DZ (Allen et al. 2007; Allen et al. 2004), which was later also observed in human GCs (Caron et al. 2009). When CXCR4 was ablated on GC B cells they became trapped in the anatomical LZ- but interestingly retained intact proportions of each cell phenotype as defined by the aforementioned surface markers, with 'DZ' phenotype cells progressing normally through the cell cycle (Bannard et al. 2013). This was concurrent with

other studies where proliferation had been observed in both zones of the GC (Allen et al. 2007; Hauser et al. 2007; Rahman et al. 2003; Wang & Carter 2005). Where previously positioning was assumed to be the sole determinant of the LZ and DZ programme, these studies showed transition between the two states occurred irrespective of environmental cues, instead being controlled by a cell-intrinsic 'bodyclock' (Bannard et al. 2013), where number of divisions in the DZ are tuned by T cell signal strength received in the LZ (Gitlin et al. 2015). However, location is important, as CXCR4 deficient cells were less able to gain high affinity mutations and became outcompeted by wild-type cells over time (Bannard et al. 2013), with other perturbations of zonal organisation also hampering efficient affinity maturation (Sander et al. 2015; Dominguez-Sola et al. 2015).

Recently came the first genetic perturbation resulting in loss of one of the GC B cell subsets. Two studies found the transcriptional regulator forkhead box protein-1 (Foxo1), was highly expressed in the nucleus of DZ GC B cells relative to LZ cells (Sander et al. 2015; Dominguez-Sola et al. 2015). Foxo1 expression is turned off by the PI3K pathway and the kinase Akt and was long suspected to play a role in GC B cell gene expression due to its frequent mutation in GC-derived lymphomas (Trinh et al. 2013). Foxo1 deficiency or silencing through introduction of a constitutively active PI3K gene in GC B cells caused a selective loss of DZ cells. Surprisingly, the overall size of GC response was unaffected. This suggests perhaps proliferation is not fundamentally tied to the DZ- or even to DZ cells. This further supports evidence of cell-intrinsic GC B cell control mechanisms, but similarly, loss of architectural integrity in the GC compromised selection of high-affinity B cell clones and class switch recombination (Dominguez-Sola et al. 2015; Sander et al. 2015; Bannard et al. 2013).

1.12 Antigen transport and presentation in the GC

Follicular dendritic cells are regarded to be the primary platform for antigen presentation in the GC (Tew et al. 1980; Mandel et al. 1980; Allen & Cyster 2008). They hold large amounts of antigen on their surfaces, in the form of immune complexes, for interrogation by GC B cells (Suzuki et al. 2009). FDCs are stromal cells of mesenchymal origin (Tew 1993) identified based on their extensive

dendritic processes, that reside in large numbers in the GC LZ. FDCs are unique in their ability to retain intact antigen on their surface for prolonged periods, thought to be in the region of months or longer (Tew & Mandel 1979; Mandel et al. 1980; Allen & Cyster 2008). It should be noted that following genetic ablation of immune complex formation in mice, GC formation could proceed, providing some evidence for alternative antigen sources, although the magnitude (or even existence) of these contributions to a full response are highly controversial (Hannum et al. 2000; Kosco-Vilbois 2003; Allen & Cyster 2008; Haberman & Shlomchik 2003).

Antigen is delivered to FDCs in a stepwise fashion by other cells in SLOs. Intact large antigen, such as viruses or bacteria may be captured and processed in the medulla by SCS macrophages or $CD11c^{+}$ LN-resident DCs (Gonzalez et al. 2010; Roozendaal et al. 2009). DCs are implicated in direct transport of processed antigen to FDCs (Heesters et al. 2014). Opsonised particulate antigen entering the SLO covered in complement or antibodies in an immune complex may be captured in the SCS by $CD169^{+}$ SCS macrophages lining areas adjacent to incoming lymphatic vessels (Batista & Harwood 2009; Phan et al. 2009). Cognate B cells can interact with antigen presented by SCS macrophages, accumulate it and carry it to FDCs (Carrasco & Batista 2007). Remarkably, non-cognate follicular B cells have also been implicated in an antigen shuttling role in the follicle (Phan et al. 2009; Phan et al. 2007). They achieve this either by collecting opsonised antigen from SCS macrophages or directly from the blood or lymph via complement component C3 binding to surface complement receptors and migrating via a random-walk motion through the follicle to meet extended FDC processes. They may then unload their cargo through receptor competition onto FDCs expressing higher levels of splice variants of the two complement receptors (CR1, CR2), which might have higher affinity for C3. Similar shuttling behaviours have been also been observed in the spleen in non-cognate MZ B cells (Cinamon et al. 2008). Mechanisms of antigen 'handover' to FDCs are not well defined, although it is known to be unidirectional, actin-dependent and may involve force generation by the CR2 receptor (Heesters et al. 2014; Heesters et al. 2013).

B cells require interactions with antigen presented in its native form. How antigen could be retained on the surface of FDCs long-term without intracellular processing or subsequent degradation (Szakal et al. 1983) was a puzzling thought. The issue was elegantly investigated using live-cell imaging (Heesters et al. 2013), where transfer of immune complexes was observed from non-cognate B cells to FDCs. Antigen was acquired and unexpectedly, was rapidly internalised. Internalisation led to trafficking through a nondegredative endosomal pathway, where complexes were protected from degradation and recycled to the cell surface periodically. Aside from long-term antigen presentation, this may have a role in controlling epitope density in the GC, where FDCs all present similar amounts of antigen, equalizing large avidity effects of antigen clustering and focussing selection of B cells in relation to their relative affinity (Chan & Brink 2012). Long-term retention of antigen by FDCs serves a functional purpose of maximising antigen exposure to late-arriving B cells to GC reaction.

1.13 The B cell receptor in germinal centre reactions

The BCR is fundamental in B cell responses, especially in the GC where it undergoes alterations to achieve improved antigen binding. In addition to genetic changes and changes in the signalling pathways described below, the surface BCR density on GC B cells becomes reduced up to 10-fold when compared with naive B cells (Chan et al. 2009), including a complete loss of the surface IgD isotype. It is possible that lower levels of surface BCR may actually improve sensitivity of affinity-based selection. In contrast to high levels of surface BCR on naive B cells, which act to maximise recruitment of cells spanning a wide range of affinities, the lower levels of surface BCRs on GC B cells and the lower levels of antigen presented on MHC work in concert to increase stringency, excluding somatically mutated variants with affinity-compromising mutations. This model is supported by findings that the high expression of the IgD BCR on naive cells promotes early B cell recruitment (Brink et al. 1995; Brink et al. 1992; Roes & Rajewsky 1993).

1.13.1 Somatic hypermutation and class-switching

Two main mechanisms exist to diversify BCRs during GC reactions, somatic hypermutation (SMH) and class-switch recombination (CSR) (Berek et al. 1991; Jacob et al. 1991; Nussenzweig & Nussenzweig 2010; Neuberger et al. 1999). Both rely on the enzyme activation-induced cytidine deaminase (AID) expressed by B cells, which deaminates cytidine bases specifically in VDJ and switch regions of the Ig genes (Honjo et al. 2002; Muramatsu et al. 2000; Nussenzweig & Nussenzweig 2010). SMH introduces stochastic mutations into the variable region sequence of Ig heavy and light chains to alter antigen binding affinity, with mutation rates of as high as 10^{3} per base pair per generation (Berek et al. 1991), 10^{6}-fold higher than background mutation rates. CSR replaces the Cμ constant region of immunoglobulin locus with genes of Cγ, Cα or Cε- altering the IgM BCR to an IgG, IgA or IgE isotype (Honjo et al. 2002). Alternate isotypes affect the Fc portion of the resultant BCR, providing different effector mechanisms of pathogen clearance without changing the antigen specificity (Pogue & Goodnow 2000). Due to dependence of both mechanisms on AID, their individual influences on B cell fate were hard to uncouple. IgG isotype-switched memory B cells appeared to have a shorter half life than IgM memory cells, but displayed more extensive SHM (Pape et al. 2011; Dogan et al. 2009). In a recent study, Gitlin *et. al.* genetically uncoupled the two processes using an approach where CSR could occur in the absence of SHM (Gitlin et al. 2016). The results confirmed that class switched memory cells had shorter lifespan because they were preferentially selected into the bone marrow PC pool and steered away from the memory fate.

1.13.2 BCR signalling in the GC

The role of signalling through the BCR in GC responses is poorly defined. In current models implicating T cell help as the determinant for selection of high affinity variants, BCR signalling is thought to play a more limited role outside of affinity-based selection. Instead, T_{FH} -derived signals through the CD40 signalling pathway are proposed as a major player in selection (Allen 2007). However, BCR signal strength and duration as well as qualitatively different signals accompanying

high and low affinity variants have also been proposed. Studying signaling in GC B cells *ex vivo* has been complicated by their propensity to die within hours of isolation. This is because they are kept in a proapoptotic state by Bcl-6, which suppresses the antiapoptotic molecule BCL-2 (Saito et al. 2009). However, some GC BCR signalling data exist; using a novel *ex vivo* fixation technique, the Shlomchik group proposed that most proliferating GC cells surprisingly showed no active BCR signalling, with signalling being controlled by the activity of two phosphatases, SHP-1 and SHIP-1(Khalil et al. 2012). These were both hyperphosphorylated and failed to dissociate from the BCR after activation as they do in non-GC cells. Additionally, conditional SHP-1 knockouts had disrupted GC maintenance. Syk phosphorylation was detected in a small fraction of cells in the G2 phase of the cell cycle, thus the authors suggested B cell signalling in the GC was based on the integration of T derived and BCR signals in a cell-cycle dependent manner. However, a major caveat of this study is the use of an IgM transgenic mouse model. CSR in the GC causes large proportions of GC B cells to display BCRs of alternate isotypes, with longer cytoplasmic domains than IgM containing additional signalling motifs (Engels et al. 2009). Indeed, significant evidence is accumulating supporting unique signalling propensities of the class switched isotypes, such as IgG and IgE (He et al. 2013; Yang et al. 2012; Talay et al. 2012; Engels et al. 2009). *In vivo,* BCR silencing was not observed to the same degree. Using a Nur77-eGFP reporter mouse as a real-time sensor of BCR signalling, active BCR signalling could be observed in an appreciable proportion of LZ GC B cells (Mueller et al. 2015). Therefore, signalling capabilities of GC B cells through the BCR- particularly after CSR- remain incompletely understood.

1.14 Affinity maturation and selection in the germinal centre

Affinity maturation is the ultimate purpose of the GC, augmenting high affinity antibody responses and commitment to the memory B cell fate. Old models of selection were based on the idea of GC B cells competing for limited amounts of antigen, as affinity maturation was more pronounced when antigen access was limiting (Eisen & Siskind 1964; Goidl et al. 1968; Nussenzweig & Benacerraf 1967). Higher affinity variants were hypothesised to block access to antigen for

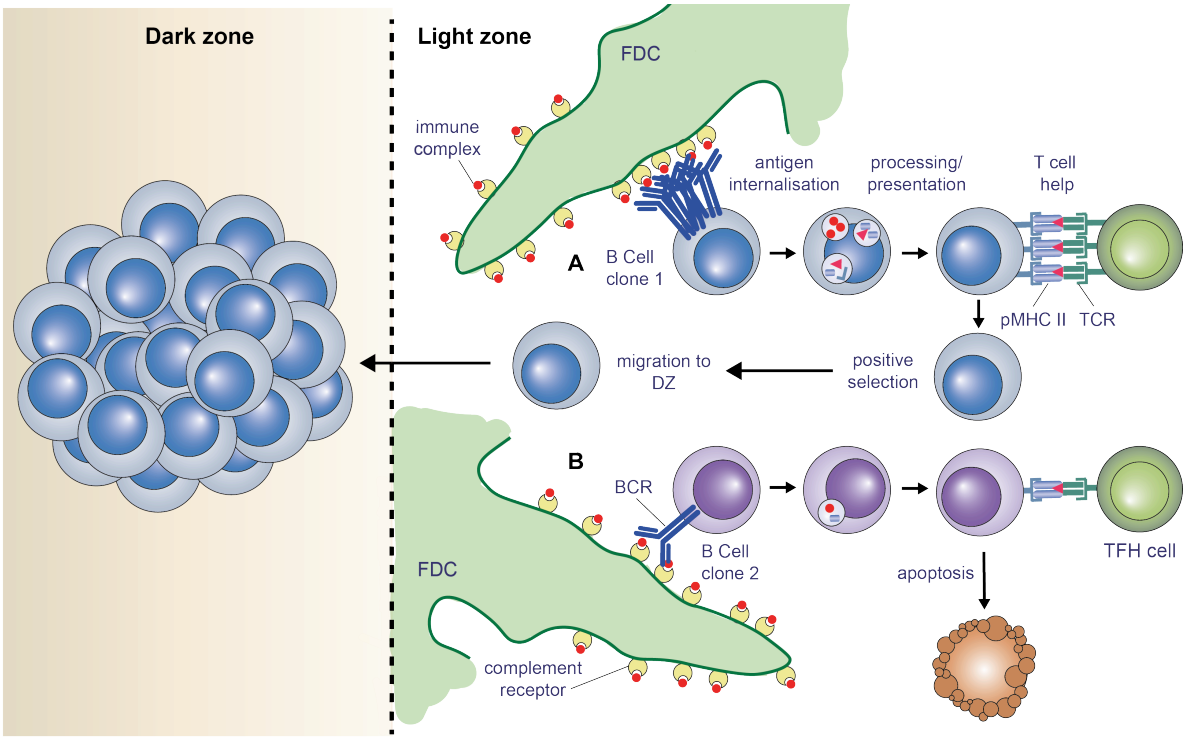

Figure 5 B cells interact with FDCs and TFH cells in the light zone in order to receive positive selection signals

B cells interact with antigen displayed on the surface of FDCs as immune complexes held in complement receptors or Fc receptors (not shown). B cells that bind antigen with the highest affinity extract more from FDCs and internalise it into endosomal compartments for intracellular processing. During intracellular trafficking, antigen is degraded into peptides and loaded into MHC II molecules. These are presented on the surface of the B cell for interaction with cognate T cell receptors (TCRs) on T_{FH} cell surfaces. Cells displaying the most pMHC II and therefore receiving the most T cell help are selected for migration back to the dark zone and subsequent mutation and proliferation (A). B cells internalising less antigen from FDCs receive less T cell help and die via apoptosis (B).

lower affinity cells by forming long-lived, shielding interactions with FDCs and sequestering all available antigen and signalling. However, this was not corroborated *in vivo* as intravital microscopy failed to identify any of these kinds of synapses (Schwickert et al. 2007; Allen et al. 2007; Hauser et al. 2007). This also fails to account for the deletion of autoreactive cells generated by SHM (Diamond et al. 1992; Davidson et al. 1987), which would exhibit strong binding to self-Ags and be selected for in this model.

Current models have evolved based on B cells acquiring antigen deposited on FDCs (Heesters et al. 2013), processing and presenting it to acquire limiting T_{FH} help, the magnitude of which is determined by the density of MHC-displayed surface antigen (Victora et al. 2010) (Figure 5). This picture of T-cell-help based selection was elucidated by an elegant set of *in vivo* experiments uncoupling antigen presentation by GC B cells from the BCR (Victora et al. 2010) so as to exclude any contributions from antigen induced signalling. In these experiments GC B cells could be decorated in cognate peptide through artificial loading of a cell surface lectin expressed on the GC B cell surface called DEC205, which caused a subsequent increase in surface peptide-MHCII (pMHCII). GCs were induced such that only a small proportion of B cells expressed DEC205 (and therefore could be artificially loaded with cognate peptide to display to T cells). These DEC205 sufficient cells with access to T cell help outcompeted $DEC205^{-/-}$ cells despite matching BCR affinities. In a situation where all cells were targeted through DEC205 to display equivalent pMHCII, GC T cells effectively became blinded to GC B cell affinity abrogating affinity maturation and selection of high-affinity mutants. Even prior to this direct evidence, a wealth of data existed implicating T cells as regulators of affinity-based selection.

T cells were previously observed discriminating between B cells on the basis of surface pMHCII *in vitro* where more contacts were formed with B cells bearing higher surface pMHCII density (Depoil et al. 2005). T cell help is delivered through CD40-CD40 ligand (CD40L) interactions (Basso et al. 2004) and through secreted products such as interleukin 21 (IL-21) (Linterman et al. 2010). Blocking either of these caused termination of the GC reaction (Linterman et al. 2010; Zotos et al. 2010; Han et al. 1995) and disturbing T_{FH} function resulted in impaired GC B cell selection and the onset of autoimmunity (Kim et al. 2010; Vinuesa et al. 2005; Arnold et al. 2007). Furthermore, in competition studies, B cells unable to effectively load peptide onto MHCII were outcompeted irrespective of BCR affinity, which was matched across all B cells using a transgenic fixed BCR specific for the hapten NP (Draghi & Denzin 2010). Multi-step selection processes (step 1: affinity-dependent antigen acquisition, step 2: cognate engagement of T_{FH} cells) where B cells binding antigen with highest affinity through the BCR are not always those

who achieve most efficient selection, is likely to have advantageous implications during an immune response. Although not necessarily the fastest route to achieving maximum affinity, introduction of noise into the system through competition for T cell help (potentially hampered by location or dynamics) may diversify Ab responses (Eisen & Siskind 1964)- an important feature in a some infection settings (Scheid et al. 2009; Klein et al. 2012; Lingwood et al. 2012). Generating breadth in responses may be preferable to simply accumulating affinity-improving mutations considering an effective Ab affinity ceiling has been observed, where subsequent mutations did not further improve responses (Batista & Neuberger 1998).

Old models of the GC as a static microenvironment were challenged by the observation that FO B cells recruited after GC establishment, perhaps travelling from distant, sites may join the reaction at any stage (Schwickert et al. 2007; Suzuki et al. 2009). This has obvious implications for affinity maturation and redefined the GC as a dynamic niche where cells continually proliferate, die, enter and leave. On this theme, a phenomenon called 'antibody feedback' has recently been described- where not cells, but antibodies (Abs) produced by recently emigrating plasma cells (PCs) replace existing Abs in GC immune complexes. As the GC reaction progresses, affinity of this secreted Ab increases, thus establishing a slowly rising competitive threshold for B cells to overcome during progressive rounds of selection (Zhang et al. 2013). Abs from any nearby PC could diffuse into any given GC, and thus antibody feedback has been proposed as a mechanism for inter-GC communication (Zhang et al. 2013; Zhang et al. 2016), tuning responses between GCs to achieve high affinity across the board. GC B cells have even been observed exchanging between GCs during an infection, or invading established GCs during multiple parallel infections (Bergqvist et al. 2013; Schwickert et al. 2009). The requirement for a significant competitive advantage to enter a GC where affinity is rapidly increasing limits B cell invasion to a small number of scenarios, and may be more relevant in sites of continual antigenic stimulation, like the gut (Bergqvist et al. 2013). Additionally, T_{FH} cells readily migrate between GCs (Shulman et al. 2013). T_{FH} populations are highly polyclonal within a single GC and similar clonal distributions may be identified across multiple GCs (Shulman et al. 2013; Zheng et al. 1996; Roers et al. 2000; Golby et al. 1999). Newly activated T_{FH}

cells may be recruited to established GCs and can gain unrestricted entry without overcoming an affinity barrier (Shulman et al. 2013). This adds robustness to selection by continually testing B cells against a broad assortment of T cells from an evolving pool; particularly pertinent in infections known to cause rapid mutation of T cell epitopes.

Over time, B cells in some GCs become increasingly monoclonal in a process known as 'homogenizing selection'. This relies on extensive proliferation of successful clones in the DZ, and often occurs after a phenomenon known as a clonal burst, where a single SHM variant is extensively expanded (Tas et al. 2016). Although transition between LZ and DZ states are intrinsically regulated by GC B cells (Bannard et al. 2013), behaviour in the DZ is influenced by T cell help. Increasing amounts of T cell help received in the LZ increases dwell time in DZ, facilitating more rounds of cell division for highest affinity clones (Gitlin et al. 2014; Meyer-Hermann et al. 2012). Additionally, successfully mutated clones have altered cell cycle dynamics, upregulating expression of cell cycle regulators downstream of the T-cell-help-associated transcription factor c-Myc (Calado et al. 2012), resulting in a shorted S phase (Gitlin et al. 2015). This means B cells receiving large amounts of T cell help migrate to the DZ for prolonged time periods and undergo accelerated rounds of proliferation. This may help to explain how a single successful clone begins to dominate a given GC and undergo a clonal burst. Notably, novel intravital imaging with a multicolor fate mapping 'Confetti' allele revealed clonal patterns in GCs are more complex than original models anticipated (Tas et al. 2016). GCs are seeded by larger numbers of clones than the 1-3 initially thought (Jacob et al. 1993) - hundreds of individual B cells, and undergo varying amounts of homogenizing selection with some maintaining clonal diversity and others becoming entirely monoclonal (Tas et al. 2016). Although all the previous data still mapping affinity maturation and selection drove forward knowledge on affinity-based selection in the GC, factors driving this observed GC heterogeneity and clonal diversity remain to be characterised, as do their knock-on implications in immune responses to specific infections.

1.15 Unresolved aspects of GCs and clinical perspectives

There are still unidentified parameters in our understanding of how successfully selected B cell clones gain dominance in the GC. Particularly, although antigen in the GC is surface-bound (Carrasco & Batista 2006a), mechanisms of immune synapse formation and antigen extraction by GC B cells remain poorly understood. Intravital imaging revealed a surprising absence of long-lived cellular contacts between GC B cells and FDCs (Schwickert et al. 2007; Hauser et al. 2007; Allen 2007) hinting at alternative regulation of synaptic contacts. However, the formation of immune synapses in GC B cells has never been observed in high enough temporal or spatial resolution. Furthermore, synapse formation in FO B cells is dependent on BCR signalling (Fleire et al. 2006), and on cytoskeleton-dependent antigen centralisation (Seeley-Fallen et al. 2014; Song et al. 2013; Liu et al. 2013; Liu et al. 2011). Accumulating evidence implies GC BCR signalling is fundamentally different to FO signalling (Khalil et al. 2012; Mueller et al. 2015), which may have consequences for the formation of GC immune synapses.

In spite of these unknown molecular aspects of the GC reaction, major strides have been made on a cellular level. As previously detailed, we now understand in detail how GC B cells are recruited, cycle between compartments and evolve clonally, with some insight into what molecular cues guide these movements. Clinically, this presents a realistic prospect for rational vaccine design against viral infections such as HIV and influenza that are notoriously refractory to current vaccination strategies (Krammer & Palese 2014; Burton et al. 2012). Where current vaccines work through induction of neutralising Abs to a few immunodominant surface epitopes, protection from rapidly evolving viruses is instead elicited through broadly neutralising antibody (bnAb) responses (Scheid et al. 2009). bnAbs often bind non-immunodominant epitopes that are in highly conserved regions, such as the stem in the influenza hemagglutinin (Krammer & Palese 2013), which is recognised by several different families of isolated bnAbs (Throsby et al. 2008; Sui et al. 2009; Corti et al. 2010; Wrammert et al. 2011). This has led to the isolation of a pan influenza neutralising antibody, raising hopes of a universal vaccine (Corti et al. 2011; Krammer & Palese 2014; Kallewaard et al. 2016). A recent study tracking

evolution of HIV-1 Ab responses in a patient revealed that bnAb clones arose when many viral variants were present in parallel (Liao et al. 2013). Therefore, integrating multiple inputs may produce clones with greater breadth that are therefore favoured on the basis of higher total avidity. Interestingly, most potent HIV-1 bnAbs have huge rates of SHM, accumulating numbers of mutations tenfold higher than those normally elicited by vaccination, and these seem to be required for their broadly neutralising function (Jiang et al. 2013; Klein et al. 2013; Klein et al. 2013b; Scheid et al. 2011). Manipulating B cell antigen presentation through extraction mechanisms may provide cues to induce the high levels of SHM required to acquire broadly neutralising function. Consequently, understanding clonal evolution of Ab responses and the GC B cell-antigen interactions that induce them will be central to the understanding of how to promote bnAb responses through vaccination.

1.16 Thesis aims

Immune synapse formation is well characterised in FO B cells, and is a prerequisite for efficient antigen extraction from APCs. To test receptor rearrangements in the GC, B cells must form a second immune synapse to extract antigen presented on the surface of FDCs and internalise it for processing. This leads to a generalised model of affinity maturation where presentation of processed antigen in the format of MHC II bound peptides facilitates access to limiting T cell help, which selects successful clones for a expansion, gradually increasing the net affinity of the GC B cell pool.

Although B cell antigen acquisition from FDCs has been observed *in vivo*, these approaches lacked sufficient resolution to observe immune synapse formation, which is presumed to form between GC B cells and FDCs during antigen acquisition. GC B cells are transient, rare and may not be produced *in* vitro and thus are poorly suited to traditional low throughput high-resolution imaging techniques. So, despite the importance of GC B cell antigen extraction from FDCs, synapse formation and its contribution to affinity-dependent extraction remains unstudied.

To address these knowledge gaps, my aims were to build a system capable of high resolution imaging of synapse formation across B cell populations in order to:
(1) Compare synaptic architecture in across B cell subsets interacting with membrane-presented antigen *ex vivo*
(2) Investigate GC immune synapse formation and antigen extraction mechanisms
(3) Link any observed alterations in synaptic patterning to affinity discrimination during GC reactions.

Chapter 2. Materials & Methods

2.1 Mice

C57BL/6 (Bl6) mice were used as the source of naive B cells unless otherwise stated. B1-8$^{flox/flox}$ Igκ$^{Ctm1Cgn/tm1Cgn}$ mice on C57BL/6 background (B1-8 mice) were used as a source of B1-8 B cells specific for the NP and NIP haptens. All mice were between 1-6 months old and were male and female. Mice were bred and treated in accordance with guidelines set by the UK Home Office and the Francis Crick Institute Ethical Review Panel.

2.2 Buffers and Media

Table 2 Composition of buffers and media

Name	Composition
Running buffer	Phosphate buffered saline solution (PBS), 0.5% bovine serum albumin (BSA) (SigmaAldrich), 2 mM EDTA
HBSS/BSA	Hank's Balanced Salt Solution (HBSS), 0.1% BSA
HBSS/ lo BSA	Hank's Balanced Salt Solution (HBSS), 0.01% BSA
Sodium Carbonate buffer	3 mL 0.1 M Na_2CO_3, 17 ml 0.1 M $NaHCO_3$. pH 9.3
Full RPMI	RPMI 1640 (SigmaAldrich), 10% fetal bovine serum (FBS) (Biosera), 1% MEM Non-Essential Amino Acids (ThermoFisher Scientific), 2 mM L-glutamine (GE Healthcare), 50 µM 2- mercaptoethanol (Thermo Fisher Scientific), 100 U/ml Penicillin and 100 µg/ml Streptomycin
Full DMEM	Dulbecco's Modified Eagles Medium (DMEM), 10% FBS, 1% MEM Non-Essential Amino Acids, 2 mM L-glutamine, 100 U/ml Penicillin and 100 µg/ml Streptomycin
Full Pro-293	Pro-293 (Lonza), 1.5% FBS, 2 mM L-glutamine

B cell media	RPMI 1640 (SigmaAldrich), 10% fetal bovine serum (FBS) (Biosera), 1% MEM Non-Essential Amino Acids (ThermoFisher Scientific), 2 mM L-glutamine (GE Healthcare), 50 µM 2- mercaptoethanol (Thermo Fisher Scientific), 20 mM HEPES buffer (ThermoFisher Scienctific), 100 U/ml Penicillin and 100 µg/ml Streptomycin
Full FDC	Dulbecco's Modified Eagles Medium (DMEM), 10% FBS, 20 mM HEPES Buffer 1% MEM Non-Essential Amino Acids, 2 mM L-glutamine, 1 µg/ml gentamicin (Gibco)
Full StemPRO	StemPRO-34 Serum-free media (Invitrogen), Nutrient supplement provided with media, 1% Antibiotic-Antimycotic (Invitrogen)

2.3 Immunisations

2.3.1 Friend virus (FV)

FV was propagated *in vivo* and prepared as 10% w/v homogenate from the spleen of 12-day infected BALB/c mice (homogenate provided by G. Kassiotis). C57Bl/6 mice received an inoculum of ~2000 spleen focus-forming units (SFFU) of FV, injected via the tail vein in 0.1 ml sterile phosphate buffered saline (PBS). Mice were sacrificed at day 12-20 post-infection (p.i.).

2.3.2 Sheep red blood cells (SRBCs)

SRBCs (Patricell) were supplied and stored in sterile Alsever's solution at 4°C and washed three times in sterile PBS before intra-peritoneal (i.p.) injection of 10% v/v SRBC solution in 0.2 ml PBS. SRBC-immunized mice were sacrificed at day 7–20 p.i., although GC's were still detectable more than 30 days p.i.

2.3.3 SRBC conjugated to the NIP hapten (SRBC-NIP)

NIP-e-Aminocaproyl-OSu (Biosearch Technologies) (NIP-Osu) was equilibrated to room temperature, and dissolved to 10 mg/ ml in anhydrous dimethyl sulfoxide (DMSO). This was further diluted to 1 mg/ml in a freshly made solution of 0.15M $NaHCO_3$ (0.126g in 10 ml dH_20). A 10% v/v solution of SRBC was prepared as

above but finally resuspended in $NaHCO_3$ rather than PBS. Equal volumes of NIP were added dropwise to SRBC with shaking and incubated at room temperature for 2 hr. Cells were washed 3 times in PBS and finally resuspended in PBS at 10% v/v. Mice received 0.2 ml SRBC-NIP via the i.p route, and were sacrificed at day 7-14 p.i. The conjugation was confirmed by staining the SRBCs with a Cy5-labelled recombinant B1-8 Fab fragment (Natkanski et al. 2013) and measuring with flow cytometry.

In each case, GC formation was evaluated by flow cytometry. For GC B cell imaging, splenocytes were pooled from two mice per experiment.

2.4 Cell Transfers

Antigen-specific GC B cells were generated by adoptive transfer of 5×10^6 splenocytes from B1-8 mice (expressing CD45.2) in 0.1 ml Iscove's Modified Dulbecco's Medium (IMDM) into congenic C57BL/6 CD45.1 or (C57BL/6 × C57BL/6 CD45.1) F1 mice via tail vein injection. Immediately after cell transfer the mice were immunized with SRBC-NIP. Mice were immunized with 0.2 ml SRBC-NIP via the i.p route and used 6-10 days p.i. For imaging, splenocytes were pooled from three mice per experiment.

2.5 Cell lines

Suspension HEK293A cells were maintained in full Pro-293 at $5x10^5$ cells/ml and agitated at 120 rpm. Adherent HEK293, PLAT-E cells and NIH 3T3 cells were grown in full DMEM and maintained until passage 35. The Burkitt (Ramos, Raji,) GCB (SUDHL-6, OCI-LY7), or ABC (OCI-LY10, U2932) human B cell lymphoma lines were cultured in suspension in full RPMI and maintained at $1x10^6$ cells/ ml. All cells were cultured in incubators humidified with 5% CO_2 at 37°C.

2.6 Primary B cell isolation and enrichment

Primary splenocytes were obtained from the spleen by passing through a 70 µm cell strainer and lysing red blood cells using ACK buffer (Gibco). Naive B cells were isolated by negative selection using anti-CD43 microbeads (Miltenyi Biotech). GC B

cells were enriched from splenocytes of immunized mice by negative selection using biotinylated anti-CD43, anti-IgD and anti-CD11c antibodies and anti-biotin microbeads (Miltenyi Biotech). For the enrichment of transferred B1-8 B cells, the negative selection was supplemented with biotinylated anti-CD45.1, which is expressed by the host cells. After enrichment, cells were recovered in Full RPMI.

2.7 Follicular dendritic cell isolation and culture

Method adapted from (Shikh et al. 2006; Sukumar et al. 2006; Heesters et al. 2013). Lymph nodes (Superficial and deep cervicals, brachial, axillary, mesenteric, inguinal) were removed from 4 Bl6 mice and digested in 0.26 U Liberase DH and 0.2 mg/ml DNase1 in DMEM supplemented with 20 mM HEPES buffer. Lymph nodes were digested at 37°C with shaking at 75 rpm for 45 mins. Cells were removed into 50 ml ice cold DMEM, 10% FCS and digestion repeated. FDCs were isolated by positive selection using an AutoMacs cell separator (Miltenyi Biotech) after sequential incubations with: FDCM1 antibody (Section 7.1), anti-rat kappa-biotin (clone, MRK1) and finally anti-biotin microbeads (Miltenyi Biotech). Cells were washed, counted and seeded onto 35mm/10mm FluoroDishes (World Precision Instruments, Inc, FD35-10-100) coated with 20 µg/ml collagen (rat tail, Roche) diluted in acetic acid. Cells were seeded at a density of $0.5x10^{6}$ per imaging FluoroDish in 100 µl warm Full FDC media (full details in Table 2). After 1hr dishes were topped up with a further 500 µl media and cultured for 5 days at 37°C, 5% CO_2 to recover full dendritic morphology. FDC cultures were used at day 5-7 post-isolation.

2.8 Antigens and stains

2.8.1 Anti-Igκ antigen

An anti-Igκ antibody fragment was used to non-specifically capture B cells on substrates for imaging. A goat $F(ab')_2$ anti-mouse Igκ (Southern Biotech) was biotinylated with a 20-fold molar excess of NHS-LC-LC-biotin (Pierce) and labelled with Cy3 or Cy5 using Monoreactive dye packs (GE Healthcare). Excess dye was removed using Zeba 7K MWCO desalting columns (Pierce, ThermoFisher).

2.8.2 NP/ NIP antigens

To capture B cells specific for the haptens 4-Hydroxy-3-nitrophenyl acetyl (NP) or 4-Hydroxy-3-iodo-5-nitrophenylacetic acid (NIP) multivalent antigen was produced. NP_{15} and NIP_{15} antigens were prepared by biotinylating and Cy5 labelling a goat IgG $F(ab')_2$ fragment (Jackson Immunoresarch) as above, followed by haptenation with 4-Hydroxy-3-nitrophenylacetic acid active ester (NP-OSu) or 4-Hydroxy-3-iodo-5-nitrophenylacetic active ester (NIP-OSu; Biosearch Technologies). Haptenation was carried out by incubating a 5-fold molar excess of hapten with labelled antibody in carbonate buffer, pH 9.3, with shaking for 1 hr before removal of free haptens using Zeba 7.000 Da molecular weight cutoff (MWCO) desalting columns (Pierce, ThermoFisher).

2.8.3 Lipid dyes

Lipids were stained with the long-chain dialkylcarbocyanine lipophilic dyes DiI or DiD. 1 mg/ ml stock solutions of dye dissolved in dimethylformamide (DMF) were stored at -20°C. PLBs or PMSs were incubated with dyes diluted 1:1000 in HBSS/ BSA for 10 min before washing with HBSS/ BSA.

2.9 Substrates for imaging synapses

2.9.1 Planar Lipid Bilayers (PLBs)

PLBs were prepared by fusing small unilamellar lipid vesicles to clean coverslips as previously described (Tolar et al. 2009). Briefly, 1,2-dioleoyl-*sn*-glycerol-3-phosphocholine (DOPC) and 1,2-dioleoyl-*sn*-glycero-3-phosphoethanolamine-N-(cap biotinyl) (DOPE-cap-biotin, both from Avanti Polar Lipids) were combined in a 100:1 molar ratio in chloroform, dried to a film with a gentle stream of argon and then further under vacuum for 1 hr. The lipid film was resuspended in PBS to 5 mM and bath sonicated for 2 hr to produce small unilamellar vesicles, which were clarified by ultracentrifugation and filtering. Glass coverslips (Menzel-Gläser) were cleaned with fresh Piranha solution (98% H_2SO_4 and 30% H_2O_2 in a 2:1 ratio), rinsed thoroughly with Milli-Q H_2O, dried with argon and glued to the bottom of Lab-

Tek 8-well imaging chambers (Nalgene Nunc). Lipids were added at 0.1 mM in PBS to form PLBs, and excess vesicles were washed away with PBS. PLBs were incubated with 1 mg/ ml streptavidin for 20 min, washed with PBS, incubated with biotinylated fluorescent antigens for 20 min and then washed again. Antigens were loaded onto PLBs at a concentration of 0.5 µg/ml unless otherwise explicitly stated.

2.9.2 Plasma Membrane Sheets (PMS)

PMSs were prepared as described (Natkanski et al. 2013). Briefly, suspension HEK293A cells were seeded onto poly-L-lysine-coated Lab-Tek 8-well glass-bottomed imaging chambers and cultured overnight in full DMEM to 100% confluency. Cells were washed in PBS and sonicated with a probe sonicator at 25°C. The exposed glass surfaces were blocked with 1% BSA in PBS and 5% v/v normal goat serum in PBS for 1 hr, and then incubated in HBSS/ BSA with 24 nM biotinylated annexin V biotin (BioVision) for 20 min. After washing, PMS were incubated with 1 µg/ ml streptavidin for 20 min, washed, incubated with biotinylated fluorescent antigens for 20 min and washed once more before imaging. Igκ antigens were loaded onto PMSs at 1 µg/ml. NP/NIP antigens or force sensors were loaded onto sheets at 1 µg/ml initially, and then adjusted so that fluorescence was matched between wells. Imaging was performed in HBSS/ BSA unless otherwise stated.

2.9.3 Glass

Lab-Tek 8-well, glass-bottomed, imaging chambers were coated with poly-L-lysine for 1 hr. Glass was washed with PBS and then coated for 2-3 hr with antigens. These were 1 µg/ml CD40L, 2.5 µg/ml anti-Igκ antigen (Jackson, labeled in-house; see section 2.8.1) or poly-L-lysine alone. Wells were washed with continual washing and finally buffer exchanged into HBSS/ BSA for imaging.

2.9.4 Follicular dendritic cells

FDCs were prepared as described in Section 2.9.4. FDCs were loaded with complement-coated immune complexes. Complement was prepared fresh per experiment from serum prepared from blood collected from a Bl6 mouse. Immune complexes were prepared by mixing 5µg rabbit anti-goat IgG $F(ab')_2$ specific

antibody (Jackson ImmunoResearch), 5µg anti-Igκ-biotin-Cy5 (called Igκ-antigen see section 2.8.1) and 10µl fresh complement and incubating together in 40µl GVB++ complement buffer (ComplementTech) at 37°C, with shaking at 300 rpm for 30 minutes. FDCs were blocked with warm PBS, 2% BSA for 30 mins before being washed by hand and incubated with immune complexes for 30 mins at 37°C. After washing in HBSS/BSA primary B cells (prepared as described in Section 2.6) were added and allowed to interact with antigen on FDCs for 30 mins at 37°C before fixing with 2% PFA, cell surface staining and imaging.

2.10 Large-scale imaging

Isolated B cells were washed and resuspended in 50 µL of warm HBSS/ BSA per well. Cell number varied depending on substrate and cell type but typically 0.5-1x10^6 were prepared for each well, with GC cells added in a 2:1 ratio with naive control B cells. For inhibitor studies cells were pre-incubated with their inhibitor prior to addition to imaging chambers containing the same buffers and inhibitors. See Table 8 and Table 9 for specific information about inhibitors, concentrations, incubation times and imaging buffers. Cells were added to pre-warmed imaging chambers with antigen-loaded substrates and incubated for 20 mins at 37°C to allow B cells to form synapses. Cells were fixed in 2% paraformaldehyde (PFA, Alfa Aesar), blocked for 1 hr using 5% v/v normal mouse serum (Jackson ImmunoResearch) and stained for surface markers using fluorophore-conjugated primary antibodies at a concentration of 1 µg/ml for 30 minutes at 25°C. Stained cells were washed by hand in HBSS/ BSA and fixed again in 2% PFA. For intracellular staining cells were fixed and then permeabilized using the FoxP3 fixation/permeabilization kit (eBioscience) on ice, washed with supplied permeablization buffer, blocked with 5% v/v normal mouse serum and then incubated with the corresponding antibody for intracellular staining. If antibodies for intracellular staining were unlabelled, an extra incubation was added with a secondary labelled antibody. F-actin was stained using fluorescently labeled phalloidin. Cells were finally fixed in 2% PFA before imaging.

2.11 Antigen internalisation assays

2.11.1 Secondary staining on PMSs

Secondary antigen staining was used to assess whether extracted antigen was inside or outside of the cell. Cells were prepared and loaded onto prepared PMSs as described (Section 2.9.2, 2.12) before fixing in 2% PFA for 30 min and blocking for 1 hr with 5% v/v normal mouse serum. A fluorescently labelled anti-goat IgG antibody was used as a secondary stain to target antigen and was added directly to blocked wells at 1 µg/ml with other antibodies during surface staining. Wells were washed and fixed in 2% PFA before imaging.

2.11.2 Soluble antigen internalisation

Splenocytes were isolated from naive or GC mice by agitation through a 70 µm cell strainer before ACK red cell lysis. On ice, cells were incubated with kappa antigen at 1 µg/ml in RB for 30 min. After washing (where used) cells were inhibited with inhibitors or DMSO according to Table 9. $5x10^6$ cells were moved from ice to 37°C and incubated for 10 or 30 min before fixation with 2% PFA on ice. A sample was left on ice and then fixed after 30 min. Cells were washed and stained with a cocktail of antibodies against surface markers which included a fluorescently labelled streptavidin molecule to label antigen remaining on the cell surface. After washing, samples were run on a LSR Fortessa (BD Biosciences) flow cytometer. Analysis was carried out using FlowJo (TreeStar) and Prism (Graphpad) to determine the extent of antigen internalisation.

2.12 Multi dimensional acquisition (MDA)

All imaging was performed using a motorized Olympus IX81 microscope with a 100X oil objective (Olympus), controlled through Metamorph softwate (Molecular Devices). For illumination, the following laser sources were used: 405 nm (Changchun New Industries), 488 nm, 514 nm (both lines from LS300, Dynamic Lasers), and 640 nm (Blue Sky Research). Laser beams were passed through excitation filters and combined into a multispectral single mode optical fibre (Oz Optics) connected to the illumination port of the microscope. Emitted fluorescence

was filtered by appropriate emission filters using a filter wheel (Sutter). Automated image acquisition was performed using a motorised stage with an integrated piezo Z-drive (Applied Scientific Instruments). Metamorph journals were used to systematically acquire images from multiple fields of view in each imaging well and move between wells. Hanging drops of oil on the bottom of the imaging chamber was used to supplement immersion oil during stage movement between chambers. Focus was maintained using either the ZDC autofocus unit (Olympus) or, in experiments using Cy7 emission, software autofocus using the antigen fluorescence from the substrates.

2.13 Large-scale image processing and analysis (Pavel Tolar)

Images were processed and analyzed by a user-guided pipeline implemented in Matlab (Mathworks) tethered to ImageJ by the MIJ plugin (http://bigwww.epfl.ch/sage/soft/mij/). Three interactive modules were programmed for (1) determination of background, flatfield and calculation of spectral bleedthroughs, (2) processing 3D multichannel images for identification of cells and their analysis, and (3) display and gating of the data, including generation of image galleries for visual inspection of the results. Code available on request (Pavel Tolar).

Background and flatfield images for each channel were obtained from spatially smoothened images of empty imaging wells, or wells with the labelled antibodies adsorbed to coverslips (respectively). 2D background and flatfield images were used for each channel. Channel alignment was pre-determined by imaging multicolor beads. Single color controls for spectral unmixing were obtained using images of fluorophore-labelled antibodies adsorbed to coverslips. Flatfield images were normalized to the mean of their pixel values. All image sets were aligned and cropped to remove poorly illuminated areas at the edges. 2D spectral bleedthrough images were obtained after background subtraction and flatfield correction of the single color images for each channel pair, generating per-pixel bleedthrough correction factors. Per-pixel spectral unmixing of experimental samples improved the accuracy of spectral unmixing for 3D multicolor images because of the significant photobleaching of the fluorophores that occurred during sequential

acquisition of the channels. All experimental image sets were cropped, aligned, background subtracted and corrected for flatfield and spectral bleedthroughs. Corrected images were saved for visual inspection of identified cells and further analysis.

Cells were detected in the B220 channel using an initial geometric detection in 2D followed by refinement of the cells' edges in 3D. Initially, object edges were detected in mean-projected images using bandpass filtering and Sobel edge detection with user defined parameters. Cell-like objects were identified using circle detection by Hugh transforms with a user-specified radius range. Circles overlapping by more than their radius were merged as one object. After this initial object detection, the images were normalized by smoothened masks of the identified objects to equalize the staining intensity of the membranes of the cells in the image. Scattering of the fluorescence was reduced by dividing fluorescence images by their corresponding brightfield images, which contain bright areas around cells. Cell edges were then refined in a 2D maximum projection image by an outward propagation algorithm, in which the cell's edge was identified in 32 radial segments as a distance from the cell's center, where the intensity of the radial segment drops by a user-defined factor compared to the mean intensity of the centripetal pixels of the segment. This algorithm was used iteratively and greatly improved performance over global thresholding for cells with uneven staining along the plasma membrane. The outer edges were limited by regions defined by Voronoi-based segmentation of the image seeded by the centers of the original circles. After identifying the edges of the cells in the maximum projections, the propagation algorithm was repeated in 3D with the 2D objects serving as an outward limit for the propagation. Cells touching the edges of the image were excluded from further analysis. The resulting 3D masks containing cell identification numbers were stored as image stacks. All subsequent analysis of cells was based on these masks.

To exclude incorrectly segmented cells as well as noncellular debris, we developed CellScore - an empirical score of the likelihood that the detected object represents an intact cell. To calculate CellScore for each object, we calculated the mean pixel

intensities in five concentric rings normalized by the mean object intensity using channels containing a membrane marker (typically B220) and brightfield. The resulting normalized profiles were correlated with mean profiles obtained from a small number of manually segmented cells. The final CellScore was an average of the correlation coefficients of the profiles in the B220 and the brightfield channels. All image data sets were then gated on intact cells using a dotplot of B220 versus CellScore.

Fluorescence intensity of the cells was calculated as the mean intensity of the pixels identified by the cell masks in each of the channels. The image plane of the antigen- containing substrate (synapse plane) was identified in each image by searching for the plane with the highest mean squared gradient of neighboring pixel values. This focal plane was used to analyze fluorescence intensities and spatial patterns of immune synapses. Synapse size was calculated as the area of the cell mask at the synapse plane. Mean fluorescence in the synapse was the mean intensity of the pixels in the synapse area. Antigen centralization was calculated as the inverse of the intensity-weighted mean of the distances of the pixels from the center of the mass of the synapse, normalized by the mean pixel distance. Synaptic cSMACs were identified from low pass-filtered antigen images as the area of contiguous above-background antigen fluorescence in the center of the synapse. Clusters in the pSMAC were detected in the antigen channel after bandpass filtering as the local maxima outside of the cSMAC.

Antigen extraction by each cell was analyzed from the *z*-stack images by an improved version of a previously described algorithm (Natkanski et al. 2013). Briefly, each image plane was bandpass- filtered and antigen clusters were identified in planes above the synapse by using a user- specified global threshold. To correct for antigen fluorescence scattered from the substrate, local background was subtracted from each identified cluster using a 3-pixel-wide rim around the cluster in each plane. Other clusters were excluded from the background. Total fluorescence of extracted antigen was calculated as the sum of pixel intensities of the background-corrected extracted clusters. The masks of the extracted antigen clusters were used to calculate the number and mean intensities of the extracted

antigen clusters in each cell. Masks containing the extracted antigen clusters were used to quantify fluorescence in other channels. For display in dot plots, cells with zero extracted antigen were assigned a random value derived from the background of the antigen channel. All data from image and object analysis, including locations of the objects in the images, were stored in an SQLite database. Data were inspected using a custom written set of visualization tools in Matlab for interactive data display in dot plots and histograms, manual gating, generation of image and cell galleries, and export of data for further statistical analysis.

Sideview reconstruction of cells was performed using deconvolution as described (Natkanski et al. 2013).

2.14 Calcium Imaging

2.14.1 Measuring calcium flux by microscopy

$5x10^6$ pre-enriched GC or naive cells were loaded with calcium indicator dyes Fura-Red and Fluo-4 (Invitrogen). Dyes were added to cells in 1 ml RPMI 5% FCS at a concentration of 5 µM and incubated at 37°C for 30 mins with shaking. Cells were washed and transferred to HBSS/ BSA for imaging on fluorescently labelled antigen-loaded PLBs. Cells were imaged for 20-30 min by time lapse 3D acquisition with z-stacks acquired every 20 s in both Fluo-4 and Fura Red channels. TIRF images of the antigen channel were acquired at the end of each time lapse. Fluo-4/Fura-Red rations were calculated from the cell body of naive cells and for cells in the GC sample that showed the characteristic synapse shape. Images of synapses were acquired in TIRF after time-lapse acquisition.

2.14.2 Measuring calcium flux by flow cytometry

$5x10^6$ cells were loaded with Fluo-4 and Fura-Red (section 2.14.1). $5x10^6$ cells were loaded alongside with each dye individually. After washing, cells were recovered at 37°C either in HBSS/ BSA or incubated with desired inhibitor according to details in Table 9. Cells were run on a LSR Fortessa X20 flow cytometer (BD Biosciences) for 1 min to set a baseline before the addition of 10 µl

anti-mouse Igκ F(ab')2 (Southern Biotech, 0.5 mg/ml). The sample was run for a further 10-15 min until observed flux returned to baseline. When testing whether reagents caused calcium flux, anti-mouse Igκ F(ab')2 was always used as the positive control. Inhibitor studies were always run alongside a DMSO control. Imaging data was analysed using ImageJ and traces produced using Prism (GraphPad).

2.15 PMA and ionomycin stimulation.

Naive and pre-enriched GC B cells were mixed and incubated with 50 ng/ml PMA and 500 ng/ml ionomycin for 10 min at 37°C, and then allowed to settle onto poly-L-lysine coated 8-well LabTek imaging chambers for 10 min. Cells were fixed in 2% PFA, stained for surface markers, permeabilized, blocked and stained for PKCs. Plasma membrane translocation for each cell was calculated as the ratio of the mean fluorescence intensity of a 3-pixel-thick perimeter region to the mean fluorescence intensity of the whole cell.

2.16 NF-κB nuclear translocation assay.

Imaging chambers were coated with 2.5 mg/ml Igk antigen or 1 mg/ml CD40L (R&D Systems). Naive and pre-enriched GC B cells were mixed in HBSS/ BSA at 37°C, added to the imaging chambers and incubated for 1 hr before fixing in 2% PFA. Cells settled on poly-L-lysine coated chambers for 15 min served as non-activated controls. Wells were blocked with 5% v/v normal mouse serum (Jackson ImmunoResearch) before surface staining, permeabilization and intracellular staining with anti-NF-kB1 p105/p50 primary antibody. Cells were then incubated with a fluorescent secondary antibody and with DAPI to stain nuclei. Cells were finally fixed in 2% PFA and imaged. Cells were segmented using the DAPI stain into the nuclear volume and the cytosol using a thresholded DAPI image. The segmentation threshold was determined in each cell as a value three times higher then the background DAPI intensity in the perimeter of the cell. Nuclear translocation of p50 for each cell was calculated as the ratio of the mean fluorescence intensity of p50 staining in the nucleus to the mean intensity in the cytoplasm.

2.17 Measurement of soluble monovalent NP/NIP binding (Sensor design and synthesis, Katelyn Spillane)

To quantify monovalent binding of NP or NIP to B1-8 naive and GC B cells, NP or NIP was coupled to the dye Atto647N in a 1:1 ratio through a double-stranded DNA oligonucleotide, which was formed through annealing single stranded oligomers with the following sequences:
Fluorescent strand: 5′ -Atto647N- TCCGGCTGCCTCGCTGCCGTCGCCA; complementary strand: 5′ – C6 NH2 - TGGCGACGGCAGCGAGGCAGCCGGA. To label the DNA with a single hapten, the oligonucleotide was exchanged into sodium carbonate buffer using a Zeba desalting column and incubated with a 20-fold molar excess of NP-OSu or NIP-OSu for 30 min at 25°C to haptenate the primary amine. Unreacted hapten was removed and the oligonucleotide exchanged into PBS using a desalting column. The 1:1 conjugation ratio was verified by UV/Vis spectroscopy. To measure binding to naive and GC B cells, cells were stained with antibodies for surface markers and incubated with the indicated concentrations of the monovalent antigens for 20 min on ice. Samples were diluted ten times with PBS immediately before running on a LSR Fortessa (BD Biosciences) flow cytometer. Background was subtracted using staining of naive B cells from Bl6 mice, or host-derived GC B cells, respectively.

2.18 Force sensors and force imaging (Katelyn Spillane)

The force sensors consist of three DNA oligonucleotides annealed through hybridization to form upper and lower handles connected by a central hairpin. At the base of the hairpin, a red fluorophore-quencher pair (Atto647N and Iowa Black RQ dark quencher) provides a digital readout of hairpin unwinding; and a second fluorophore, Atto550, on the upper handle reports on the position of the sensor and allows clustering-independent ratiometric analysis. The upper handle of the sensor is covalently attached to the protein antigen, and the lower handle of the sensor is tethered to a membrane substrate through a double biotin-streptavidin linker. The F1/2 values of the hairpins, the forces at which 50% of the hairpins unfold, were

calculated based on the total free energy of the hairpins as described (Woodside et al, 2006) and were approximately 7, 9, and 14 pN. For control measurements, the hairpin sequence was replaced with a single nucleotide, which prevents separation of the Atto647N from the quencher. Opening of this control sensor would require shearing of the DNA by a force of approximately 57 pN. Control experiments using sensors lacking the quencher showed that quenching of the closed state was better than 95%. The DNA sequences were:
7 pN hairpin strand sequence: 5′ – C6 NH2 - TCACGACAGGTTCCTTCGCATCGATATTATATATTAATATATAATTTTTTTTTTTTTTATATATTAATATATAATAATTTACTCACAAGCAGTGTGTACA – biotin; 9 pN hairpin strand sequence 5′ – C6 NH2 - TCACGACAGGTTCCTTCGCATCGATATTATATATTAATATATAATTTTTTATATATTAATATATAATAATTTACTCACAAGCAGTGTGTACA – biotin; 14 pN hairpin strand sequence: 5′ – C6 NH2 - TCACGACAGGTTCCTTCGCATCGAGAGTCAACGTCTGGATCCTGTTTTCAGGATCCAGACGTTGACTCATTTACTCACAAGCAGTGTGTACA – biotin; control strand sequence 5′ – C6 NH2 - TCACGACAGGTTCCTTCGCATCGATATTTACTCACAAGCAGTGTGTACA – biotin; upper handle complementary strand sequence 5′ – Atto647N - TCGATGCGAAGGAACCTGTCGTGA – S-S; lower handle complementary strand sequence 5′ – biotin - TGTACACACTGCTTGTGAGTAAAT – Iowa Black RQ.
To conjugate sensors to antigen, goat F(ab')2 anti-mouse Igk (Southern Biotech) was purified by anion exchange chromatography (Mono Q, GE Healthcare) using a buffer gradient composed of 25 mM Tris, pH 8.0, and 100-1000 mM NaCl. The protein was exchanged into degassed 1 mM EDTA in PBS, pH 7.3 (PBS-EDTA) using a 7 kDa MWCO desalting column (Zeba, Pierce) and then incubated with a 20-fold molar excess of sulfo-SMCC (Cambridge Biosciences) for 30 min at 25°C. Unreacted sulfo-SMCC was removed with two passes through desalting columns. Equal volumes of 100 mM HPLC purified, single-stranded oligonucleotides (IDT) in 30 mM HEPES, pH 7.5, 100 mM potassium acetate were mixed and annealed in the presence of 2 mM $MgCl_2$. The annealed sensor was exchanged into 0.1 M sodium carbonate-sodium bicarbonate buffer, pH 9.1, using a desalting column and then incubated with a 3-fold molar excess of Atto550 NHS ester for 30 min at 25°C

to label the upper-handle primary amine. Excess dye was removed and the sample exchanged into PBS-EDTA using a desalting column. The upper handle dithiol was reduced with 50 mM DTT for 30 min at 25°C and the sensor was passed twice over desalting columns to remove DTT and exchanged into PBS-EDTA. The sensor was mixed with the SMCC-activated antigen in a 1:5 ratio and incubated at 25°C for 2 h. Conjugation was verified by a shift in size on a 2% agarose gel. DNA-protein conjugates were purified by anion exchange chromatography using the same buffer gradient as above.

To measure opening of the force sensors in B cell synapses, imaging chambers were assembled by placing a 10 ml CultureWell gasket (Grace Bio-Labs) onto a piranha-etched glass coverslip attached to a 1-well Lab-Tek chamber. Biotin-containing PLBs were formed in the wells as described above and then loaded with 1 mg/ml streptavidin, washed and loaded with 6 nM force sensor. Naive or enriched GC B cells were added to the wells in 0.1% protease-free BSA in HBSS. Images of the Atto550 and Atto647N fluorescence were acquired using 514 and 640 nm illumination with five second time resolution at 37°C. The images were aligned, background subtracted and flatfield corrected in ImageJ. Fluorescence in BCR clusters in time-lapse experiments was tracked using previously described algorithms (Tolar et al. 2009). For quantification of sensor opening, synapses were analyzed after 20 min of incubation of the cells with the PLBs. Areas around the cell were cropped and the antigen clusters were identified in the Atto550 channel using the threshold function in ImageJ. The ratio of Atto647N to Atto550 fluorescence in each cluster was determined, and the average ratio for each cell was recorded.

2.19 Measuring antigen degradation using a degradation sensor (Katelyn Spillane)

Degradation was measured used a DNA based degradation sensor. The degradation sensor consists of a double stranded DNA oligonucleotide formed through annealing the fluorescent and quencher single stranded oligomers with the following sequences:

Fluorescent strand sequence: 5′ – Atto647N – TCCGGCTGCCTCGCTGCCGTCGCCA – biotin; quencher strand sequence: 5′ – TGGCGACGGCAGCGAGGCAGCCGGA – Iowa Black RQ.

2.19.1 Membrane-bound antigen degradation from PMSs

PMSs were prepared and loaded with Cy3 labelled anti-Igκ antigen, incubated with streptavidin at 1 μg/ml for 20 min then loaded with degradation sensors for 30 min. After loading PMSs with sensors, imaging was carried out as previously described. Extracted antigen was considered degraded in pixels where the Atto647N/Cy3 fluorescence was two times higher then the ratio on PMSs outside of cells.

As an additional control, 2′-OMe phosphorothioate-modified oligomers that are resistant to nuclease degradation were used: control fluorescent strand sequence: 5′ – Atto647N – mU*mC* mC*mG*mG* mC*mU*mG* mC*mC*mU* mC*mG*mC* mU*mG*mC* mC*mG*mU* mC*mG*mC* mC*mA – biotin; control quencher strand sequence: 5′ – mU*mC* mC*mG*mG* mC*mU*mG* mC*mC*mU* mC*mG*mC* mU*mG*mC* mC*mG*mU* mC*mG*mC* mC*mA – Iowa Black RQ.

2.19.2 Soluble antigen degradation

Splenocytes were isolated from naive or GC mice by agitation through a 70 μm cell strainer before ACK red cell lysis. On ice, cells were incubated with kappa antigen at 1 μg/ml for 30 min, streptavidin at 1 μg/ml for 30 min then sensor at 100 nM for 30 min. All incubations were in RB with washes between each step. After cell labelling samples were moved from ice to 37°C for 5, 15, 30 or 45 min then fixed with 2% PFA on ice. Cells were stained for surface markers by incubating with fluorescently labelled primary antibodies at 1 μg/ml for 20 min on ice. After washing, samples were run on a LSR Fortessa (BD Biosciences) flow cytometer. Analysis was carried out using FlowJo (TreeStar) and Prism (Graphpad) to determine the extent of antigen degradation.

2.20 Live-cell imaging

Imaging substrates and cells were prepared as described previously. Primary naive or GC B cells were recovered in full RPMI for at least 20 minutes before $1x10^6$ cells were removed and washed in HBSS/ BSA. Cells were resuspended in 100 µl warm HBSS/ BSA and stored briefly under a heated stage set to 37°C. Substrates were pre warmed on a heated stage and objective set to 37°C. Live-cell imaging was carried out using Total Internal Reflection microscopy (TIRF), with the TIRF angle set as shallow as possible to extend the depth of field further away from the coverslip. 50 µl cells were applied gently to the centre of the well and imaged immediately, with a time resolution of 5 s for 20-30 min in the antigen fluorescent channel and brightfield channel. A prepared aliquot of cells was used for two separate time-lapse acquisitions. Acquired images were aligned, background-subtracted and corrected for spectral bleedthough and photobleaching.

2.21 Analysing cell populations using flow cytometry

Flow cytometry was used to assess the expression of surface markers or activity of intracellular signalling molecules from splenic B cells. Freshly isolated splenoctyes were incubated with primary fluorescently labelled antibodies in Running Buffer for 20 min on ice. Typically, cells were stained with antibodies at 1 µg/ml per $1x10^6$ cells. After washing, cells were run on an LSR Fortessa or Verse flow cytometer (BD Biosciences). For intracellular staining, after surface staining, cells were fixed and permeablised using a FoxP3 fixation/ permeabilization kit (eBioscience) following the manufacturers protocol. Cells were blocked with 5% v/v normal mouse serum (Jackson ImmunoResearch) before the addition of antibodies for intracellular staining. Where these antibodies were unconjugated, a secondary fluorescently-labelled antibody was added after primary incubation and washing. This antibody was washed off and cells were fixed with 2% PFA for 20 min on ice before running on an LSR Fortessa or Verse flow cytometer. Data was analysed using FlowJo software (TreeStar). For antibody details see Table 9.

2.22 PKC retrovirus production

Retrovirus was produced by TransIT-LT1 (Mirus Bio) -mediated transfection of PLAT-E cells (Morita et al. 2000) with the pMSCV PZ MCS vector containing PKC-β or PKC-δ constructs joined by a short linker to a modified, non-dimerising form of GFP (Huse lab, (Quann et al. 2011)).

2.23 PKC retroviral infection

2.23.1 NIH 3T3 infection

NIH 3T3 cells were maintained as described in Section 2.5. Cells were seeded at a density of 50,000 cells/well into a 12-well tissue culture dish in 500 µl full DMEM overnight. Retrovirus-containing supernatants were added to cells and incubated at 37°C for two days before analysis by flow cytometry.

2.23.2 Fetal liver cell infection

Frozen Bl6 fetal liver cells (> 6 months old) were thawed and were cultured for 24 hrs in full StemPRO media (see Table 2) supplemented with 100 ng/ml recombinant murine SCF, 100 ng/ml recombinant murine Thrombopoeitin, 10 ng/ml recombinant human IL-6, 6 ng/ml recombinant mouse IL-3, 20 ng/ml recombinant mouse Flt3-ligand (all Peprotech). Cell were seeded at $0.5x10^5$ cells/well in a 12-well tissue culture plate in 250 µl full StemPRO and spinfected with 1ml unconcentrated retrovirus-containing supernatant in the presence of 16 g/ml polybrene for 90 mins at 2500 rpm, 4°C. After spinfection cells were cultured overnight at 37°C, 5% CO_2 with 1ml full StemPro before transfer. Cells were assessed by flow cytometry for efficiency of infection

2.24 PKC-GFP fetal liver cell transfers

Fetal liver cells infected with PKC-GFP expressing retroviruses were transferred into CD45.1 Bl6 recipient mice. $0.5x10^6$ infected cells in 0.1 ml IMDM were transferred via the i.v. route. Recipients were sub lethally irradiated (500 rads) prior to cell transfer. Mice were maintained on antibiotics (Baytril, 0.2%) for 4 weeks

post-irradiation in drinking water. Mice were reconstituted for 8 weeks prior to tail bleeds and 12 weeks prior to immunisation with SRBCs (as described, section 2.3.2). Cell transfers were analysed by flow cytometry.

2.25 Lentiviral PKC vector preparation

PKC inserts were extracted from retroviral vectors via PCR using the following primers: PKC-β-forward TAA CAC TAG TAC GAT GGC TGA CCC GGC TG, PKC-δ-forward TAA CAC TAG TAC GAT GGC ACC CTT CCT GCG, universal reverse-GFP CGGAATTCTCACTCAGTCAGGATCCTC. Forward primers included insertion of the restriction site SpeI for downstream instertion into the p.Lenti.puro lentiviral vector. PCR cycling conditions as follows:

Step	Temperature (°C)	Time
1	98	30 s
2	98	5 s
3	58-71	30 s
4	72	2 min
Repeat steps 2-4 x 29 cycles		
5	72	10 min

Following PCR amplification, both inserts and the p.Lenti.puro vector were cut with the restriction enzymes SpeI and BamHI before ligation, transformation and DNA preparation. Successful insertion was confirmed with sequencing.

Chapter 3. Large-scale imaging identifies variation in synapses of splenic B cell subsets

3.1 Introduction

In vivo, unprocessed antigen is largely retained on the surfaces of specialised antigen-presenting cells (APCs) (Carrasco & Batista 2006a; Junt et al. 2007; Qi et al. 2006; Phan et al. 2007; Bergtold et al. 2005; Gonzalez et al. 2010). Membrane-tethered antigen has been shown both *in vivo* and *in vitro* to be accessible to B cells (Batista et al. 2001; Schwickert et al. 2007). *In vitro,* BCR interaction with membrane-presented antigen results in the formation of an immune synapse (synapse).

Synapse formation in lymphocytes is a well-characterised process. The initial phenomena of cSMAC and pSMAC formation were observed first in T cells (Grakoui et al. 1999), and later in B cells (Fleire et al. 2006; Tolar et al. 2009). These data were predominantly elucidated using high-resolution fluorescent imaging on synthetic membrane systems such as planar lipid bilayers (PLBs), which act as surrogate APC membranes. The synthetic nature of these substrates made it possible to engineer model fluorescent antigens that can be anchored to the phospholipid bilayer and retain unhindered two-dimensional mobility. Key events in mature synapse formation are now very well described, including signalling-mediated B cell spreading (Weber et al. 2008), microcluster formation (Reth & Wienands 1997; Tolar et al. 2009) and B cell contraction (Fleire et al. 2006). Although PLBs unveil lateral reorganisation of molecules in B cell membranes, they have a major disadvantage in that they do not support internalisation of antigen clusters seen when B cells interact with live APCs (Natkanski et al. 2013).

Lymphocyte synapses vary, and are adapted to a range of specialised effector functions. For example, cytotoxic T cells and NK cells form synapses to directionally deliver lytic granules to kill virus infected cells (Griffiths et al. 2010), whereas helper T cells form synapses to recognise and respond to infinitesimal

amounts of presented peptide (Davis et al. 2007) with high sensitivity. Synapse formation may even be hijacked during infections such as HIV, where helper T cells become able to extrude vesicles into the synapse to facilitate the spread of virus between cells (Choudhuri et al. 2014). In B cells, antigen is gathered and internalised from presenting APC membranes for intracellular processing and presentation to helper T cells (Batista et al. 2001), and hence B cells are said to form 'endocytic synapses'. Transfer of membrane-attached material between cells is known as 'transendocytosis' (or 'trogocytosis') and is important in a variety cell-cell contacts (Qureshi et al. 2011; Miner et al. 2015; Steele et al. 2016). In follicular B cells, this internalisation event is known to be a prerequisite to B cell activation, differentiation and antibody production (Moseman et al. 2012; Chappell et al. 2012; Carrasco & Batista 2007; Schwickert et al. 2007; Phan et al. 2007; Junt et al. 2007; Suzuki et al. 2009; Wang et al. 2011) . Using a flexible substrate derived from mammalian cell membranes, known as Plasma Membrane Sheets (PMS) (Natkanski et al. 2013) we are able to effectively model internalisation of BCR-antigen clusters during synapse formation *in vitro*.

Knowing that immune synapses can have diverse functions, we hypothesised that different organisation of synapses can support distinct functions of certain B cell subsets. We built a large-scale imaging platform to capture key synaptic processes in B cell subsets outside the most common follicular B cells. Heterogeneity in synaptic morphology is common in immortalised human B cell lines (unpublished observations) and unusual, multifocal synapses have been found to exist in immature T cells (Hailman et al. 2002), although synaptic differences through developmental B cell stages were as yet unstudied. This was in part due to the 'single-cell' or low-throughput nature of previous live-imaging approaches, and the low cell numbers of more unusual B cell populations. With an unbiased snapshot of the entire splenic B cell compartment, we aimed to uncover novel differences in synapse formation, BCR signalling or antigen internalisation when specific B cells engage antigen presented in the context of a membrane.

3.2 Results

3.2.1 Synapse formation on Planar Lipid Bilayers (PLBs)

PLBs are a good model to study synaptic architecture in high-resolution. PLBs were formed by the fusion of unilamellar vesicles to glass coverslips and attachment of fluorescent, biotinylated antigen to biotinylated phospholipids via streptavidin linkage. Goat anti-mouse Igκ F(ab')2 fragment labelled was used as a model antigen. This antibody fragment binds to the kappa light chain of the BCR (expressed on 95% of splenic B cells) to capture B cells in a non-antigen-specific manner.

After incubation on PLBs naive B cells formed classical cSMACs (Figure 6, Movie 1) defined by fusion of antigen clusters followed by movement into a central focus. Small clusters became visible as early as 30 seconds after B cells touched down onto the bilayer, with classic synapses discernable after as little as 5 min. By 20 minutes, the mature synapse was fully formed.

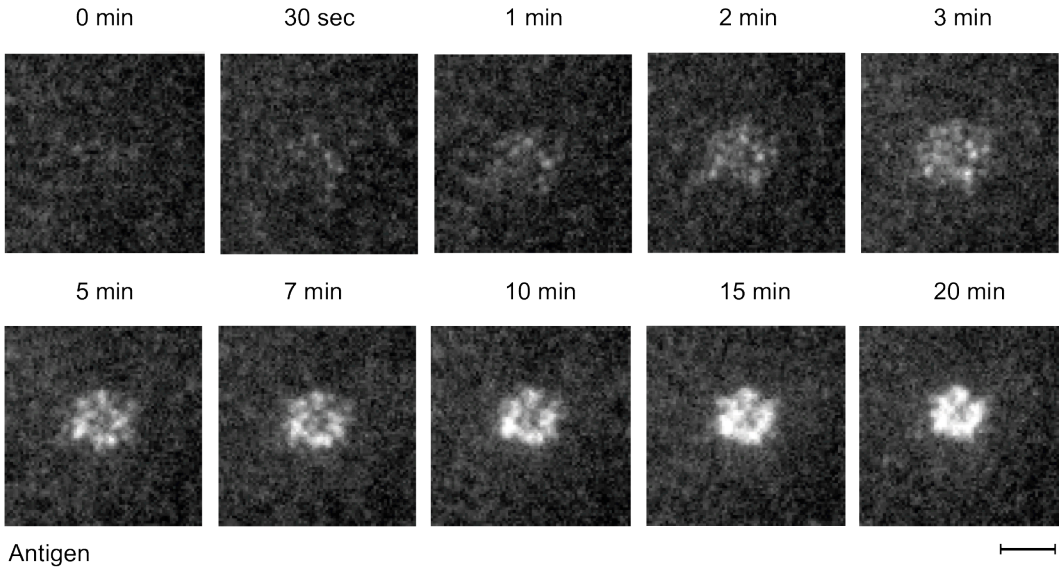

Figure 6 Synapse formation on PLB by naive B cells

Stills from time-lapse live cell TIRF microscopy. Untouched splenic B cells were applied to anti-Igκ-loaded PLBs and imaged at 37°C. Images were acquired in TIRF at a time resolution of 5 seconds. Scale bar = 5 μm.

3.2.2 Large-scale imaging setup: imaging many cells in many colours

In order to examine synapse formation simultaneously in multiple B cell populations we built a large-scale imaging platform initially using PLBs as a surrogate antigen-presenting membrane (Figure 7). B cells isolated from the spleen of naive C57Bl/6 (Bl6) mice were applied untouched to these bilayers, allowed to interact with fluorescent antigen and then fixed. Following fixation, cells were stained with fluorescent antibodies against a panel of surface markers in as many as 6 colours to phenotype cells. Multi-dimensional acquisition (MDA) was carried out using journals compiled in the microscope software MetaMorph. This involved acquiring Z-stacks of 31 0.5 μm slices per field of view, encompassing 15 μm from the bilayer through the top of the cell inclusively. This 3D Z-stacking was automatically repeated for up to 1,000 fields of view, in up to 7 different 'coloured' channels (fluorescent channels and a brightfield channel). Multicolour imaging was possible by passing 4 separate laser lines through excitation filters and coupling into a single optical fibre. A software-controlled filter wheel collected emitted light for each channel. A hardware-based autofocus was used to maintain the objective-sample distance during movement of the microscope stage between fields of view.

After image correction, cells could be seen spread over the bilayer (Figure 7b) with B cells staining positive for the cell surface marker B220. Each B220 stained cell had a corresponding fluorescent synapse visible in the antigen channel. When looking across other fluorescent channels positive and negative cells were clearly identifiable based on levels of surface markers (Figure 7c), and so by using the right combination of cell surface markers different populations could be identified; the example in Figure 7 shown by a yellow arrow identifies a $B220^{+}$ $CD21^{+}$ $CD23^{lo}$ IgM^{+} marginal zone B cell.

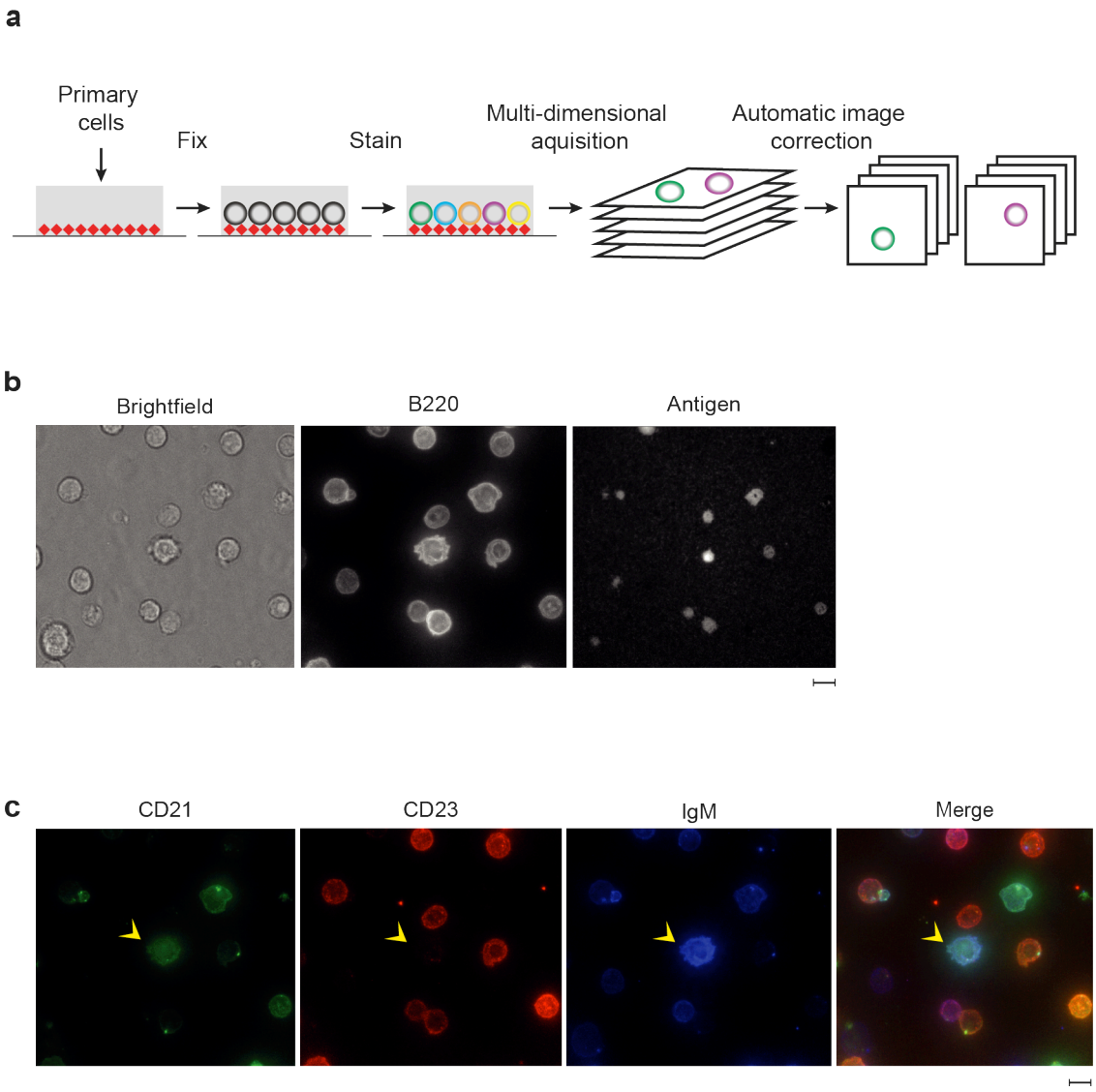

Figure 7 Large-scale multicolour imaging workflow

(a) Schematic depicting experimental setup of a typical large-scale experiment. Splenic anti-CD43 enriched B cells were imaged after 20 min on anti-Igκ-Cy5 loaded bilayers.
(b) Images of cells in the brightfield and B220 channels, with their corresponding immune synapse in the antigen channel.
(c) Cells were stained with B220-ef450, CD21-FITC, CD23-PerCP-Cy5.5, IgM-PeCy7, AA4.1-PE (not shown). Arrow shows a $B220^{+}$ $CD21^{+}$ $CD23^{lo}$ IgM^{+} marginal zone B cell.
Scale bar = 5 μm.

3.2.3 Analysis tools can extract useful information from Multi-Dimensional Acquisition (MDA) data (Pavel Tolar)

Following standard image corrections: background subtractions, flatfield corrections and spectral overlap removal using single colour controls, images were passed through a number of in-house algorithms for analysis. Automatic object detection algorithms (written by Pavel Tolar, Figure 8a) detected B220 fluorescence, identified cell boundaries and created ‘cell masks’; a term referring to the area identified from which all other data was extracted from that cell.

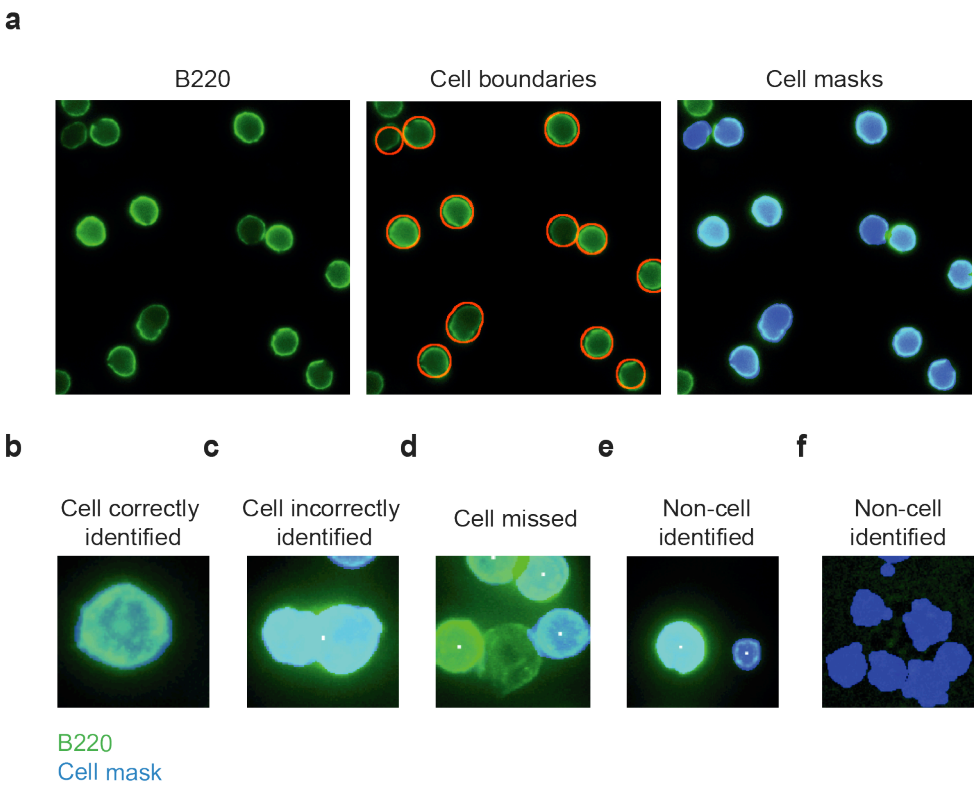

Figure 8 Automatic object identification from MDA

(a) Objects positive for B220 (green) with identified cell boundaries (red circles) and cell masks (overlay, blue).
(b-f) Different outcomes of automatic object identification, green B220 staining, blue cell masks.

Table 3 Efficiency of automatic object detection in identifying B cells

Cell correctly identified	Cell incorrectly identified	Cell missed	Non-cell identified
>81%	11%	6%	Variable

Generally, automatic object detection worked well at identifying B cells. Mis-identification of objects as cells happened in rare cases (17%, Table 3, Figure 8 c,e,f), but was minimised by altering sample preparation. For example, applying too many cells to a sample well resulted in overcrowding and henceforth mis-identification of cells sitting on top of one another (Figure 8 c, d).

The frequency of non-cells being identified as cells was highly variable, and occurred in two distinct circumstances; either when there were no (or few) cells in a sample or when autofluorescent debris was present. Optimisation of the technique almost entirely eliminated both of these kinds of mis-identifications.

Contaminating debris or mis-identification can skew downstream analysis. A measure termed CellScore was built into the analysis as a second layer of stringency to ensure only true B cells were analysed. CellScore compared the fluorescence radial profile of the B220 channel to the illumination pattern in the brightfield channel (Figure 9b), creating a ratio where a true cells' CellScore equalled 1. When plotted against B220 fluorescence, two distinct populations appeared (Figure 9c) where $B220^{+}$ $CellScore^{+}$ objects were bone fide B cells whereas the corresponding negative population was debris (Figure 9d). Therefore, CellScore served as the most robust way to pre-gate on true B cells prior to downstream analysis.

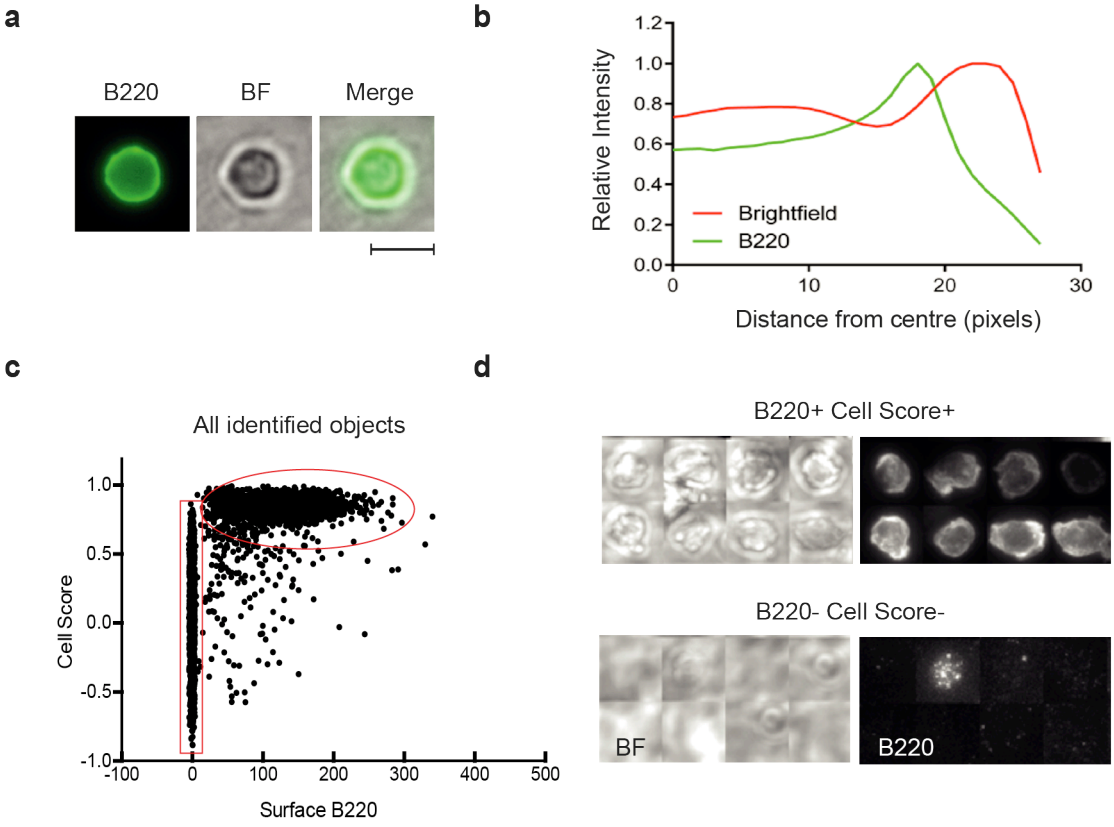

Figure 9 CellScore: A numerical score assigned to identified objects, which can classify them as true B cells

(a) B220 and brightfield images from MDA following correction.
(b) Intensity of illumination plotted from the centre of an identified cell outwards. Green line, B220, red line, brightfield. Lines representative of a single, typical cell.
(c) CellScore ratios plotted against B220 for an entire data set. Gates indicate $B220^-$ $CellScore^-$ objects (debris) and $B220^+$ $CellScore^+$ objects (cells).
(d) Image galleries show random objects recalled from either gate described.

BF = Brightfield. Scale bar = 5 μm.

3.2.4 Naive splenic B cells have varied synaptic architecture

Frequencies of naive B cell populations in the spleen are well known (Allman & Pillai 2008). To determine whether our system was unbiased in it's reporting of splenic B cell population frequencies, we first identified these populations by flow cytometry in our internal Bl6 mouse colony (Figure 10), based on the surface markers detailed in Table 4 (Chung et al. 2003).

Table 4 Surface marker expression used to identify murine B cells in the spleen

Splenic B cell subset	Surface markers
Mature B cells	B220+ AA4.1-
All Transitional B cells	B220+ AA4.1+
Transitional B cells subset 1	B220+ AA4.1+ IgM+ CD23-
Transitional B cells subset 2	B220+ AA4.1+ IgM+ CD23+
Transitional B cells subset 3	B220+ AA4.1+ IgM^{int} CD23-
Marginal zone B cells	B200+ AA4.1- CD38+ Fas- CD21+ CD23-
Follicular B cells	B200+ AA4.1- CD38+ Fas- CD21+ CD23-
Germinal centre B cells	B220+ AA4.1- CD38- Fas+

These proportions were typical compared to published values (Allman & Pillai 2008; Loder et al. 2012; Chung et al. 2003). The MZ compartment showed some variability (5-12% of total B cells), as did the resting GC population (0.01-1% of total B cells) but these populations are known to fluctuate with age, gender and health status.

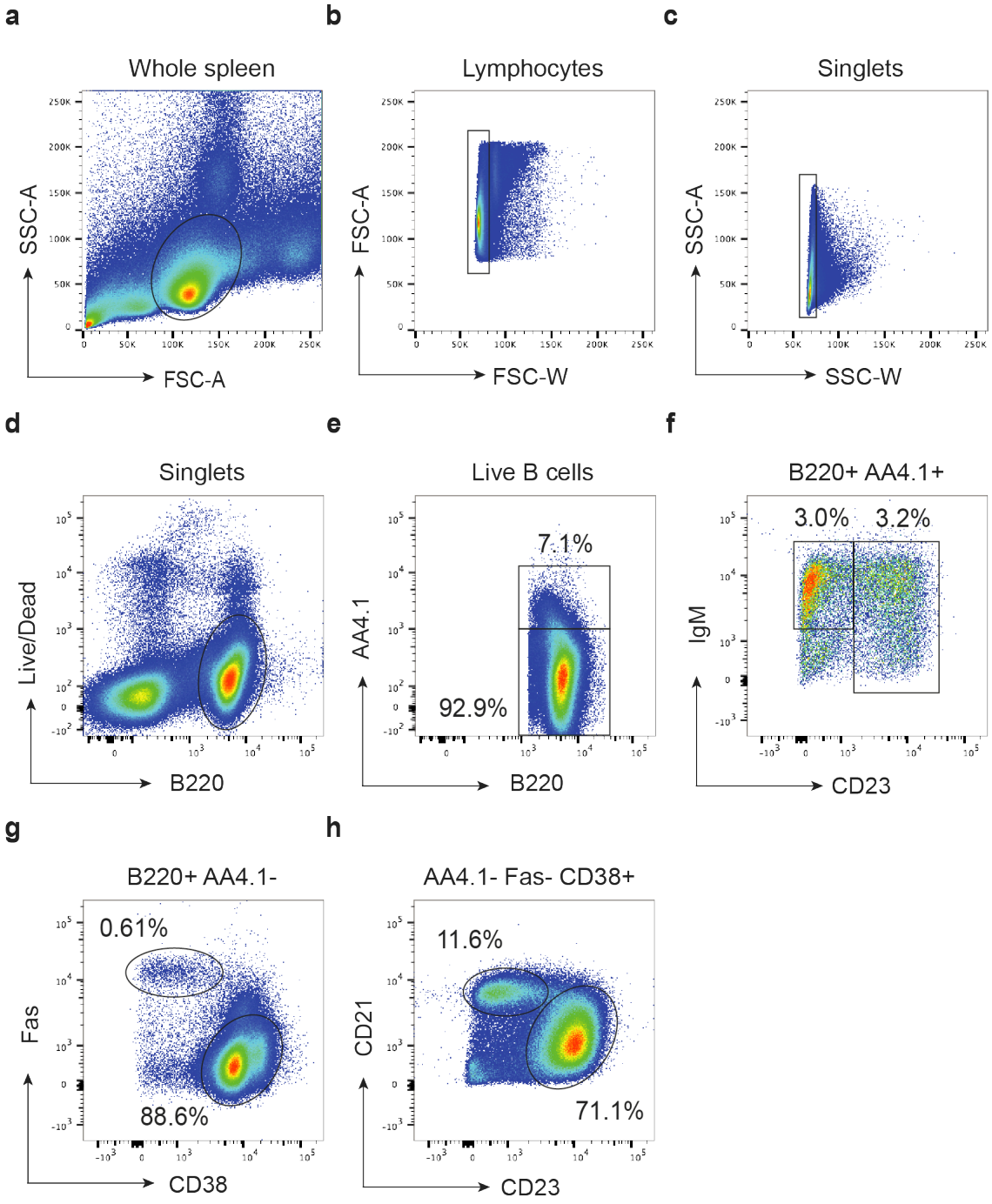

Figure 10 Splenic B cell populations identified from the spleens of naive C57Bl/6 mice

Figure 10 Splenic B cell populations identified from the spleens of naive C57Bl/6 mice

Splenocytes were stained for 30 min on ice and data plotted using FlowJo. Percentages refer to percentage of total live B cells. Gating strategy as follows:

(a) Dot plot showing all events and gated on lymphocytes based on forward-scatter/ side-scatter characteristics
(b-c) Doublet exclusion
(d) Total live B cells, Live/dead– B220+
(e) Transitional B cells, AA4.1+ B220+, 7.1%. non-transitional B cells, AA4.1-B220+
(f) T1 B cells, IgM+ CD23-, 3.0%, T2/T3 B cells IgM variable CD23+, 3.2%
(g) Germinal centre B cells, Fas+ CD38-, 0.61%, non-germinal centre cells, Fas- CD38+, 88.6%
(h) Marginal zone B cells, CD21+ CD23-, 11.6%, follicular B cells, CD21int CD23+, 71.1%

Dotplot displays of microscopy data acquired via MDA allowed the identification of naive splenic B cell subsets (Figure 11a). Visually, these plots resembled plots obtained by flow cytomtery (Figure 10f, h compared to Figure 11a) and furthermore, frequency of each subset was also consistent with flow cytometry (Table 5).

Table 5 B cell frequencies obtained from flow cytometry or MDA microscopy

Data from one experiment, representative of 5 independent experiments

Splenic B cell subset	Flow cytometry frequency (%)	Microscopy frequency (%)
T1 B cells	3.0	1.2
T2/3 B cells	3.2	2.1
MZ B cells	11.6	7.8
FO B cells	71.1	82.0
GC B cells	0.61	0.013

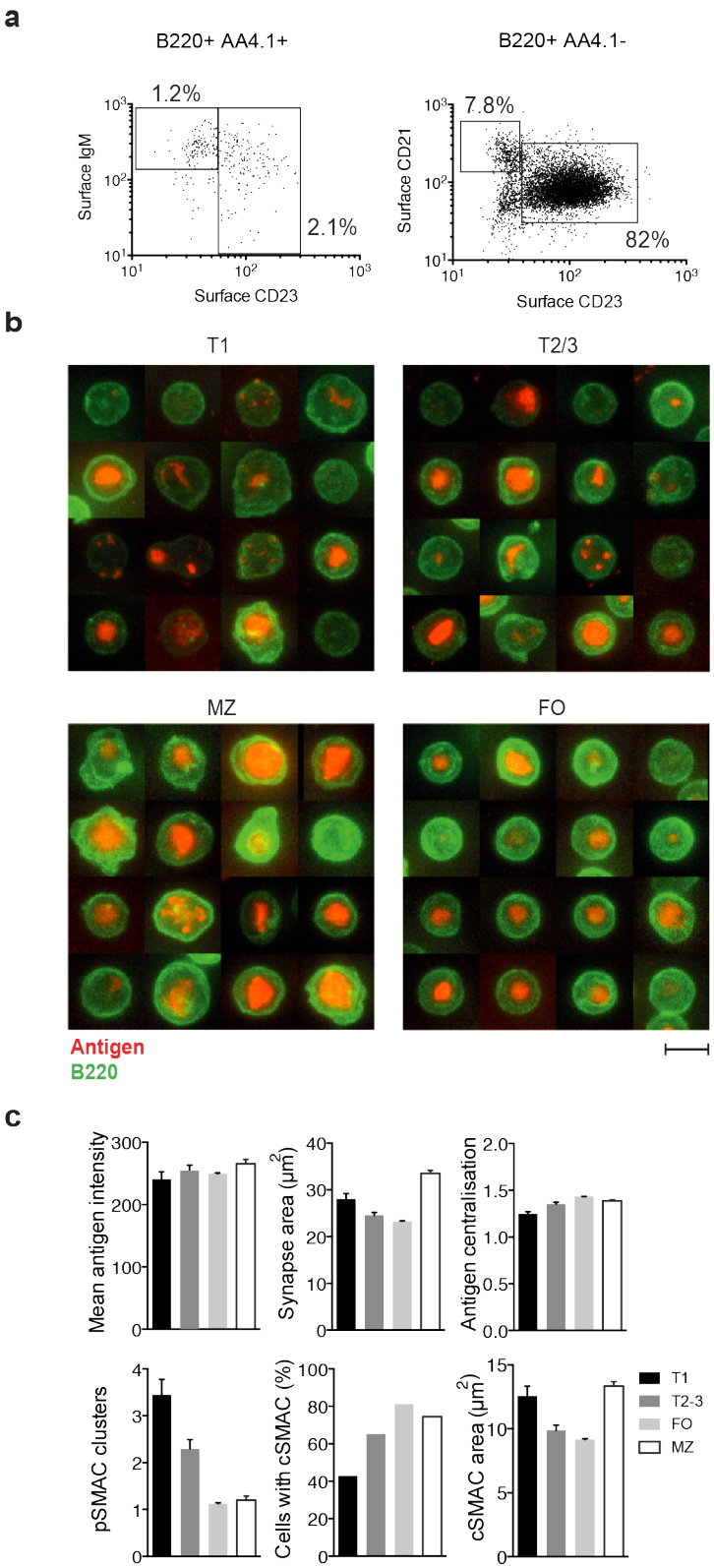

Figure 11 Large-scale imaging reveals subset-specific differences in naive B cell synapses

Figure 11 Large-scale imaging reveals subset-specific differences in naive B cell synapses

MDA data displayed as a (a) dotplots followed by gating in image datasets on B cell subsets using fluorescence intensities of membrane markers and (b) image galleries of B cell synapses after 20 min incubation with antigen (anti-Igκ) on PLBs.

(a) Left graph, gates show T1, IgM^{+} $CD23^{-}$, 1.2% and T2-3, $IgM^{+/int}$ $CD23^{+}$ cells, 2.1%. Right graph, gates show marginal zone (MZ), $CD21^{+}$ $CD23^{-}$, 7.8% and follicular (FO), $CD21^{lo}$ $CD23^{+}$ cells, 82%.

(b) Image galleries from indicates gates showing synapses (antigen, red) and B cells (B220, green)

(c) Quantification of synaptic features.

Data are means and s.e.m. from n = 92 T1, 161 T2-3, 4504 FO, and 459 MZ cells from one out of three experiments.

Scale bar = 5 μm.

When gates were applied to identified subsets and images recalled, synaptic differences were immediately visible (Figure 11b). These differences were quantified numerically, and although overall mean intensity of antigen in synapses was similar; FO B cells were most efficient at contracting antigen into tight central cSMACs as defined using a segmentation algorithm (Pavel Tolar, Figure 12). Mature synapses (in FO cells) tended to have a smaller synapse area, both in the cSMAC and over the entire synapse (more contracted), less pSMAC clusters and a higher degree of centralisation (Figure 11d).

In contrast, centralisation of antigen was lowest in T1 B cells and intermediate in T2/3 B cells. A higher number of cells in these fractions made synapses, which were disorganised and lacked a proper cSMAC. It should be noted, however, that a substantial number of these cells still made a synapse with a typical looking cSMAC.

Interestingly, cells in the MZ formed unusual diffuse synapses. MZ B cell synapses had the largest synapse area of all the naive subsets. These cells displayed efficient antigen centralisation, with low numbers of pSMAC clusters present and a high percentage of cells forming cSMACs; albeit larger, spread ones. To summarise, all naive subsets formed synapses with cSMACs, but to varying degrees.

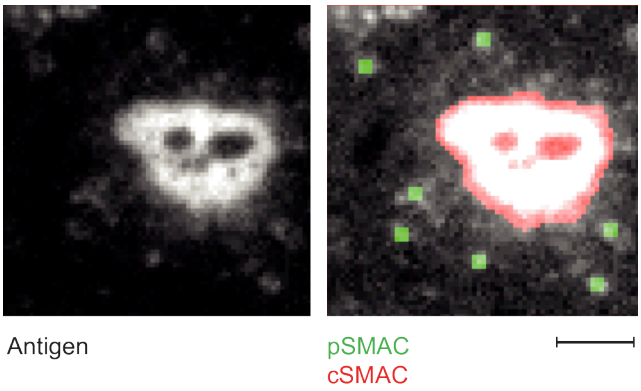

Figure 12 Automatic cSMAC and pSMAC identifcation

Images of fluorescent antigen from a single cell incubated for 20 min on an anti-Igκ loaded PLB. Cell representative of a typical FO B cell synapse. Tools identify the cSMAC (red) and pSMAC clusters (green)
Scale bar = 2 μm

3.2.5 Naive B cell subsets internalise antigen efficiently from Plasma Membrane Sheets (PMS)

To examine antigen internalisation from synapses of B cell subsets, we next set up our large-scale imaging platform with Plasma Membrane Sheets (PMS), a flexible antigen-presenting substrate used previously to model internalisation in B cells (Natkanski et al. 2013). PMS were prepared as described (Natkanski et al. 2013); briefly, mammalian HEK293 cells were cultured directly onto poly-L-lysine coated glass, and then sonicated to shear cells, revealing the inner leaflet flexibly bound to the glass. These uncovered portions of membrane were then loaded with the same fluorescent anti-Igκ antigen used on PLBs (Figure 13a). Prepared PMS covered glass to varying degrees (Figure 13b) with some areas of glass left exposed and free from antigen. This resulted in B cells landing either on (Figure 13b, white arrow) or outside (yellow arrow) of an area of sheets. Cells outside of sheets served as internal non antigen-stimulated controls.

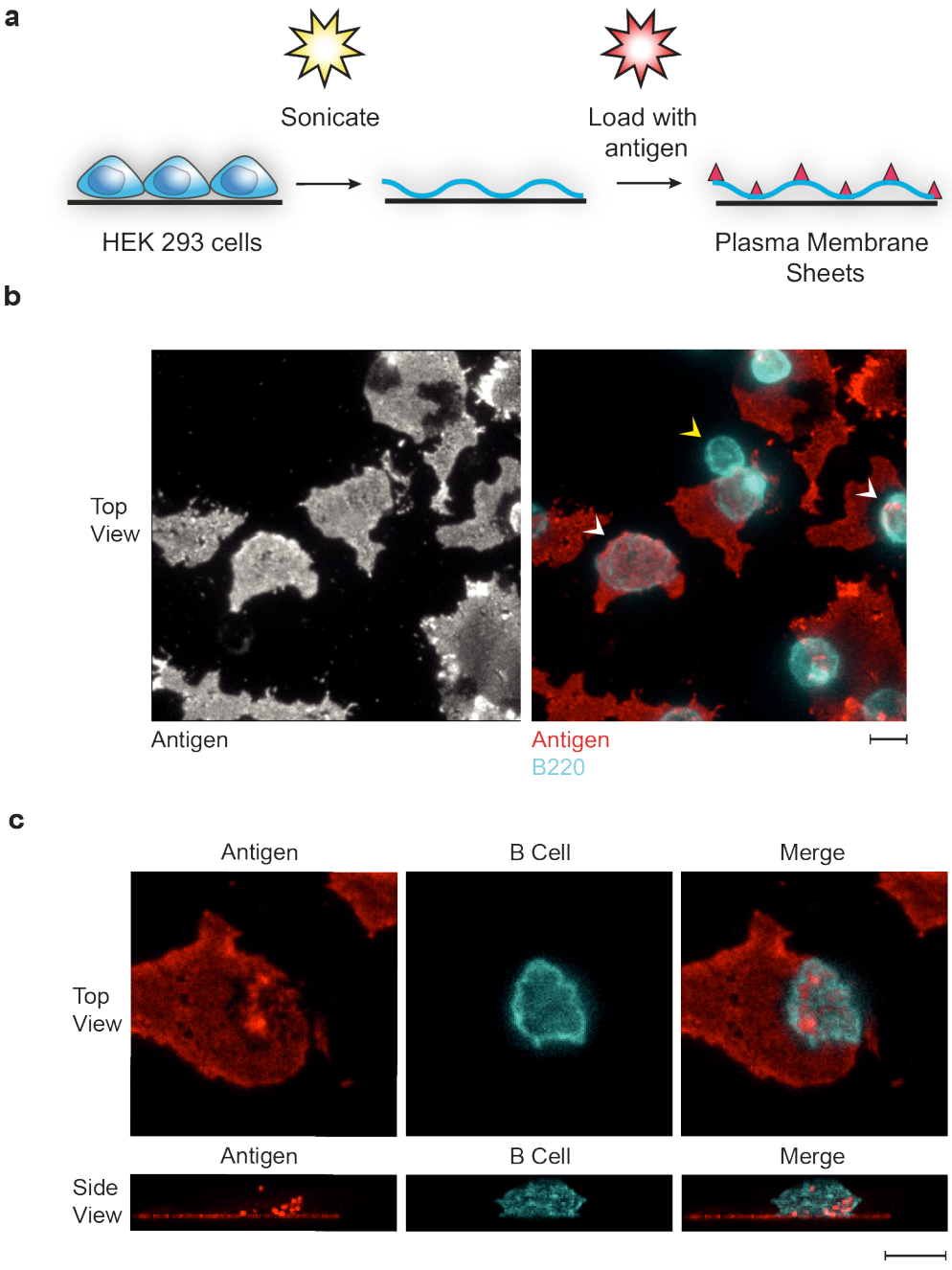

Figure 13 Plasma Membrane Sheets (PMS) are a flexible substrate which support antigen internalisation from B cells

(a) Schematic outlining PMS preparation for imaging
(b) Image of prepared PMS loaded with fluorescent antigen (left) and after the addition of B cells (right, cyan) to PMS (red). White arrows show B cells interacting with a sheet; yellow arrow shows a B cell outside of a sheet.
(c) Antigen forming a synapse on a PMS. Top view shows synapse formation, side view shows antigen (red) inside a B cell (cyan).

Scale bar = 5 μm

Synapse formation was clearly visible when B cells were incubated on PMS (Figure 13c). The cSMAC appeared as a bright cluster of gathered antigen under the cell when viewed from the top down. When side views were reconstructed from acquired information in the z-plane, antigen clusters were seen inside the cell on endosomes, extracted and internalised from the PMS.

When applied to large-scale imaging, MZ and FO B cells were successfully identified on the basis of their surface marker expression (Figure 14a) and it was possible to gate on these populations, view their synapses and examine their antigen internalisation capabilities.

Observed differences in synaptic architecture were mirrored on PMS, where MZ cells formed more irregularly shaped synapses (Figure 14b, top row) compared with the prominent cSMACs formed by FO cells. Stills starting at the focal plane of the synapse and moving up in increments of 1 μm (2 z-steps of 0.5 μm) show antigen clusters removed from the sheet up inside both cell types (Figure 14b). Although MZ B cells did not internalise significantly different amounts of antigen compared to FO B cells (Figure 14c), internalised antigen did appear to be distributed over significantly more endosomes in MZ B cells, which correlates with their diffuse synaptic architecture.

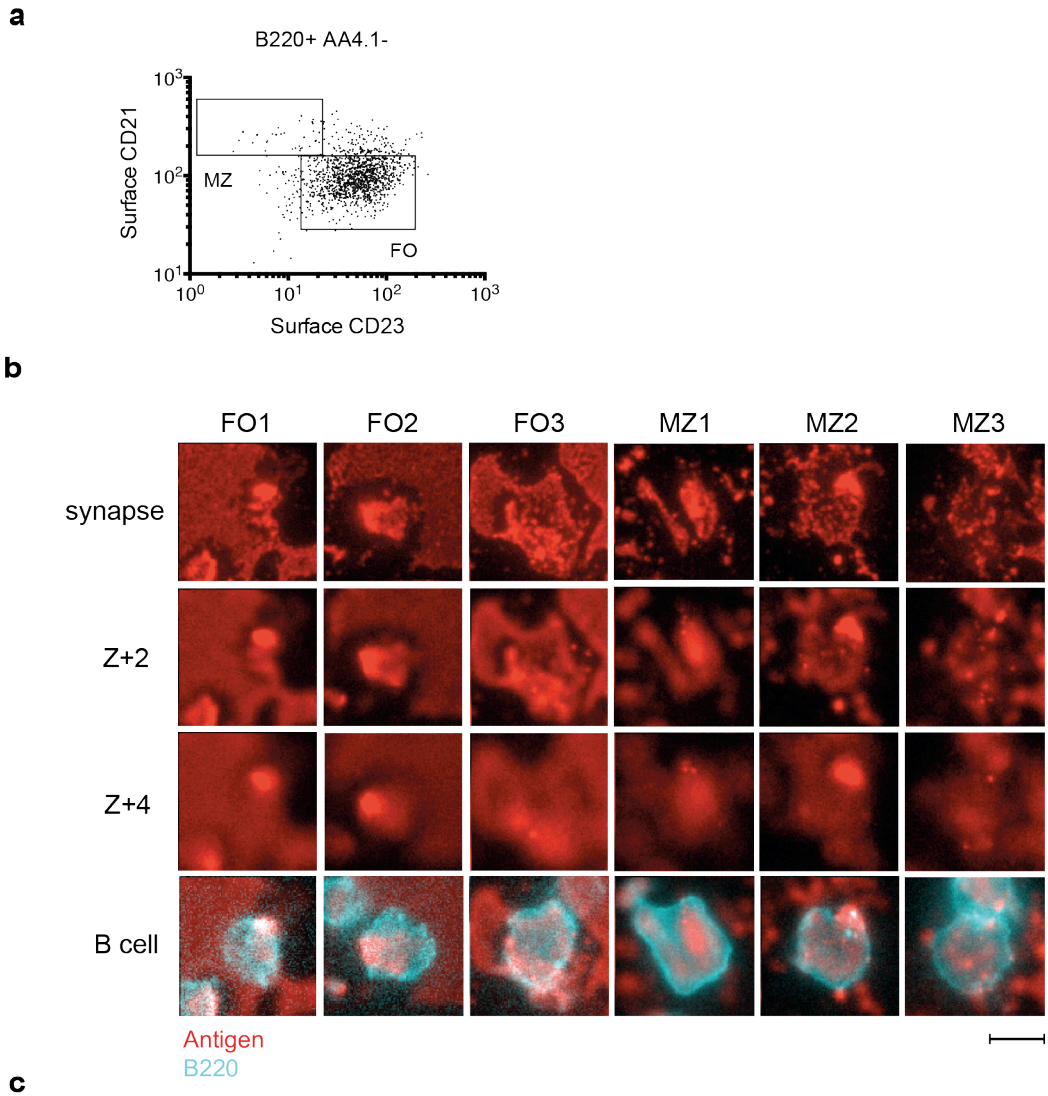

Figure 14 MZ and FO B cells both internalise equivalent amounts of antigen from PMS

Figure 14 MZ and FO B cells both internalise equivalent amounts of antigen from PMS

(a) MDA data displayed as a dotplot based on surface marker expression. Gates show B220+ AA4.1- CD21+ CD23- MZ cells and B220+ AA4.1- CD21int CD23+ FO cells
(b) Stills of three cells from each gate showing synapses and internalised antigen (red) removed from sheets when moving up through z-planes. Z+2 = two 0.5 μm z-steps above synaptic focal plane. B cell (cyan) shown interacting with PMS.
(c) Quantification of total antigen internalised and number of endosomes observed inside each cell. F.U = fluorescence units, n.s = not significant, * = $p < 0.05$

Scale bar = 5 μm

3.2.6 Developing a live FDC imaging substrate to image cell-cell interactions

In order to expand our imaging toolbox to more physiologically relevant scenarios we attempted to image B cells interacting with live FDCs. After isolating FDCs from lymph nodes of Bl/6 mice, the cells were cultured on FluoroDish imaging culture dishes coated with collagen for 5 days to fully recover their dendritic morphology. When imaged with a 10x objective many cells can be seen spread over the collagen-coated dish (Figure 15a). These cells have the classic dendritic morphology expected of FDCs, with many cells having multiple, long projections emanating from a central cell body. Cells stained positive for the surface molecule CD21/35 (complement receptor 1/2, CR1/CR2) and with the antibody FDC-M1 (a marker of FDCs) confirming that a significant number of isolated cells were in fact FDCs.

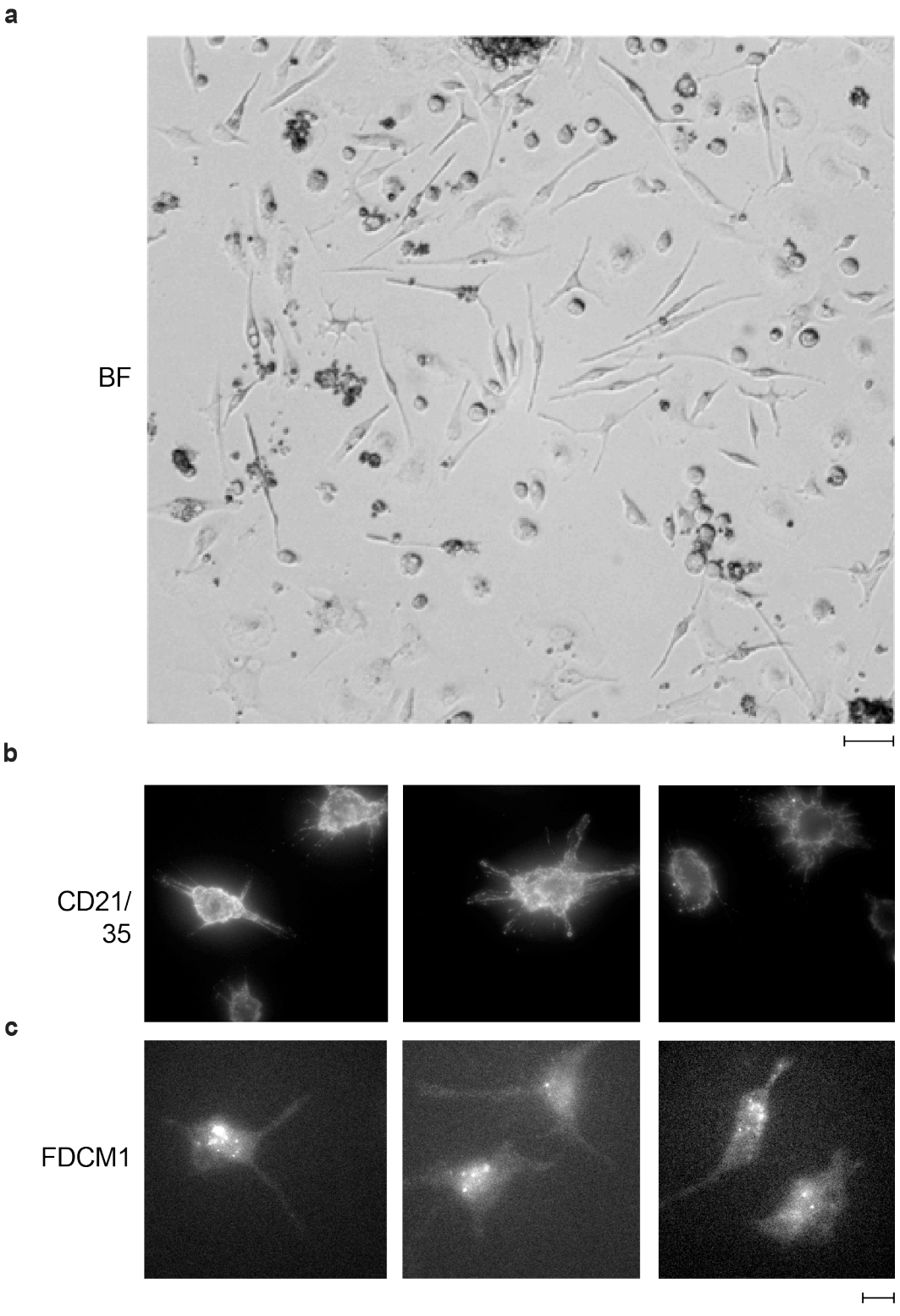

Figure 15 Primary follicular dendritic cells isolated from mouse lymph nodes

Figure 15 Primary follicular dendritic cells isolated from mouse lymph nodes

(a) Follicular dendritic cells in their imaging chamber following 5 days of culture. Cells imaged with a 10x air objective on an inverted widefield microscope. Scale bar = 25 μm
(b) Three images of FDCs stained with CD21/35
(c) Three images of FDCs stained with FDCM1 unlabelled antibody with secondary fluorescent staining. (b,c) Scale bar = 10 μm

After successful FDC isolation and culture we tested several strategies to load the FDC surface with antigen for B cells to interact with. Loading with full-length fluorescent version of anti-Igκ antibodies was unsuccessful, probably due to the relatively low affinity of the antibodies for Fc receptors. Next we attempted to bind a biotinylated anti-CD16/32 antibody followed by streptavidin and biotinilated $F(ab')_2$ anti-Igκ. This was also unsuccessful and caused extensive clustering on the cell surface. We eventually decided to target the complement receptors, especially CR2, by binding complement-coated immune complexes, which is the physiological mechanism by which FDCs present antigens *in vivo*. The immune complexes were prepared by combining our $F(ab')_2$ anti-Igκ antigen with an $F(ab')_2$- specific full length IgG antibody and incubating with freshly isolated murine complement in GVB++ complement buffer. This uniformly loaded FDCs with the antigen (Figure 16), with some clustering of the immune complexes visible. When B cells were applied to antigen loaded FDCs, they interacted with the FDCs, preferentially with the dendrites extended from the main FDC cell body (Figure 16, Movie 5). B cells rarely interacted with the middle portion of FDCs, instead preferring the flatter processes. B cells also successfully extracted antigen from the FDCs, as small clusters of antigen could be observed inside B cells after incubation with FDCs for 30 mins at 37°C.

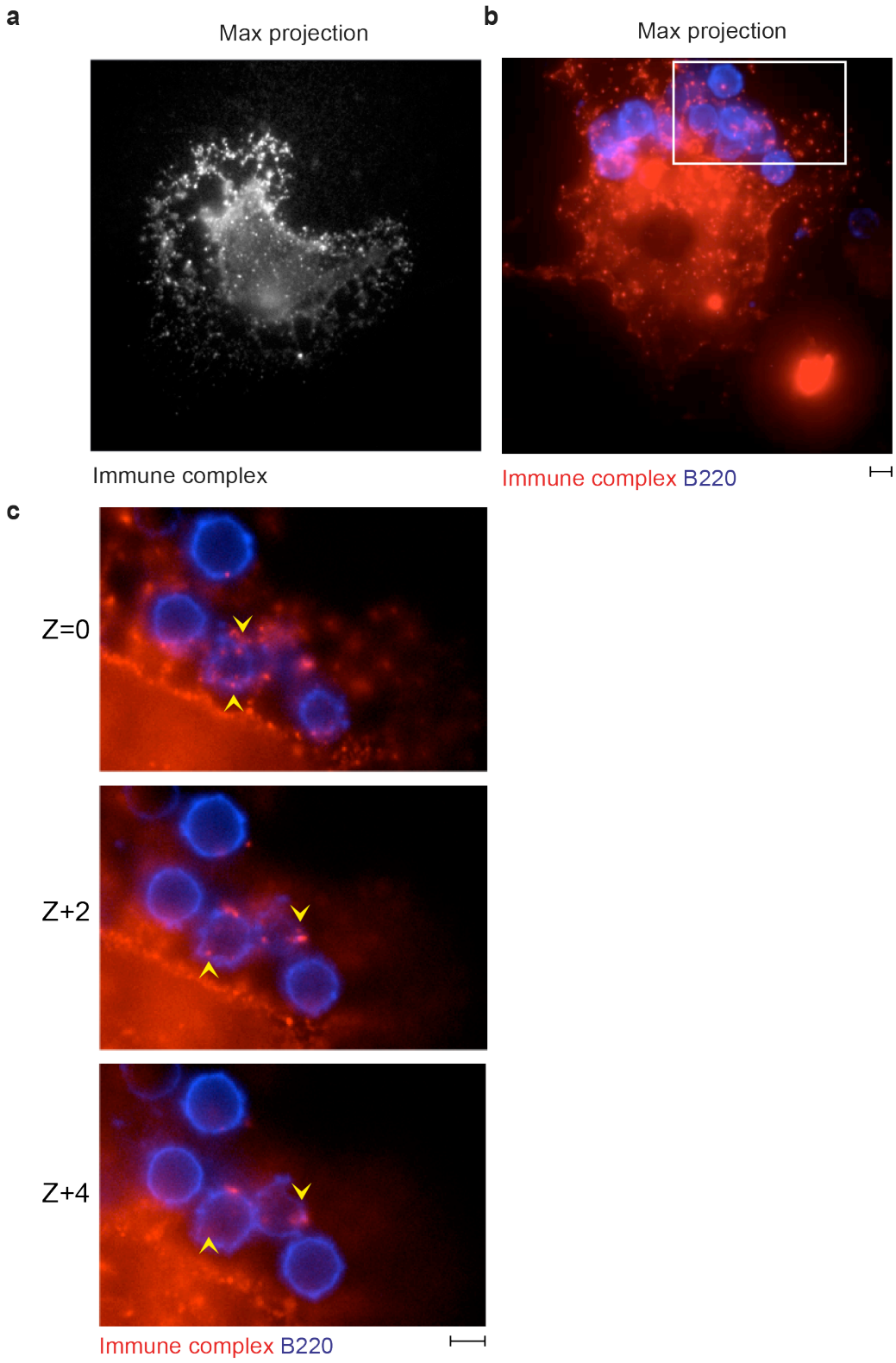

Figure 16 B cells extract antigen loaded as immune complexes from the surface of FDCs

Figure 16 B cells extract antigen loaded as immune complexes from the surface of FDCs

(a) Max projection of an FDC loaded with fluorescent complement-coated immune complexes (ICs).
(b) Max projection of B cells (blue) interacting with an FDC loaded with anti-Igκ antigen in immune complexes (red)
(c) Enlarged stills from area marked with white rectangle from (b) showing anti-Igκ-ICs (red) internalised by B cells (blue) from FDCs when moving up through z-planes. Z+2 = two 0.5 μm z-steps above synaptic focal plane. Arrows show antigen clusters inside B cells.

Scale bar = 5 μm

3.3 Discussion

Using a large-scale imaging approach, quantitative differences have been observed in synapse formation across different populations of murine splenic primary B cells. We were able to replicate the synapse formation data of others using similar surrogate membrane formats (PLBs and PMS) (Fleire et al. 2006; Natkanski et al. 2013; Tolar et al. 2009), but could uniquely extend this by generating large, rich data sets of many cells interacting simultaneously with antigen presented on a membrane. This analysis provided information on sufficiently large numbers of B cells to cover even rare B cell populations often overlooked by single-cell imaging approaches.

We were able to image in 7 colours, including fluorescent antigen and 6 distinct surface markers. This produced data analogous to flow cytometry in its identification of naive B cell subsets, proving the system and analysis tools built were robust and unbiased. Further increase in the number of colour channels may be possible by using wider range of fluorophores and corresponding fluorescent filters. Useful features of MDA data include custom data display tools. We were able to display processed data as dotplots based on a wide range of fluorescence and other parameters, gate on populations of interest, and, uniquely, retain an image link to recall images of cells and synapses from each gate as well as extracting quantitative numerical data.

The system itself was built with inherent flexibility, demonstrated by our use of two surrogate membrane formats, PLBs and PMS, each with their own strengths. PLBs are rigid, flat surfaces (Attwood et al. 2013; Natkanski et al. 2013) which exhibit excellent lateral mobility. This has made them excellent substrates for imaging both the formation and organisation of the synapse using high-resolution TIRF microscopy. Although we know PLBs do not support antigen internalisation (Natkanski et al. 2013), they are still informative for the study of microcluster formation and antigen dynamics before internalisation.

We attempted to extend our imaging capabilities to observe B cell synapse formation directly with live FDCs for the first time. FDCs could be isolated and loaded successfully with complement-coated immune complexes and we were able to observe many B cells extracting antigen from the FDC surface. However, we were not able to detect canonical synaptic patterns in the B cell synapses using this system. For example, naive B cells did not form detectable cSMACs. This could be due to the relatively low antigen amounts and high levels of preclustering of antigen on the FDC surface or due to rapid extraction of the antigen from the FDCs. Nevertheless, the system is promising and with some alteration of antigen density or antigen-loading techniques and with the application of live cell imaging, it seems likely that synapse formation could be investigated in this physiological format. We are currently optimising the protocols to make high-resolution cell-cell imaging a reality in the future.

Using PLBs loaded with anti-Igκ more than 5,000 cells were captured, imaged, processed and identified in 4 different subsets, T1, T2/3, MZ and FO. For the first time, differences were identified in synaptic architecture in primary B cell populations. There was a trend towards increasing synaptic organisation through developmental stages, with centralisation of antigen increasing from transitional B cells through to FO B cells. In other immune cells, differential synaptic structures are known to exist. Synapses formed without receptor rearrangement have been described in some inhibitory NK cell synapses (Carlin et al. 2001; Miner et al. 2015) and multifocal synapses were described in other inhibitory NK cell-target cell contacts (Carlin et al. 2001). Interestingly, in T cells, multifocal synapses were observed in immature thymocytes (Hailman et al. 2002; Richie et al. 2002) during negative selection, and it was once suggested that multifocal synapses were a hallmark of immaturity in T cells. This idea drew parallels with our observations of synaptic organisation increasing with maturity, hinting that this may be a common observation amongst lymphocytes. Since then however, multifocal synapses were seen in contacts between dendritic cells and mature T cells (Brossard et al. 2005), and we saw diffuse synaptic organisation in marginal zone B cells, confirming that although synapses may become more organised with development, differences in synaptic architecture are also present in mature lymphocyte subsets.

Unexpectedly, MZ B cells displayed distinct synaptic morphology. They formed synapses that scored very highly for centralisation of antigen, but seemed to bypass the last contraction phase of cSMAC formation, leaving them with an unusual, diffuse appearance. MZ cells are often described as 'innate like' B cells and vary from FO B cells in a number of key ways. For example, MZ B cells are localised in the marginal zone of the spleen, and upon activation, MZ B cells rapidly differentiate into plasmablasts and produce large quantities of low affinity antibodies in a T-cell independent manner. The low activation threshold of marginal zone B cells facilitates a rapid primary antibody response (Zouali & Richard 2011) and might mean MZ B cells have less of a requirement to cluster antigen to achieve full activation.

Using PMS to investigate antigen internalisation we could compare the antigen extraction capabilities of MZ and FO B cells interacting simultaneously with the same substrate. Naturally, this controls for any differences that may arise during substrate preparation, and also includes non-stimulated control cells (that land outside sheets) imaged at the same time. Although PMS differ from APCs in their lack of co-stimulatory molecules known to be important for *in vivo* antigen internalisation (Carrasco & Batista 2006b; Carrasco et al. 2004; Suzuki et al. 2009), they do match APCs in their viscoelastic properties (Natkanski et al. 2013), the importance of which is rapidly becoming more appreciated (Wan et al. 2013). MZ B cells internalised equivalent amounts of antigen when compared to FO B cells, but antigen could be detected on significantly more endosomes, suggesting it had been picked up from smaller clusters. This aligns with PLB data describing the dispersed shape of MZ synapses, and serves to highlight the strength of combining these two substrates to answer different, but related questions.

Based on our data, it is possible to speculate that the differences in synaptic architecture in more mature B cell subsets (like MZ B cells) might read-out into functional differences in cell behaviour. The multifocal synapses formed during thymocyte interactions with PLBs were associated with increased and sustained T cell receptor (TCR) signalling (Hailman et al. 2002), and in B cells, cytoskeleton-

dependent antigen centralisation has been associated with negative regulation of BCR signalling (Liu et al. 2013; Seeley-Fallen et al. 2014), suggesting that the degree of antigen centralisation could govern B cell activation in a subset-specific manner.

This question will require further study of specific signalling pathways. The flexibility in our large-scale system would allow for such investigations by incorporating stains for BCR signalling molecules and members of the cytoskeleton.

Chapter 4. Germinal centre B cells internalise antigen though specialised extraction mechanisms after forming unique synapses

4.1 Introduction

It is well established that during immune responses, naive B cells must physically interact with and internalise membrane-bound antigens from APCs and display them on their surface after endocytic processing in order to receive the T cell signals required for full activation (Phan, Green, et al. 2009; Batista et al. 2001; Junt et al. 2007). What is also known, but less well characterised, is the importance of context of antigen encounter for activated B cells that have acquired the germinal centre (GC) phenotype. The GC is a transient structure that forms during an active infection, through recruitment of nearby T-cell-activated B cells drawn into the specialised GC niche (Victora & Nussenzweig 2012; Shlomchik & Weisel 2012a). These form characteristic foci in secondary lymphoid organs where GC B cells proliferate and undergo processes that improve their antigen responsiveness, support very high affinity antibody production and lay the foundations of immunological memory (Eisen & Siskind 1964; Berek et al. 1991; Neuberger et al. 1999; MacLennan 1994).

Decisions in the GC are a topic of great interest and intense study. Mechanisms of how GC B cells read out improvements in receptor affinity over time remain illusive, although signalling and location are known to play indispensible roles. GC B cells themselves show a number of fundamental differences compared with their follicular (or naive) counterparts; including a large, more polarised morphology (Hauser et al. 2007; Allen et al. 2007; Schwickert et al. 2007), upregulation of surface Fas, and absence of surface IgD and CD38 (in mice) (Bhan et al. 1981). The default fate for a GC B cell is death by apoptosis, high levels of surface Fas coupled with absence of BCL-2 result in cell death in culture within a matter of hours (Liu et al. 1991). *In vivo,* this may be overcome by receiving signals to upregulate antiapoptotic proteins such as Mcl-1 (Vikström et al. 2010; Peperzak et al. 2013).

After each progressive round of B cell receptor mutagenesis there is competition in the GC, such that high affinity clones are chosen for expansion or further mutagenesis over low affinity clones, which die via apoptosis (Shokat & Goodnow 1995; Shih et al. 2002; Rajewsky 1996), gradually increasing net affinity of the entire GC. This process is independent of inherent BCR affinity, and instead favours the selective expansion of the highest affinity clones available- illustrated by the ability of very low affinity B cells to be selected, expanded and recalled from memory in the absence of competition (Dal Porto et al. 2002). This hints at the presence of some sort of 'winning' signal acquired by GC B cells succeeding productive BCR rearrangements in the GC dark zone.

Light and dark zones (LZ, DZ) of the GC are established by chemokine gradients and cellular composition (Allen et al. 2004; Ansel et al. 2000); the DZ being occupied exclusively by B cells where the LZ contains B cells intermingled with specialised follicular dendritic cell (FDC) networks and T follicular helper cells (Cyster et al. 2000; Schaerli et al. 2000; Breitfeld et al. 2000). FDCs hold intact antigen on their surfaces in aggregates known as iccosomes (immune complex-coated bodies, or immune complexes) for prolonged timespans (Suzuki et al. 2009; Tew et al. 1993). It is within this light zone that activated B cells encounter antigen on FDC surfaces (Suzuki et al. 2009), and presumably rely on the formation of an immune synapse for antigen extraction.

Following antigen extraction from FDCs, GC B cells present peptides on their surface complexed with MHCII molecules, facilitating access to T cell help. It was recently shown that competition for T cell help was the limiting factor for GC cell selection, and for the first time provided evidence of a 'winning' signal rewarded to the highest affinity competitors (Victora et al. 2010). This challenged traditional models implicating direct competition for antigen as the limiting factor to GC B cell expansion (Tarlinton & Smith 2000). Although competition for antigen *per se* is not the determinant of successful clonal expansion, amount of antigen extracted from FDCs does correlate with antigen affinity, thus making surface-presented peptide density a surrogate readout for BCR affinity (Batista et al. 2001; Batista et al. 2007). T cells were shown to form synapses preferentially with B cells displaying higher

levels of surface peptide MHC *in vitro*, and this was supported by studies *in vivo* where T cells formed more conjugates with B cells bearing more successive affinity-improving mutations in their BCRs (Reinhardt et al. 2009; Depoil et al. 2005). Moreover, after loading of T-cell specific antigen to the surface of a subset of GC cells via the DEC205 receptor, the resultant T-cell help influenced their selective expansion despite similar BCR affinities in non-targetted controls (Victora et al. 2010). Thus, we hypothesise synapse formation and subsequent antigen internalisation events are essential processes in the GC for obtaining T-derived selection signals, although to date this remains unstudied at length.

The contribution of BCR signalling to selection in the GC reaction is currently not well understood. Rather than GC cells receiving qualitatively different signals, more recent studies utilizing transgenic mouse strains suggest that the magnitude of signalling influences GC selection. Gene expression profiling of LZ and DZ subsets identify gene signatures supporting both BCR and CD40 T- cell- derived signals (Victora et al. 2012; Basso et al. 2010). These responses are challenging to study due to the hidden heterogeneity of the GC often masked by population wide analysis. However, a recent study removed some of this heterogeneity by using a transgenic B1-8 mouse, bearing a hapten-specific BCR exclusively expressing the IgM isotype. They saw a general silencing of BCR signalling in the GC, facilitated by high activity of the phosphatase SHP-1 (Khalil et al. 2012). Another study, using an *in vivo* reporter of BCR signalling reports a similar phenotype, although they could detect active BCR signalling in a proportion of LZ cells (Mueller et al. 2015). These data together support a role for BCR signalling in the GC, but imply it is not sufficient for effective GC selection.

Although B cell-FDC encounter has been observed *in vivo* (Suzuki et al. 2009), GC synapses have never been investigated in high resolution, probably owing to the fact that the cells themselves are transient and rare. In the following chapter we aim to uncover the structure of the immune synapse in *ex vivo* GC B cells by using our large-scale MDA imaging platform and a combination of fluorescent markers. Furthermore, we also aim to explore BCR signalling in combination with contributions from members of the membrane cytoskeleton to more fully understand how GC B cells make fate decisions upon antigen encounter.

4.2 Results

4.2.1 Generation of Germinal Centres in mice

Germinal centre formation and maintenance is reliant on the presence of on-going infection. A number of laboratory systems exist to cause potent induction of GCs in mice, either using infectious agents or immunising adjuvants. We successfully induced GC formation using Friend Virus (FV), a murine retrovirus causing an early acute, non-lethal infection of B cells when mice were infected intravenously with spleen homogenate from a FV-infected mouse. After 14 days, a population of GC cells (3.64% of all splenic B cells) had formed in response to FV. This proportion was in line with published data, where even at its peak, the GC reaction is known to only comprise 1-5% of B cells (Chan & Brink 2012). GC light zone (LZ) and dark zone (DZ) cells were detectable by flow cytometry (Figure 17), as well as induction of non-GC plasma cells. As expected, both GC cells and plasma cells were present in very low numbers in an uninfected control mouse (0.9 and 0.03% respectively). These results were mirrored when sheep red blood cells (SRBCs) were used as an immunogen in place of FV (Figure 18). GCs were detectable from 7 days p.i. with either immunogen and were maintained for at least one month, consistent with GC data from others in various infection settings (Bachmann et al. 1996; Gatto et al. 2007; Shlomchik & Weisel 2012a).

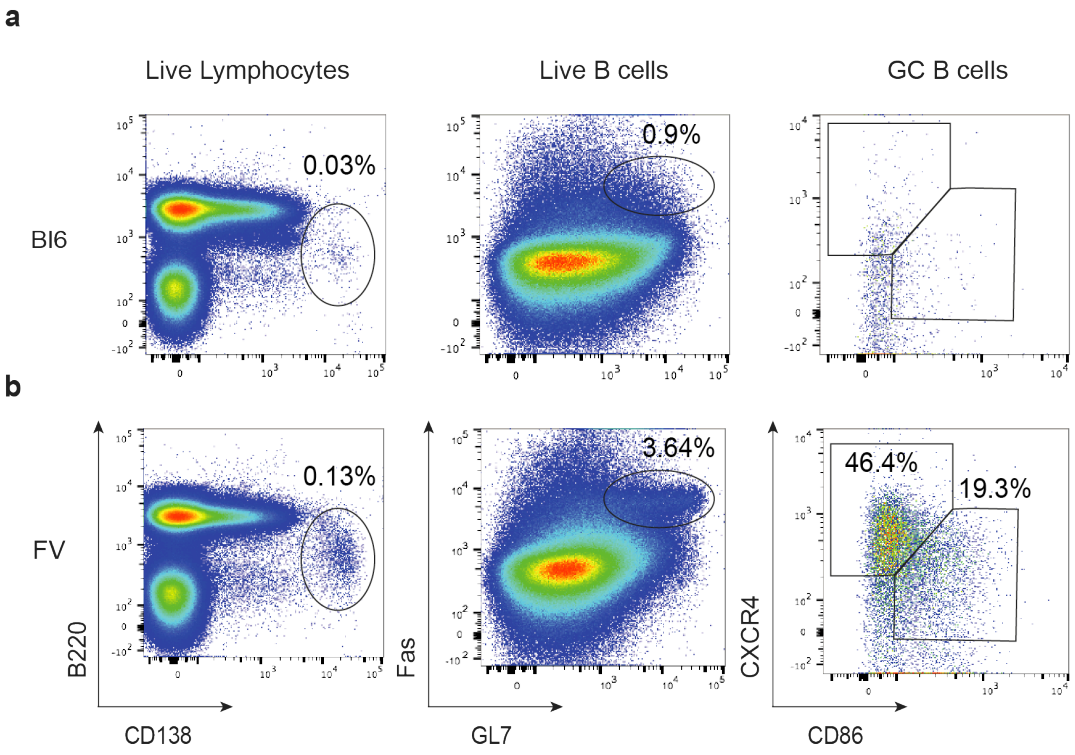

Figure 17 Friend Virus infection causes germinal centre formation in mice
Splenocytes were stained for 30 minutes on ice and data was plotted using FlowJo. Percentages refer to percentage of parent population (detailed above plot). Cells pre-gated on live, doublet-excluded lymphocytes based on FSC-SSC characteristics and live/dead viability dye.

(a) Uninfected Bl6 splenocytes, B220int CD138+ plasma cells, 0.03%, B220+ Fas+ GL7+ GC cells, 0.9%, GC cells further gated on CXCR4 and CD86. Dark zone cells defined as CXCR4+ CD86-, light zone cells defined as CXCR4- CD86+.

(b) Friend Virus infected splenocytes at day 14 p.i. All cell populations as described in (a). Plasma cells, 0.13%, GC cells, 3.64%; 46.4% DZ, 19.3% LZ.

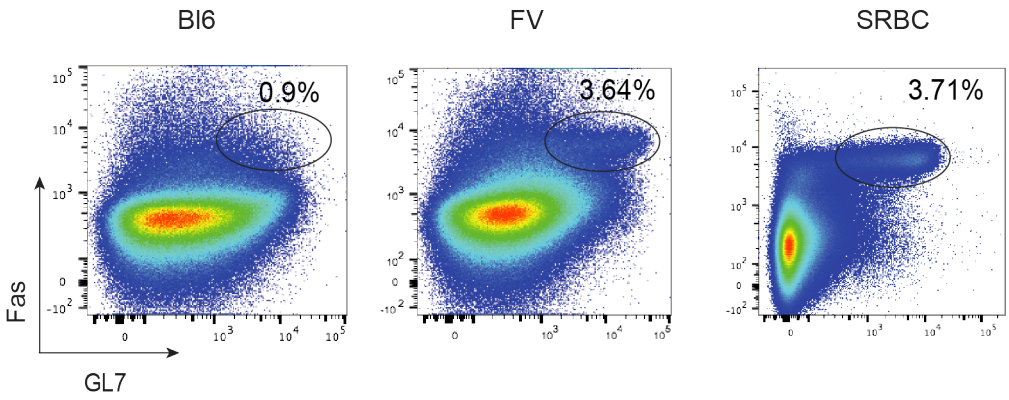

Figure 18 Germinal Centre induction by different agents

Cells prepared as detailed in Figure 17
Cells shown are single, live B220+ B cells. Percentages are % of single, live B cells. Bl6 = C57Bl/6 uninfected FV = Friend Virus, SRBC = Sheep Red Blood Cells

4.2.2 Germinal centre B cells form synapses with a distinct morphology

Using the large scale imaging platform described in Chapter 3, GC cells could be identified based on surface marker staining from the spleens of either FV infected or SRBC immunised mice after incubation on anti-Igκ loaded PLBs (Figure 19). Due to low frequency of GC cells in the spleen, an enriched GC fraction (obtained by a MACS depletion of CD11c, CD43 and IgD positive cell populations) mixed with naive control B cells was generally used for large-scale imaging experiments (Figure 19c). This resulted in up to 50% GC B cells in a given imaging sample compared to the typical 1-5%.

When synaptic characteristics were plotted, a small population of cells showed very low synapse centralization (Figure 19a), implying these cells were not forming canonical cSMACs. Furthermore, when presence of cell surface markers was examined, these cells were predominantly enriched in the CD38-Fas+ GC gate (Figure 19b, marked in red). After images were recalled at random from identified cells from either gate, GC cells were visibly larger and irregularly-shaped, with numerous lamellipodia-like protrusions; and, concurrent with the centralization data, indeed these cells did not form canonical cSMACs (Figure 20).

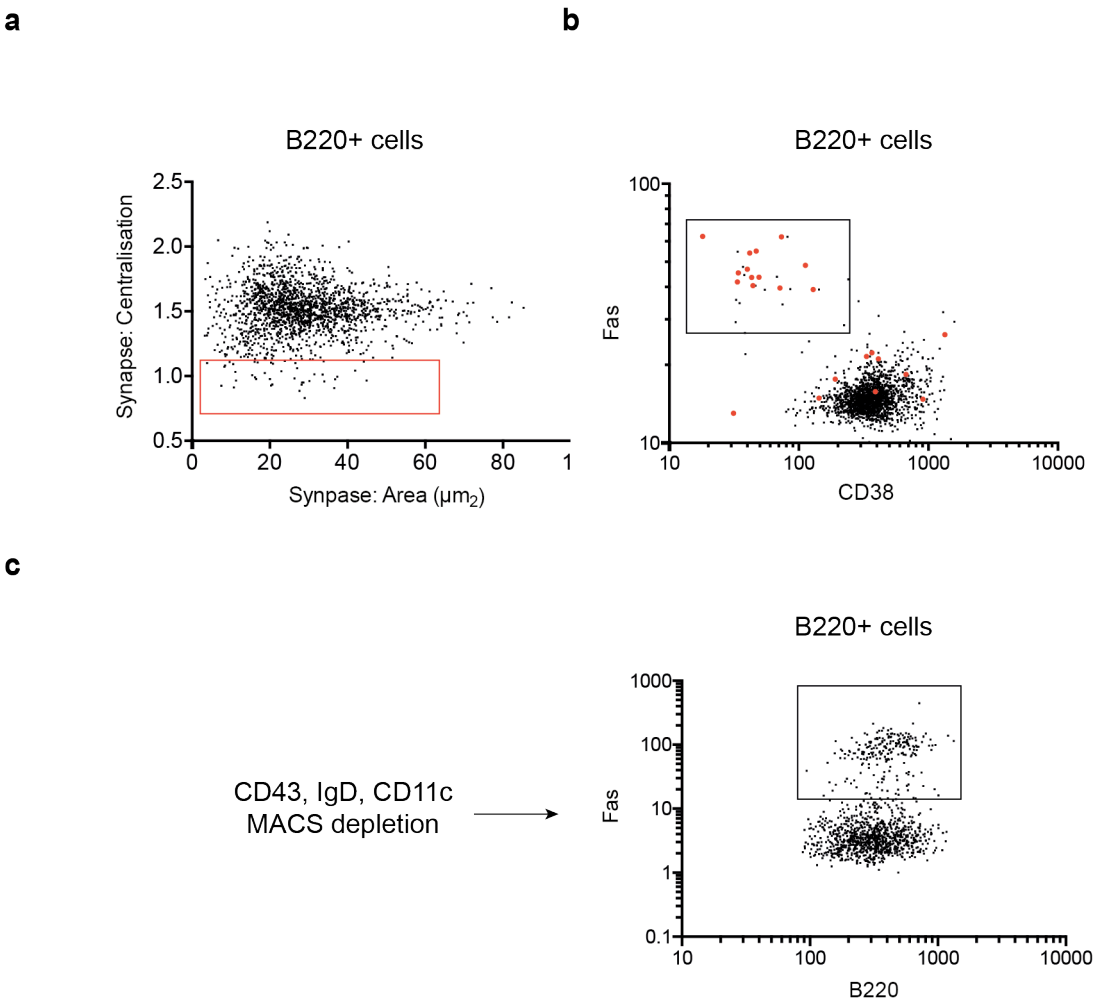

Figure 19 Identification of GC B cells by multi-dimensional acquisition

CellScore+ B220+ cells from spleens of immunised mice from an MDA of 900 fields-of-view. Each dot represents a single cell.

(a) Centralization of antigen (Igκ) in synapses of B220+ B cells. Gate indicates cells with low centralization.

(b) Cells from (a) plotted according to surface marker expression. Gate shows CD38- Fas+ GC cells. Red dots indicate cells from low centralization gate in (a)

(c) Data showing Fas+ GC cells after enrichment by MACs depletion of non-GC cells.

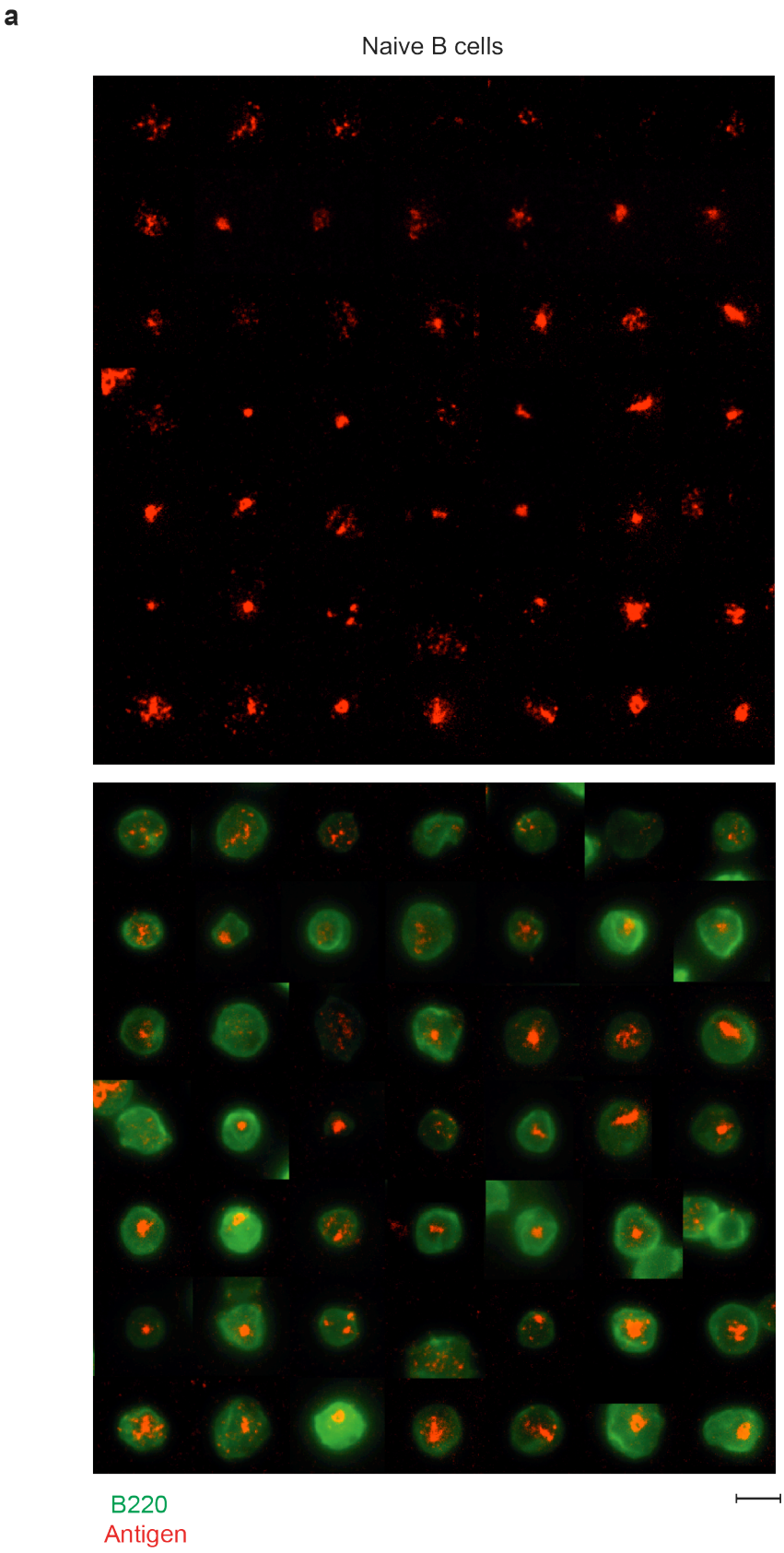

Figure 20 Naive and GC synapse formation on planar lipid bilayers

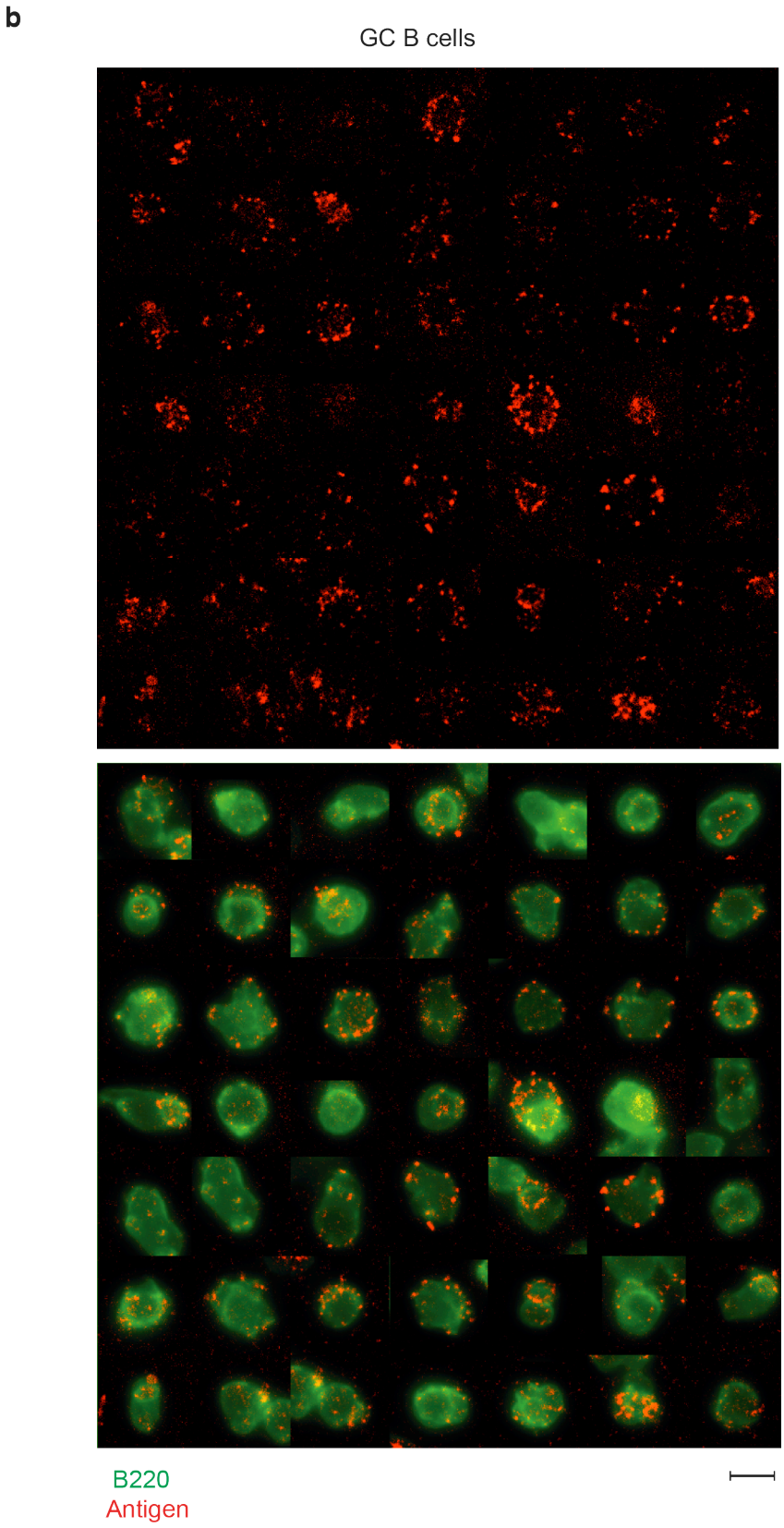

Figure 20 Naive and GC synapse formation on planar lipid bilayers

Figure 20 Naive and GC synapse formation on planar lipid bilayers

Image galleries of synapses (and cells) recalled at random from gated populations described in Figure 19c.

(a) B220+ Fas- naive B cell synapses shown by anti-Igκ antigen fluorescence (top panel) together with B220 cell overlay (bottom panel) after incubation for 20 minutes on antigen-loaded planar lipid bilayers.

(b) B220+ Fas+ B GC B cells from the same imaging well, imaged under the same conditions.

Scale bar 5μm.

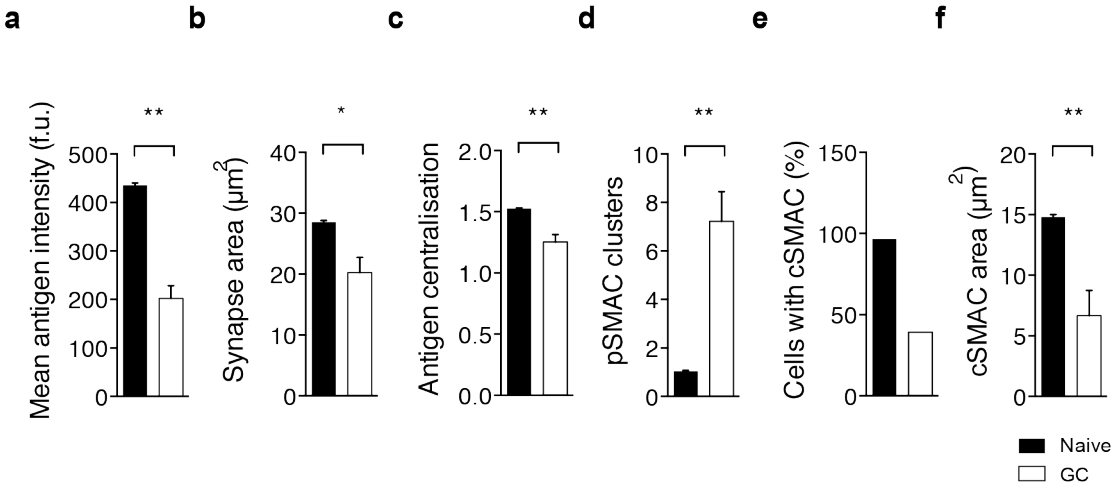

Figure 21 Quantification of synaptic features of naive and GC B cells

Data are from one experiment representative of three independent experiments, mean and s.e.m. of n = 1,596 naive B cells and 28 GC B cells. *P < 0.005, **P < 10^{-4} in unpaired t-tests.

In fixed images of GC B cell synapses (Figure 20b), cells did not centralize antigen into classical cSMAC structures seen in naive cells (Figure 20a). This was independent of immunisation or infection protocol, and occurred reproducibly when GCs were induced with FV, SRBC, or NP-CGG (data not shown). Although occasionally antigen clusters were seen in the centre of the contact, generally GCs formed large, spread synapses, where small antigen clusters were moved outwards towards the periphery of the contact. Further quantitative analysis of these synapses (Figure 21) uncovered that GC cells bound less antigen than naive cells overall. A significant number of cells did not form any identifiable cSMAC, and in the small fraction of cells that did centralise antigen, cSMACs were smaller than their naive counterparts. Actin localisation in GC B cells was distinct compared with naive B cells. Naive B cells localised antigen predominantly in peripheral lamellipodia, with some small spots sporadically present in cSMACs (Figure 20a), whereas in GC B cells actin was co-localized with antigen, forming close associations with peripheral antigen clusters (Figure 22, Figure 23b). Tubulin was also upregulated in GC B cells, although MTOC polarisation to the synapse was reduced (Figure 24). In most naive B cells individual microtubules visibly overlaid the synapse, positioned low and close to the plasma membrane. This was largely absent in GC cells, although in some cells the MTOC was polarised to the synapse.

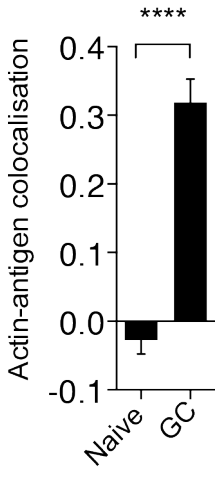

Figure 22 Actin colocalization with antigen in naive or GC synapses

Analysis of pre-enriched GC cells and naive control cells on PLBs. Data from one experiment representative of two independent experiments, mean and s.e.m from n = 543 naive and 65 GC B cells. ****$P < 10^{-4}$

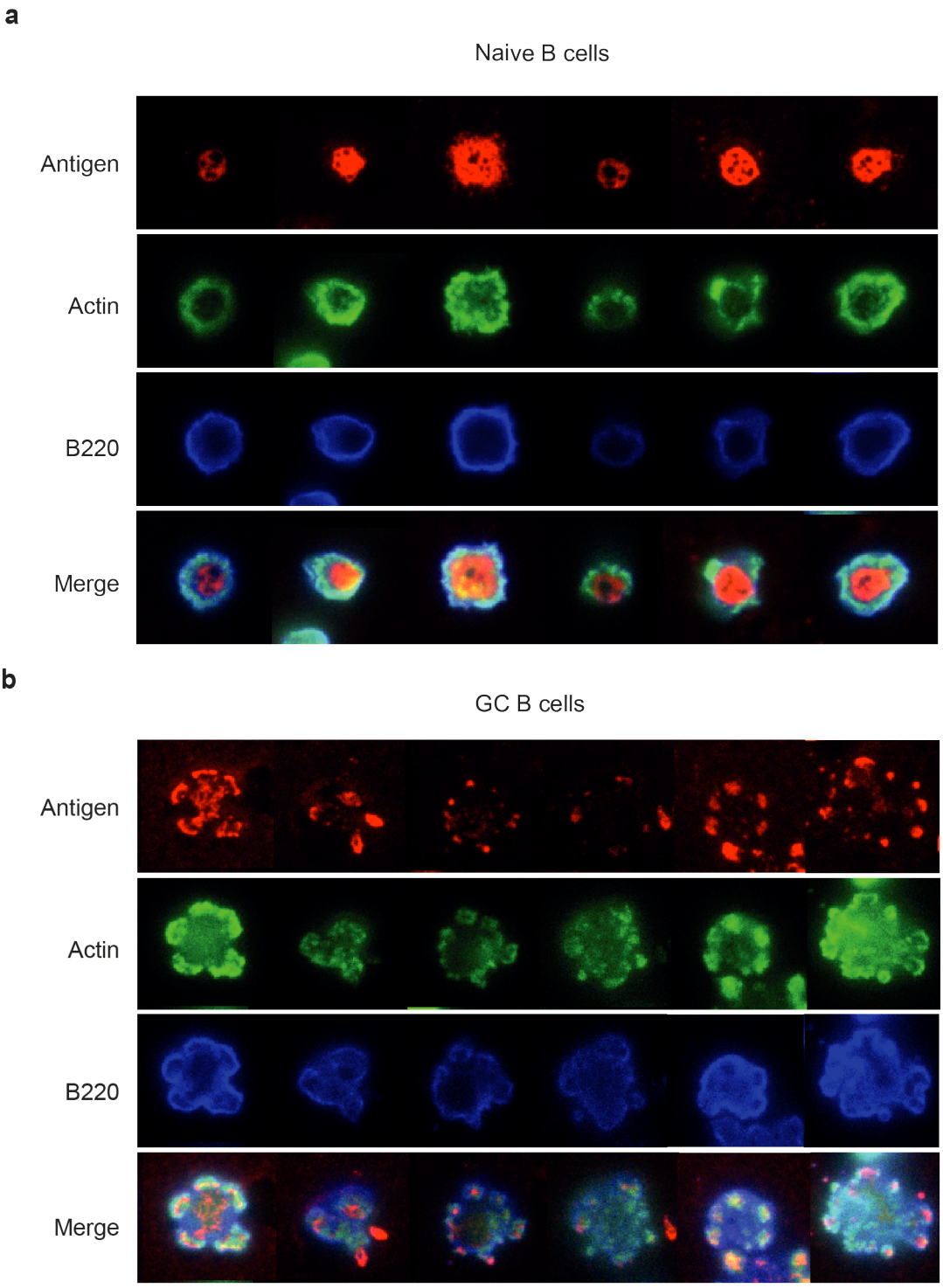

Figure 23 Actin patterning in naive and GC B cells forming synapses on PLBs

Image galleries showing F-actin staining with phalloidin in the synapse plane of naive (a) or GC (b) cells after 20 mins on anti-Igκ loaded PLBs.

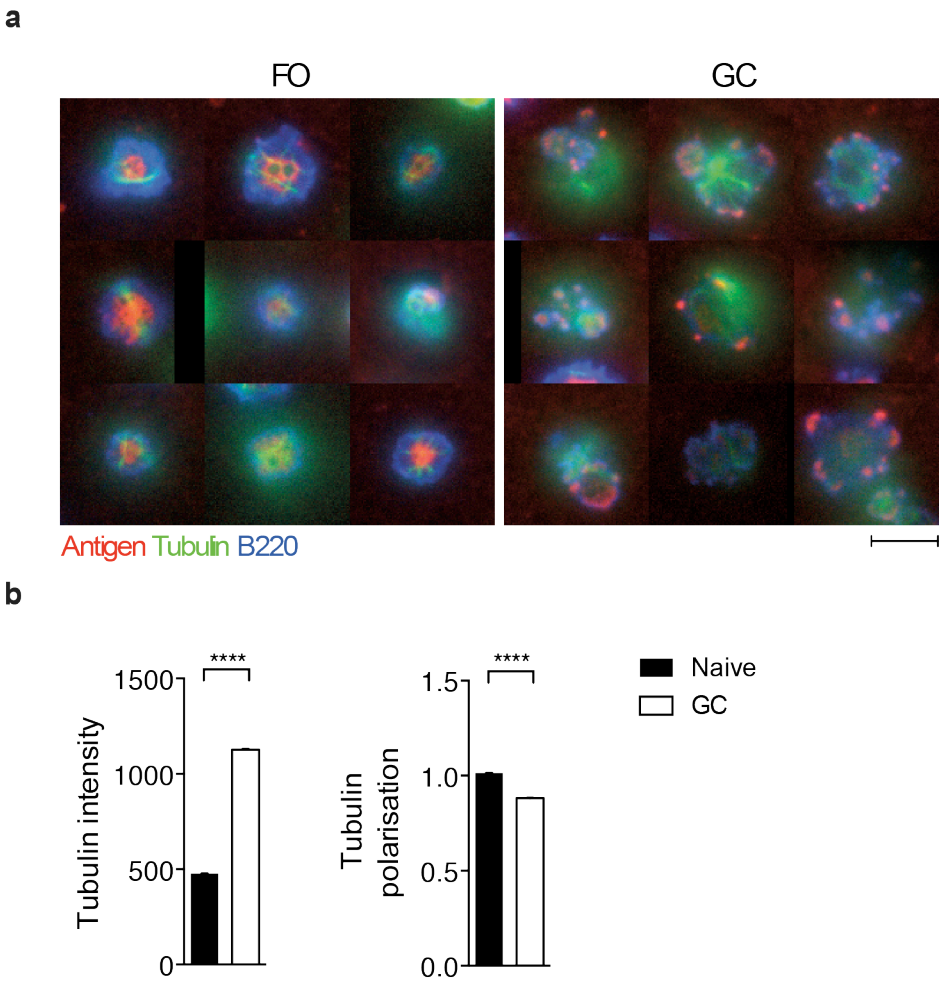

Figure 24 GC cells have reduced tubulin polarisation to the synapse

(a) Galleries of synapses from naive or GC B cells interacting with antigen on PLBs. Synaptic plane showed. Brightness of tubulin staining was matched between the two cell types in order to easily visualise individual microtubules despite the high tubulin intensity in GC cells. Scale bar 5μm.

(b) Quantification of total tubulin levels (left) and tubulin polarisation (right), calculated as the ratio of mean tubulin intensity in the synapse as compared to mean tubulin intensity in the entire cell. Data from one experiment representative of two independent experiments, means and s.e.m from n = 4429 naive and 3138 GC cells

4.2.3 GC synapse morphology is independent of kinetics

In order to better understand the peripheral nature of these unusual GC synapses, cellular dynamics were examined using live TIRF imaging on enriched GC populations. TIRF imaging allowed for a combination of high spatial and time resolution in the synapse. GC B cells were first identified by synapse shape and then confirmed by surface staining *in situ* post-acquisition with fluorescent peanut agglutinin (PNA). Live cell imaging showed that initial antigen binding and spreading phases looked very similar between GC cells and naive control cells (Figure 25, Movie 1). In naive cells a robust centralisation phase followed B cell spreading, involving BCR-antigen microcluster formation and growth during centripetal movement into the mature cSMAC, resulting in an aggregation of antigen under the centre of the contact interface between the cell and PLB. Although GC cells formed microclusters, these grew slowly, often due to a failure of individual microclusters to fuse with their neighbour, or due to dynamic cluster growth and reduction over the lifetime of the contact (Figure 26).

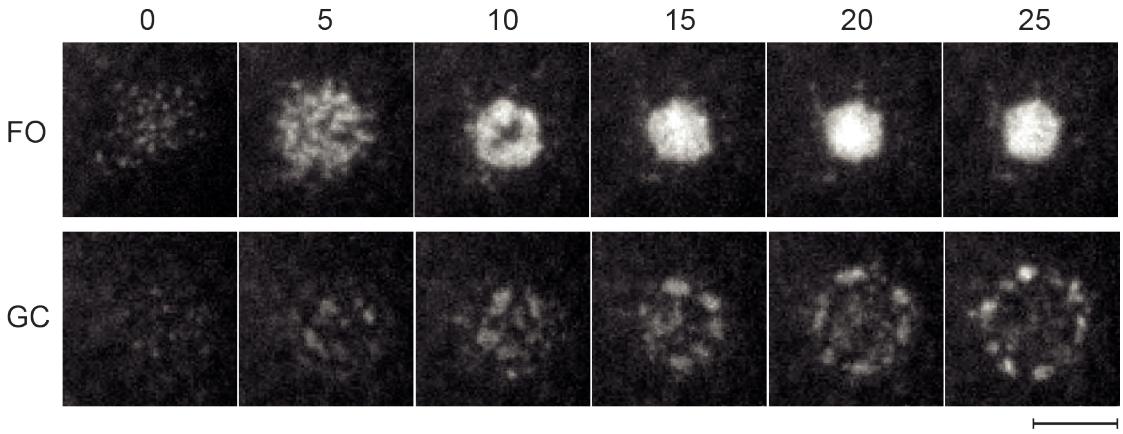

Figure 25 Tracking BCR receptor dynamics live in GC B cells

Stills showing antigen from time-lapse live TIRF microscopy. FO cells were isolated from the spleen; GC cells were isolated and enriched before imaging on anti-Igκ PLBs at 37°C. Cells were imaged at a time resolution of 5 seconds, numbers above panels describe time in minutes. Scale bar = 5μm.

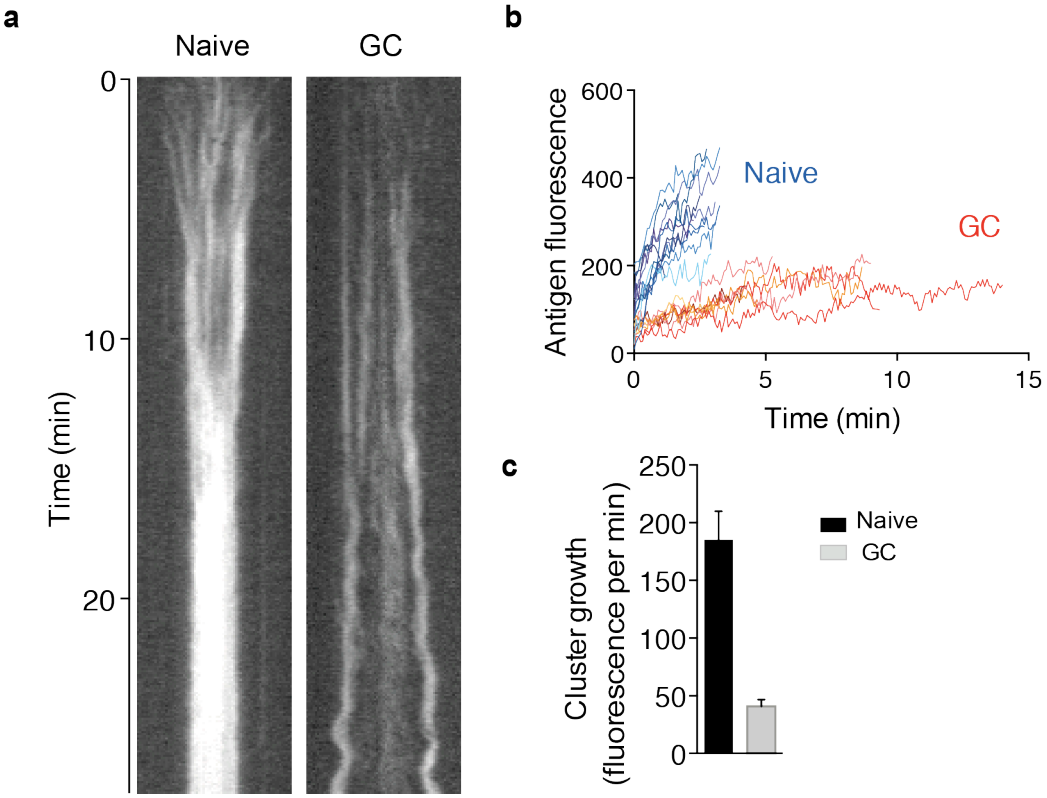

Figure 26 Cluster dynamics revealed by live time-lapse microscopy

(a) Kymographs of antigen (anti-Igκ) in synapses on PLBs.
(b) Fluorescence intensities of antigen clusters tracked from their appearance to either fusion with other clusters or their disappearance.
(c) Growth rates of antigen clusters in the first 2 min of synapse formation. Scale bar, 5 μm. *$P < 10^{-4}$ in an unpaired t-test. Data are from one representative cell from three experiments (a,b) or are from three experiments (c; mean and s.e.m. of n = 29 naive cell antigen clusters and 24 GC cell antigen clusters).

Instead of fusing, growing and moving towards the centre of the contact, GC clusters continually grew and shrank, ultimately remaining at a fairly constant size (Figure 26b). They were actively dispersed towards the periphery of the contact, leaving the central region predominantly clear of antigen-BCR microclusters. This effect did not change with time; clusters fluctuated dynamically, and were dragged both in and out over time (Figure 26 a,b). Clusters were surprisingly dynamic, often disappearing from view altogether, especially in the centre of the contact. They seemed to oscillate radially, sometimes in pulsating waves, which probably accounted for the occasional centralised antigen seen in fixed samples.

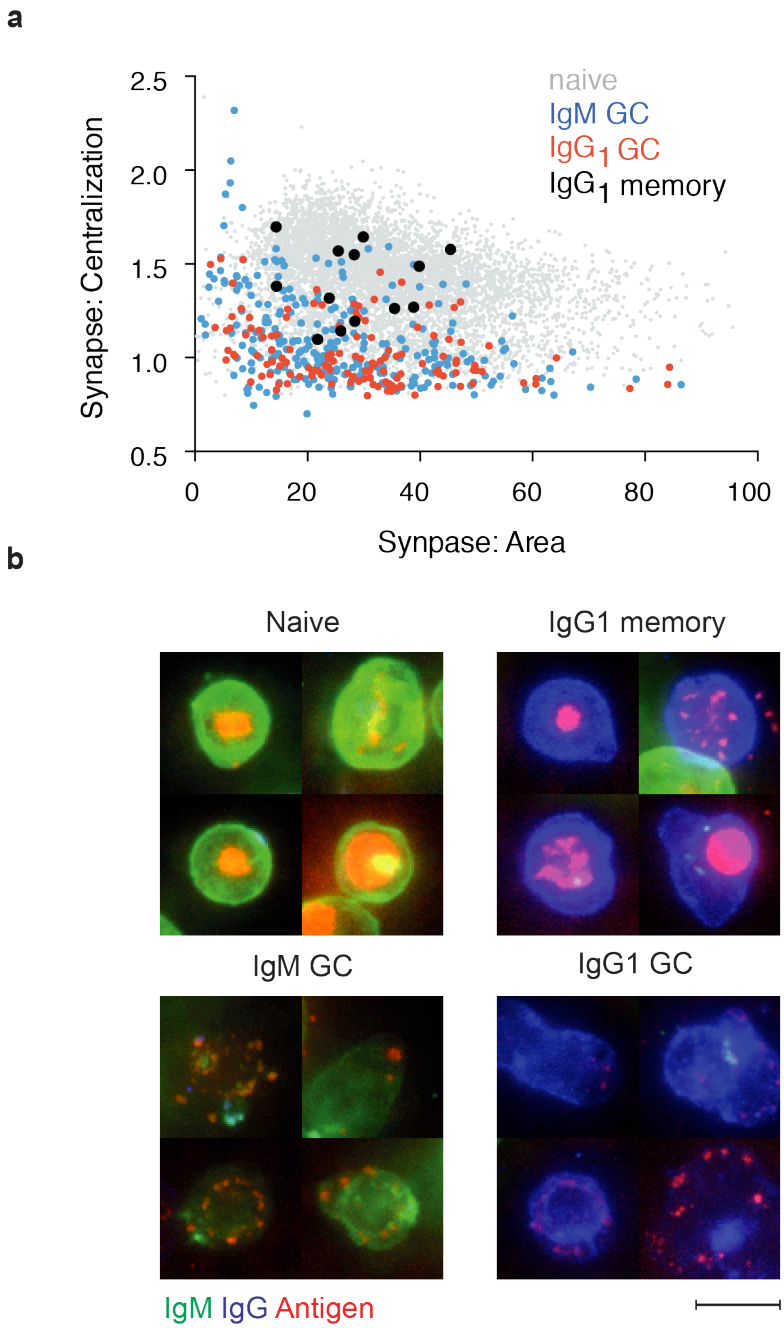

Figure 27 GC synapse architecture was independent of class-switch status

(a) Antigen centralization plot, each dot indicates and individual CellScore+ B220+ cell

(b) Maximum projections of synapses of cells from naive (B220+ Fas- CD38+ IgM+ IgG-), pre-enriched GC (B220+ Fas+ CD38- IgM+ IgG- or B220+ Fas+ CD38- IgM- IgG+) or memory (B220+ Fas- CD38+ IgM- IgG+) B cells from the same PLB and imaging chamber.

Data is from one experiment representative of four independent experiments

To investigate whether the BCR class-switching in the GC was responsible for synapse morphology, we stained for surface IgM and IgG. This was combined with staining for GC markers to separate GC non-switched, GC switched and non-GC switched cells. When extent of synapse centralization was plotted against total synapse area the two GC groups clustered together (low centralization), with non-GC switched cells clustering with naive cells (higher centralization, larger total synapse area) (Figure 27a). Image inspection of synapses confirmed that class-switch status did not affect GC synapse phenotype (Figure 27b)

4.2.4 Signalling in GC B cells

4.2.4.1 GC B cells flux calcium after BCR binding to membrane-presented antigens

To investigate the effects of membrane-presented antigen binding on the cellular signalling capabilities of GC cells compared with naive cells we first measured calcium fluxing with live, 3-D, time-lapse microscopy. Enriched GC B cells or naive B cells were loaded simultaneously with a ratiometric pair of calcium indicators, Fluo-4 and Fura Red. During imaging, Fluo-4 fluorescence rapidly increased before levelling out over time (Figure 28a, Movie 2), and when Fluo/Fura ratios were plotted GC cells produced typical calcium traces, where a characteristic flux occurred immediately after antigen binding (Figure 28b). Compared to naive cells, traces looked very similar, although overall, GC cells fluxed slightly more calcium over time when total levels were quantified (Figure 28 b,c).

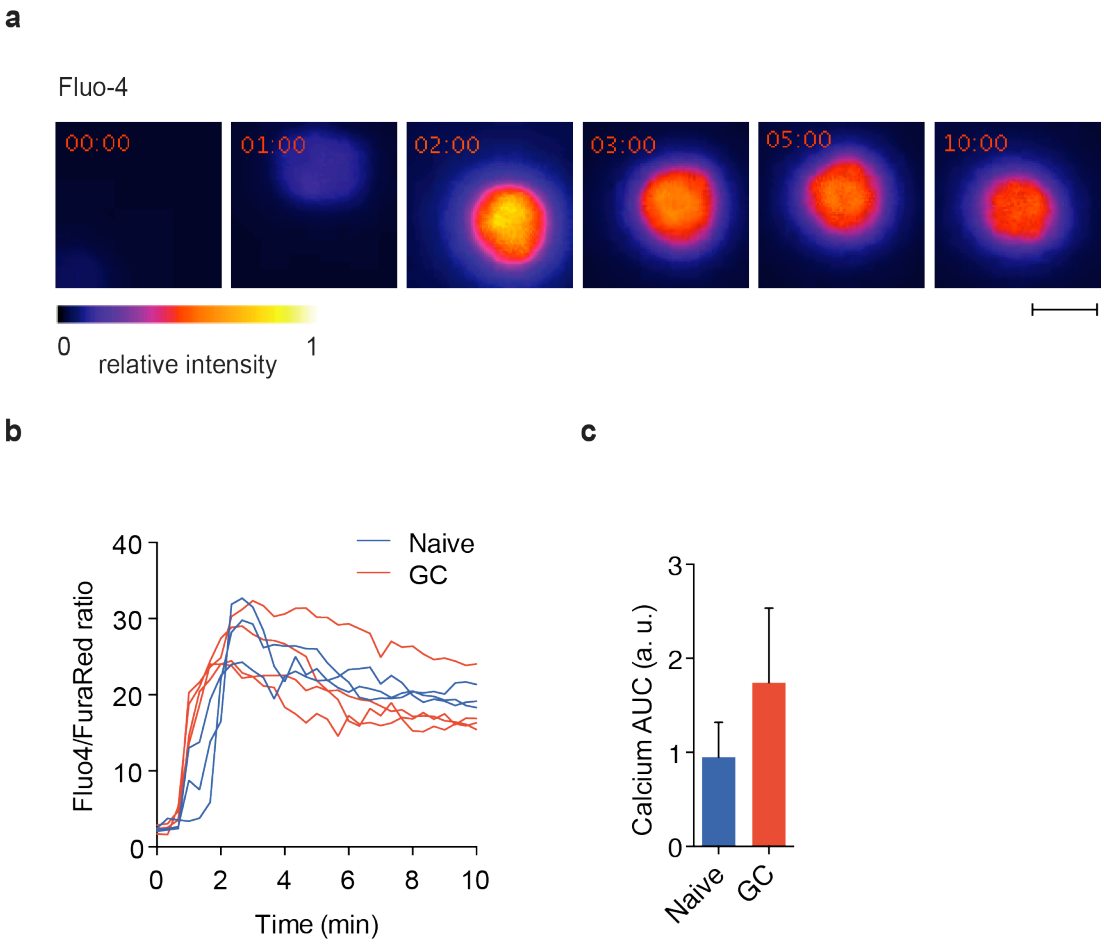

Figure 28 GC cells flux calcium after binding membrane-bound antigen

(a) Stills from live imaging of a GC-cell loaded with Fura red (not shown) and Fluo-4 calcium indicators, colours denote indicated fire-scale. GC cells were isolated from the spleen and pre-enriched before dye loading. GC phenotype determined by synapse shape and *in situ* PNA staining post-acquisition. Time resolution 20 seconds, numbers above panels are time in minutes. 4 Z-slices per acquisition, Fluo-4 and Fura Red channels imaged simultaneously. Scale bar = 5µm.

(b) Traces of Fluo-4/Fura Red ratios from multiple GC or naive B cells over time.

(c) Quantification of total calcium levels, AUC = Area Under Curve.

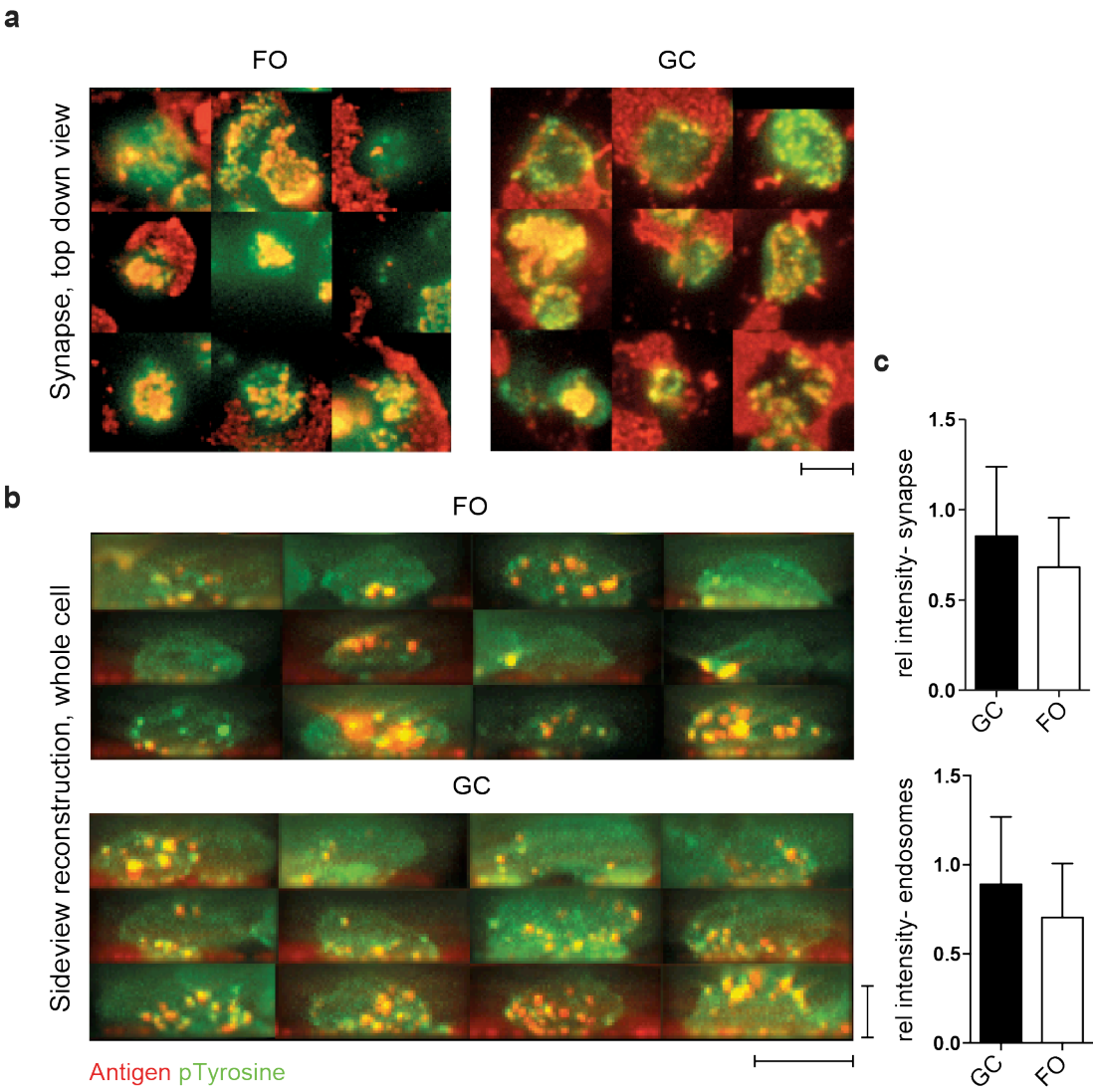

Figure 29 Phospho-tyrosine staining can read out BCR signalling in GC and naive B cells

Naive and pre-enriched GC cells were incubated together on anti-Igκ-loaded PMS for 20 minutes before fixing, surface staining and pTyr intracellular staining. GC cells identified as B220+ Fas+.

(a) Galleries of a top-down view of the synapses of naive and GC B cells recalled at random from gates applied to a Fas/B220 dot plot (not shown).

(b) Sideview reconstruction galleries showing internalised antigen and pTyr staining on endosomal compartments in naive and GC B cells.

(c) Quantitation of intensity of pTyr in either synapses or on endosomes of naive and GC B cells. Data from 3 independent experiments.

Scale bar = 5μm

4.2.4.2 BCR signalling in GC B cells

The BCR signalling cascade occurs through a highly regulated network of tyrosine kinases, and henceforth, we carried out intracellular staining of phospho-tyrosine (p-Tyr) as a broad readout of BCR signalling. GC B cells had a tendency towards higher levels of p-Tyr compared with naive B cells, both in the synapse and on extracted clusters of antigen (Figure 29). To better dissect the contribution of different components of the BCR signalling cascade in GC cells we systematically stained for a range of molecules downstream of the BCR individually, beginning with phosphoylated BLNK (p-BLNK) (Figure 30).

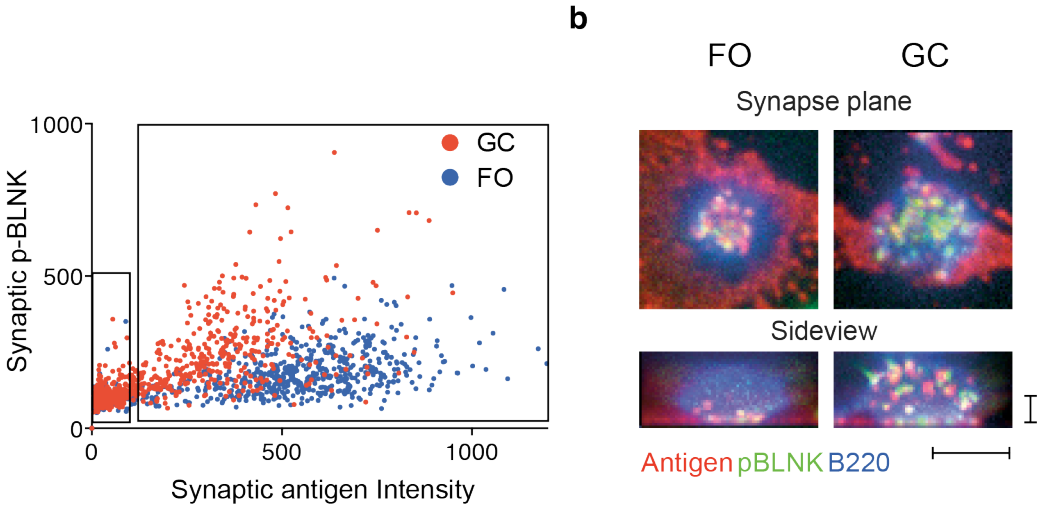

Figure 30 Phosphorylated BLNK is upregulated in GC B cells

(a) Dotplot of synaptic p-BLNK levels in naive and pre-enriched GC synapses imaged simultaneously on anti-Igκ-loaded PMS. Large gate= cells on PMS, small gate = cells outside of PMS.

(b) Images of a single naive or GC cell showing p-BLNK staining both in the synapse and on endosomes (lower panel, sideview reconstruction). Scale bar = 5μm

In the single cell images, p-BLNK was clearly more abundant in the GC B cell (Figure 30b), and was present in similarly high levels on extracted antigen clusters as well as in the synapse. This was in contrast to the naive B cell, whose p-BLNK was localised mostly in the synapse with decreased signalling after antigen extraction. On the population level, this observation was substantiated across dot plots of a single data set (Figure 30a) and in bar graphs collated from multiple data sets (Figure 31). When other members of the BCR signalling cascade were investigated, they too displayed matching signalling profiles both visually and quantitatively over populations of cells (elevated upon antigen binding) (Figure 31, Figure 32).

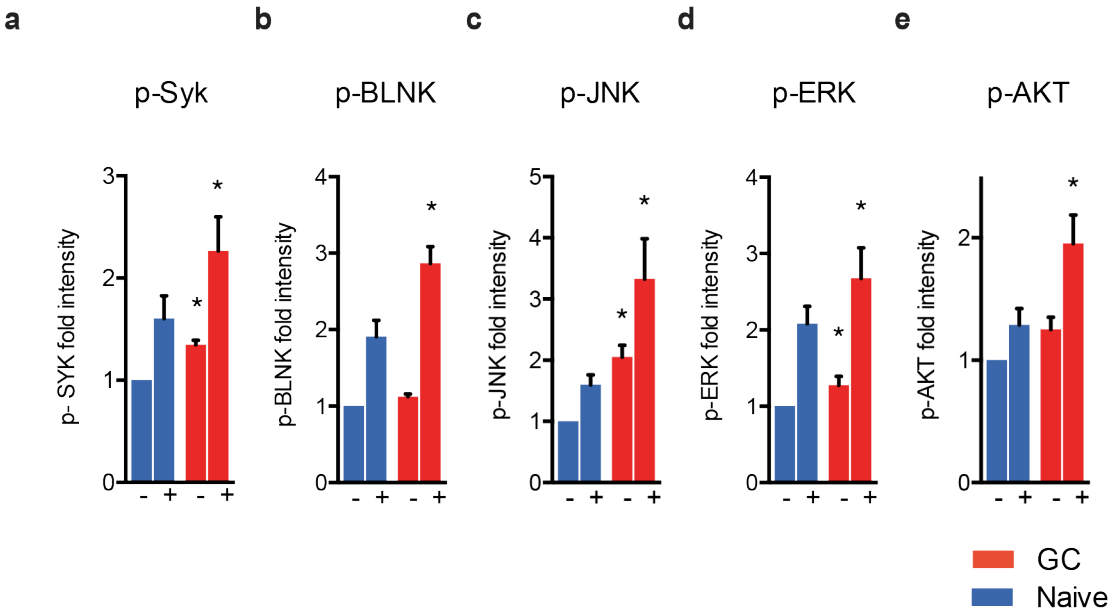

Figure 31 GC B cells exhibit increased BCR signalling when stimulated with membrane-bound antigen

(a-e) Quantification of intracellular BCR signalling in naive or GC B cells either outside (-) or on (+) anti-Igκ loaded PMS. Synapses analysed after either 10-mins (SYK) or 20 mins (all other staining) on PMS. Data are normalised to the signal of naive B cells, outside of PMS. *P < 0.05, GC vs naive cells in paired t-tests. Data are mean and s.e.m. from three independent experiments per molecule.

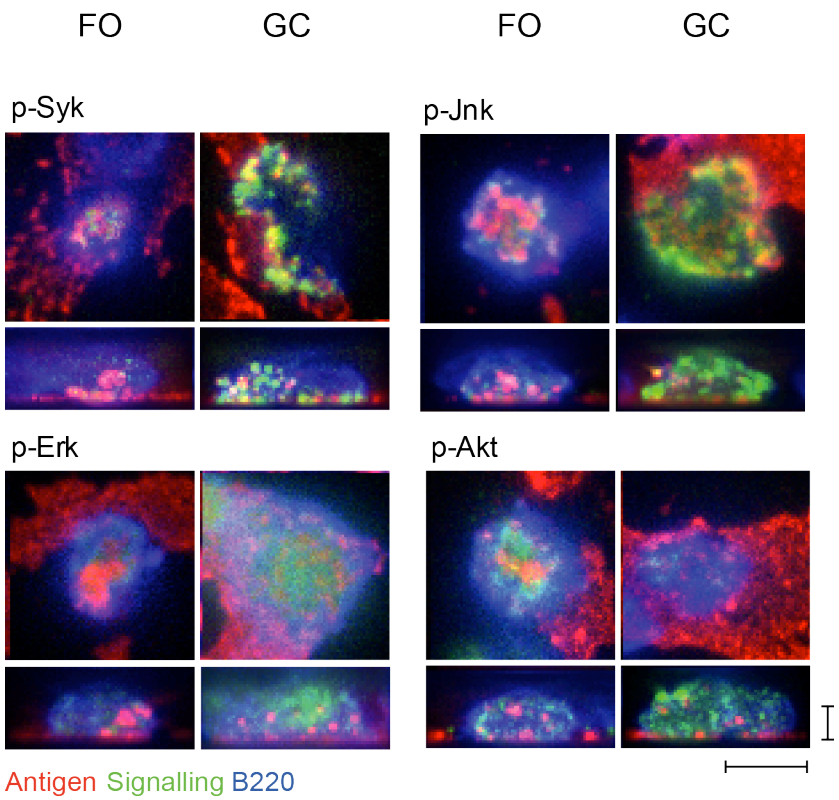

Figure 32 Galleries of intracelluar signalling stains in naive and GC B cells

Top- down synapse views (top panel) and sideview reconstructions (bottom panel) of a single naive and GC cell for each of the BCR signalling molecules shown in Figure 24. Naive or pre-enriched GC cells were incubated on anti-Igκ loaded PMS for 10 minutes (SYK) and 20 minutes (all others) before signalling molecules were stained by intracellular staining. Scale bars = 5μm.

In addition to significant upregulation of phospho-BCR signalling molecules after BCR-crosslinking, GC B cells exhibited significantly higher basal signalling levels (p-SYK, JNK and ERK) (Figure 31 a,c,d), and thus we refer to this phenotype as the 'GC signalling profile'. Cellular localisation of signalling molecules varied, appearing to correlate with position in the BCR signalling cascade. Early signalling molecules Syk and BLNK and JNK were localised in close proximity to membranes at the synapse and on endosomes, colocalised with antigen clusters, whereas later molecules such as ERK and AKT were dispersed throughout the entire cell and rarely colocalised with antigen.

These data show that GC B cells respond proficiently when stimulated with antigen presented in the context of a membrane, and upon antigen internalisation BCR signalling is not dampened, but rather is sustained and propagates up throughout the cell.

4.2.4.3 Inhibitory signalling in GC B cells

Molecules known to be important in an inhibitory or regulatory capacity are also able to signal through tyrosine phospohorylation. One such molecule in B cells is CD22. CD22 was lower in GC cells than in naive B cells, and levels remained unchanged following antigen binding in either cell type (Figure 33 a,c). This data implied CD22 did not contribute to the high levels of antigen-dependent p-Tyr seen in GC B cells after activation.

We also checked levels of p-SHIP-1, a phosphatase known to be important in modulation of BCR signalling and implicated in dampening BCR signalling in GC B cells (Khalil et al. 2012). Surprisingly, this phosphatase also followed the GC signalling profile observed in activating BCR signalling (Figure 33 b,c), suggesting that enhanced BCR signalling in GC B cell synapses proceeds despite high levels of this phosphatase.

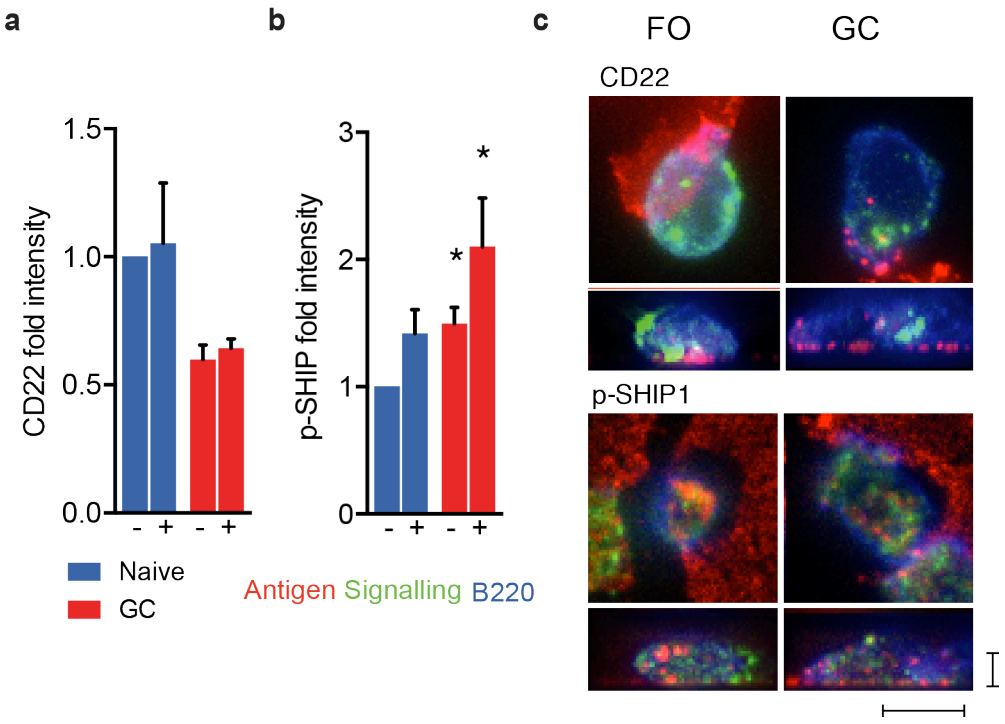

Figure 33 Inhibitory signalling in GC B cells

(a,b) Quantification of intracellular inhibitory BCR signalling molecules in naive or GC B cells either outside (-) or on (+) anti-Igκ loaded PMS after 20 minutes. Data are normalised to the signal of naive B cells, outside of PMS. Data from three independent experiments (p-SHIP) and one experiment (CD22).

(c) Top- down synapse views (top panel) and sideview reconstructions (bottom panel) of a single naive and GC cell for each inhibitory molecule.

*P < 0.05, GC vs naive cells in paired t-tests. Data are mean and s.e.m.
Scale bar = 5μm.

4.2.4.4 Cytoskeletal signalling in GC B cells

The importance of various members of the cytoskeleton for synapse formation has long been established. As an extension of earlier studies establishing differences in microtubule and actin patterning we used a range of specific intracellular stains to quantitate total levels of tubulin (Figure 24, shown again in Figure 34 for comparison), filamentous (f)-actin (using phalloidin) (Figure 34b) and activated myosin IIA (using an antibody against activated phosphorylated myosin light chain (MLC)) (Figure 34, Figure 35b). As stated previously, tubulin levels were more than doubled in GC cells, though mictrotubule polarisation was reduced.

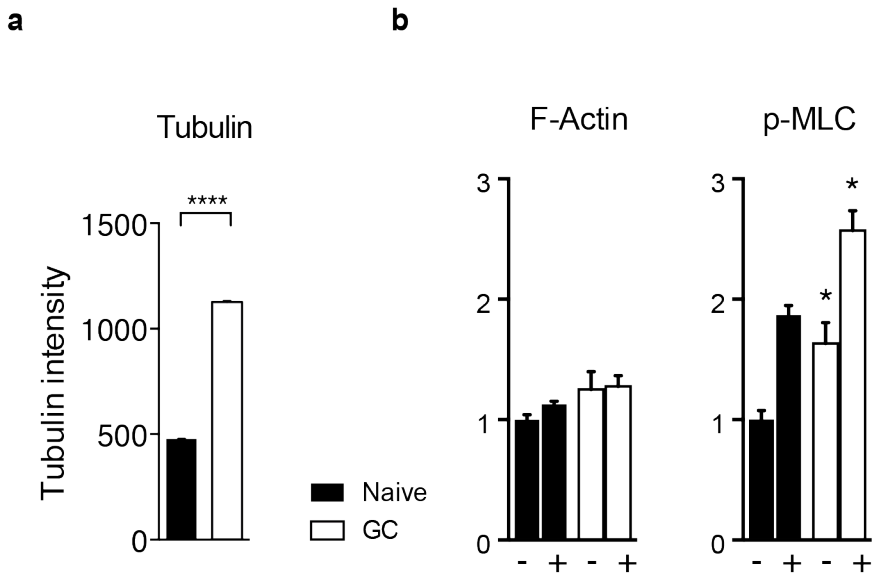

Figure 34 Cytoskeletal signalling in GC B cells

(a) Quantification of total tubulin levels tubulin in whole naive or pre-enriched GC cells (as shown previously in Figure 24) ****$P < 10^{-4}$

(b) Quantification of intracellular actin or myosin in naive or GC B cells either outside (-) or on (+) anti-Igκ loaded PMS after 20 minutes. Data are normalised to the signal of naive B cells, outside of PMS. *$P < 0.05$

Data are means and s.e.m. from three independent experiments .

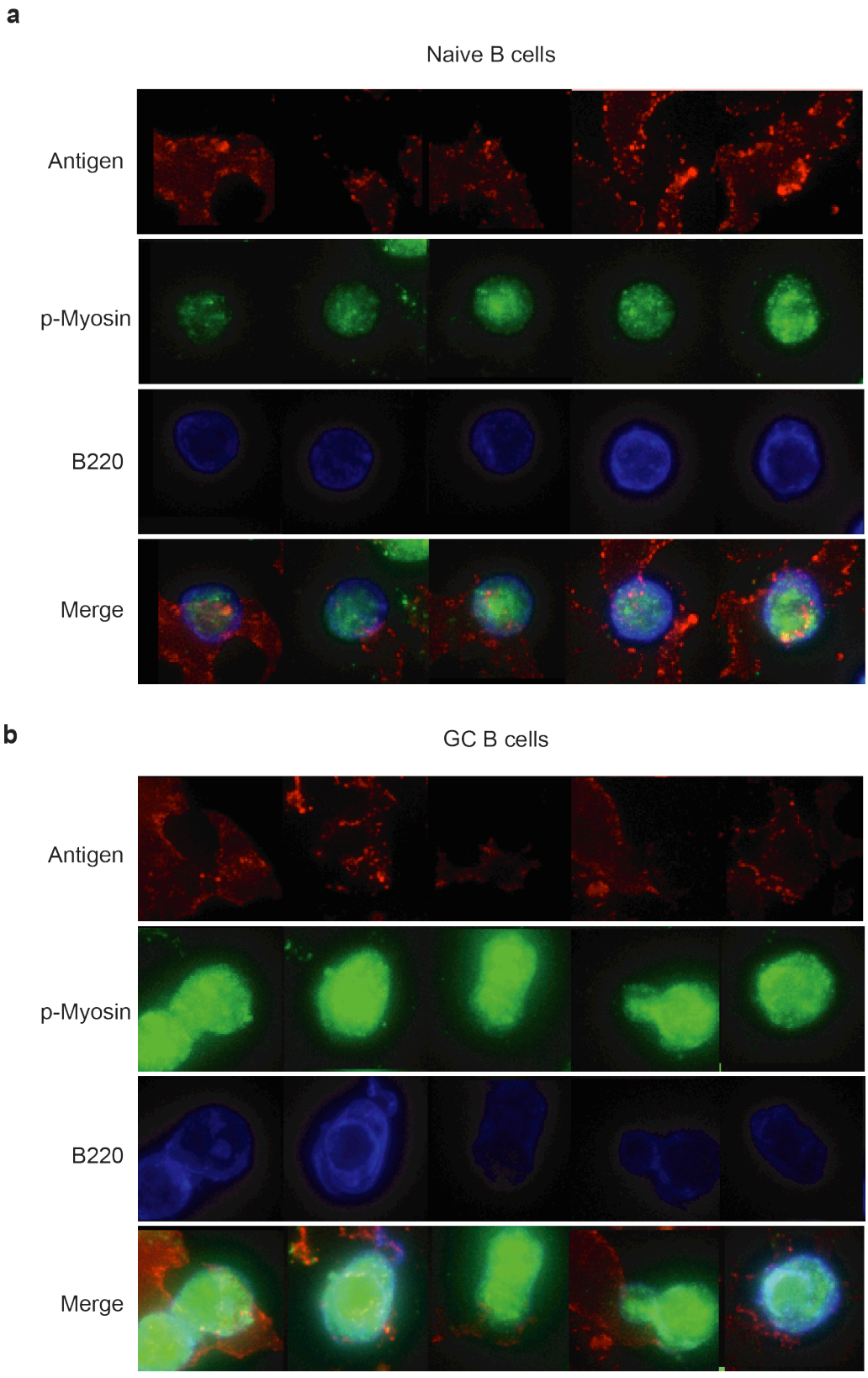

Figure 35 Galleries showing myosin IIA relative intensity in naive and GC cells

Figure 35 Galleries showing myosin IIA relative intensity in naive and GC B cells

Galleries showing myosin IIA staining in 5 naive and GC B cells after activation on PMS. Fluorescence was matched in all channels.

Although actin-antigen localisation was noticeably altered in GC cells, total amounts of F-actin were very similar between the two cell types (Figure 34b). This was in sharp contrast with activation of the contractile force-generating molecule, myosin IIA. Myosin IIA is known to play important roles in the contraction phase of synapse formation and is indispensible for antigen internalisation in naive B cells (Natkanski et al. 2013). In GC B cells, myosin also fits the stereotypical 'GC profile' of signalling as it was significantly more phosphorylated at baseline as well as after activation (Figure 34, Figure 35b). Myosin localisation was altered in GC cells, where, instead of gathering in spots above the synapse, it was localised in the periphery, closely associated with antigen clusters (Figure 36).

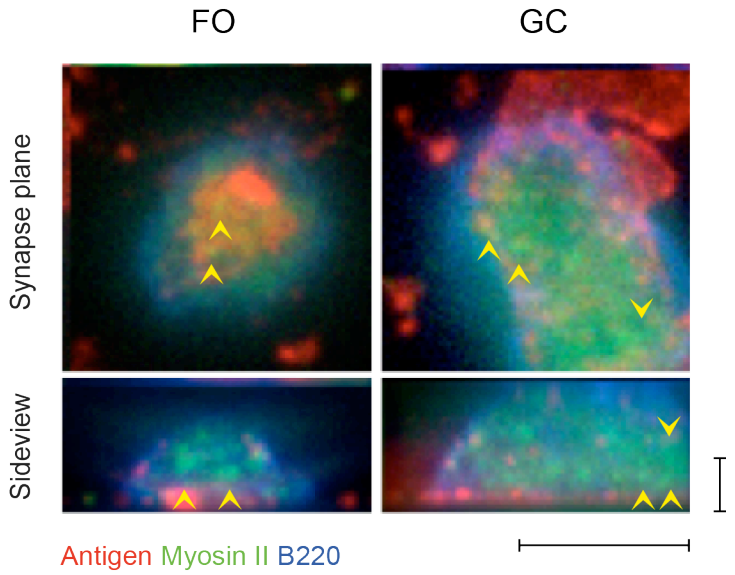

Figure 36 Myosin IIA localisation in naive and GC cells

Top down and sideview reconstructions of single cells to show where myosin IIA localised after synapse formation and antigen internalisation on PMS. Arrows show myosin IIA clusters. Scale bars = 5μm.

All staining carried out in this section (4.2.4- BCR signalling in the GC) was sensitive to inhibition by pharmacological inhibitors of upstream signalling molecules (Figure 37).

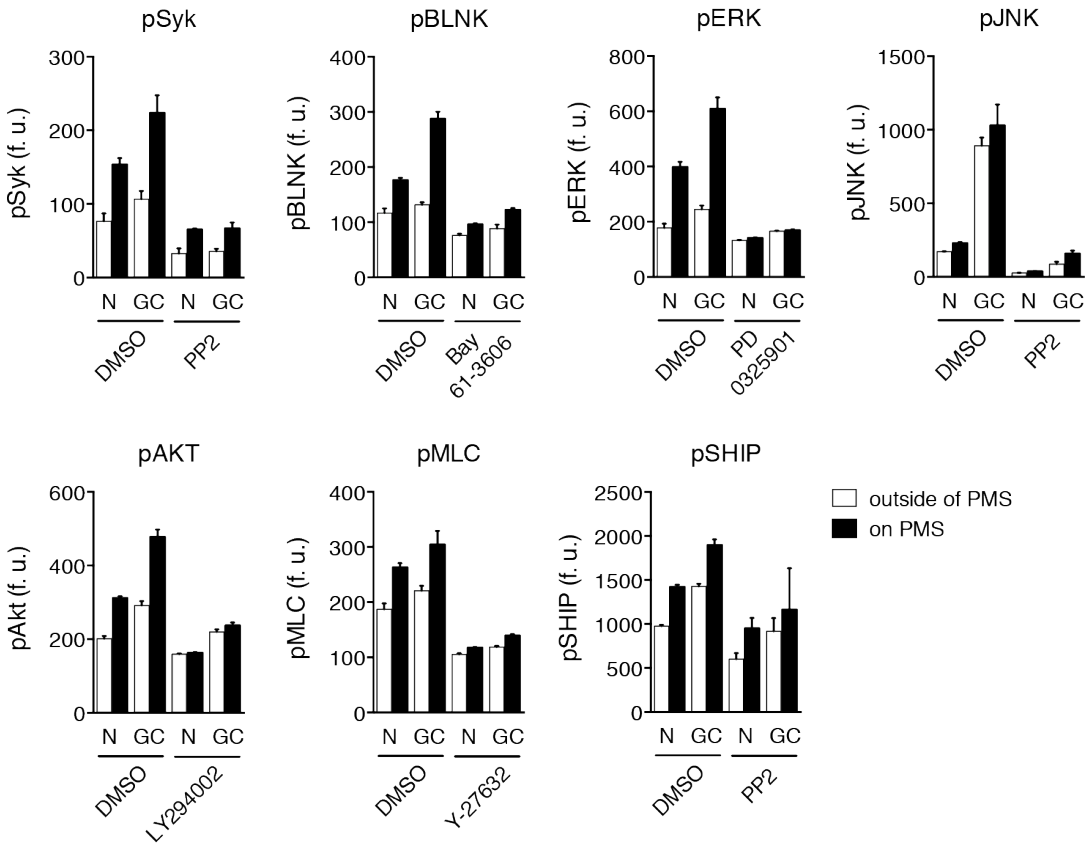

Figure 37 Pharmacological inhibitors confirm effective intracellular staining of signalling molecules

Naive and enriched GC B cells were treated with DMSO or the indicated inhibitors, incubated with PMSs containing anti-Igκ antigen, fixed and stained with the phospho-specific antibodies. Staining was analyzed in synapses (p-Syk, p-BLNK, p-JNK, p-SHIP) or whole cells (p-Erk, p-Akt, p-MLC) gated on naive (N) or GC B cells outside and on the PMSs. Inhibitor names under bars on graph, molecule inhibited above graph.

4.2.4.5 Characteristics specific to stimulating antigens or presenting membranes affect GC signalling

As more information is gleaned surrounding antigen acquisition by B cells, the importance of antigen format has become more pertinent. Antigen format, and its related accessibility to the BCR, is expected to play a role in signal propagation through the BCR. To this end, we stimulated GC B cells with the same antigen in a soluble rather than membrane-bound form to investigate whether antigen format affected signalling in GC B cells. Naive cells phosphorylated all tested BCR signalling molecules to a higher extent than GC cells after soluble antigen stimulation and measurement by flow cytometry, the exception being p-JNK which neither cell type upregulated (Figure 38).

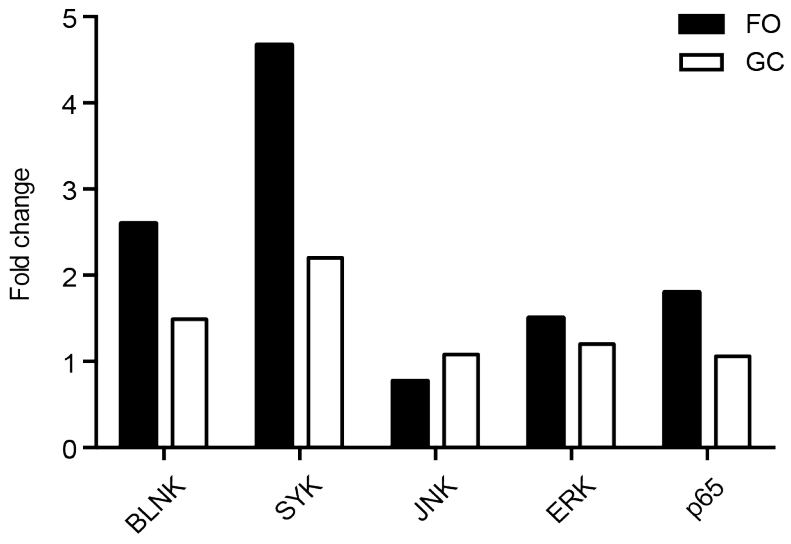

Figure 38 Soluble antigen stimulation results in less signalling by GC B cells
Bar graphs comparing naive and GC flow cytometry data for a range of signalling molecules. Data normalised to unstimulated cells. Data from two independent experiments.

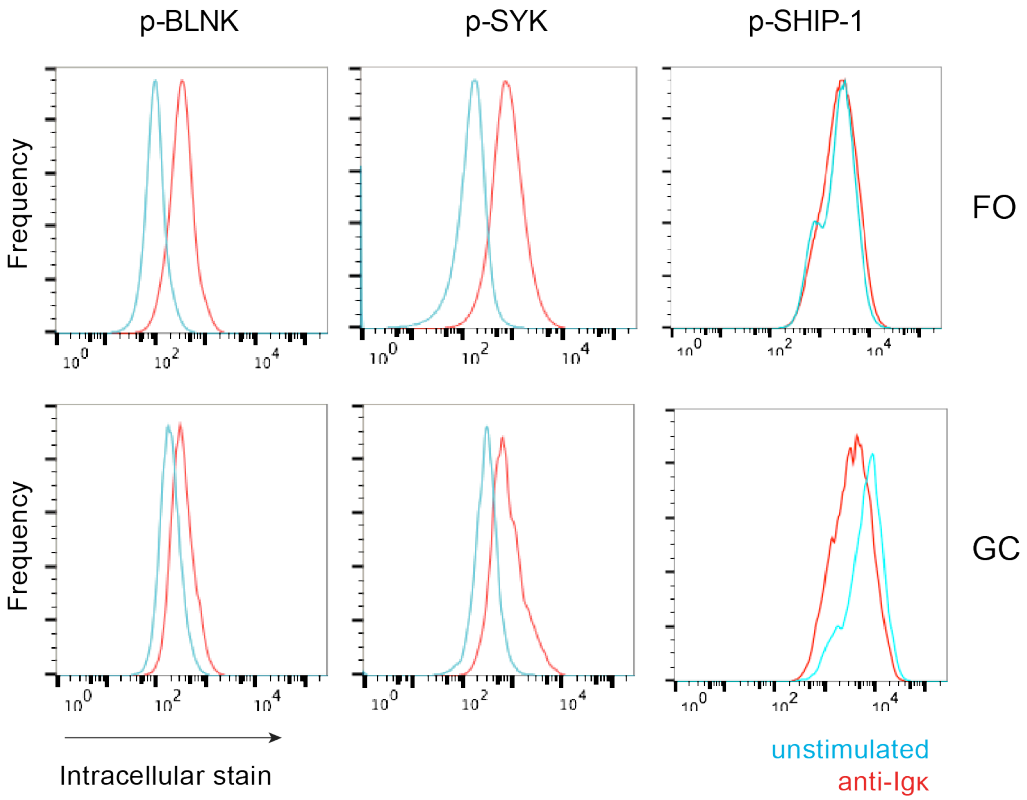

Figure 39 BCR signalling after soluble antigen stimulation

Intracellular staining in unstimulated and anti-Igκ stimulated naive and GC B cells analyzed by flow cytometry. Signalling molecules stained above plots.

GC cells had raised basal p-SHIP levels, which decreased after antigen stimulation (Figure 39). Levels of p-SHIP in naive cells remained unchanged following antigen stimulation. This profile of dampened BCR signalling and high phosphatase activity following stimulation with soluble antigen is in agreement with previously published data (Khalil et al. 2012). The discrepancy between signalling profiles in soluble vs. membrane-bound scenarios confirms that antigen format is important, and GC cells tune their signalling responses depending on the nature of their BCR engagement.

We observed another interesting phenomenon relating to the characteristics of the presenting membrane. In these experiments we compared signalling induced by antigens on PLBs or PMSs. A major difference between PMS and PLBs is membrane flexibility, with PLBs providing a much stiffer membrane than PMS.

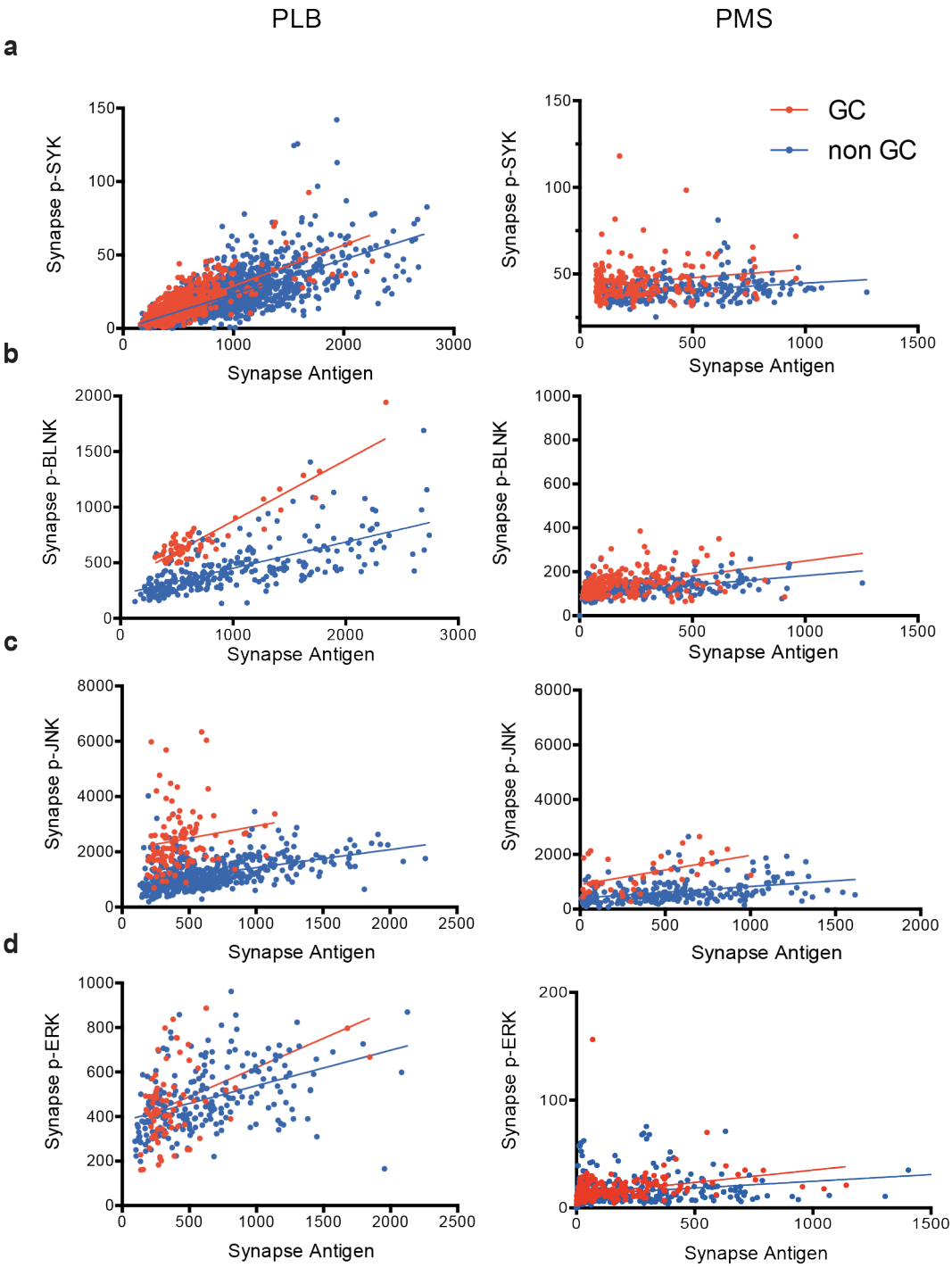

Figure 40 Induction of BCR signalling is dependent on membrane stiffness

Dotplots of p-signalling molecules in the synapses of naive and GC B cells after incubation on PLBs or PMS. Each dot represents a single B220+ Fas+ GC cell (red) or a single B220+ Fas- naive cell (blue).

After incubation on anti-Igκ-loaded PLBs (stiff substrate), BCR signalling was more potently upregulated than on PMS (soft substrate) (Figure 40). On both substrates GC signalling was higher than naive, but differences were amplified as substrate stiffness increased. This trend remained visible in some preliminary data obtained from antigen immobilised on a completely inflexible glass coverslip (data not shown), where BCR signalling was most intensely induced. The effect of substrate stiffness therefore appeared to affect all B cells in surrogate membrane systems, but amplified existing differences observed between naive and GC cells.

4.2.5 Antigen Internalisation by GC B cells

Antigen extraction and internalisation was investigated in GC B cells using PMS, which we previously showed supported antigen internalisation by naive B cells (Section 3.2.5) (Natkanski et al. 2013). We first investigated whether GC cells were capable of efficient internalisation of antigen, and how this compared to their naive counterparts. Following image recall and sideview reconstruction of naive and GC cells on PMS antigen could be seen inside both cell types (Figure 41), showing GC cells certainly were internalisation-competent.

Following formal quantification, we saw that whilst there was not a significant difference in total antigen amount internalised (Figure 42 a, b), other differences could be detected by more richly mining our dataset. When we examined features of antigen clusters internalised by either cell type we saw GC B cells internalised significantly more clusters than naive cells and these correspondingly were smaller in size (Figure 42 c,d). Therefore, GC B cells internalised a greater number of small sized antigen clusters, localised in the periphery of synaptic contacts formed with membrane-presented antigen.

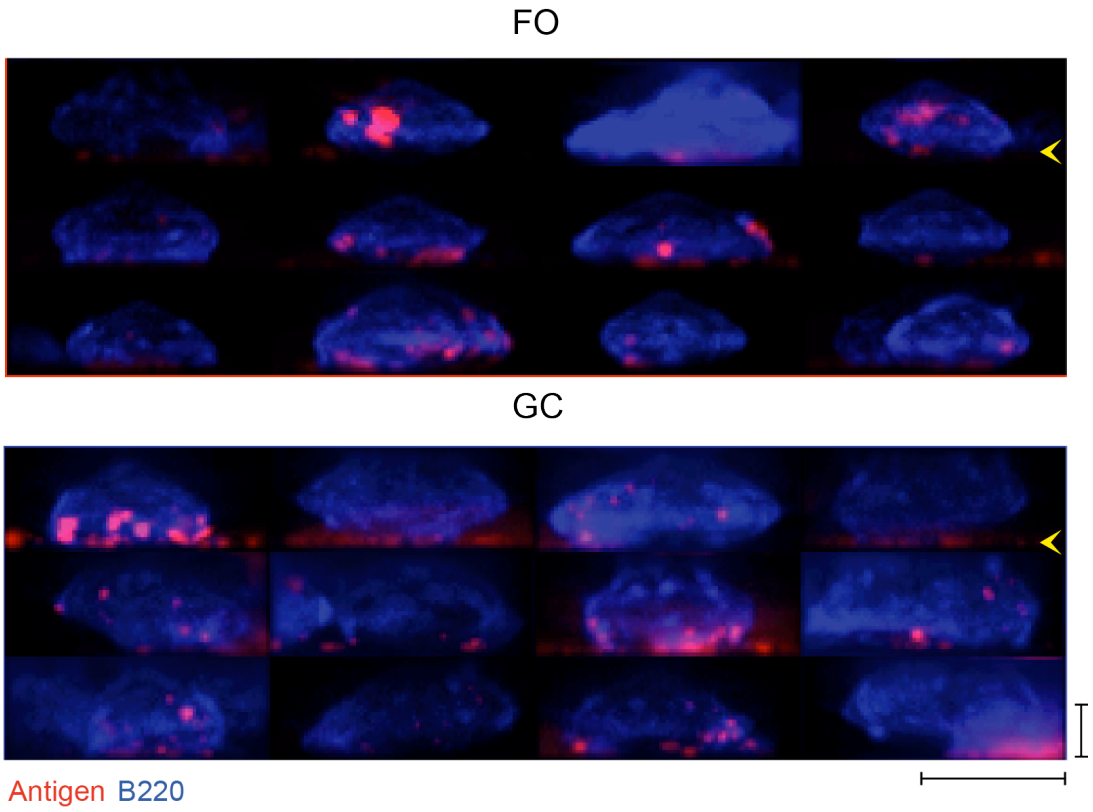

Figure 41 GC B cells internalise antigen from PMS

Sideview reconstruction galleries of naive and GC (Fas+) B cells incubated with anti-Igκ-loaded PMSs for 20 min. Images recalled at random from FO and GC gates set on surface marker expression of B220 and Fas. Yellow arrows indicate PMS. Scale bars = 5μm

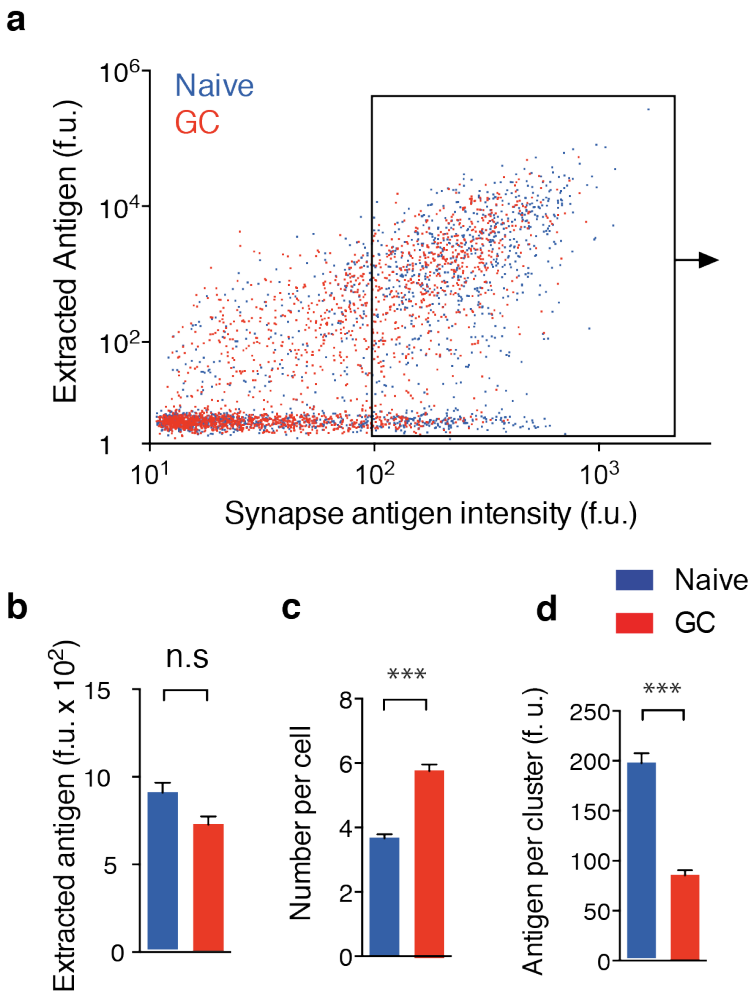

Figure 42 Quantification of internalisation in naive and GC B cells on PMS

(a) Quantification of total extracted antigen per cell after 20 min on PMS. For visualisation, cells with zero antigen extraction were assigned a random background value. The box shows cells that interacted with PMSs and were therefore considered for analysis. FU, fluorescence units. Data representative of five independent experiments

(b) Quantification of features of extracted antigen clusters, Data representative of five independent experiments, mean and s.e.m. of *n* = 982 naive cells or 854 GC cells. ***P < 10^{-4} n.s = not significant.

4.2.6 Antigen internalisation in GC B cells is signalling-dependent

In naive B cells various molecules have been identified as important mediators of the antigen internalisation process. Internalisation of antigen is a process unique to B cells, although it is as yet unknown whether a conserved mechanism exists within B cell populations. To investigate mechanisms by which GC cells extract, internalise and process antigen a range of pharmacological small-molecule inhibitors were used to block regulators of internalisation (Figure 43).

Blocking various cytoskeletal and endocytic proteins resulted in a reduction in antigen extraction in all B cells. Blocking dynamin (with Dynasore), a protein critical for endocytosis, caused the most dramatic phenotype in both naive and GC cells. Blocking myosin IIA (with Blebbistatin) also significantly reducing antigen extraction.

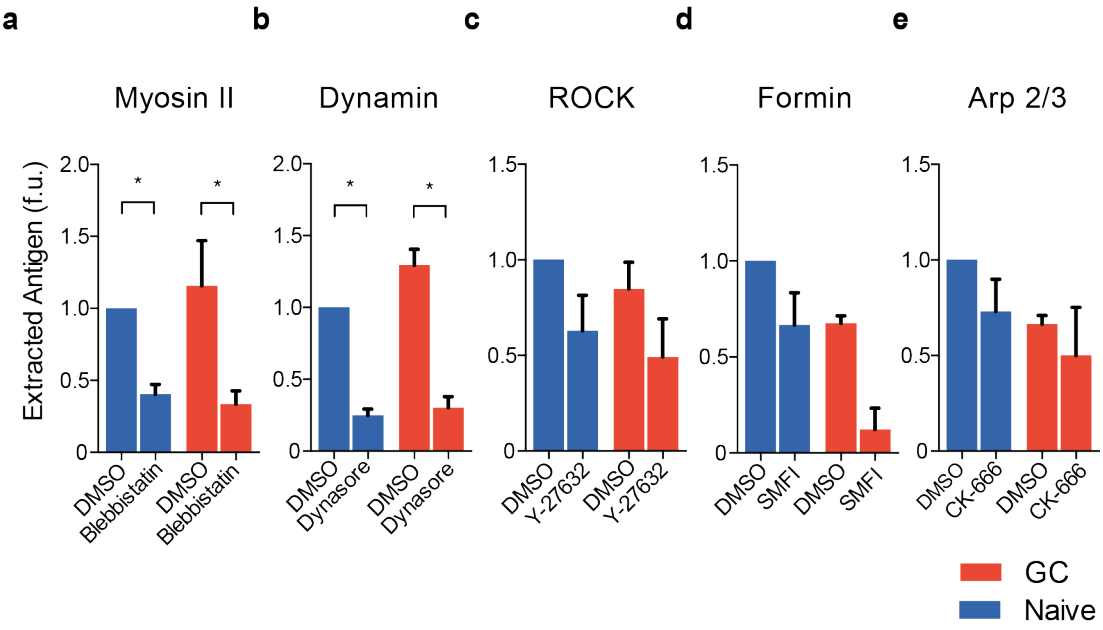

Figure 43 Inhibiting cytoskeletal molecules affects antigen extraction in naive and GC B cells

Effects of inhibition of a range of molecules in the cytoskeleton on antigen extraction. Results normalised to extraction in DMSO treated naive control B cells. *P < 0.05 in paired t-tests. Data are means and s.e.m. of three (a,b), two (c,d) or one (e) independent experiments. f.u., fluorescence units

Rho-associated protein kinase (ROCK) increases activity of myosin IIA by directly phosphorylating myosin light chain through serine-threonine kinase activity. When inhibited however, modest effects were seen on antigen extraction in both cell types compared with inhibition of myosin IIA itself (Figure 43 a,c). Formins and actin-related protein (Arp) 2/3 are both actin nucleators, controlling either polymerisation or branching of filamentous actin in the cortical cytoskeleton. Similarly, inhibiting these molecules had varying, usually modest effects on antigen extraction in both cell types (Figure 43 d,e).

BCR signalling was inhibited in a number of ways- ranging from broad-spectrum SRC-family kinase inhibitors (PP2, Bosutinib), to specific, single-kinase inhibitors, such as the very potent SYK inhibitor, PRT062607. When any element of proximal BCR signalling was inhibited antigen extraction was severely compromised in both cell types (Figure 44 a-c). These data suggest that GC B cells, similarly to their naive counterparts, are dependent on BCR signalling and myosin IIA contractility for efficient internalisation of antigen from membrane substrates.

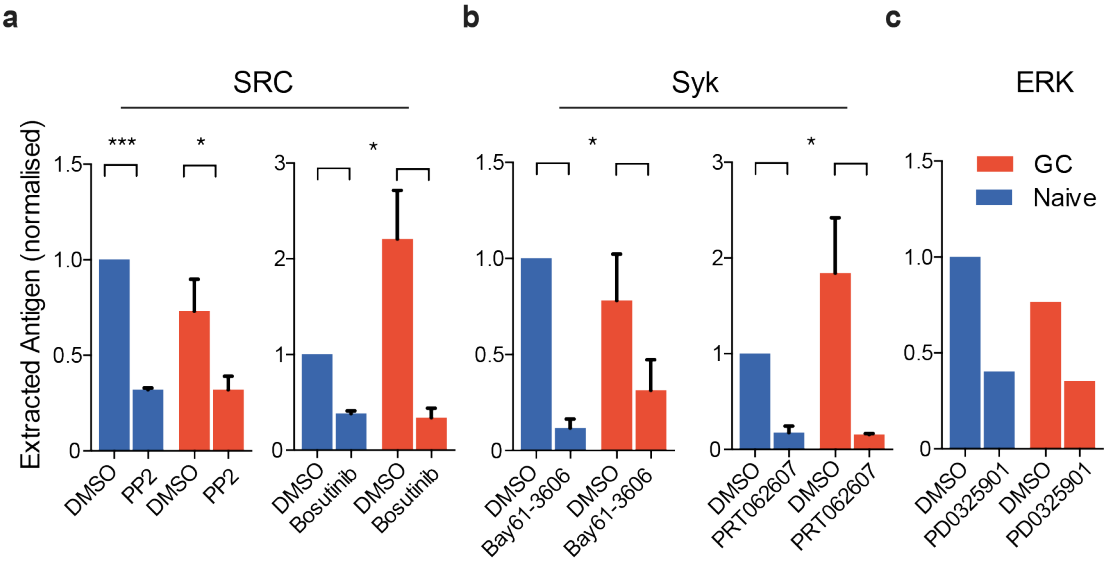

Figure 44 Antigen extraction is BCR signalling-dependent in all B cells

Effects of signalling inhibition on antigen extraction in naive and GC B cells. Results normalised to extraction in DMSO treated naive control B cells. Inhibitor name, x-axis, molecule inhibited, above graph. ***$P < 10^{-3}$,*$P < 0.05$ in paired t-tests. Data are means and s.e.m. of three (a,b) or one (c) independent experiments.

4.2.7 GC cells extract antigen in a molecularly distinct mechanism

Whilst GC cells were dependent on BCR signalling and cytoskeletal involvement for antigen extraction, they seemed to be insensitive to PI3K inhibition. We used the broad-spectrum small molecule inhibitor LY294002, which abolished most antigen extraction in naive B cells, but had a much less striking effect in GC B cells, only moderately effecting amount of antigen extracted from PMS (Figure 45a). Additionally, the class-1 PI3K specific inhibitor GDC-0941, despite significantly affecting naive antigen extraction, had no effect on GC B cells. These data suggested that GC B cells extract antigen through a molecularly distinct mechanism than that of naive B cells.

We wondered whether PI3K-dependent antigen internalisation was unique to antigen presented in the context of a membrane, or rather if it was a general feature of internalisation. To address this we used the same inhibitors in a soluble internalisation assay analysed using flow cytometry. Naive and GC cells internalised similar amounts of soluble antigen, although GC cell kinetics appeared slightly different. GC cells internalised most antigen rapidly (within the first 10 minutes) and then plateaued, internalising less antigen at later time points. Contrastingly, naive cells internalised constant amounts of soluble antigen over time. During soluble antigen encounter the PI3K pathway was dispensable for internalisation in both B cells (Figure 45b). Pathway blockade by either inhibitor had no measurable effect on internalisation of soluble antigen. This supported our findings that GC B cells use molecularly distinct mechanisms to extract antigen, and this was dependent on antigen being presented in a membrane-bound format.

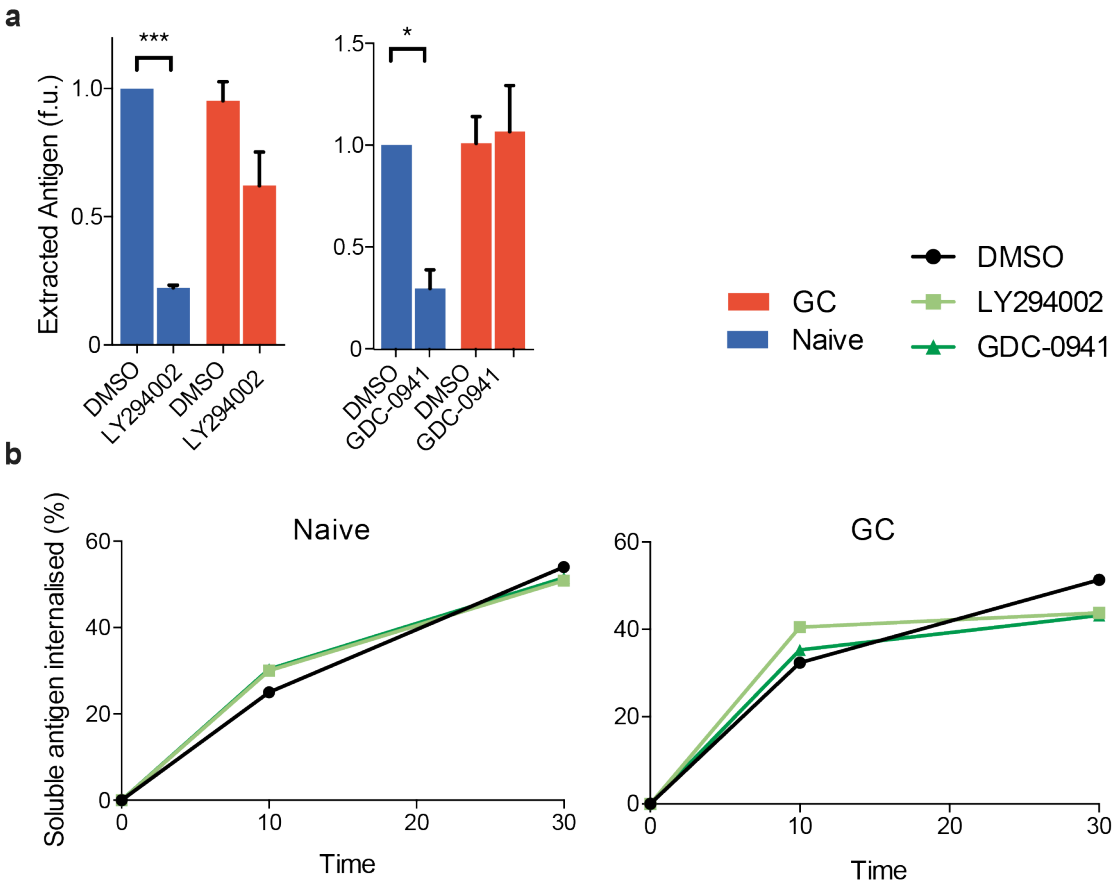

Figure 45 PI3K inhibition has no effect on GC membrane-bound antigen extraction

(a) The effects of inhibiting PI3K on antigen extraction in naive and GC B cells interacting with anti-Igκ antigen on PMS. Results normalised to extraction in DMSO treated naive control B cells.****P < 10^{-4},*P < 0.05 in paired t-tests. Data are means and s.e.m. of three independent experiments.

(b) Time course of soluble antigen stimulation with the same Igκ antigen in solution, analysed by flow cytometry. % internalised relative to ice incubated control cells.

4.2.8 Investigating mechanisms of antigen acquisition in GC B cells

In order to quantify antigen processing in GC B cells, a DNA-based degradation sensor was designed to quantify amounts of antigen that reached degradative endosomal compartments. Antigen was conjugated to the sensor (shown in Figure 46a), which was comprised of a double-stranded DNA oligomer with an Atto647N dye/ quencher pair on one end and a biotin tether on the other. After internalisation, enzymatic cleavage of the sensor in endosomes caused liberation of the fluorophore from its quencher and a subsequent increase in Atto647N fluorescence (Figure 46b). After incubation of naive and GC cells on the same sensor-loaded PMS for 30 mins, naive B cells degraded most of their internalised antigen. GC cells showed significantly less efficient degradation of antigen over the same time frame (Figure 46c). Interestingly, in soluble antigen internalisation assays using the same antigen-bound degradation sensor this difference was absent (Figure 46d), indicating this phenomenon was specific to membrane-bound antigen extraction.

We hypothesised that low amounts of degraded antigen may have been the result of delayed antigen internalisation in GC cells relative to naive B cells. To test this, cells were stained with a secondary antibody specific to the hinge-region of the Igκ $F(ab')_2$ antigen, identifying only surface antigen. The vast majority of antigen in naive synapses was inaccessible to secondary staining, indicating it had been internalised. Higher amounts of colocalised secondary staining was observed on the outer edges and up the sides of GC B cells, and after quantification we saw significantly less internalisation (Figure 47). Thus, we show that naive B cells endocytose antigen directly from the synapse, and process it immediately in endosomal compartments. Alternatively, GC B cells first extract antigen from presenting surfaces, transport it towards the opposite pole of the cell, hold it on their surface for a period of time and then eventually internalise it. This differential decoupling of extraction and internalisation in GC B cells was restricted once again by antigen format, with no effect seen after soluble antigen stimulation (Figure 47c).

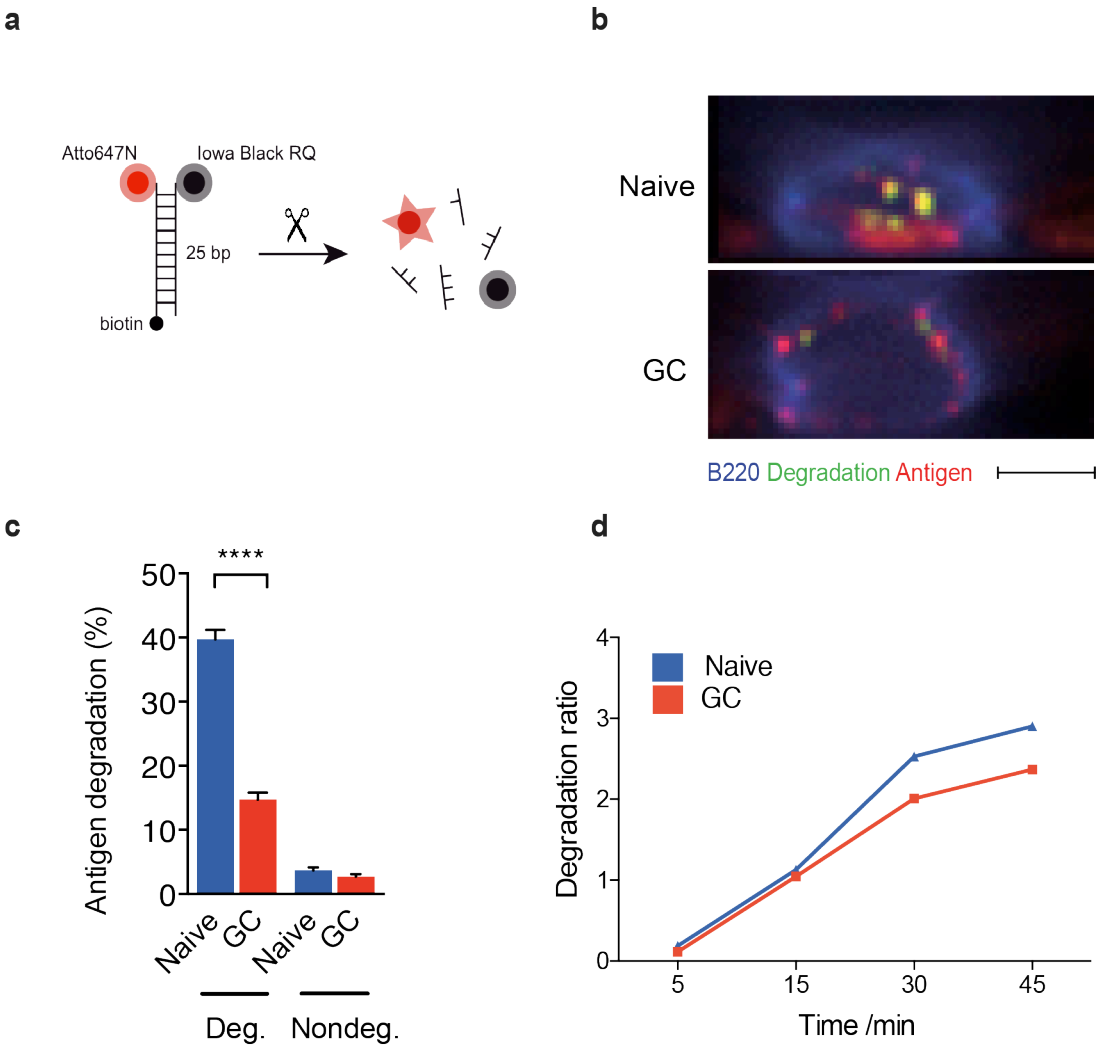

Figure 46 Antigen in endosomes may be visualised using a DNA-based degradation sensor (Katelyn Spillane)

(a) Design of the DNA degradation sensor showing position of tethers, fluorophore and quencher
(b) Sideview reconstruction showing endosomal degradation in naive and GC B cells after 30 mins on PMS. Scale bar = 5μm
(c) Quantification of antigen degradation after 30 min on PMS. ****P $<10^{-4}$. Deg. = degradation sensor, nondeg. = a non-degradable control sensor.
(d) Flow cytometry data showing antigen degraded over time as a ratio compared to samples incubated on ice.

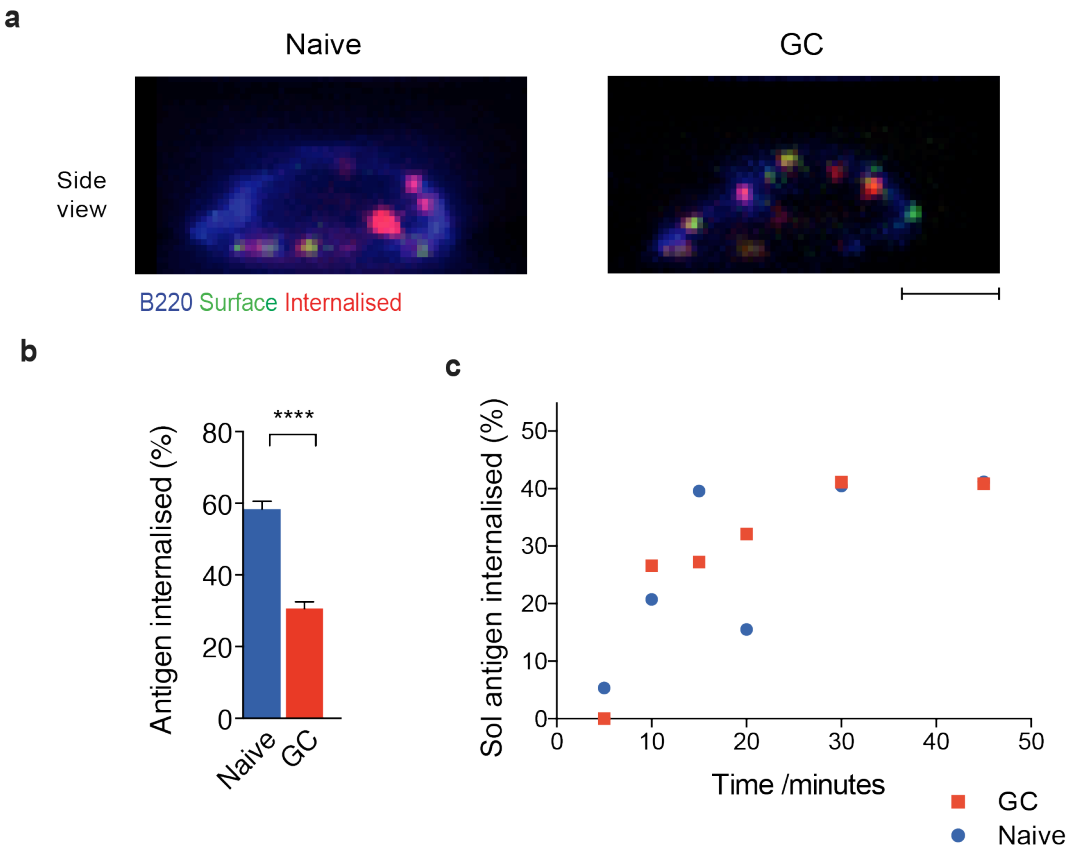

Figure 47 Secondary staining reveals high levels of surface antigen on GC B cells

(a) Sideview reconstructions of naive or GC B cells with surface and internalised antigen staining after 20 mins on PMS. Scale bar = 5μm
(b) Quantification of internalised antigen from cell populations after 20 mins on PMS
(c) Flow cytometry data showing soluble antigen internalisation percentages over time compared to ice incubated samples.

4.2.9 Forces in GC B cells

The observation that GC B cells had high levels of myosin activity and formed small antigen clusters led us to query whether GC B cells were mechanically more active and used contractile forces to regulate antigen binding and extraction. We have previously established a role for myosin IIA-generated mechanical forces in naive B cells (Natkanski et al. 2013).

To compare forces generated in both cell types we engineered a second DNA-based sensor that could monitor location, dynamics and magnitude of vertical tugging forces in live B cells. This sensor, shown in Figure 48, incorporated a fluorophore/ quencher pair located at the opening-end of a DNA hairpin, designed to unravel at a pre-determined force (7, 9 or 14 pN) (Woodside et al. 2006). The resultant increase in Atto647N fluorescence normalized by the fluorescence of the force-insensitive Atto550 and plotted as a ratio. Igκ-antigen was conjugated to one end for interaction with incoming B cells, and a biotin tether to the other for anchoring to PLBs.

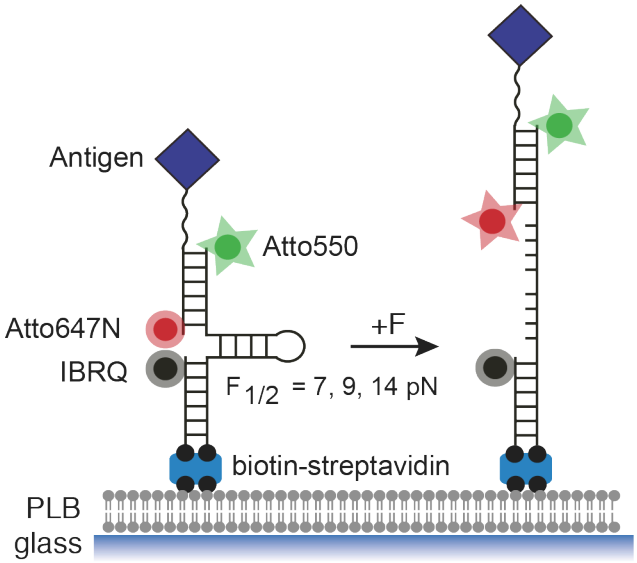

Figure 48 Force sensor design (Katelyn Spillane)
PLB = Planar lipid bilayer, IBRQ = dark quencher, F = force

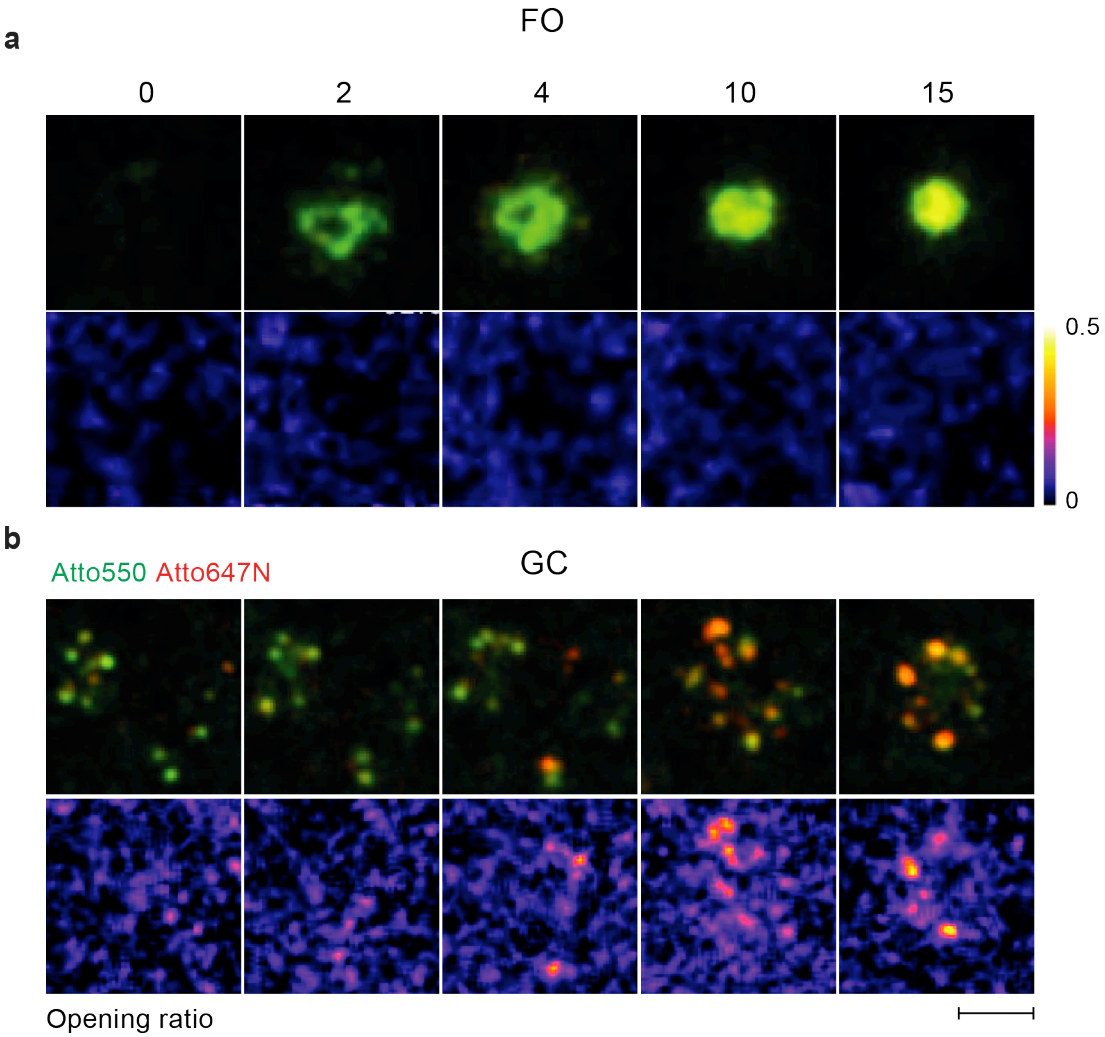

Figure 49 GC B cells produce higher forces in live imaging studies with force sensors

Time-lapse stills of sensor fluorescence and fluorescence ratios using a 9 pN sensor on PLBs in (a) naive B cells and (b) GC B cells. Numbers above panels indicate time in minutes. Scale bar = 5μm.

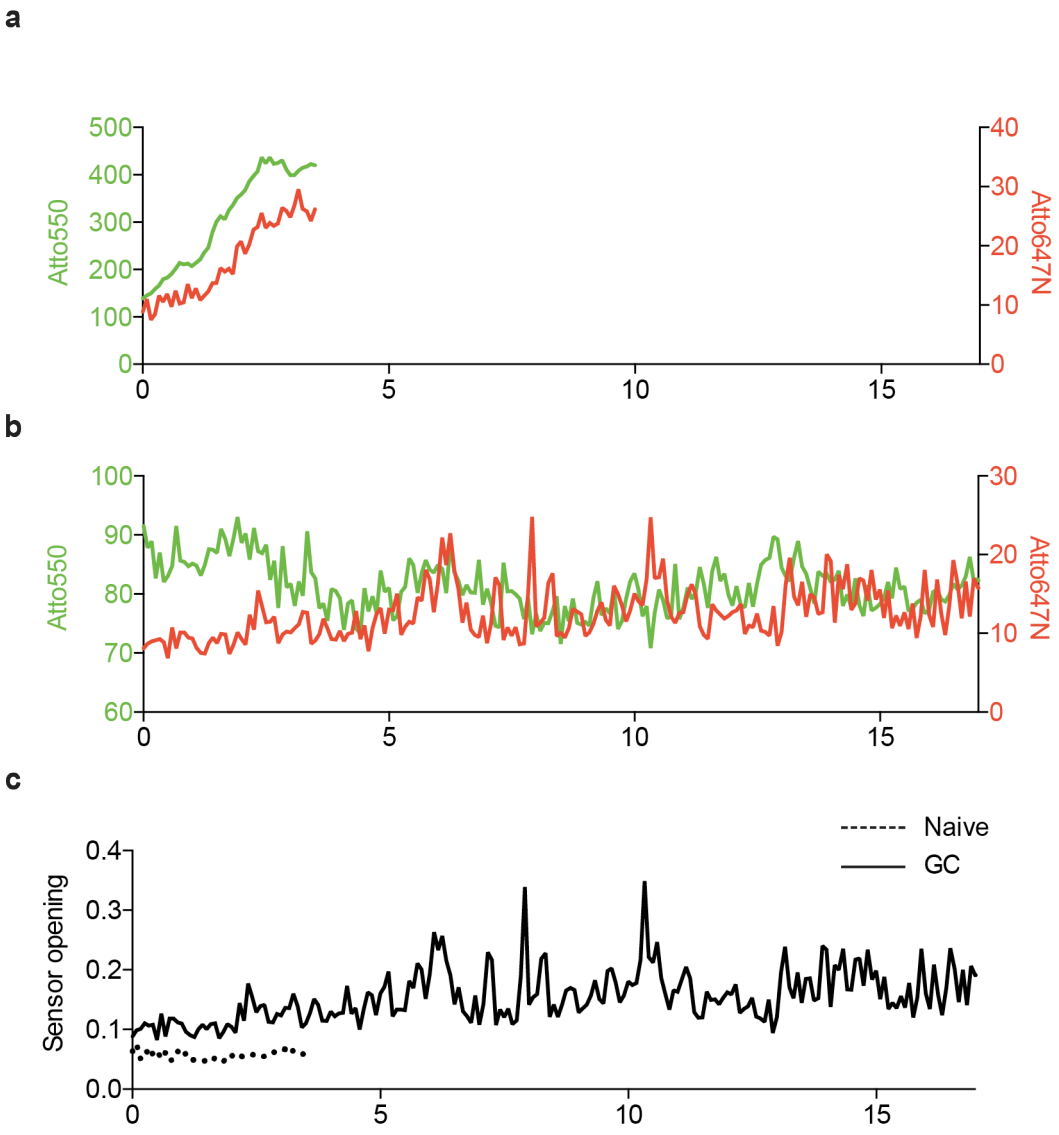

Figure 50 Single cluster tracking of cells interacting with force sensors

Tracking of fluorescence from a single cluster identified in a (a) naive or (b) GC synapse over time from a PLB loaded with an antigen-conjugated 9 pN force sensor. Sensor opening shown as a function of time (c) in either cell type.

PLBs were the most suitable substrate for force sensor imaging as they provided unrestricted lateral movement but strongly resisted vertical, tensile forces, which would otherwise lead to extraction of the sensor and disappearance from the TIRF field. Time-lapse TIRF imaging with the 'medium' force 9 pN sensor revealed only occasional sensor opening by naive B cells. Not only were these forces infrequent, they were also very transient in nature (Figure 49a, Figure 50a, Movie 4). GC cells were able to dynamically interact with the same sensor, opening it in the majority of synaptic clusters. These were visualised as spots of red fluorescence in time-lapse stills or movies (Figure 49b, Movie 4) or areas of high intensity in ratiometric representations of the two fluorophores (Figure 49b, Movie 4).

On the single cluster level, Atto647N fluorescence was highly dynamic, fluctuating often as the sensor was tugged upon, pulled open and snapped shut. Despite this cluster fluctuation, over the entire lifetime of the contact, on average cluster force application became stronger and more sustained (Figure 49b, Figure 50b). Forces were generated rapidly and applied in short bursts, lasting around 5-10 seconds each, with burst frequency increasing over time. Sometimes opening of a sensor (increase in A647N fluorescence) coincided with decreased antigen binding (loss of A550 fluorescence). This was in contrast with naive cells, which relied upon antigen clustering and fusion into a cSMAC before any force generation took place.

Naive B cells opening significantly less of the sensor in all force strengths tested (Figure 51). They opened small amounts of the 'low' 7 pN sensor, but failed to open any of the medium or high force sensors to levels significantly above background (measured with a control sensor lacking a hairpin). GC cells, on the other hand opened every available sensor, albeit to a lesser degree as force increased. This data shows that GC cells apply more forces to BCR-antigen bonds and that these forces are stronger than in naive B cells.

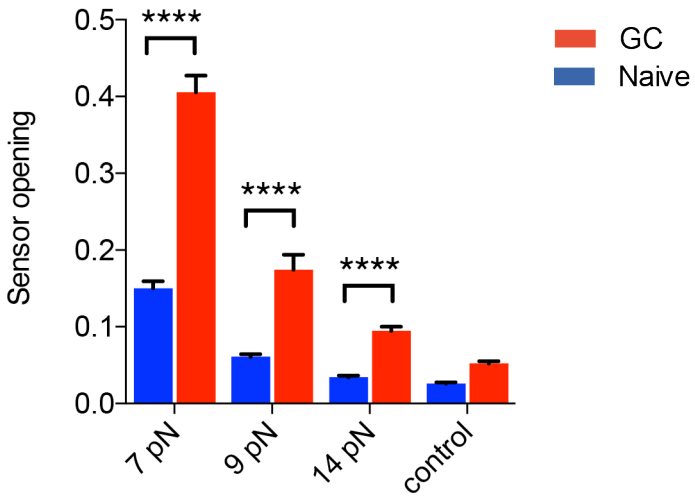

Figure 51 GC cells open force sensors more effectively than naive B cells

Sensor opening ratios displayed as a function of the sensor opening force. The control sensor lacked the force-sensitive hairpin. Data are means and s.e.ms from two independent experiments. **** $P < 10^{-4}$ in paired t-tests. n = 33-49 naive synapses, 16-59 GC synapses.

After uncovering the force-generating capabilities of GC cells, we aimed to elucidate the source of these forces, and their role in synapse formation. We postulated that myosin IIA could be the molecule responsible for force generation, based on its role in naive cells and earlier quantification data showing elevated levels during GC synapse formation. After inhibiting myosin IIA with blebbistatin, cells were live-imaged to observe any defects in synapse formation.

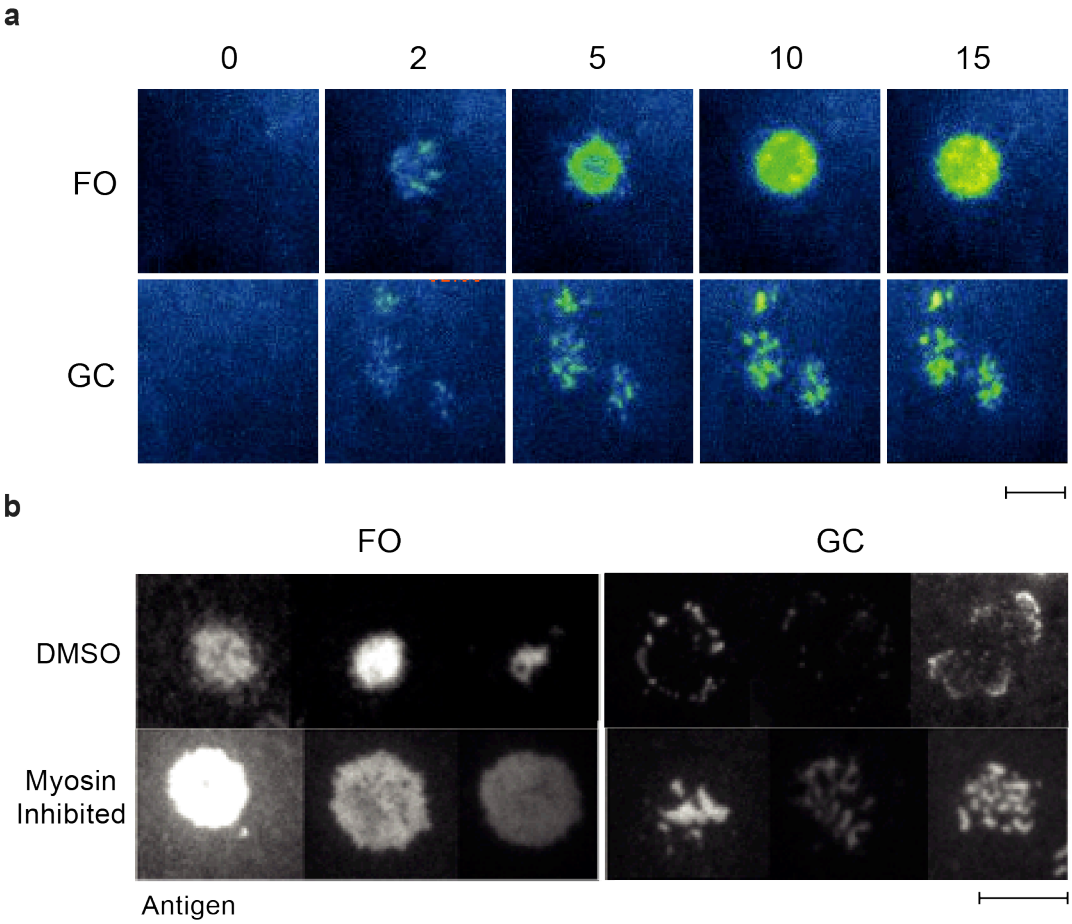

Figure 52 Myosin-inhibited synapses show altered morphology in GC B cells

(a) TIRF time-lapse stills of synapse formation over time (in minutes- shown above panels) in blebbistatin treated naive or GC B cells.
(b) TIRF synapse images comparing DMSO treated or blebbistatin treated naive or GC B cells.

Scale bar = 5 μm.

After myosin inhibition GC B cells did not centralise antigen or become more 'naive-like' in their synaptic architecture. Instead, they formed unusual contacts lacking most of their aforementioned vigour; antigen became relatively immobile, although was still arranged in small clusters (Figure 52a, Movie 3a, 3b). In stills from multiple inhibited cells compared with DMSO-treated controls this difference became more striking. GC cells had arrested antigen where it bound, giving the appearance of small confetti strands of antigen covering the contact, appearing over the entire interface- including the central region (Figure 52b). Naive cell synapses were also somewhat affected, and lacked the final contraction phase of mature cSMAC formation, resulting in enlarged but well organised cSMACs.

Cells were imaged interacting with anti-Igκ live on PLBs to dynamically measure quantity of antigen contacted in synapses. This allowed for the quantification of mean Igκ antigen intensity over time (Figure 53). Blebbistatin treatment marginally increased antigen binding in naive synapses, whilst strongly increasing antigen binding in GC synapses. This suggested GC B cells use myosin IIA contractility to negatively regulate antigen binding in their synapses, keeping cluster size small, through the application of strong and persistent mechanical forces.

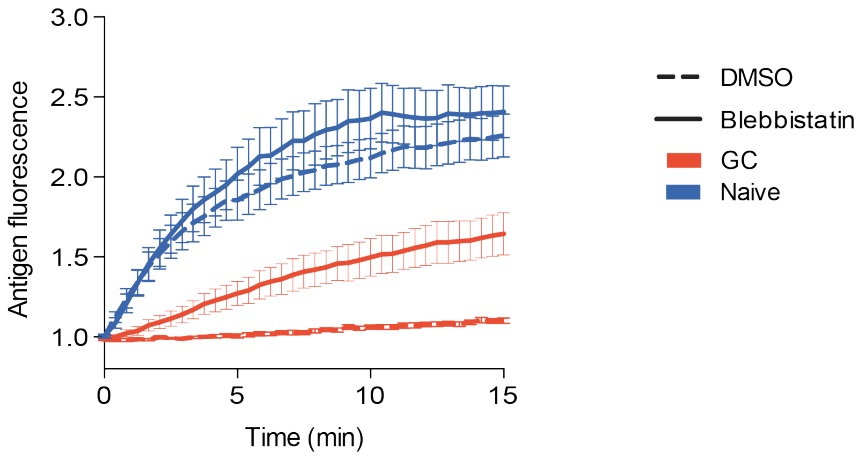

Figure 53 Quantification of antigen intensity over time in live imaging

Antigen (anti-Igκ) fluorescence in synapses of cells with or without blebbistatin treatment, normalized to antigen fluorescence outside of cells. Data from three independent experiments, n = 12-19 naive and 11-12 GC synapses.

4.2.10 GC B cells are more effective at affinity discrimination than naive B cells

The duration, strength and coordination of mechanical forces were previously shown to have an effect on stringency of selection and affinity discrimination (Natkanski et al. 2013). To detect these effects in GC B cells, an antigen-specific cell transfer system was established using the B1-8 knock-in mouse strain. B1-8 mice have a BCRs specific for the low-affinity 4-hydroxy-3-nitrophenylacetyl (NP) and the high-affinity 4-hydroxy-3-iodo-5-nitrophenylacetyl (NIP) haptens when they express the immunoglobulin lambda (Igλ) light chain. Our B1-8 mice were previously crossed to an Igκ-null background therefore resulting in a full repertoire of hapten-specific Igλ-expressing BCRs. B1-8 mice did not form GCs when immunised with NIP-conjugated SRBCs (Figure 54).

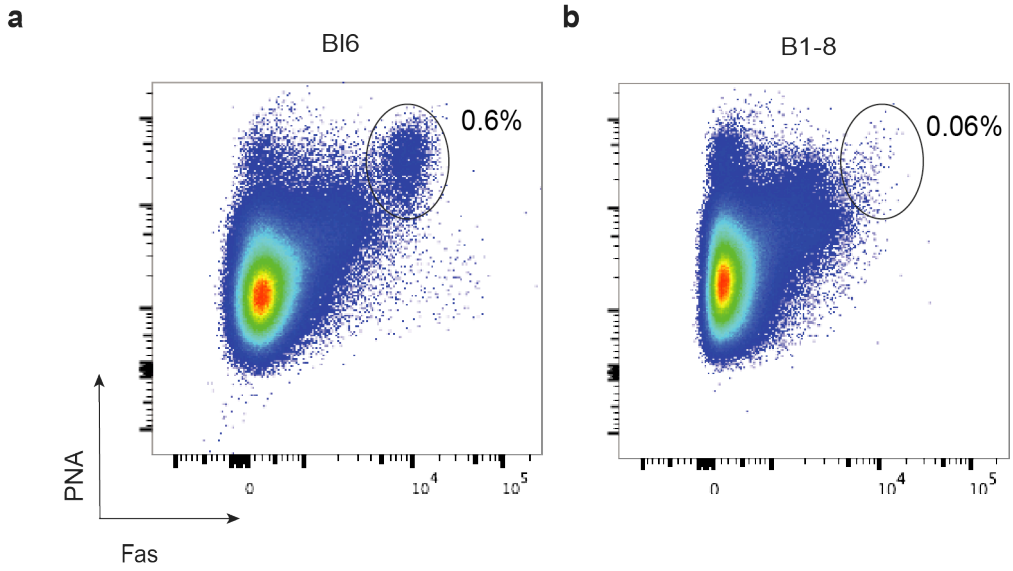

Figure 54 B1-8 mice do not form GCs when immunised with NIP-conjugated SRBCs

Splenocytes were stained for 30 minutes on ice and data was plotted using FlowJo. Percentages refer to percentage of parent population (detailed above plot). Cells pre-gated on live, doublet-excluded B220+ B cells. (a) wild-type B6 mice (b) B1-8 mice. Gates show PNA+ Fas+ GC cells.

Transfers were carried out as detailed in Figure 55; where up to 5 million B1-8 splenocytes were delivered i.v. immediately followed by immunisation with NIP-conjugated SRBCs i.p. After 6-10 days, splenocytes were analysed by flow cytometry to check for efficient cell transfer and GC formation. 7 days p.i. GC cells were present in the expected frequency (3.5% Figure 56d). Transferred cells could be located in the spleen based on CD45.2 expression, with 85.3% of these cells bearing the GC phenotype (Figure 56 e,f). A large proportion (85.5%) of transferred GC cells bound NIP, compared to a negligible percentage of host GC cells (Figure 56 g,h).

B1-8 cells were inherently able to bind both the high and low affinity to the same extent when receptors were maximally loaded with fluorescent multivalent NP or NIP15 antigens and analysed using flow cytometry (Figure 57a). Following GC formation in the B1-8 transfer model, cells still maintained the one order of magnitude affinity difference present in naive B1-8 cells between the two haptens (Figure 57b). This showed that even following affinity maturation in the GC, the two haptens maintained a sufficient affinity difference to be comparable to B1-8 control cells in downstream imaging assays.

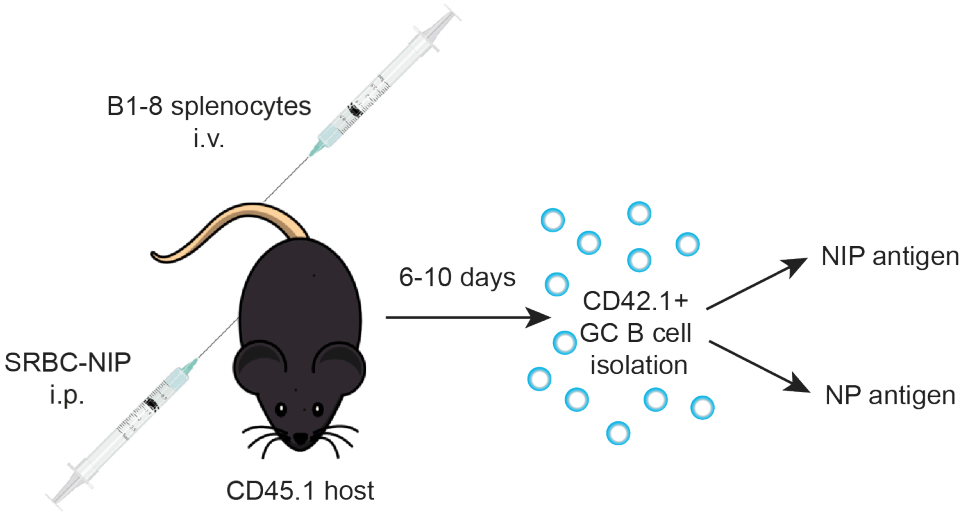

Figure 55 Schematic of B1-8 cell transfer and immunisation of B6 mice

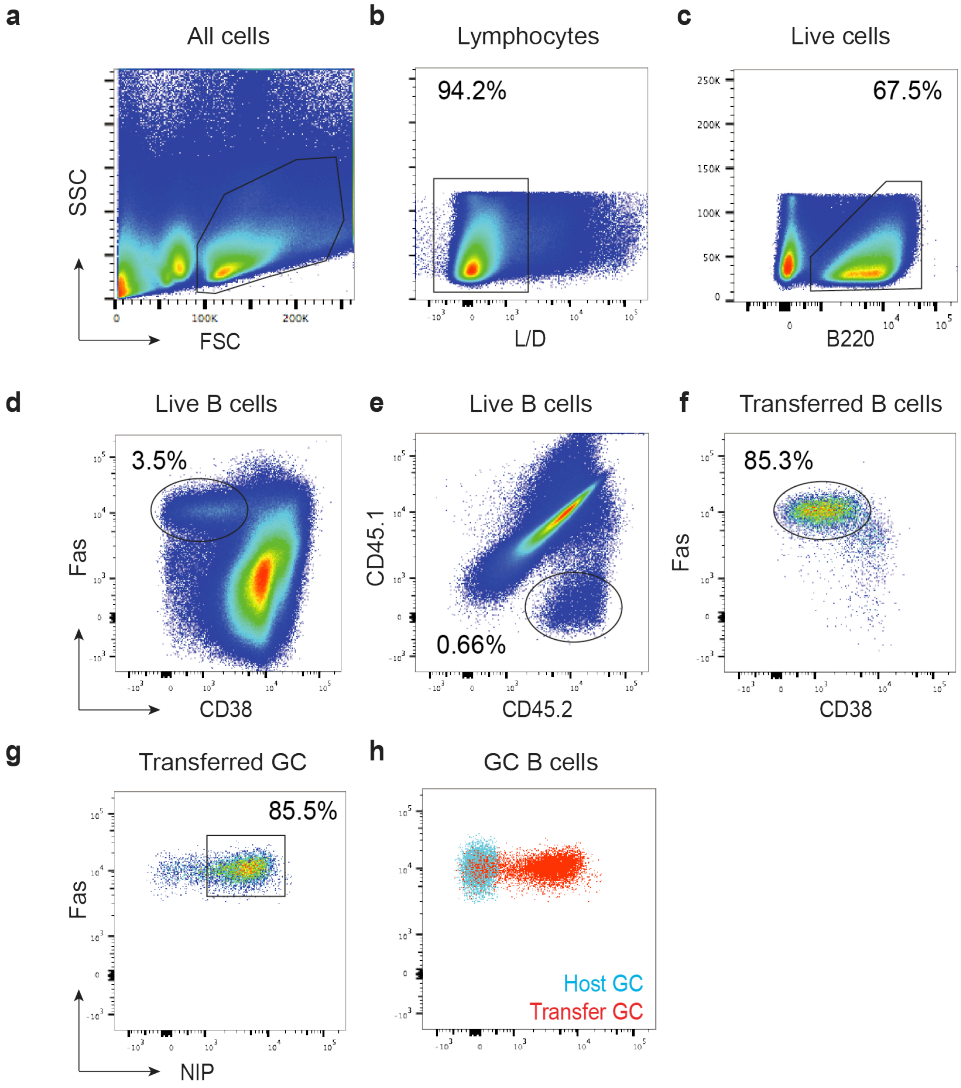

Figure 56 Antigen-specific GC transfer cells were present in host mice after SRBC-NIP immunisation

Splenocytes were stained for 30 minutes on ice and data was plotted using FlowJo. Full gating strategy shown. Percentages refer to percentage of parent population (detailed above plot). Mice sacrificed day 7 p.i.

(a) Lymphocytes gated on FSC/SSC characteristics
(b) Live/ dead viability dye negative cells (live cells)
(c) Live B220+ B cells
(d)B220+ CD38- Fas+ GC cells, 3.5%
(e)B220+ CD45.2+ transfer cells, 0.66%
(f) B220+ CD45.2+ CD38- Fas+ GC transfer cells, 85.3%
(g)B220+ CD45.2+ CD38- Fas+ NIP+ antigen-specific transfer cells, 85.5%
(h) Overlay comparing NIP binding of host and transfer GC cells

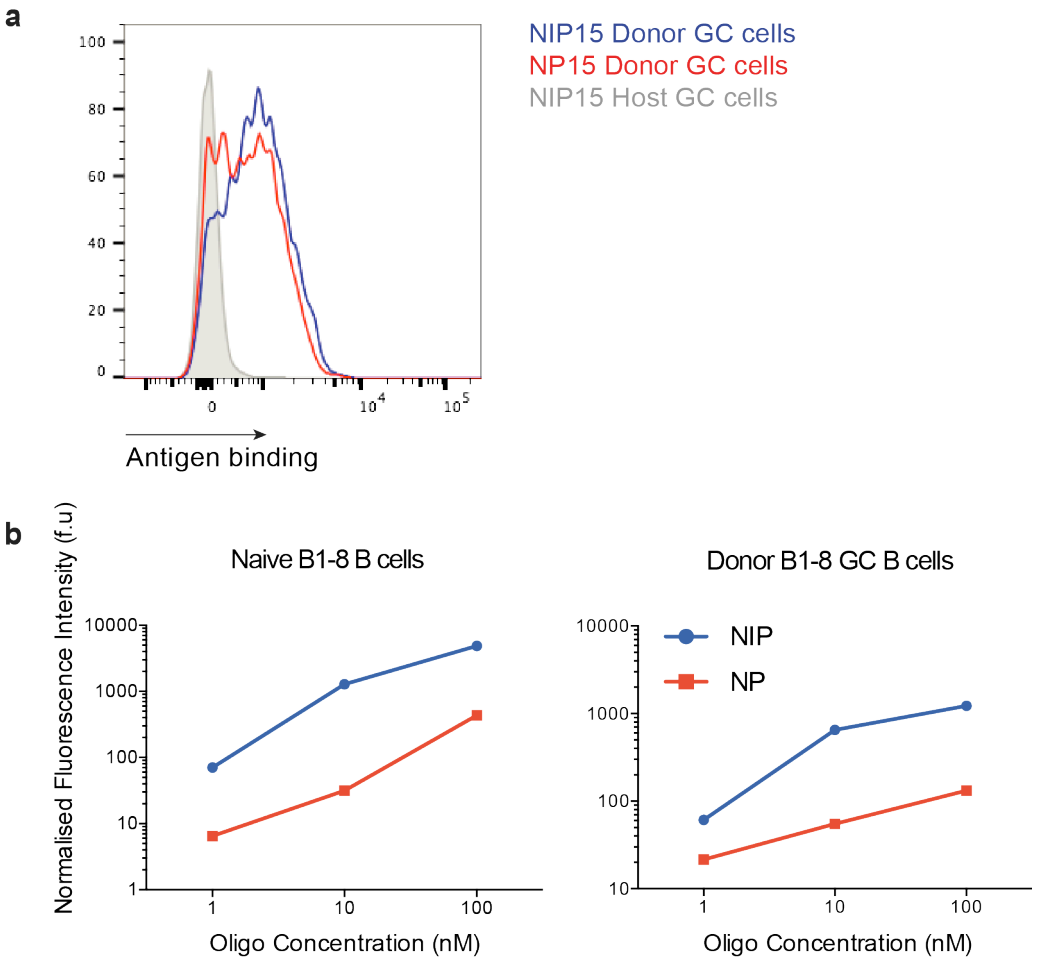

Figure 57 B1-8 antigen binding controls following cell transfer

(a) Cells were stained on ice for NIP or NP using multivalent antigens. Histograms show antigen fluorescence in various cell populations compared to host control cells.

(b) Monovalent NP or NIP oligos were added to cells in varying concentrations immediately before data collection. Graphs show oligo fluorescence vs concentration in B1-8 non-immunised control cells or GC cells from the B1-8 transfer model.

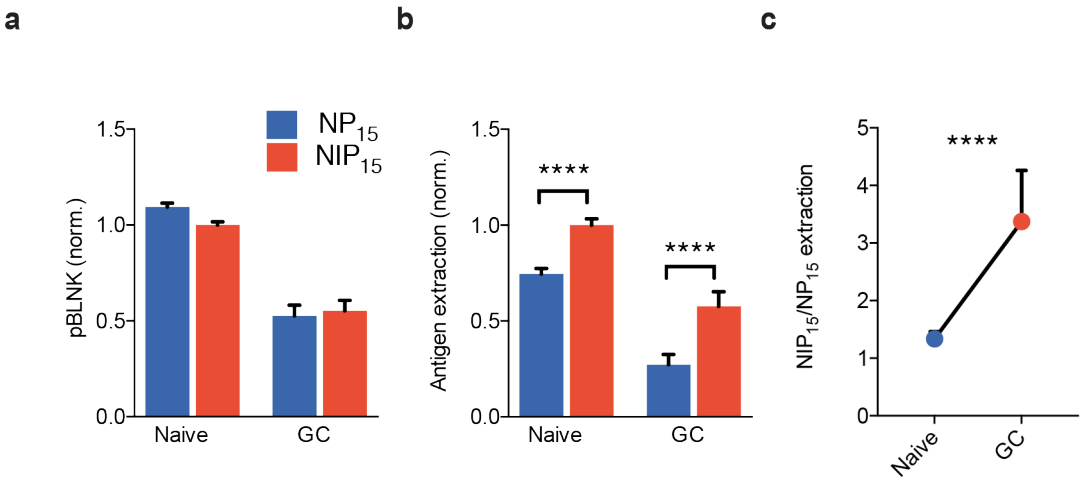

Figure 58 Affinity discrimination in naive and GC B cells

Naive, CellTrace Violet (CTV)-labeled B1-8 B cells were imaged on NP15- or NIP15- containing PMSs together with donor-enriched B cells from mice that received B1-8 B cells and were immunized with SRBC-NIP.

(a) Levels of phospho-BLNK by B1-8 naive (CTV+Fas−) and GC (CTV−Fas+) B cells, normalized to values of naive B cells.

(b) Antigen extraction by B1-8 naive (CTV+Fas−) and GC (CTV−Fas+) B cells, normalized to values of naive B cells.

(c) Ratio of NIP15 to NP15 antigen extracted from PMSs by the B1-8 naive and GC B cells.

****$P < 10-4$ (nonparametric test (b) or paired *t*-test (c)). Data are pooled from five experiments (a,b; mean and s.e.m. of $n = 1,693$ (a) or 1,517 (b) naive cells or $n = 81$ (a) or 84 (b) GC B cells) or are from five experiments (c; mean and s.e.m.).

In transfer imaging experiments BLNK phosphorylation was similar between the high and low affinity antigens, implying affinity discrimination was not influenced (on the receptor level) by BCR signalling. Interestingly, and in a departure from data gathered with the very high affinity anti-Igκ antigen, levels of p-BLNK were reduced in GC cells compared to naive B1-8 cells (Figure 58a). Both cells internalised more of the high affinity NIP antigen than the lower NP from PMS (Figure 58b), but GC cells were significantly more effective at extracting the high affinity NIP_{15} antigen in favour of the lower NP_{15} antigen. (Figure 58c, ratio of high vs low antigen extraction). This data supports the concept of GC cells more stringently discriminating between antigen affinities during the GC reaction.

4.3 Discussion

The GC is a site of intense proliferation, where high-affinity B cell clones are expanded and memory cells are produced (Shlomchik & Weisel 2012a; Victora & Nussenzweig 2012). Although antigen presentation to T cells is known to be critical, precise mechanisms governing affinity-selection are unknown. Our data suggest that this process is supported by a distinct architecture of the synapse in GC B cells. Strategies described in Chapter 3 to capture high-resolution imaging data from rare B cells were employed to visualise immune synapse formation in cells isolated from germinal centres (GCs) of mice. Using GC cells generated by various immunisation strategies and isolated and enriched by a MACs depletion approach (Cato et al. 2011) we could simultaneously image naive and GC B cells interacting with substrate-presented antigen. This revealed unique peripheral synapses lacking centralisation, which were enriched in GC cell populations after surface marker staining.

Synapses with compromised centralisation have been observed in some contexts in other immune cells (Brossard et al. 2005; Hailman et al. 2002; Carlin et al. 2001) but these tended towards a lack of antigen centralisation compared to GC cells who rearranged antigen clusters using a vigorous centrifugal flow. This was an active process independent of kinetics; during live-cell imaging clusters were pulsated dynamically initially both inwards and outwards before being restricted to the outer cell edge. This novel synapse morphology was highly stereotypical amongst GC cells and was not dependent on class switching or qualitatively different BCR signalling. We instead propose that peripheral synaptic architecture is regulated by alterations on the GC cytoskeleton imposed during the GC differentiation program. This was demonstrated by tubulin upregulation, F-actin patterning in structures co-localising with antigen clusters and high levels of myosin IIA contractility.

This dynamic contractile profile aligns with models proposed for contact-mediated repulsion (Wilkinson 2015). During live cell imaging GC cells were observed contacting the substrate by membrane pedestals in later phases of synapse formation, as if the membrane were being retracted from the presented antigen.

How immune cells cease synaptic contacts with APCs is yet to be fully understood. In T cells rapid desensitisation at inflammatory sites following synapse formation was observed as a preventative measure against hyper responsiveness, and corresponding autoimmunity, via upregulation of surface PD-1 (Honda et al. 2014; Dustin 2014a). Although ligands for PD-1 (PDL-1 and PDL-2) are upregulated on GC cells and PD-1 signalling is known to influence quality and quantity of the plasma cell and memory responses (Good-Jacobson et al. 2010), this PD-1-dependent regulation of BCR has never been explored in B cells. Targetted vesicle secretion into synaptic clefts has also been proposed as a mechanism of both information transfer and synapse cessation in T cells (Choudhuri et al. 2014). Although we did not explore vesicle secretion in GC B cell synapses at length, in previous studies where B cell membrane lipids were marked with a lipid dye no membranous vesicle deposits (via dye accumulation) could be observed during synapse formation or antigen extraction [our unpublished observations].

Extra layers of stringency are imposed in the GC in order to only select higher affinity variants. Dynamic behaviours may serve to maintain competition from newly entering FO B cells throughout the response (Schwickert et al. 2007). Alternatively, GC B cells may be using contact mediated repulsion to terminate synaptic contacts with individual FDCs in order to continuously sample the antigen pool in the GC LZ (Meyer-Hermann et al. 2012). F-actin-dependent reaching of membrane pseudopods known as 'probing' was shown to rapidly terminate upon microcluster formation in naive B cells (Wang et al. 2016). Perhaps small, dynamic microclusters that never really fuse or grow allow for more extensive detachment and probing behaviours by the GCs on individual or even multiple FDCs. This idea is supported by *in vivo* intravital imaging which failed to identify long, stable contacts between GC B cells and FDCs during antigen acquisition (Schwickert et al. 2007; Allen et al. 2007; Hauser et al. 2007). We have never considered the possibility of GC cells sampling and integrating inputs from multiple antigen sources simultaneously, but given their morphology (many dynamic membrane processes), synaptic architecture (individual and spatially separate BCR-antigen pools) and the dense FDC network in the GC, this idea could be feasible, although complex intravital imaging studies may be required to observe these behaviours in real time.

Robust signalling in GC B cells could be observed using calcium imaging and pTyr staining on both PLBs and PMS. As initial staining for pTyr could not exclude contributions from inhibitory signalling molecules we systematically stained for proximal BCR signalling components individually, both excitatory and inhibitory. This led to our description of what we term the 'GC signalling profile', referring to the robust signalling we observed, often including an elevated basal level of phosphorylation as well as potent upregulation following synapse formation. This profile seemed to fit most of the proximal BCR signalling cascade, excitatory and inhibitory, as well as myosin IIA. Although seemingly at odds with observations from others regarding GC BCR signalling, when we used soluble antigen to stimulate GC B cells, we could recapitulate the dampened signalling phenotype observed by others (Khalil et al. 2012). The B cells we used generally exploited a fully polyclonal BCR repertoire and retained the ability to class switch, both potentially influencing their signalling capacity, although based on our limited investigations, probably not significantly. Further, more extensive staining for Ig isotype coupled with signalling molecules could better address this in the future.

The major contributor to efficient BCR signalling in GC cells was synapse formation itself. Early models of synapse formation suggested the cSMAC might serve as a platform for effective signal propagation; bringing molecules in close proximity or physically excluding inhibitors of BCR triggering (Batista et al. 2001). Mechanical stimuli have also been implicated in the initiation of cellular responses in immune cells, such as T cells, where mechanical forces potentiate signalling (Zhang et al. 2014; Hong et al. 2015; Chen et al. 2015; Elosegui-Artola et al. 2016; Chen & Zhu 2013; Liu et al. 2016) and killing (Basu et al. 2016) of target cells. Membrane-presented antigens may provide the mechanical stimuli required for effective BCR signalling in GC B cells. Presently, it is unclear precisely how this may occur in synapses with physiological FDCs. This could include secreted factors or signals delivered directly via receptor-ligand interactions to the interacting GC cell or the stiffness properties of the FDC presenting membrane. Presenting membrane flexibility is known to play a role in antigen extraction in B cells (Natkanski et al. 2013; Wan et al. 2013), and consistent with our findings, stiffer presenting membranes produce higher levels of signalling. Our current data does not fully

address how signalling is elevated- by some amplification event, through lack of signal termination or by another undefined mechanism. We also never investigated the stiffness properties of FDC membranes, so may only hypothesise that they are more rigid through our GC observations of high and sustained BCR signalling and longer, stronger pulling forces. In any case, efficient BCR signalling occurs in GC B cells when they interact with membrane-presented antigens, and BCR signalling is essential for antigen extraction. Therefore, we expect BCR signalling to be indispensible for antigen presentation and eventually, acquisition of T-cell help.

We used our PMS surrogate membrane system to extensively investigate processes governing antigen internalisation in from GC synapses. Despite lack of antigen centralisation, GC cells achieved efficient microcluster internalisation from PMS, albeit by a novel mechanism. GC cells internalised antigen from membranes independently of PI3K. In naive B cells antigen is clustered, pulled up in a large bundle and then internalised in clathrin-coated pits in a PI3K-dependent fashion (Natkanski et al. 2013). This means that extraction of antigen from presenting membranes occurs in a synchronous and coordinated movement with internalisation, where in naive cells, antigen and small chunks of presenting membrane are rapidly internalised together and quickly degraded in endosomal compartments. This was different in GC synapses, where antigen was extracted and could move up the sides of the cell before internalisation. It is not yet clear how long antigen is held on the outside of GC cells prior to internalisation, or what governs its eventual internalisation. We can however, speculate as to the purpose of this delay. Separation or division of large antigen containing immune complexes from FDC surfaces may be necessary prior to internalisation, purely from a geometric point of view. Although *in* vivo some presenting membrane was detected on the B cell surface after antigen extraction (Suzuki et al. 2009), it is very difficult to discern the original size of the immune complex contacted by a given B cell, and whether physical dispersion of the immune complex is necessary for efficient internalisation.

During this process of extraction, the B cell would have to outcompete any antibody coating the complex and binding it to specialised receptors on FDCs. This could serve to establish a selection pressure where B cells must outperform existing

circulating antibody specificities secreted by themselves or other participating GC cells earlier in the reaction (Zhang et al. 2013). Another interesting scenario that might arise as the outcome of this internalisation delay is that the B cells may serve themselves as antigen presenting cells in the GC. This phenomenon has been observed outside of the GC where naive B cells may perform antigen shuttling and presentation roles (Phan et al. 2009). In the GC, prolonged surface exposure of extracted intact antigen would allow other nearby B cells binding different epitopes with higher affinity to acquire the antigen directly from a competing B cell, adding another dimension to the stringency measures employed in the GC.

The organisation of GC synapses steered us towards investigating mechanical forces and force-generators in more detail and more specifically how these might interplay with affinity discrimination. Affinity discrimination is tuned in T cells by multiple mechanisms including: force-mediated bond rupture by cytoskeletal components of the opposing membrane (Ilani et al. 2009) or regulation of antigen-TCR microcluster size, where smaller clusters decreased the effects of avidity usually caused by clustering (Ilani et al. 2009; Schamel et al. 2005). We investigated both of these phenomena in turn in our GC cells. We tested whether the high levels of force-generating molecule myosin IIA might be controlling the cluster size in GC B cells. When we inhibited myosin IIA with the small-molecule inhibitor blebbistatin, GC B cells were no longer able to regulate the amount of antigen they contacted, which instead of being kept uniformly low, rose steadily over the lifetime of the contact. This was most likely caused by increased bond dissociation following strong waves of myosin contractility. Alongside, we used a DNA-based force sensor (Zhang et al. 2014; Blakely et al. 2014; Wang & Ha 2013) to read out the magnitude of force applied to BCR bonds in GC or naive B cells. GC B cells applied stronger, more sustained forces than naive B cells. We propose that decrease in surface GC BCR density in combination with low antigen binding and stronger force generation- both mediated by the contractility of large amounts of myosin IIA- contribute to increased stringency of selection in the GC. In order to successfully extract antigen from FDC surfaces, GC cells must withstand high forces exerted on small microclusters, and also potentially overcome any effects actively contributed by the FDC that our passive surrogate membrane systems cannot recapitulate. Membrane integrity of the APC in T cell-dendritic cell synapses

has already been shown to be important for proper T cell activation (Comrie et al. 2015; Malinova et al. 2016), so we speculate the specific APC in this context, the specialised FDC, has underappreciated influences over GC synapse formation.

In a competitive, antigen-specific setting, we could see these stringency measures in action. GC B cells were better at discriminating between the haptens NP and NIP, where NIP bound the B1-8 BCR with ten times higher affinity than NP. Although naive B cells did extract more NIP than NP from PMS, the effect in GC B cells was significantly improved. This agrees with the general principles of many published models, which describe an inherent affinity sensing capability within all B cells, which improves and becomes more specific when B cells move through the GC reaction (Shlomchik & Weisel 2012b; MacLennan 1994; Victora & Nussenzweig 2012; Cyster 2015).

We have shown that distinct biomechanical mechanisms are in place during synapse formation in the GC to introduce layers of stringency into the process of membrane-presented antigen extraction. These measures lead to higher force generation, small cluster size, delayed antigen internalisation and prolonged BCR signalling- not present when GC cells are stimulated with soluble antigen. We propose a model where not only is initial binding strength between BCRs and antigen important, GC B cells must retain antigen on their surface without being outstripped by a competitor before eventual internalisation. Whilst we certainly acknowledge T cell help as the final rate-limiting step for GC selection, we implicate antigen extraction as a fundamental process preceding T-cell help, which is tightly regulated after B cells enter into the GC differentiation programme.

Chapter 5. Elucidating molecular mechanisms of immune synapse formation in the GC

5.1 Introduction

The GC represents a unique niche maintained by specific chemokine gradients (Allen et al. 2004) and is a site where B cells receive a number of soluble and cell-bound stimuli, which may have roles in modulating synapse formation. Such molecules include the cytokines interleukin (IL)-6 and IL-21. IL-21 is especially important for B cells, promoting antibody production, class-switching and plasma cell differentiation (Kasaian et al. 2002; Ozaki et al. 2004; Ozaki et al. 2002; Pène et al. 2004; Ettinger et al. 2005; Kuchen et al. 2007) in T-dependent responses in collaboration with IL-4 (Avery et al. 2008; Vogelzang et al. 2008). IL-21 also acts directly on GC B cells where it is required for formation and maintenance of GCs and optimal affinity maturation (Linterman et al. 2010). Among the effects of IL-21 on B cells is the upregulation of the transcription factor B cell lymphoma-6 (BCL-6) (Linterman et al. 2010). BCL-6 has been long known to be intrinsically required in B cells for their development into GC B cells (Crotty et al. 2010; Klein & Dalla-Favera 2008; Nurieva et al. 2009; Yu et al. 2009) and may be important in selection events recruiting naive cells into developing GCs (Kitano et al. 2011). BCL-6 acts transcriptionally as a repressor, and functions in the GC on a suite of target genes, preventing apoptosis during DNA-damage responses and blocking plasma cell differentiation (Klein & Dalla-Favera 2008).

Another possibility is that the GC B cell synapse is a consequence of the GC differentiation programme on the B cell cytoskeleton. The membrane cytoskeleton is profoundly involved in immune synapse formation, and its reorganisation is known to contribute to microcluster formation (Song et al. 2013), pSMAC and cSMAC segregation (Batista et al. 2010) and antigen internalisation (Natkanski et al. 2013), as well as regulating a number of key signalling networks (Harwood & Batista 2011; Kumari et al. 2014). Although we previously uncovered a role for actin and myosin in regulation of antigen binding, other cytoskeletal components

have remained less well explored, despite known links with synapse formation in other immune cells. In particular, the microtubule cytoskeleton is known to be important for polarisation of various cellular components to immune synapses. For example, reorientation of the microtubule organising centre (MTOC, or sometimes called the centrosome) in CD8+ T cells to a position just below the centre of the synapse interface is central to effective cytotoxic synapse formation (Le Floc'H & Huse 2015). This is vital in CD8+ T cells for the establishment of a 'privileged' site where toxic cargo is secreted directionally to the target cell only, minimising bystander damage (Stinchcombe et al. 2011; Huse et al. 2008).

Recently, molecular mechanisms of MTOC polarisation have been elucidated in T cells. Using a photocleavable antigen molecule, micron-sized regions of antigen could be specifically induced to bind the TCR with a pulse of UV light, bypassing confounding effects from signalling pathways associated with adhesion molecules also active during synapse formation. Using this approach, MTOC polarisation was found to be dependent on the lipid second messenger diacyl glycerol (DAG), which is produced by phospholipase-C-γ (PLCγ) and accumulates at the synapse following TCR signalling (Quann et al. 2009; Huse 2012; Spitaler et al. 2006). The discovery of DAG's involvement in MTOC polarisation led to the study of the protein kinase C (PKC) family of proteins. PKCs were known DAG binders and additionally were strongly implicated in an aspects of TCR signalling, due to their recruitment to the membrane following artificial, TCR-independent activation by phorbol esters and calcium ionophores (Chatila et al. 1989). PKCs exist in conventional, novel and atypical isoforms. Novel PKC isoforms, PKC-θ, PKC-η and PKC-ε were observed being recruited to the cytotoxic T cell synapse in a specific sequence (PKC-ε and η first, then PKC-θ) preceding MTOC reorientation (Quann et al. 2011). Elsewhere in the synapse, PKC-θ is known to work in concert with Wiskott Aldrich Syndrome protein (WASp) to maintain synapse stability through breaking and relocating symmetry (Sims et al. 2007).

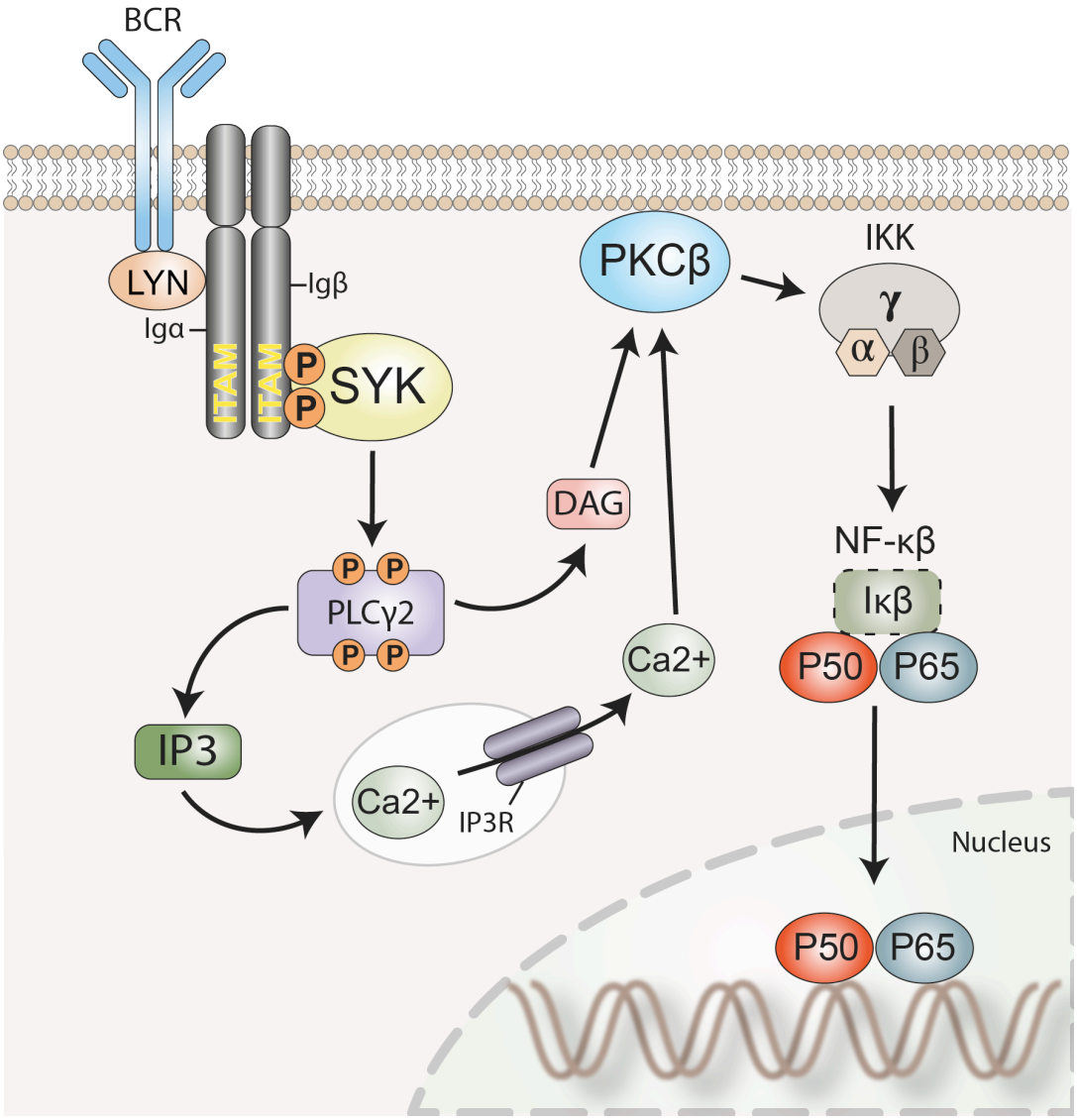

Figure 59 An overview of the BCR-mediated NF-κB signalling cascade

BCR crosslinking and phosphorylation of ITAM residues induces activity of SYK and other SRC-family kinases, culminating in the assembly of the full B cell signalosome (not shown). Phospholipase C γ 2 (PLCγ2) activity promotes the accumulation of the second messengers' diacylglycerol (DAG) and inositol trisphosphate (IP3) and the mobilization of intracellular calcium stores. PKCβ responds to DAG and calcium and localises to the plasma membrane. Activated PKCβ acts on the inhibitor of κB kinase complex (IKK), which in turn causes degradation of the inhibitor of κB (IκB). This leaves active NF-κB (shown as p50 and p65 subunits) free to translocate into the nucleus, bind DNA and carry out its effector functions.

The PKC family have known roles in BCR signalling. The novel PKC isoform, PKC-δ is specifically required in tolerance mechanisms (Guo et al. 2004), whereas the conventional PKC, PKC-β is involved with signalling downstream of the BCR. Src-family kinase signalling and the formation of the mature signalosome causes accumulation of second messengers inositol-1,4,5-trisphosphate (IP_3) and DAG (Niiro & Clark 2002). These initiate calcium fluxing and signalling through multiple pathways involving calcium signalling and various PKC isoforms to activate a key network of B cell transcription factors (Guo et al. 2004; Su 2002), PKC-β acts specifically to mediate the translocation of nuclear factor-κB (NF-κB) (Gugasyan et al. 2000) into the nucleus (Figure 59- PKC signalling cascade), through phosphorylation and assembly of the CARMA1/Bcl10/MALT (CBM) signaling complex in BCR microdomains (Thome et al. 2010; Su et al. 2002). The CBM complex acts through the inhibitor of κB kinase (IKK), which is recruited to lipid rafts in the plasma membrane and degraded, allowing movement of free NF-κB into the nucleus where it mediates B cell activation and survival (Li et al. 2003; Su et al. 2002).

Interestingly, PKC-β has been observed to regulate myosin IIA in mast cells (Ludowyke et al. 2006). The actomyosin cytoskeleton represents a site for signal integration and translation into mechanical forces, but mechanisms underlying this force output remain elusive. Myosin IIA is a heterotrimer, made up of two heavy chains (MyHCs), two essential light chains (MLCs) and two regulatory light chains (RLCs) (Apgar 1991). Although RLCs were initially assumed to be the major site for myosin regulation, accumulating evidence places phosphorylation of the MyHC as a major inhibitory regulatory mechanism in myosin IIA (Bresnick 1999; Brzeska & Korn 1996). PKC-β phosphorylates MyHC at serine 1917 (Ser1917) and regulates secretion of inflammatory mediators by mast cells (Ludowyke et al. 2006)- a process under tight control to limit host pathology.

The GC environment, microtubule organisation and myosin regulation are all implicated in GC B cell responses and antigen interaction but no clear links are yet established with any of these pathways and synaptic architecture. In this chapter, we aim to assess the contribution of these pathways to regulation of peripheral

synapse shape in GC B cells. We aim to elucidate, in more detail, the molecular mechanisms, determinants and outcome of differential synapse architecture on GC responses. We hope with this knowledge to be able to manipulate these factors specifically and drive differences in GC dynamics or synaptic architecture.

5.2 Results

5.2.1 Immune synapse patterning could not be artificially altered through cell culture conditions

In order to examine what factors are responsible for the GC synapse architecture, we attempted to alter synapse shape through specific manipulation of signalling pathways that have been implicated in the GC response. Because GC cells are resistant to *ex vivo* cell culture and cannot be differentiated *in vitro,* we first investigated a panel of human immortalised B cell lines.

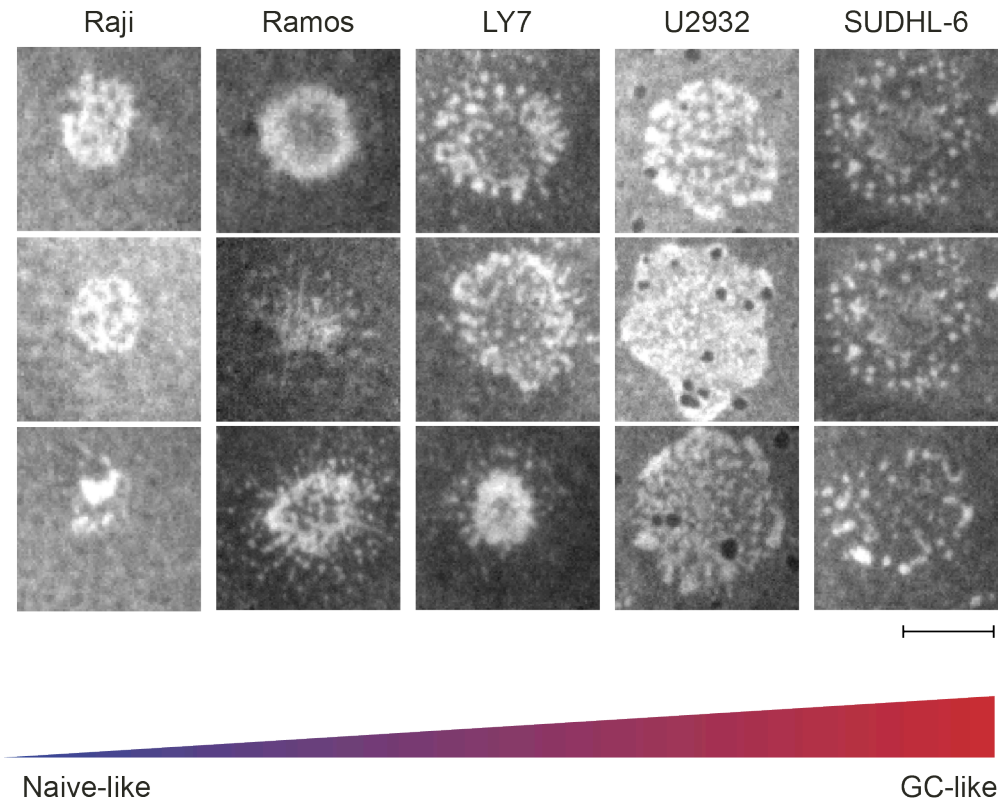

Figure 60 Synapse morphologies in human B cell lines

Three representative images of synapses formed by B cell lines after incubation for 20 min on anti-IgM-Cy5 loaded PLBs.
Scale bar = 5μm

Human B cells (Raji, Ramos, LY7, U2932 and SUDHL-6) were incubated on PLBs loaded with a human IgM $F(ab')_2$ fragments and allowed to form synapses. All human B cell lines formed synapses that exhibited an appreciable range of morphologies, with varying degrees of heterogeneity. Broadly, they fell into 'naive-like' or 'GC-like' categories, with Raji and Ramos B cells forming synapses with a high degree of centralisation and appearing most similar to naive mouse primary B cells (Figure 60). Contrastingly, SUDHL-6 B cells formed atypical synapses with a spread, speckled 'firework' configuration, appearing more similar to primary GC B cells.

We thought this panel would serve as a useful model to identify the master regulators of GC synapse organisation. We began by stimulating 'naive-like' Ramos B cells overnight under a range of conditions and then incubating them on PLBs loaded with human anti-IgM-Cy5 as a model antigen. After incubation cells were fixed, stained and imaged to examine any resultant changes in synaptic architecture. Ramos human B cells are an immortalised cell line derived from a human Burkitt's lymphoma. We found that in the absence of any stimulation Ramos cells actually formed a heterogeneous range of synapse morphologies (Figure 60, Figure 61, condition 'UN'), which was unaffected by any of the culture conditions (Figure 61). This was also true for a range of stimulants and across a number of different human B cell lines across a time course from 1-24 hours (data not shown).

1, 12 or 24-hour stimulation of primary mouse B cells produced similar results (data not shown). After stimulation with each factor individually, although some conditions did appear to cause spread synapses, this effect occurred only in fraction of the cells and often was not reproducible (Figure 62). Instead these synapses could reflect the poor health of the stimulated B cells in the culture. Alternatively, as these B cells were bulk-isolated, diffuse synapses may reflect the presence of other populations than FO B cells (discussed in Chapter 3 and Chapter 4).

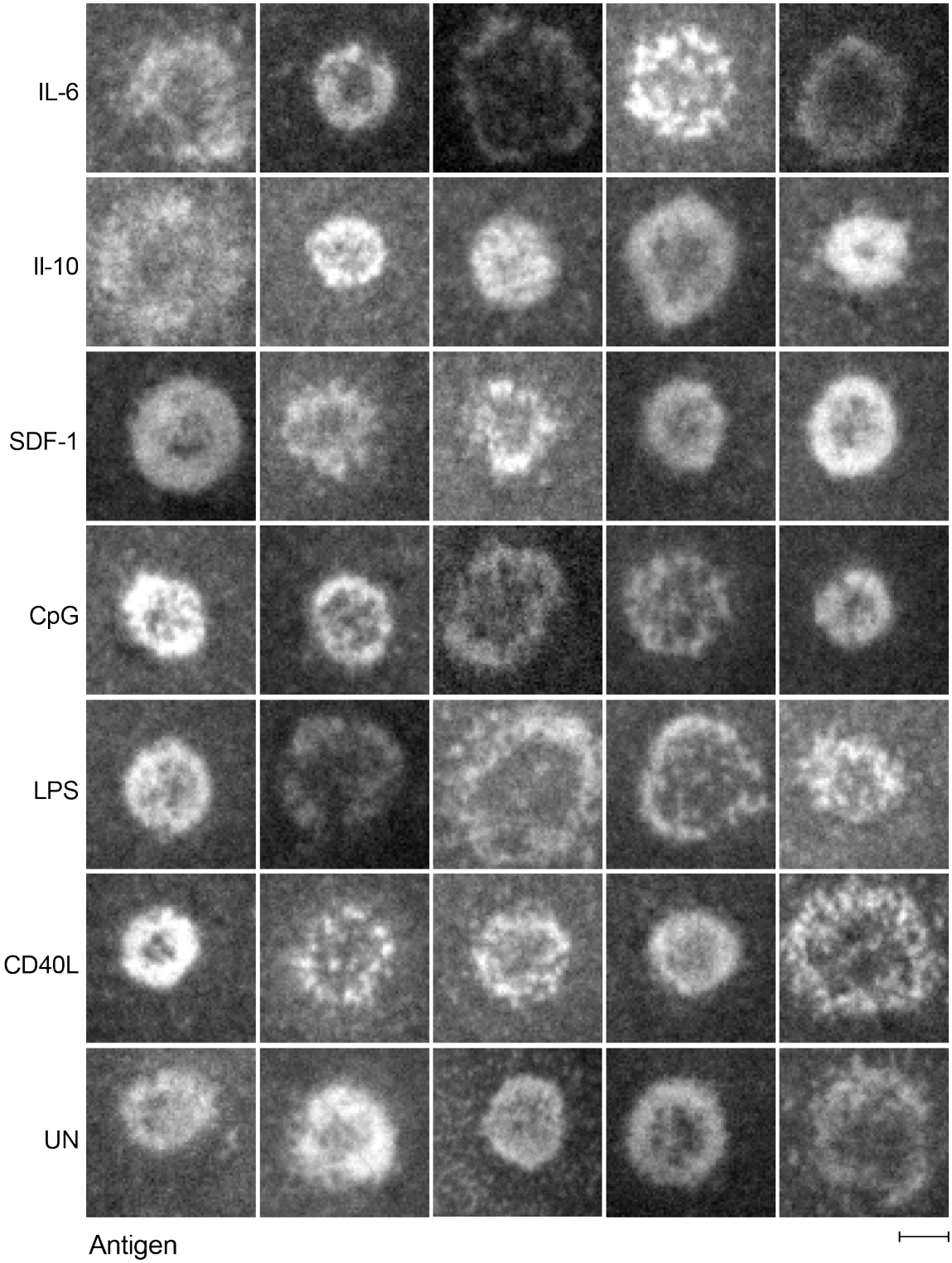

Figure 61 Synapses formed after stimulation of Ramos human B cells with various activating stimuli

Figure 61 Synapses formed after stimulation of Ramos human B cells with various activating stimuli

Image galleries of 5 typical synapses formed after 20 min incubation of Ramos cells (from an overnight stimulation with the indicated stimuli) on human IgM-loaded PLBs. Stimuli as follows:
IL-6, Interleukin-6
IL-10, Interleukin-10
SDF-1, stromal cell-derived factor-1
CpG, 5'-C-phosphate-G-3'
LPS, lipopolysaccharide
CD40L, CD40 ligand
UN, unstimulated cells

Scale bar = 5μm

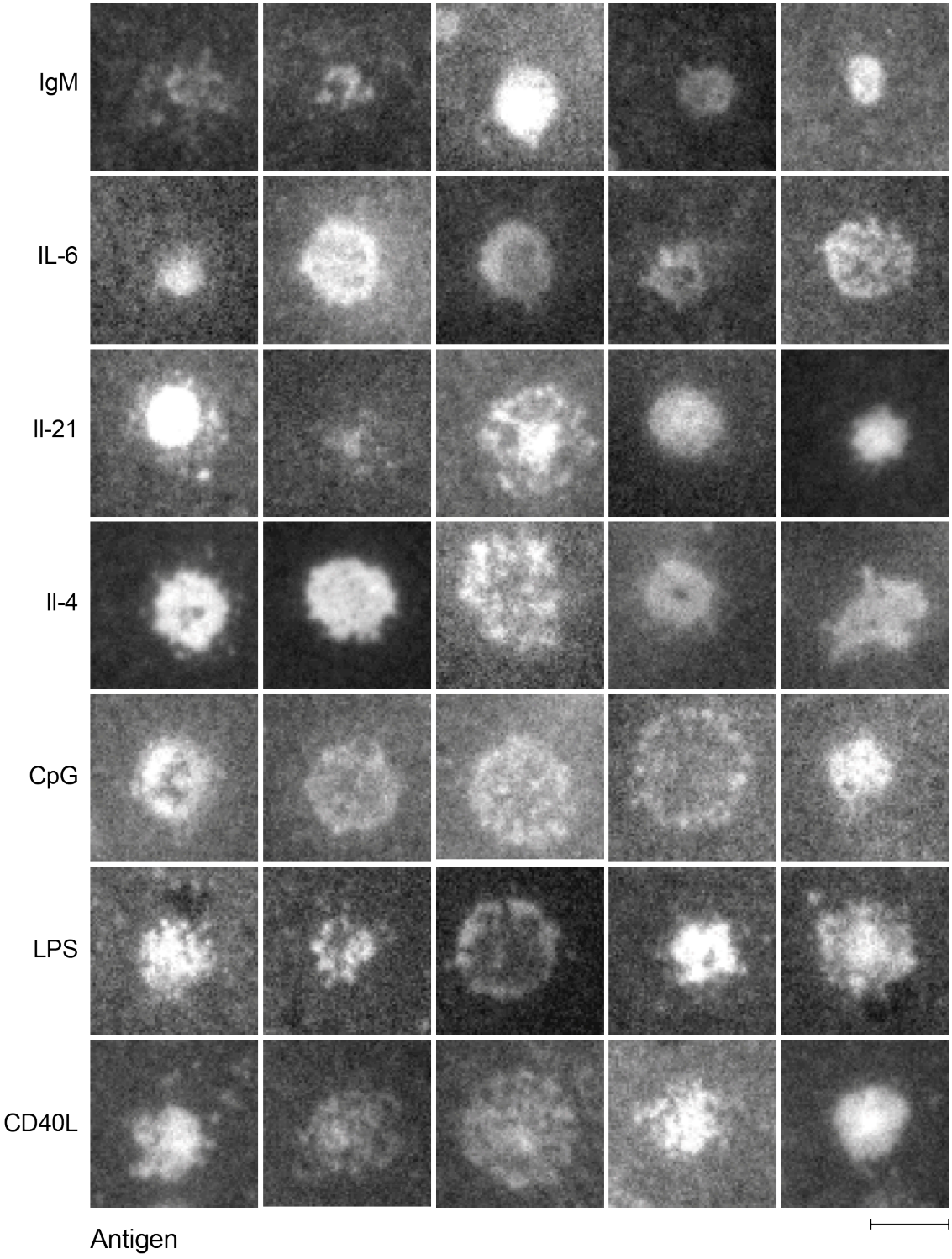

Figure 62 Synapses formed after stimulation of primary mouse B cells with various activating stimuli

Figure 62 Synapses formed after stimulation of primary mouse B cells with various activating stimuli

Image galleries of 5 typical synapses formed after 20 min incubation of B cells (from an overnight stimulation with the indicated stimuli) on anti-Igκ-loaded PLBs. Stimuli as follows:
IgM, Immuglobulin M
IL-6, Interleukin-6
IL-21, Interleukin-21
IL-4, Interleukin-4
CpG, 5'-C-phosphate-G-3'
LPS, lipopolysaccharide
CD40L, CD40 ligand
Scale bar = 5μm

Table 6 Effect of small molecule inhibitors on Ramos synapse morphology

Molecule inhibited	Effect on synapse
MEK	Heterogeneous synapses, no visible effect
BCL-6	Synapse shape similar- tendency to spread more. Tubulin distribution altered, MTOC not polarised properly
JAK	Heterogeneous synapses, no visible effect
PI3K	Heterogeneous synapses, no visible effect
IKK2	Heterogeneous synapses, no visible effect
P38α	Heterogeneous synapses, no visible effect

5.2.2 Inhibition of BCL-6 in cell lines causes a GC-like tubulin phenotype

Taking a complementary approach, we used a range of small molecule inhibitors to try to identify pathways that may be important in controlling synaptic shape. Ramos B cells were cultured overnight with each inhibitor before being allowed to interact with an IgM-Cy5-loaded PLB for 20 mins. Results are summarised in Table 6. Inhibition of BCL-6 was the only condition that resulted in a visible synaptic phenotype (Figure 63). Here, synapses were less heterogeneous, and instead all formed the more spread shape sometimes observed in Ramos cells. Strikingly, MTOC polarisation (visualised with α-tubulin staining) was severely disturbed after inhibition of BCL-6 compared to DMSO control cells (Figure 63, lower panel). After BCL-6 inhibition, the MTOC did not reorient to the centre of the synapse and was instead often off-centre and much higher up the cell. This was reminiscent of GC B cells, where MTOC also did not polarise to the synapse.

This observation prompted us to investigate MTOC positioning in the more 'GC-like' cell lines to establish a link between MTOC polarisation and extent of centralisation. Tubulin organisation diminished as synapse centralisation did, with the most GC-like cell lines exhibiting little MTOC polarisation compared to Ramos B cells (Figure 64). There was also a correlation between MTOC polarisation and antigen centralisation in untreated Ramos cells- individual cells that centralised antigen did polarise their MTOC, whereas cells that did not centralise antigen did not (data not shown). These data suggested that organisation of the microtubule cytoskeleton is a determinant of synaptic shape.

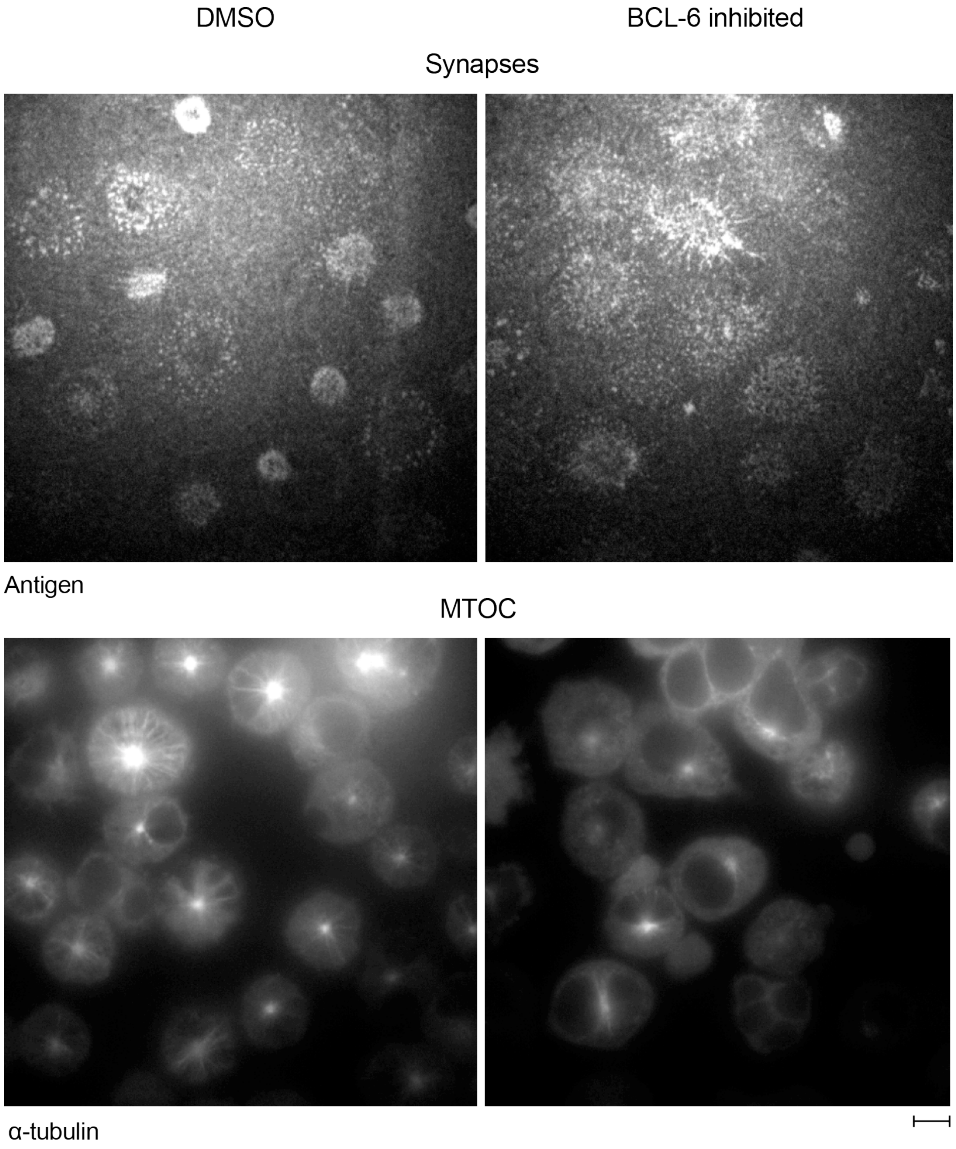

Figure 63 Ramos B cells fail to polarise the MTOC after BCL-6 inhibition

Images show synapses and tubulin staining after 20 min incubation on IgM-Cy5 loaded PLBs. Ramos B cells were inhibited overnight with BCL-6 inhibitor 79-6. MTOC visualised as a single bright spot of α-tubulin fluorescence (lower panels). Scale bar = 5μm

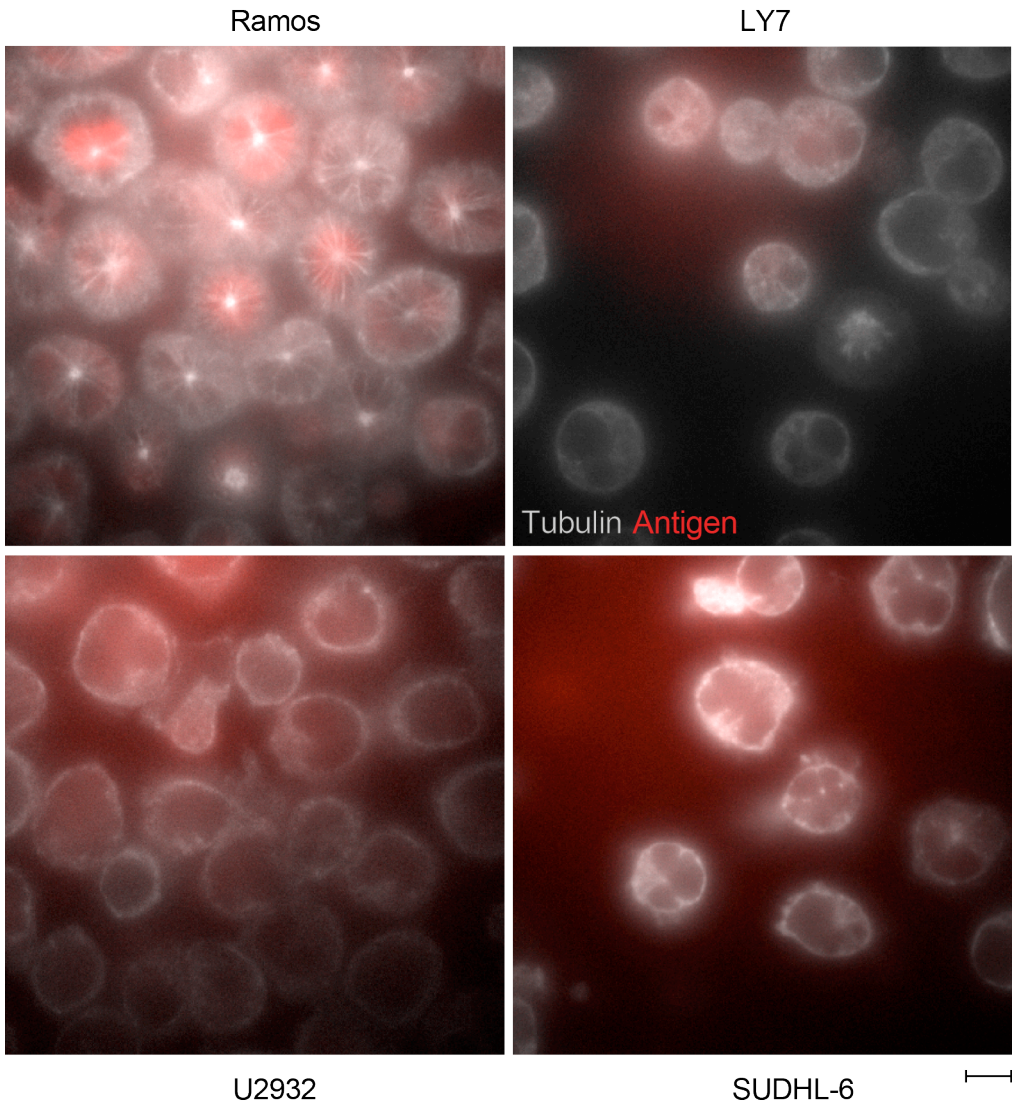

Figure 64 Differential tubulin patterning across human B cell lines

Images of human B cells incubated for 20 min on IgM-Cy5-loaded PLBs. α-tubulin shown in pale grey, antigen shown in red. All images shown in the same z-plane. Scale bar = 5μm

5.2.3 GC B cells have a selective loss of protein kinase C β

The protein kinase C (PKC) family of kinases have been implicated previously in regulation of the cytoskeleton in lymphocytes, and especially in regulation of MTOC reorientation (Quann et al. 2011; Krzewski et al. 2006; Ludowyke et al. 2006). Given the aforementioned data highlighting a connection between MTOC polarisation and synaptic shape, we decided to investigate the contribution of PKCs to GC synapse formation. Expression of PKC family members in cell lines did not recapitulate the expression in primary naive or GC B cells, therefore these investigations were exclusively carried out in primary mouse B cells. We stained primary mouse B cells for 8 different PKC isoforms: the conventional PKCs: PKC-α, PKC-β, PKC-γ, the novel PKCs: PKC-δ, PKC-ε, PKC-η, PKC-ι and the atypical PKC-ζ (data not shown). PKC-β and PKC-δ were the most abundantly expressed PKC isoforms in B cells (Table 7) and stained most brightly in primary naive murine B cells. The staining also increased after activation and was diffusely recruited to the synapse during antigen contact (Figure 65).

GC B cells generally had higher levels of each PKC isoform than their naive counterparts (shown for PKC-δ in Figure 65, c,d). This was with the notable exception of PKC-β (Figure 65,a,b), which was stained at significantly lower levels in GC cells than naive cells. GC B cells also failed to recruit PKC-β to the membrane during synapse formation (Figure 65a, synapse/cell ratio is a measure of membrane recruitment to the synapse). The initial staining was performed with antibodies that recognise the phosphorylated, catalytically competent PKC-β, but also PKC-α. To exclude the possibility of contributions from PKCα (which is minimally expressed in B cells), two other PKC-β-recognising antibodies (one recognising total protein and one recognising the phosphorylated form) were used to stain primary B cells, all with similar results (Figure 66).

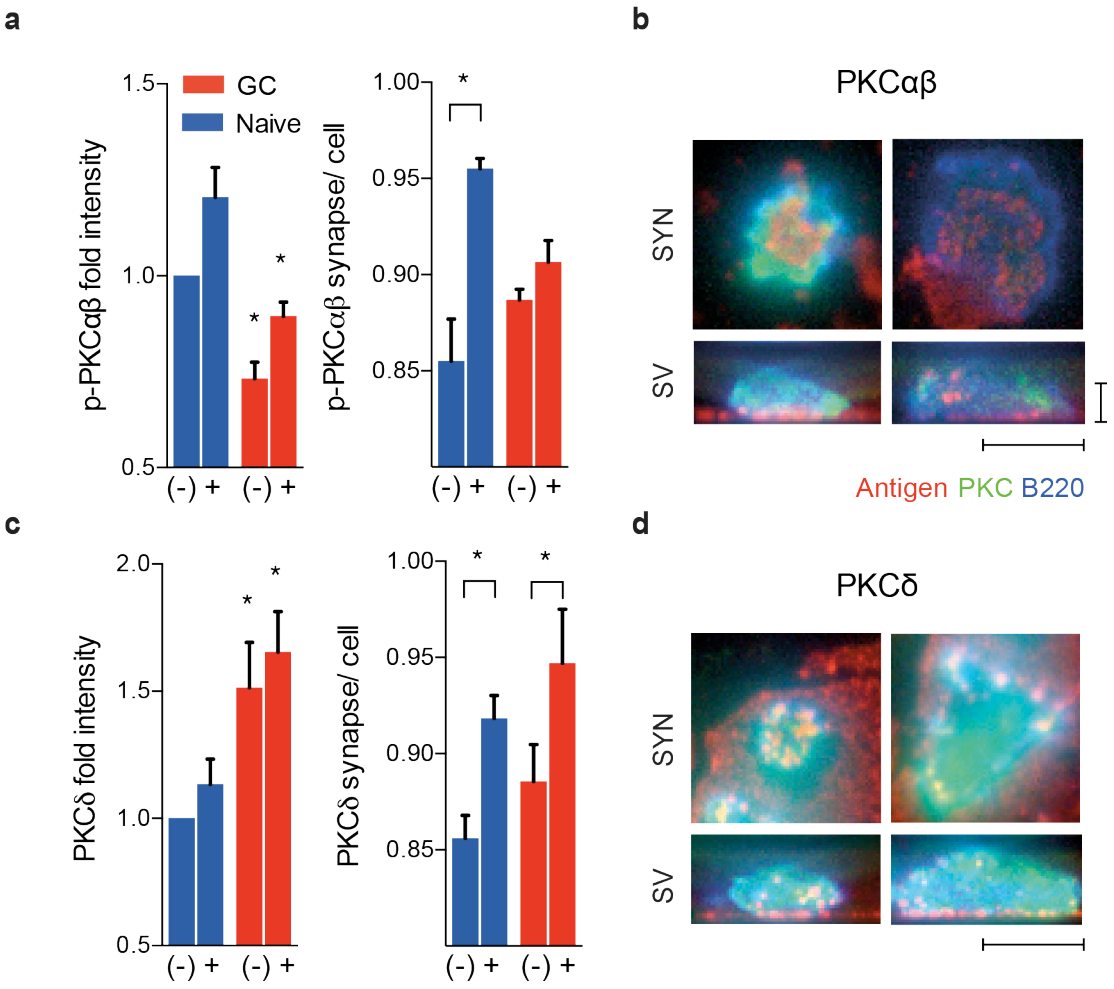

Figure 65 GC B cells have less p-PKCβ, which fails to be recruited to the synapse

Cells were incubated on anti-Igκ-loaded PLBs for 20 min before fixing and staining for PKC isoforms.

(a) Total or synaptic p-PKCαβ levels in naive or GC B cells on (+) or outside of (-) PMSs.
(b) Images of a naive (left) or GC (right) cell stained for p-PKCαβ. SYN = synaptic plane, top down view, SV = sideview reconstruction
(c) Total or synaptic PKCδ levels in naive or GC B cells on (+) or outside of (-) PMSs.
(d) Images of a naive (left) or GC (right) cell stained for PKCδ.

*P < 0.05, GC vs naive cells in paired t-tests. Data from 3 independent experiments. Data are mean and s.e.m. Scale bar = 5μm

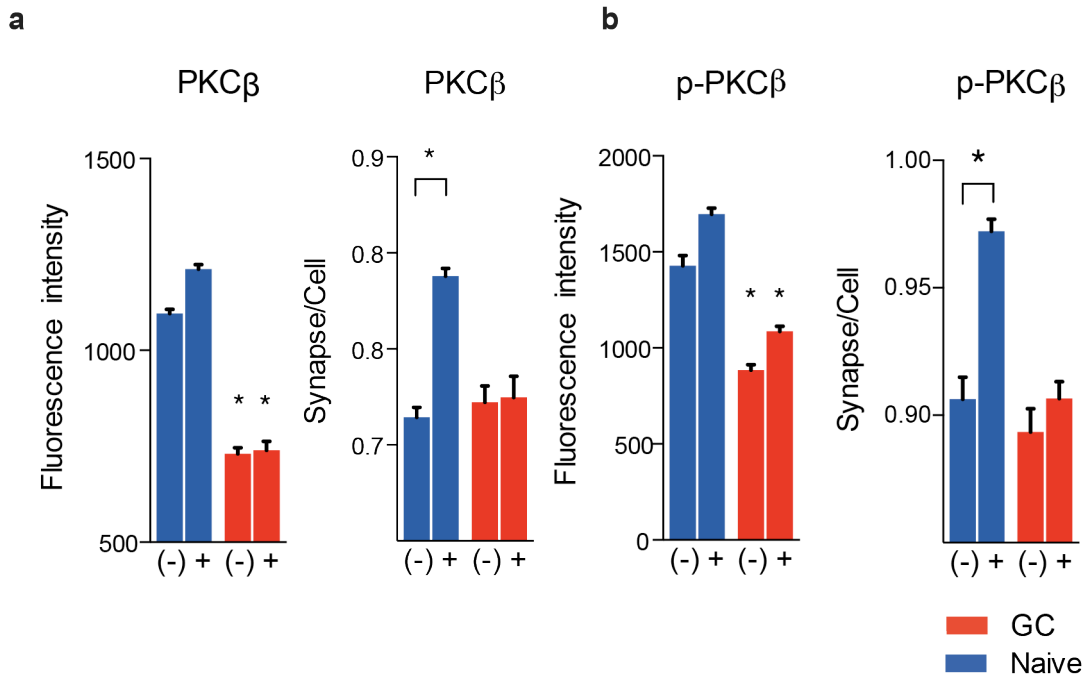

Figure 66 PKC-β antibody staining controls

Cells were prepared in the same manner as in Figure 65 and stained for either total PKC-β (a) or phospho-PKC-β (b). *P < 0.05, GC vs naive cells (or resting vs activated where indicated) in paired t-tests. Data are from 3 independent experiments and are means and s.e.m.

To understand if reduced PKC-β recruitment to the GC synapse is because of a defect of upstream BCR signalling, we stimulated naive and GC B cells with the phorbol 12-myristate 13- acetate ester (PMA) and the calcium ionophore Ionomycin to induce B cell activation independently of the BCR. In this case GC B cells still failed to mobilise PKCβ to the plasma membrane (Figure 67). In contrast PMA/ionomycin induced robust recruitment of the δ-isoform to the plasma membrane in both naive and GC cells. These data indicated a fundamental PKC-β deficiency in GC cells, rather than differential BCR-mediated regulation of the PKC-β recruitment during synapse formation.

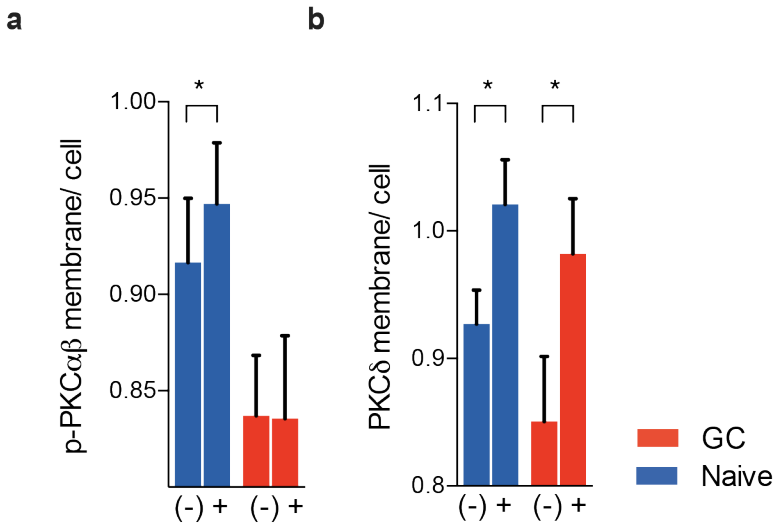

Figure 67 PKC recruitment to the plasma membrane following stimulation with PMA and ionomycin

Cells were stimulated with PMA/ionomycin, before fixing and staining for intracellular (a) PKC-β or (b) PKC-δ. *P < 0.05, unstimulated vs stimulated in paired t-tests. Data are from 3 independent experiments. Data are mean and s.e.m.

5.2.4 Consequences of low PKC-β levels on signalling requirements of GC B cells

To investigate the consequences of reduced PKC-β on GC B cells, we first investigated the role of PKC-β in the NF-κB pathway (see Figure 59 for further details of the PKC/ NF-κB signalling cascade). We designed an assay to quantify translocation of NF-κB into the nucleus, a process mediated by PKC-β. We found that after stimulation through the BCR with antigen GC B cells failed to translocate NF-κB into the nucleus (via staining of the NF-κB subunit p50) (Figure 68). When we provided stimulation via CD40 signalling, bypassing the BCR and therefore bypassing PKC-β-mediated signalling, NF-κB translocation proceeded to the same extent as in naive cells.

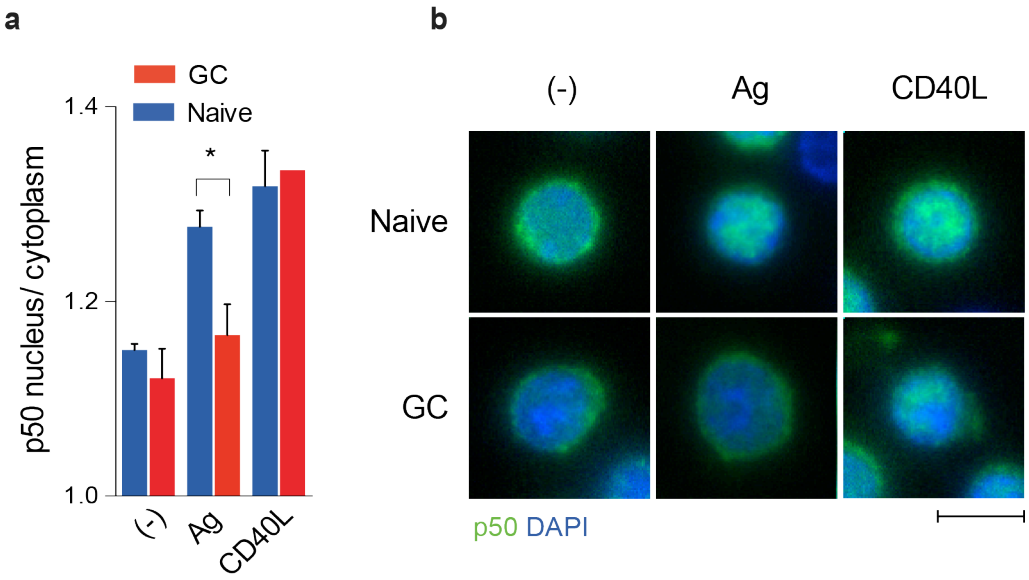

Figure 68 NF-κB translocation is compromised when GC B cells are stimulated through the BCR

(a) Large-scale image quantification of p50 nuclear-to-cytoplasm ratio. *P < 0.05 in paired t tests between bracketed groups. Data are means and s.e.m from three independent experiments.

(b) Staining of p50 and DAPI in naive and GC B cells left unstimulated or stimulated with glass-attached antigen or CD40L Scale bar, 5 μm.

5.2.5 Consequences of low PKC-β levels on the cytoskeleton of GC B cells

In addition to the signalling role of PKC-β we concentrated on aspects of the cytoskeleton reported to interact with the PKC family. We first inhibited PKC-β with the small molecule PKC-α/β inhibitor Gö-6976 and observed effects on antigen extraction and synapse shape. We wondered if PKC-β inhibition in naive cells would induce GC synapse architecture. Although centralisation decreased moderately in naive B cells following PKC-β inhibition, synapses still retained the same naive-like morphology and architecture as DMSO-treated cells (Figure 69, a,b). There was little effect on GC synapses, which remained significantly less centralised than naive B cell synapses. We also found that antigen internalisation was unaffected by PKC-β inhibition in either cell type (Figure 69c).

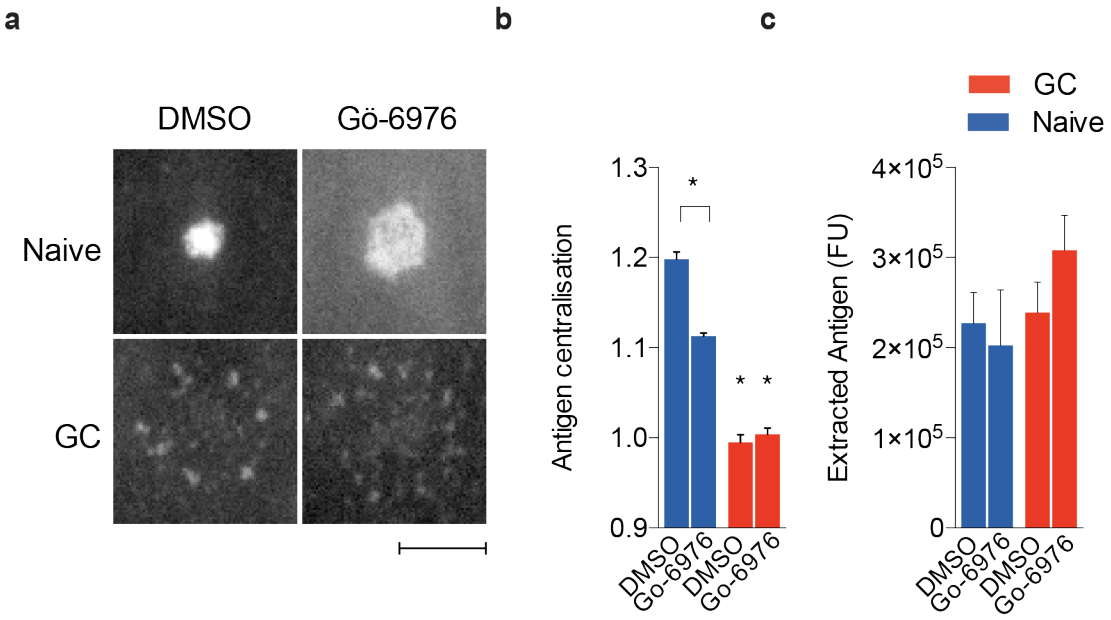

Figure 69 Inhibiting PKC-α/β has no effect on synapse shape or antigen internalisation

(a) Top- down synapse views of a single naive and GC synapse in DMSO and PKC-α/β treated cells. Scale bar = 5μm.

(b,c) Quantification of antigen centralisation or antigen extraction in naive or GC B cells treated with DMSO or PKC-α/β inhibitor before interaction with anti-Igκ loaded PMS for 20 minutes. Data are from three independent experiments. *P < 0.05, GC vs naive cells (or DMSO vs inhibitor where indicated by brackets) in paired t-tests. Data are mean and s.e.m.

Although PKC inhibition had little effect on visible synaptic architecture, it did have some profound effects on the behaviour of myosin IIA. Myosin IIA provides the contractile forces in B cells that support synapse contraction and antigen internalisation. We previously showed that myosin IIA is important in GC cells for regulation of antigen binding and force generation (section 4.2.8, 4.2.9). PKC-β has been reported to interact and phosphorylate inhibitory sites on the heavy chain of myosin IIA in mast cells (Ludowyke et al. 2006). When PKCs were inhibited in B cells either by the aforementioned Gö-6976 inhibitor or the broad-spectrum PKC inhibitor, Gö-6983, differences in phosphorylation of both myosin chains was observed across both B cell types (Figure 70).

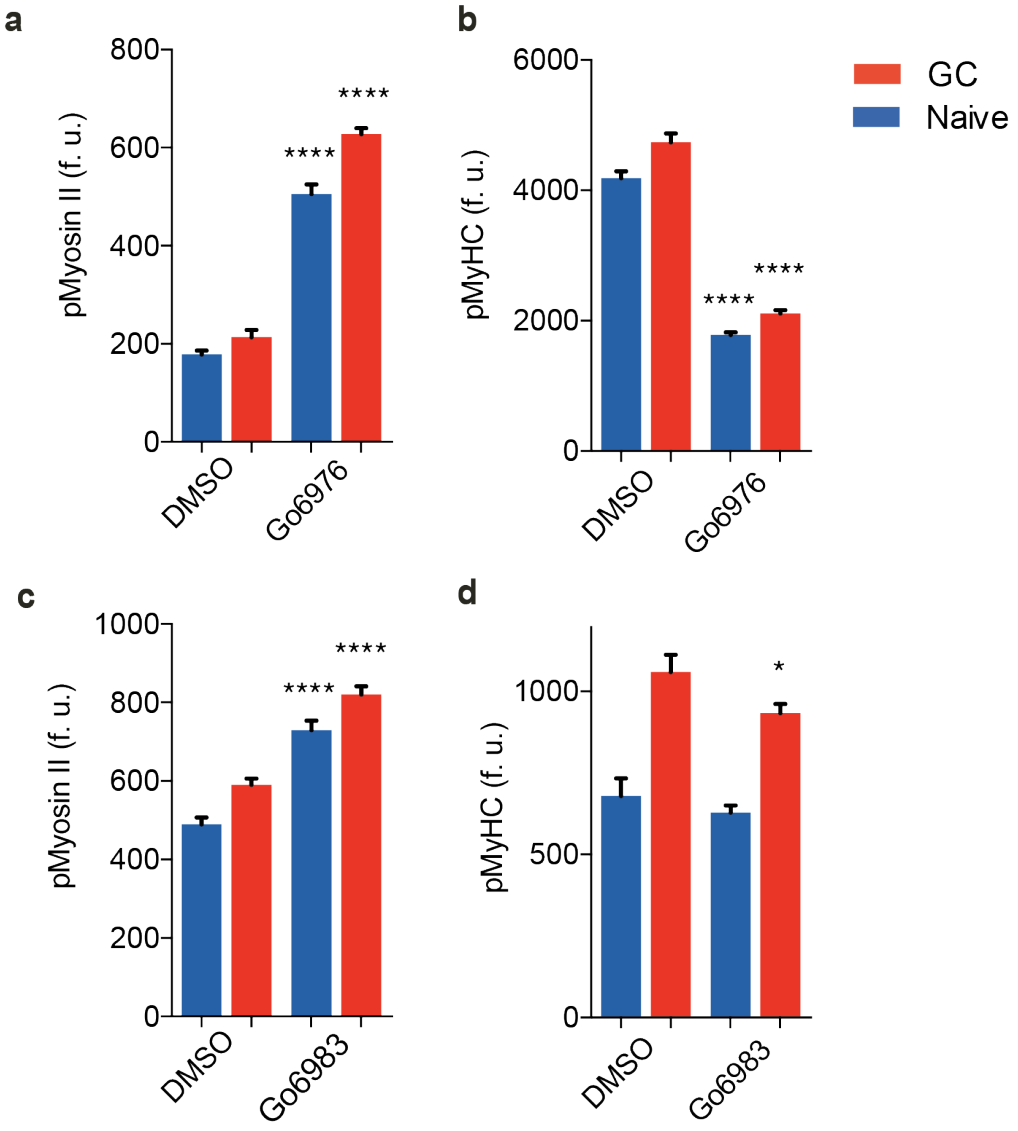

Figure 70 Effect of PKC inhibitors on phosphorylation of myosin heavy and light chains

Naive and GC B cells were treated with DMSO or (a,b) narrow spectrum or (c,d) broad spectrum PKC inhibitors before staining for myosin. MyHC = myosin heavy chain. ****P < 10^{-4} *P < 0.05 in paired t-tests comparing DMSO to inhibitor-treated cells. Data are means and s.e.m. of three (a,b) or two (c,d) independent experiments. f.u., fluorescence units

PKC-β inhibition by Gö-6976 significantly decreased phosphorylation of the heavy chain of myosin IIA (MyHC), but increased phosphorylation of the myosin light chain (MLC) in both naive and GC B cells. Broad-spectrum inhibition caused the same phenotype, but to a lesser degree (Figure 70). Thus, PKC-β is tipping the balance of myosin phosphorylation in favour of the inhibitory sites and this occurs in both naive and GC B cells. However, it should be also noted that despite lower levels of PKC-β in GC cells, phosphorylation of the inhibitory site on the MyHC was always higher in GC cells compared to naive cells. This suggests that the residual PKC-β activity in GC cells is sufficient to phosphorylate MyHC and that other mechanisms exist in GC cells that differentiate their regulation of myosin from naive B cells.

Nevertheless, we hypothesised that inhibition of PKC-β would translate into an increase in applied forces, especially in naive B cells with high levels of PKC-β available. To test this, we imaged either DMSO, Gö-6976 or Gö-6983 treated cells interacting with antigen-conjugated force sensors that unwind at a medium force of 9 pN. As previously shown, GC B cells opened more of the 9 pN sensor than naive B cells under DMSO-treated conditions (Figure 71). Specific inhibition of PKC-α/β with Gö-6976 significantly increased sensor opening in naive B cells as hypothesised. This was further enhanced upon inhibition of a wider range of PKCs with the broad spectrum Gö-6983. Interestingly, sensor opening was also enhanced in GC cells under the same inhibition conditions, to a similar extent to naive cells. In GC cells, specific inhibition of PKC-α/β could not be enhanced much further by inhibition of other PKC isoforms as it was in naive B cells. Thus PKC-β is a negative regulator of B cell contractility, but additional mechanisms independent of PKC-β must exist in GC cells to increase forces applied on antigen.

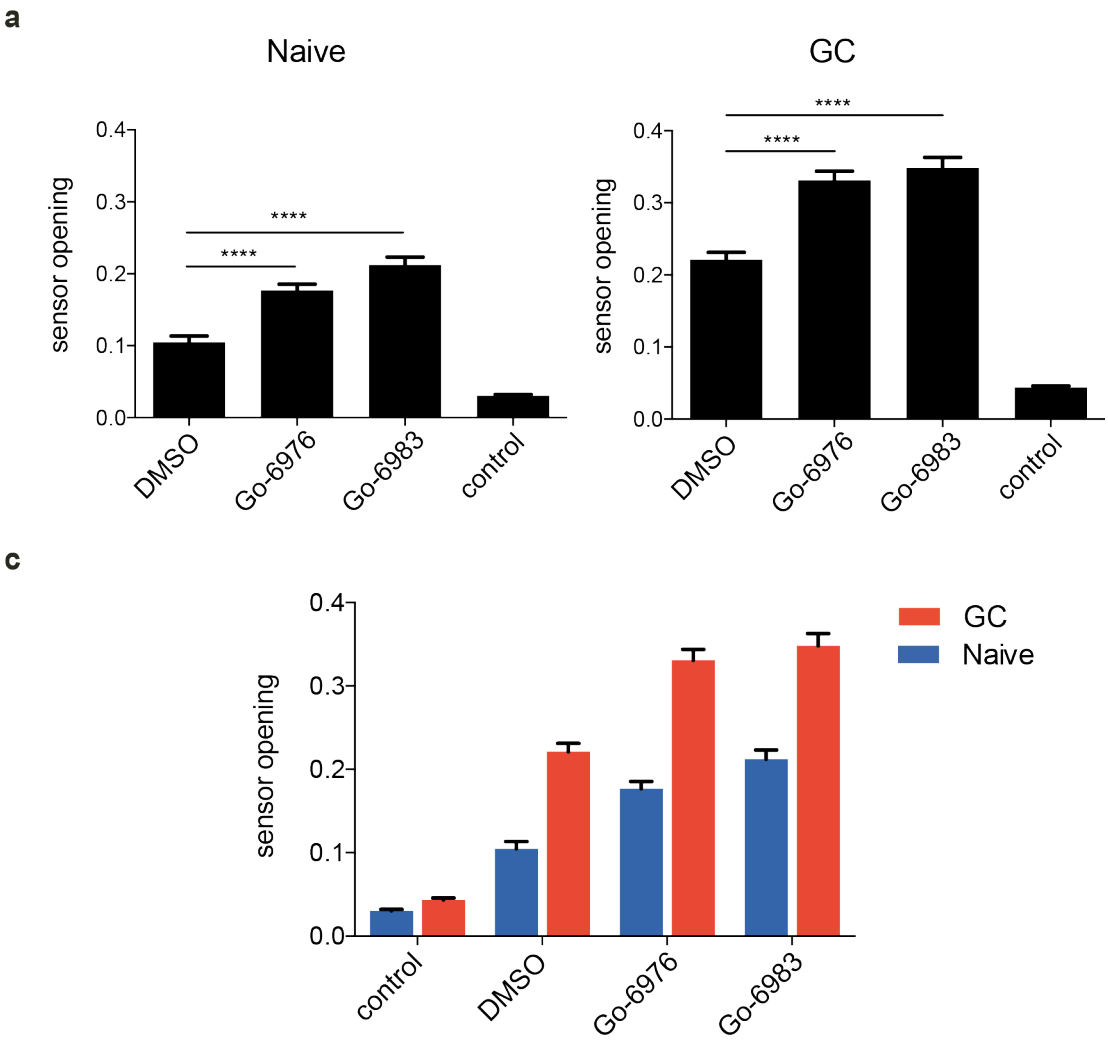

Figure 71 PKC inhibition increases force generation in B cells

Sensor opening ratios displayed as a function of the sensor opening force. The control sensor lacked the force-sensitive hairpin.

(a) Naive B cells

(b) GC B cells

(c) Grouped data of naive and GC synapses for comparison

Data are means and s.e.ms from two independent experiments. **** $P < 10^{-4}$ in paired t-tests. n = 88-133 naive synapses, 63-79 GC synapses.

5.2.6 Manipulating levels of PKCs in B cells *in vitro*- work in progress

To validate the inhibitor experiments and establish a role for PKC-β in regulation of myosin in B cells, we are manipulating the expression levels of PKC-β genetically using cell line models. Our prediction is that overexpression of PKC-β will inhibit myosin activity, whereas knock out of PKC-β will lead to myosin activation. For overexpression, we are using Ramos B cells, which do not express any PKC-β. We intended to transfect Ramos cells with a GFP-tagged PKC-β construct in a lentiviral vector. Overexpression of PKC-δ-GFP and GFP alone will serve as controls. We obtained these constructs in ecotropic retroviral expression vectors from Morgan Huse (Quann et al. 2011).

To infect the human Ramos B cells, we first cloned these constructs into the lentiviral expression vector p.Lenti.puro following the cloning strategy set out in Figure 72. Briefly, this included sequencing of the insert provided by the Huse lab followed by extraction of the insert by PCR. During this PCR step, an additional SpeI restriction site was cloned into the 5' end of the insert, upstream of the start site of the PKC sequence for insertion into the multiple cloning site in the destination vector. The resultant PCR product and target vector were both digested with SpeI and BamHI restriction enzymes and then ligated together to produce the final lentiviral vector complete with PKC-linker-mGFP insert for virus production. This work is currently ongoing, with lentiviral overexpression of PKC-β in Ramos cells planned in the near future.

These experiments will be later followed up in the lab by knocking out PKC-β in the SUDHL4 cell line using CRISPR/Cas9 tools.

Table 7 Human PKC expression levels (data from immgen.org)

Name	Gene symbol	Primary	Ly7	Raji	Ramos	SUDHL6	BJAB	Daudi
PKCα	PRKCA	+	+	+	++	++	+	+
PKCβ	PRKCB	+++++	+	++	-	++	++	++
PKCδ	PRKCD	++	++	++	++	++	++	++
PKCε	PRKCE	+	+	+	++	+	+	+
PKCγ	PRKCG	+	-	+	+	-	+	-
PKCη	PRKCH	+	-	+	+	+	+	+
PKCι	PRKCI	++	+	+	++	+	++	++
PKCθ	PRKCQ	+	-	-	-	-	-	-
PKCζ	PRKCZ	++	-	+	+	-	+	-

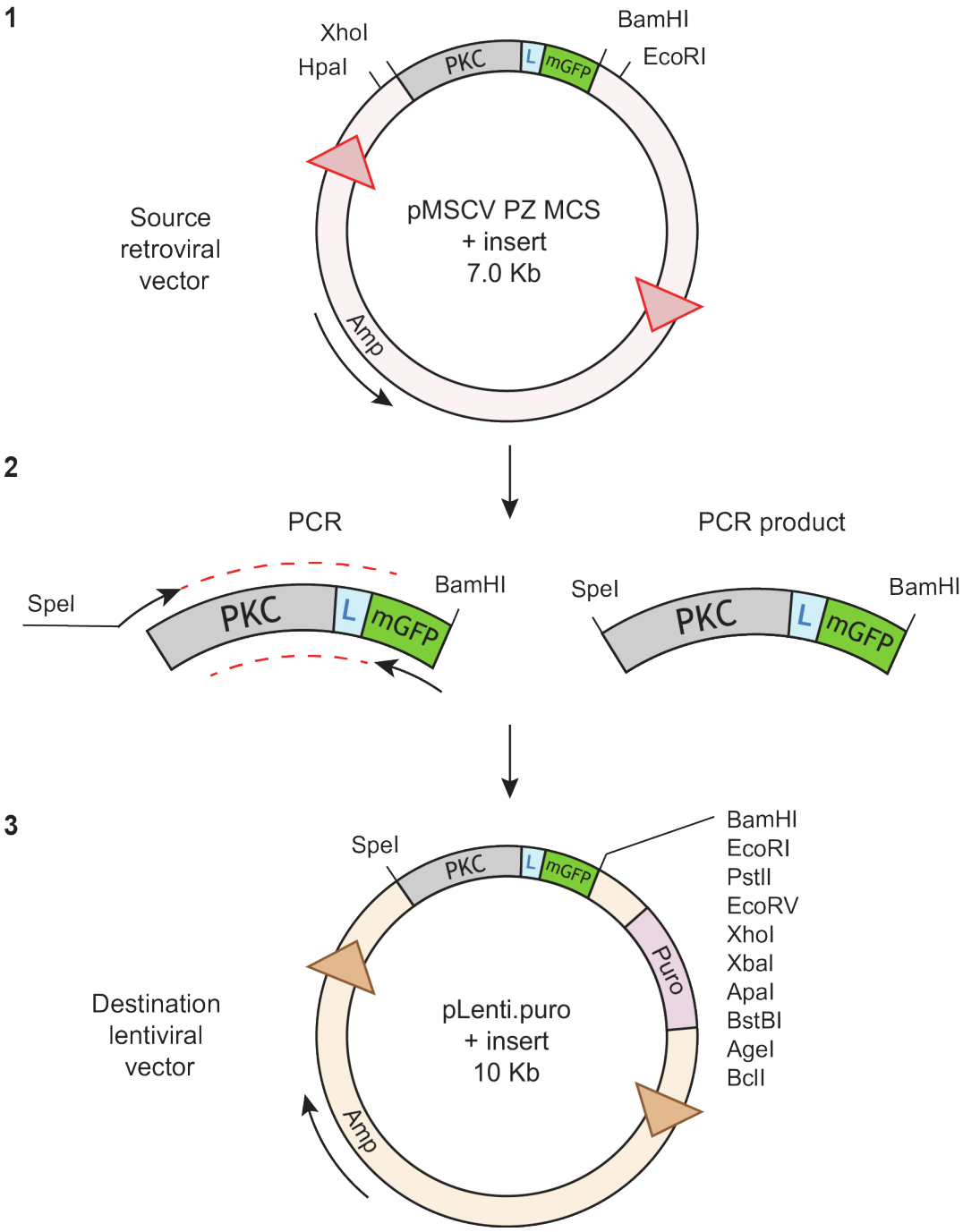

Figure 72 Cloning strategy to produce lentiviral constructs containing PKCs tagged with GFP

5.2.7 Manipulating levels of PKCs in B cells *in vivo*- work in progress

To investigate the role of PKC-β in the GC reaction we also intend to overexpress PKC-β *in vivo* and assess the GC recruitment and dynamics of PKC-β overexpressing B cells. To achieve this aim we will use the retroviral expression vectors mentioned previously to transfect bone marrow (BM) or fetal liver (FL) hematopoietic stem cells using material from Hen Egg Lysozyme (HEL)-specific mice. BM of FL cells overexpressing PKCs will be used to reconstitute sub-lethally irradiated mice. After full reconstitution of the immune system, the B cells will be transferred into wild type mice and immunised with HEL proteins conjugated to SRBC to induce GC formation. The frequency of PKC-β overexpressing cells (marked by GFP) will be assed in naive, GC, and plasma cells at different timepoints after immunisation.

So far, a series of pilot proof-of-concept experiments have been performed to establish the infection and transfer protocols. After retrovirus production, NIH 3T3 murine embryonic fibroblasts were infected with PKC-β, PKC-δ, or GFP only viruses and analysed by flow cytometry to assess infection rates. This produced up to 20% GFP positive cells, confirming competent virus was produced (Figure 73).

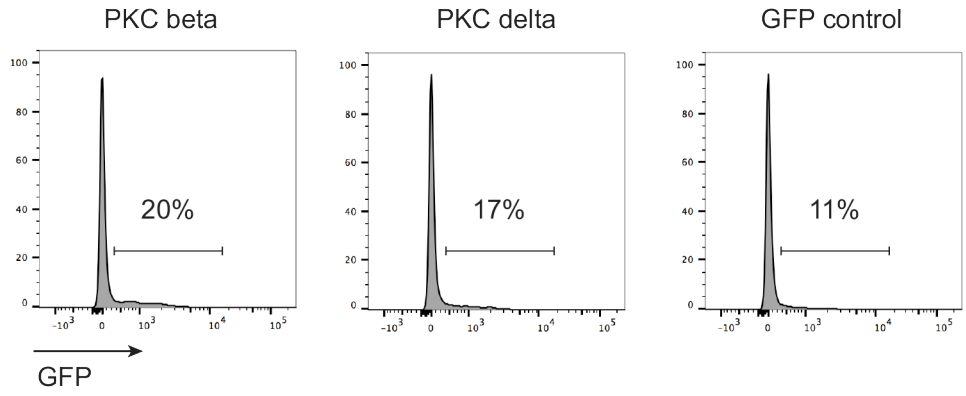

Figure 73 Retroviral infection of NIH 3T3 cells with PKC-mGFP

Plots show histograms of GFP expression after viral infection. Cells were pre-gated to exclude doublets and dead cells. Percentages refer to frequency of GFP+ single, live cells.

Following successful infection of the 3T3 cell line, we went on to infect primary mouse FL cells. In pilot studies, wild type mice were used in place of HEL-specific FL cells. Successful infection of stem cells was confirmed by flow cytometry, following the gating strategy outlined in Figure 74.

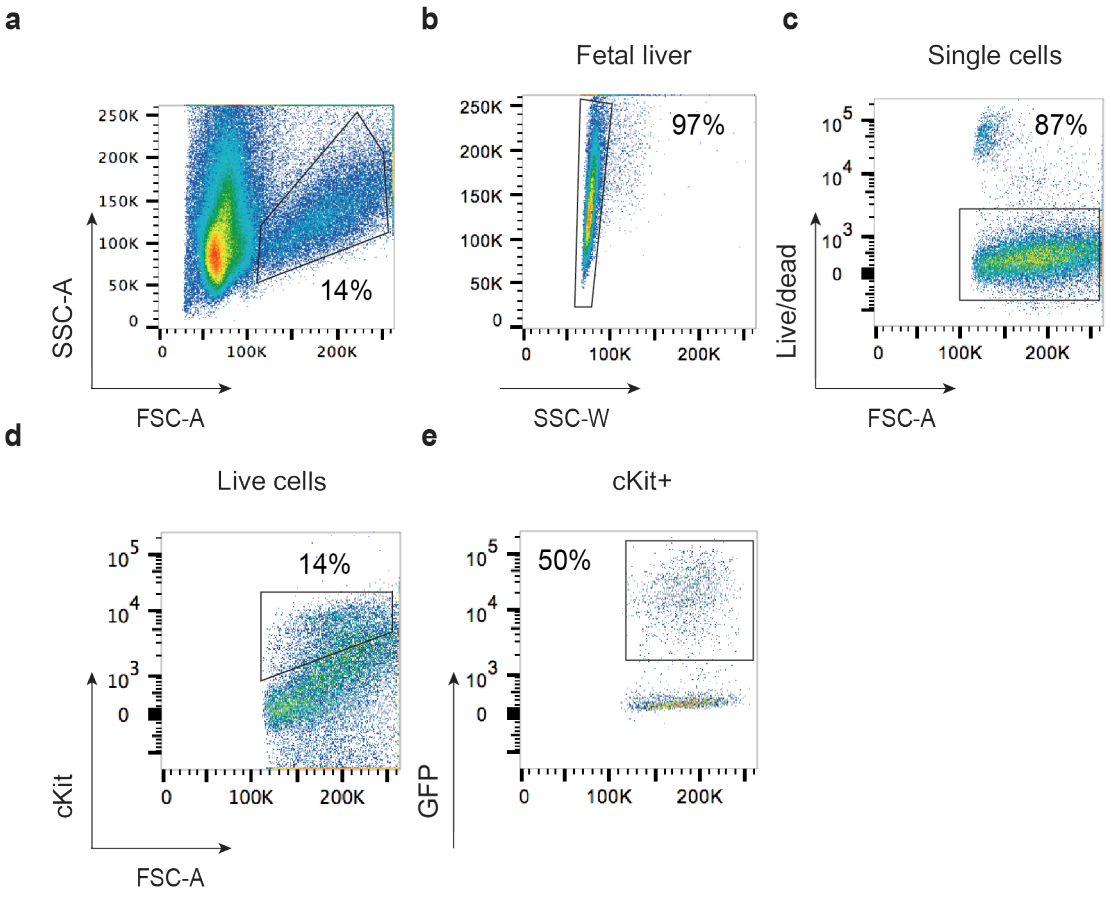

Figure 74 Fetal liver gating strategy

Fetal liver cells were stained for 30 min on ice and data plotted using FlowJo. Percentages refer to percentage of parent populations. Gating strategy as follows:

(a) Dot plot showing all events and gated on cells based on forward-scatter/ side-scatter characteristics
(b) Doublet exclusion
(c) Total live B cells, Live/dead-
(d) Stem cells, cKit+, 14%
(e) Successfully infected stem cells, cKit+, GFP+, 50%

Infection was consistent amongst PKC isotypes and GFP control viruses (Figure 75) Typically around 50% of cKit+ FL stem cells were GFP+, with very low background GFP fluorescence in polybrene-only control samples. After confirmation of successful infection, $0.5x10^6$ fetal liver cells were injected i.v into sub lethally irradiated congenically marked host mice to reconstitute their immune systems. After 12 weeks of reconstitution, mice were immunised with SRBCs to induce GC formation and their spleens analysed 12 days later. One fully successful reconstitution was achieved, where significant numbers of PKC-β overexpressing GFP positive donor cells could be identified by flow cytometry in blood after 8 weeks, and in the spleen after immunisation at 12 weeks (Figure 76).

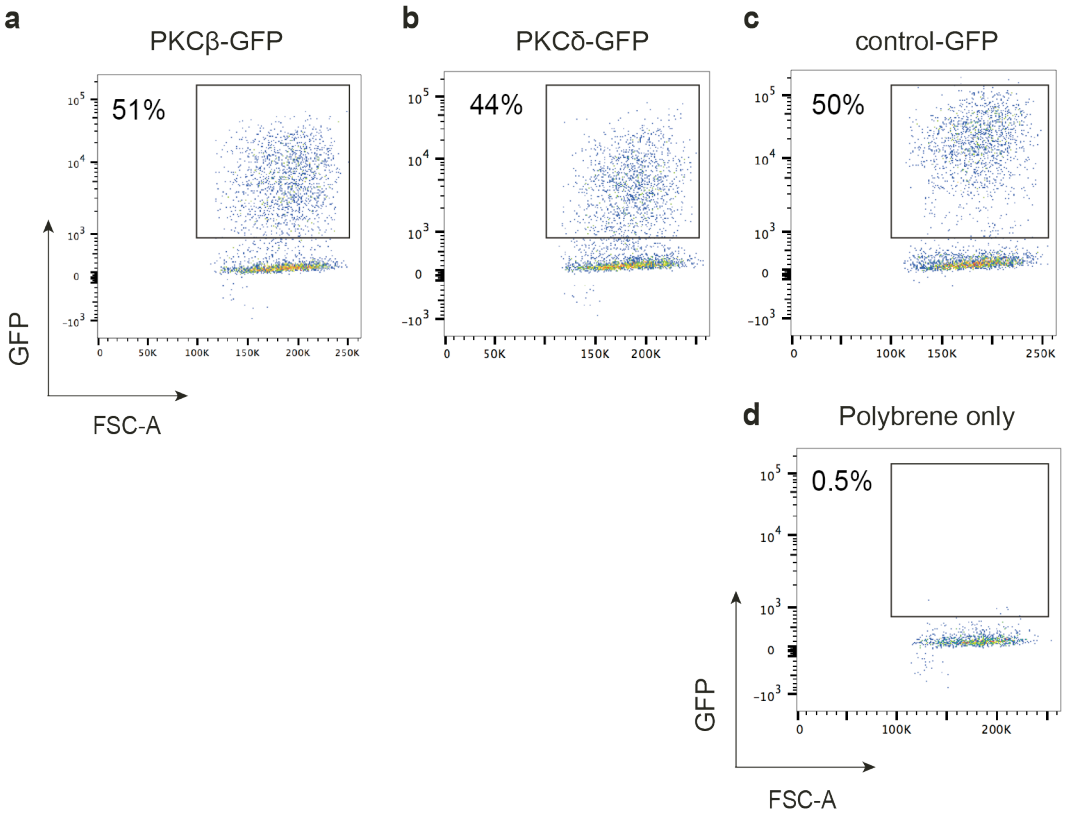

Figure 75 Successful infection of fetal liver cells with PKC-mGFP constructs
Cells were stained and pre-gated as described in Figure 74. Percentages refer to frequency of single, live, GFP+, cKit+ cells.

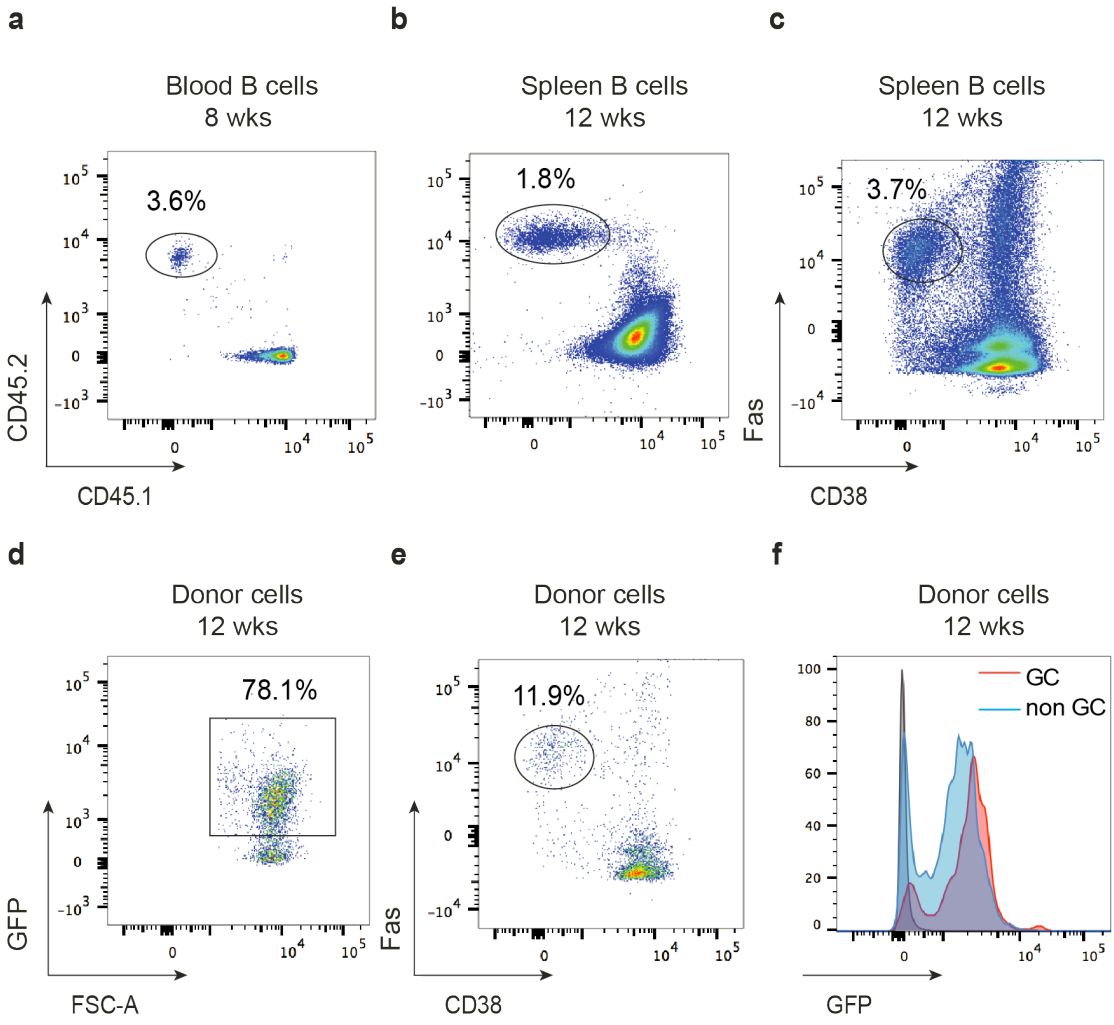

Figure 76 PKC-β overexpressing B cells can be identified in the spleen and in GCs after immunisation

Splenocytes were stained for 30 min on ice and data plotted using FlowJo. Percentages refer to percentage of parent populations, detailed below. Cells were pre-gated on single, live, B200+ B cells

(a) 8 week blood sample, CD45.2 donor B cells, 3.6%
(b) 12 week spleen sample, CD45.2 donor B cells, 1.8%
(c) 12 week spleen sample, Fas+, CD38- GC cells, 3.7%
(d) 12 week donor B cells, GFP+ fraction, 78.1%
(e) 12 week donor B cells, Fas+, CD38- GC cells, 11.9%
(f) 12 week donor B cells, GC vs non GC GFP levels

Successful immune reconstitution and immunisation produced GCs in the spleen at day 12 p.i. (3.7%, Figure 76c). Donor cells made up 1.8% of all splenic B cells, but were overrepresented in the GC, where 11.9% of all donor B cells were GC cells compared to 3.4% of host B cells. Whereas 51% of the starting cKit+ fetal liver stem cells expressed GFP, 78.1% of surviving donor cells were GFP+. GC and non-GC donor populations differed in their expression of GFP. Donor GC cells were 85.8% GFP+, and expressed higher levels of GFP on average (Figure 76f) than non-GC donor cells, 72% of which were GFP+. Therefore based on this pilot experiment, overexpression of PKC-β in B cells may aid either recruitment into the GC, or selection within an ongoing GC. It should be noted however, that immunisation with SRBC does not allow specific investigation of antigen specificity and therefore no information related to affinity selection of GC B cells may be gleaned from this data at this stage. These preliminary data provide good evidence that retroviral overexpression of PKC-β is possible, and may provide useful information concerning the GC reaction in future studies.

5.3 Discussion

We attempted to dissect the determinants driving synapse shape in GC B cells to understand their impact on cellular outcome. However, stimulation of both immortalised B cell lines and primary B cells with a wide range of stimuli produced no reproducible differences in synaptic architecture that would mimic GC synapses. Some stimuli did produce some subtle alterations in synaptic patterning. Stimulation of primary B cells with the Toll-like receptor 9 (TLR9) agonist CpG caused some spreading of synapses. TLR9 recognises unmethylated bacterial DNA (Hemmi et al. 2000), termed a 'pathogen-associated molecular pattern', and TLR9 activation is often associated with rapid differentiation of B cells into plasma cells (Capolunghi et al. 2008). Therefore, this phenotype may represent an intermediate B cell plasmablast population, with specific synaptic characteristics. Synaptic architecture in antibody secreting plasma cells or plasmablasts has not yet been studied in our system or any other, but is feasible and could be an interesting avenue for future study.

It is likely that a combination of inputs integrated from many pathways contribute to the GC synapse architecture. The complex nature of the GC-microenvironment cannot be fully recapitulated *in vitro*. Consequently, naive B cells cannot be driven towards full GC differentiation *in vitro* either, supporting the notion that context-specific signals derived from the microenvironment, from other immune cells and from supporting stromal cells all contribute to the induction and maintenance of the GC phenotype. Thus, the architecture of GC synapses seems to be a cell-intrinsic feature of the GC differentiation programme to equip cells for affinity discrimination. We do not yet understand which upstream signals or later transcriptional alterations drive this, or when these occur, but given that GC cells respond with peripheral synapses *ex vivo* after stimulation with any crosslinking antigen we can conclude commitment to the GC phenotype designates peripheral synapses.

To understand which upstream signals or transcriptional pathways may contribute to the GC synapse, we inhibited a range of molecules involved in B cell differentiation. Of these, BCL-6 inhibition in Ramos cells produced a synapse

phenotype with more peripheral antigen distribution and with a lack of MTOC polarisation, features observed in primary GC B cells. This effect was unexpected, because BCL-6 is a transcription factor that positively regulates GC B cell differentiation. One possibility is that the function of BCL-6 is altered in the lymphoma cell line, as supported by data showing that BCL-6 targets partly different genes in normal GC cells and in lymphomas (Ci et al. 2009). Alternatively, BCL-6 inhibition may cause differentiation of the cells towards plasmablasts, which also seem to have a more peripheral distribution of antigen in their synapses as noted above.

Nevertheless these data suggested a connection between synapse architecture and MTOC polarisation, which in turn led us to investigate the PKC family of proteins. PKC proteins are known to play indispensible roles in microtubule dynamics via interaction with tubulin in T cells (Huse 2012). Novel PKC isoforms were implicated in proper MTOC positioning during cytotoxic T cell polarisation and cell killing in a TCR-signalling dependent manner (Huse et al. 2008; Quann et al. 2011). Some key similarities and differences exist for PKCs in the B cell system. Firstly, expression pattern of PKC isoforms do not match T cells, where all isoforms are expressed (Huse 2012). Instead, expression data from public databases in combination with our own imaging showed PKC-β and PKC-δ to be the predominant isoforms present in murine and primary human B cells. PKC-β is a conventional PKC isoform that is regulated by lipid second messengers like DAG as well as calcium whereas PKC-δ is a novel isoform regulated solely by DAG (Nishizuka 1992). We found PKC-β recruitment to the synapse to be reduced in GC cells following antigen stimulation and after PMA/ionomycin stimulation acting independently of the BCR. This implied a fundamental lack of PKC-β activity, as opposed to a failure of upstream pathways. Indeed we saw normal or slightly increased calcium flux in GC B cells, indicating good activation of PLCγ, a step in BCR signalling directly preceding recruitment of PKC-β. Publically available databases (immgen.org) list reduced PKC-β mRNA in GC B cells, suggesting silencing of the pathway at the transcriptional level.

There is significant controversy surrounding the capacity of GC B cells to activate BCR signalling and about the contribution of BCR signalling to selection in the GC (Khalil et al. 2012; Mueller et al. 2015). Our data suggest that although GC cells induce robust proximal BCR signalling during interaction with membrane-bound antigen, propagation of signalling by PKC-β is impaired. Consistently with this notion, we found that GC B cells were inefficient in nuclear translocation of the p50 component of NF-κB a step that requires PKC-β. The NF-κB pathway is central to GC establishment and maintenance through the induction of the transcription factor c-Myc (Heise et al. 2014). c-Myc is a master regulator of cellular proliferation and has key roles in driving cyclic re-entry and proliferation of positively selected GC cells during affinity maturation (Calado et al. 2012; Dominguez-Sola et al. 2012). Our finding supports models suggesting BCR signalling is not sufficient to alone drive selection during the GC reaction (Victora et al. 2010). These models implicate T cell help in GC selection, through signals delivered by T_{FH} through the CD40 signalling pathway (Victora & Nussenzweig 2012; MacLennan 1994). Indeed, when we stimulated primary GC B cells with CD40L, we fully restored their ability to translocate NF-κB into the nucleus. Therefore, we show that despite proximal BCR signalling being intact and fully functional in GC B cells, low PKC-β levels hamper BCR-derived NF-κB activity, creating a reliance on T-cell derived signals delivered through CD40. This model fits well with current understanding of affinity selection in the GC, where GC cells internalising and presenting more pMHCII acquire higher levels of T cell help, achieving more efficient activation and thus becoming positively selected.

Inhibiting PKC-β in naive B cells did not result in a GC phenotype in terms of synapse patterning or amount of antigen internalised. However PKC-β inhibition did alter the balance of phosphorylation of myosin chains, and did increase pulling forces generated in B cell synapses. When we specifically inhibited PKC-β in naive B cells, we could detect significant increases in MLC phosphorylation accompanied by the opposing decreases in phosphorylated MyHC at Ser1917. This translated into increased opening of 9 pN force sensors. PKC-β was shown to be the signalling molecule responsible for inhibitory phosphorylation of the MyHC in mast

cells (Ludowyke et al. 2006), but its role in B cells is currently undefined. Our data indicate that PKC-β is a negative regulator of myosin contractility in B cells.

Given these results, we propose that lower levels of PKC-β in GC B cells may be responsible for the higher levels of pMLC observed in GC B cells. Mechanistically, PKC-β could control the balance of activation in myosin chains, where the excitatory light chain is robustly phosphorylated downstream of BCR signalling (Natkanski et al. 2013) but lacks the regulation of inhibitory signals delivered from the direct phosphorylation of the heavy chain at Ser1917 by PKC-β. In turn, the resultant increased activity of myosin is responsible for the increased force generation capabilities and regulation of antigen binding observed in GC B cells. However, our current data using inhibitors do not fully support this model as an explanation for the difference between naive and GC cells. Namely, PKC-β inhibitors showed similar changes in myosin phosphorylation and in pulling forces in both naive and GC cells. In addition, staining with antibodies recognising the inhibitory site Ser1917 was higher in GC cells than in naive cells. This was somewhat unexpected given the reduction in GC pPKC-β levels. One possibility is that GC B cells contain enough PKC-β activity to regulate myosin, but that this PKC-β is not sufficiently available to carry out signalling in the immune synapse. It is also possible that blanket inhibition may produce effects overriding physiological differences that exist between naive and GC cells. In summary, we implicate PKC-β as a regulator of myosin in B cells, capable of balancing activating phosphorylation of the MLC with regulatory phosphorylation of the MyHC.

Some outstanding questions developing from this data are currently being addressed experimentally. Firstly, to better characterise the effects of PKC-β on MLC and MyHC phosphorylation without the use of pharmacological inhibitors, we have created lentiviral vectors carrying either PKC-β or PKC-δ fused via a short linker to a mutant non-dimerising GFP protein suitable for high-resolution imaging. We intend to infect Ramos B cells (an ideal B cell model for this purpose due to their lack of endogenous PKC-β) and analyse the resultant cellular outcome. We are interested in imaging PKC-β localisation during synapse formation through live-

cell imaging. We would also like to use this system to fully characterise the contribution of PKC-β to phosphorylation of MyHC and to force generation.

In parallel, we are preparing bone marrow and fetal liver chimeras to investigate effects of PKC-β overexpression on GC dynamics *in vivo.* We hope that this may provide insight into the role of PKC-β downregulation in the entry into and selection of cells within the GC. It is possible, for example, that excessive PKC-β activity will confer advantage to GC B cells because they will be less dependent on T cell help. Alternatively, excessive PKC-β activity may promote exit from the GC and differentiation into plasma cells or memory cells.

In summary, we have shown GC-specific dampening of BCR-induced signalling through PKC-β to NFκB and a general role for PKC-β in regulation of myosin contractility. This has added to our understanding of the GC response on two levels. Firstly, we established a mechanism by which direct interaction of PKC-β with myosin regulates the strength of antigen extraction forces, which is a potential mechanism to increase stringency of affinity discrimination in GC B cells. Secondly, we showed that in addition to antigen extraction and internalisation, the acquisition of T cell help is paramount to fulfilling transcriptional requirements for effective positive selection in the GC.

Chapter 6. Perspectives

During this PhD I characterized a novel mechanism for affinity-based selection in GC B cells, through regulation of the immune synapse. This was achieved by developing a large-scale imaging platform to capture interactions of cell populations with membrane-presented antigens. This was the first time GC cells have been imaged *ex vivo* in high-resolution and provided insights into immune synapse function and how its modulation can promote specific cellular outcomes. The novel link between mechanical forces and signalling induced cytoskeletal reorganisation is summarised in our working model, depicted and explained in Figure 77.

Naive B cell synapses are optimised for sensitive activation of all cells recognising antigen, whereas GC synapses are specialised for selection of cells binding antigen with the highest affinity. This body of work describes the multiple mechanisms that increase stringency at key points during GC cellular interactions. GC B cells have fewer surface BCRs (Chan & Brink 2012) and lack the IgD BCR isotype thought to function as an amplifier of surface BCR events in naive B cells (Brink et al. 1995; Brink et al. 1992; Roes & Rajewsky 1993). In spite of this, we saw that GC B cells contacted similar amounts of antigen but formed highly unusual peripheral synapses, able to function efficiently to internalise antigen without the requirement of cSMAC formation. GC cells arrange antigen in smaller clusters, which they actively segregate to the poles of the contact for interrogation by strong mechanical forces, generated by increased myosin IIA contractility. The combination of low receptor density, small cluster size and increased bond breakage represents the first layer of stringency imposed on GC B cells, mediated largely by novel cytoskeletal rearrangements of F-actin, tubulin and myosin IIA.

Additionally, signalling responses were tuned as a function of substrate stiffness, with stiffer substrates promoting stronger BCR signalling responses, a phenomenon similarly observed by others (Natkanski et al. 2013; Wan et al. 2013). In other systems, such as the DC-T cell synapse, cytoskeletal contributions from the DC (or APC) side of the synapse had implications for resultant T cell outcome (Comrie & Burkhardt 2016; Comrie et al. 2015; Comrie et al. 2015;

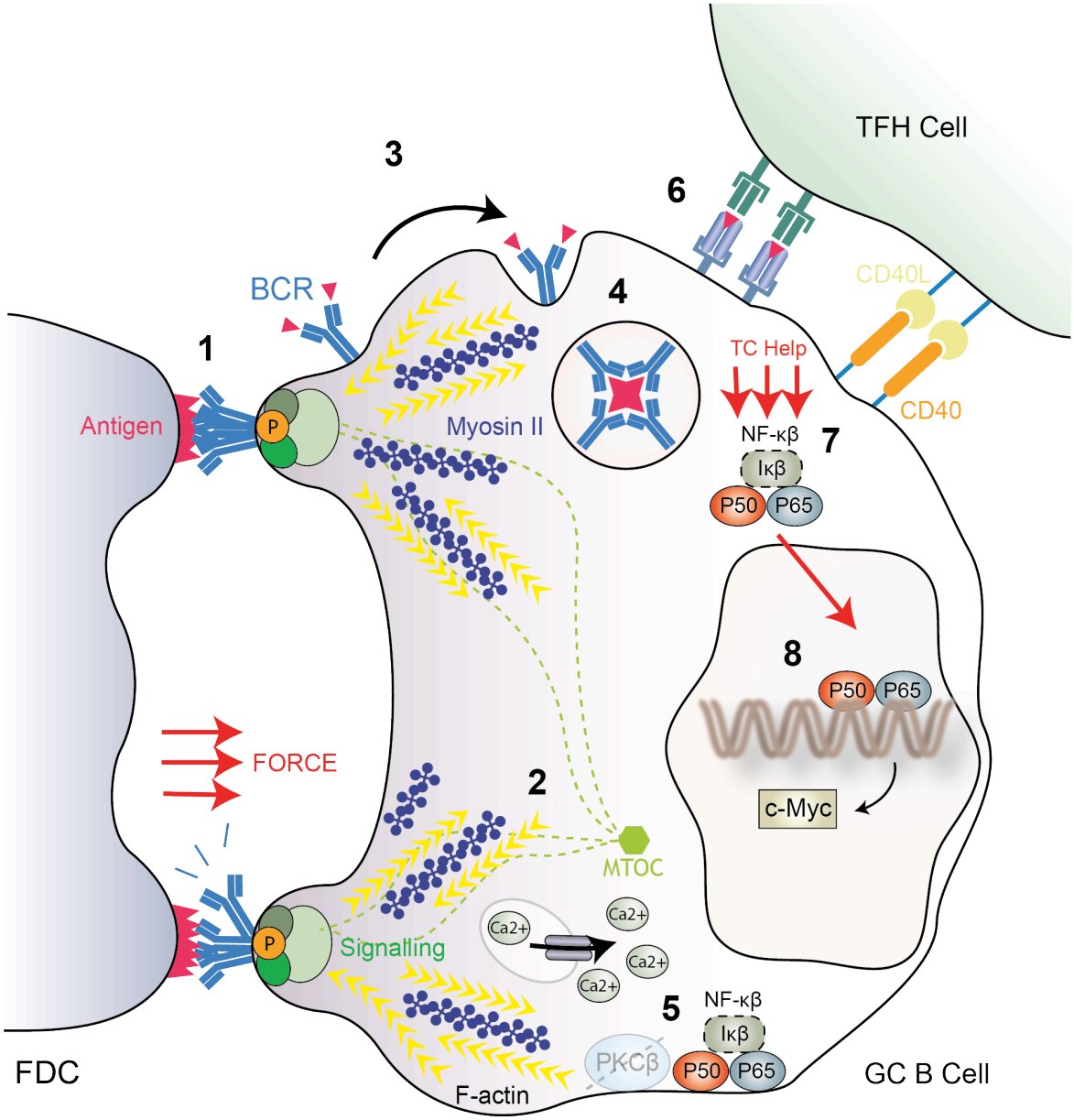

Figure 77 GC synapse formation: a working model

Figure 77 GC synapse formation: a working model

Germinal centre synapse structure supports affinity discrimination during clonal selection

1. GC B cells bind antigen held on the surface of FDCs in immune complexes. To increase stringency in situations where antigen is in excess GC B cells form microclusters that do not fuse and grow, and segregate them to the periphery of the contact interface.
2. Cytoskeletal components are arranged in novel configurations to support peripheral synapses. The MTOC is not polarised to the center of the contact, and F-actin and myosin associate directly with microclusters. Myosin is in close association with microclusters and produces strong upward forces on BCR-antigen bonds, often breaking weaker bonds.
3. Antigen microclusters that can withstand myosin-generated forces are separated from the FDC surface by a distinct PI3K-independent mechanism and moved up the sides of the cell. This may be an opportunity for antigen sampling from other incoming B cells.
4. After internalisation antigen enters into endosomal compartments for degredation and processing. Antigen peptides are generated and loaded onto MHC II molecules for trafficking to the cell surface.
5. GC synapse formation is BCR signalling-dependent. GC cells signal robustly though the BCR signalling pathway and form mature signalosomes. This leads to efficient calcium fluxing and accumulation of second messengers. However, low levels of PKC-β prevent NF-κB translocation to the nucleus.
6. Presentation of the extracted antigen as surface peptide-MHCII engages T_{FH} cells through binding of cognate TCRs
7. TCR binding allows the delivery of T cell help via interactions between CD40 on the B cell surface and CD40L on the T_{FH} cell. More antigen presentation recruits increasing amounts of T cell help. Signals delivered via the CD40 signalling pathways can support the translocation of Nf-κB into the nucleus independently of PKC-β.
8. Nf-κB is a transcription factor that binds DNA to induce transcription of a large number of target genes. Specifically, Nf-κB can promote expression of c-Myc, a cell cycle regulator promoting cyclic re-entry.

Malinova et al. 2016; Kumari & Dustin 2015). Whether FDCs in the GC regulate their stiffness as a means of controlling resultant BCR signalling or actively tune GC force requirements via distortion of their own membrane protrusions as affinity is improved is a fascinating prospect for future investigation. This is a complex interaction to unravel, and will require further optimisation of imaging on live FDCs to fully address APC-B cell interactions in high resolution.

The next layer of stringency appeared during antigen extraction. We saw GC B cells physically separating antigen from the presenting surface and transporting it to the edge of the contact, delaying internalisation. This is very different to antigen internalisation in naive B cells, which occurs concurrently with extraction via a PI3K-dependent, clathrin-mediated pathway (Natkanski et al. 2013). This uncoupling could act as a mechanism to prolong signalling, if indeed signalling thresholds for activation are altered in the GC. As we saw active signal propagation from endosomal compartments this is perhaps not the primary function for a differential extraction pathway. Currently unexplored, but very interesting, is the prospect of surface-held antigen establishing inter-clonal B cell competition, where newly recruited B cells could strip antigen from the surface of older, previously successful clones if their BCR binding is of sufficient strength. This could be important for newly activated GC B cells entering into existing GC reactions or in contexts of GC re-utilization or invasion, where newly activated B cells invade on-going GCs specific for entirely different pathogens during periods of dual infection (Schwickert et al. 2009; Bergqvist et al. 2013; Schwickert et al. 2007). These kinds of responses have only been observed in a handful of specific settings, so it would be worthwhile to investigate this phenomenon further. Long-term intravital imaging of live tissues would be required to investigate the possibility of GC B cell antigen stripping.

Although a role for T cell help in GC B cell selection was already established (Victora et al. 2010), it was not clear how this was integrated with BCR-derived signalling. We reconciled this discrepancy by uncovering an additional layer of stringency regulated at the signalling level. We saw that signals propagated through the CD40 signalling pathway (delivered by T cells *in vivo*) could overcome

the inability of GC B cells to mobilise NF-κB to the nucleus purely through BCR-mediated pathways. Low levels of PKC-β were discovered to be responsible for the failure of NF-κB to localise to the nucleus, and were later proposed to play a role in regulation of myosin IIA. Thus, as this body of work concludes, we come full circle-implicating an intrinsic loss of PKC-β in both the acquisition of T cell help to supplement inefficient signalling and for some of the altered cytoskeletal regulation described to control antigen extraction. This drew a link between mechanical force and affinity discrimination for the first time in the germinal centre. As blocking PKC-β in naive cells did not induce a GC phenotype, we clearly cannot attribute this molecule entirely to the effects we see in GC B cells. Nonetheless, we are currently exploring this interaction in more detail, both from a cytoskeletal and signalling viewpoint in order to better understand how GC B cells regulate the cytoskeleton and signalling in tandem to 'read-out' receptor improvements dynamically.

A major outstanding issue left unresolved in our system and others is the question of what occurs in the steps between antigen extraction and pMHCII presentation. It is known that higher affinity cells capture and present more antigen (Batista & Neuberger 1998), but precise mechanisms are unknown. In fact, it is unknown how the magnitude of antigen extraction relates specifically to surface levels of pMHCII. For example, although we know BCR crosslinking induces MHC synthesis, how BCR signalling might influence intracellular trafficking of pMHCII is unexplored. It is tempting to speculate that strong BCR signalling could accelerate antigen processing in some way and act as a way of amplifying small differences in extraction and translating them to larger differences in surface pMHCII density, especially as the GC response becomes more focussed at later stages. At this stage, these pathways remain relatively unstudied.

How a cell that is mutated so rapidly can completely clear and replace all pMHCII so as to be evaluated exclusively on the basis of its current BCR was difficult to imagine, especially as pMHCII molecules were reported to have long half-lives discordant with the GC reaction (De Riva et al. 2013). Recently, data emerged tracking pMHCII dynamics in the GC, showing dynamic regulation of complexes at different stages of the GC reaction, controlled by the differential activity of ubiquitin

(Bannard et al. 2016). This study found decreased pMHCII levels on extensively expanded cells, but could not link this with amount of T cell help received or affinity. Extending our system to include B cell antigen presentation would be a neat way of tracking endosomal processing efficiency and whether antigen presentation has a non-linear relationship with antigen extraction that creates an increased advantage when receiving limiting T cell help.

We showed that the output of cytoskeletal reprogramming was stronger upward pulling forces generated by GC B cells on antigen clusters, which improved affinity discrimination. Hence, mechanical testing provides a seemingly simple, yet elegantly multi-layered mechanism to increase stringency in the GC. This may have implications in other receptor-ligand systems where organization of the contact interface and force generation are only beginning to be appreciated (Hong et al. 2015; Basu et al. 2016; Wang & Ha 2013). This is particularly relevant in the immune system, where cells have to interact with a huge range of molecules and integrate incoming signals from numerous surface receptor interactions in order to make effector decisions (Carter & Fearon 1992; Carrasco et al. 2004; Nitschke et al. 1997). An especially relevant example is the poorly characterised process of antigen handover from incoming immune cells to FDCs, which is known to be actin-dependent and unidirectional (Heesters et al. 2013; Heesters et al. 2014). It is proposed that force generation by CR2 on the FDC surface is involved in facilitating effective antigen acquisition (Heesters et al. 2014). This bears more than a passing resemblance to B cell antigen acquisition where force generation by the BCR is implicit in unidirectional antigen extraction (Natkanski et al. 2013). Force sensors designed in the lab would be an ideal tool to study the force-generating capabilities of CR2 on FDCs during antigen extraction from macrophages or B cells in a *ex vivo* imaging setup to elegantly address this outstanding question. The ability to utilise force sensors *in vivo* is our ultimate aim, with protocols under development in the Tolar Lab.

In the wider context, the MDA imaging platform we created is incredibly versatile and has far-reaching applications to view spatiotemporal dynamics in cellular interactions. The ability to combine mechanical and molecular signalling

information is a powerful advantage of our system over others. We would love to use the setup to explore other rare, uncharacterised B cell populations, with particular emphasis on anergic or regulatory B cells, which we imagine might have similarly divergent synaptic architectures. Outside of the immune system, the platform has the ability to accommodate any cell type or any mixed cell population to study membrane interactions, internalisation of membrane-bound molecules, or indeed (although not presented in this thesis) secretion of cargo into synaptic clefts. The system is incredibly flexible, where intracellular signalling, subcellular localisation and receptor trafficking may all be studied over large numbers of heterogeneous, primary cells. With some optimisation, infection settings or complex migratory niches could be recapitulated for large-scale imaging- although this would require some customisation of the imaging hardware to include flow-chambers or similar devices to mimic chemoattractant or cytokine gradients.

In summary, a novel *ex vivo* imaging approach was designed to uncover hidden heterogeneity in rare germinal centre B cells. Using this unbiased, high-content platform we discovered surprising links between mechanical forces, cytoskeletal reprogramming and BCR signalling pathways. This has important biological implications in redefining mechanisms of positive selection in the GC. Biologically, selection in the GC is critical for effective resolution of infections, as well as being the major hurdle to overcome for rational vaccine design. We hope these data can improve the understanding of the molecular strategies employed by GC cells to improve stringency of antigen binding, and that this information can add to the expanding body of knowledge unravelling responses in the germinal centre.

Chapter 7. Appendix

7.1 Table of antibodies

Table 8 Antibody details

FC= flow cytometry, MDA= multi dimensional acquisition, ICs= immune complexes, CI= cell isolation

Antibody	Clone	Dilution/ conc.	Use	Supplier	Catalog number
anti-Rabbit IgG F(ab')$_2$ –AlexaFluor488	(Secondary antibody)	1:2000	MDA	Cell Signaling	4412S
anti-Rabbit IgG F(ab')$_2$ –AlexaFluor647	(Secondary antibody)	1:2000	MDA	Cell Signaling	4414S
anti-Rat Igκ light chain-biotin	MRK-1	1:100	CI	BD Biosciences	553871
B220-BV421	RA3-6B2	1:200	FC, MDA	BioLegend	103254
B220-BV510	RA3-6B2	1:200	FC	BD Biosciences	563103
B220-eFlour450	RA3-6B2	1:200	FC	eBioScience	48-045-82
B220-PerCP/Cy5.5	RA3-6B2	1:200	MDA	BioLegend	103236
CD117 (Ckit)-APC	ACK2	1:200	FC	Biolegend	135108
CD11c-biotin	N418	1:100	CI	eBioScience	13-0114-82
CD138-APC		1:200	FC	BD Biosciences	
CD138-PerCP/Cy5.5	281-1	1:200	FC, MDA	Biolegend	142509
CD184-PE	2B11/ CXCR4	1:100	FC	BD Biosciences	561734
CD21-FITC	7G6	1:400	FC	BD Biosciences	561769

CD22-PE	Lyb-8.2	1:200	MDA	BD Biosciences	553384
CD23-PE	B3B4	1:100	FC	eBioscience	12-0232-83
CD38-FITC	90	1:500	FC	BD Biosciences	558813
CD38-PerCP/Cy5.5	90	1:200	FC, MDA	BioLegend	102722
CD43-biotin	eBioR2/60	1:100	CI	eBioScience	13-0413-82
CD45.1-APC	A20	1:200	FC	BD Biosciences	558701
CD45.1-biotin	6C3	1:100	CI	BD Biosciences	553159
CD45.1-PE	A20	1:200	FC	BD Biosciences	553776
CD45.2-eFluor450	104	1:200	FC	eBioscience	48-0454-82
CD45.2-PerCP/Cy5.5	M1/69	1:200	FC	BD Biosciences	562360
CD86-V450	GL1	1:100	FC	BD Biosciences	560449
CD93 (AA4.1) -APC	AA4.1	1:100	FC	eBioscience	17-5892-83
CD93 (AA4.1) -FITC	AA4.1	1:100	MDA	BD Biosciences	561990
CD95-BV421	Jo2	1:200	FC, MDA	BD Biosciences	562633
CD95-PE	Jo2	1:200	FC, MDA	BD Biosciences	561985
CD95-PE/Cy7	Jo2	1:200	FC	BD Biosciences	557653
Follicular dendritic cell	FDCM1	1:100	CI	BD Biosciences	551320
GL7-AlexaFluor488	GL-7	1:100	FC, MDA	BD Biosciences	53-5902-82
Goat $F(ab')_2$ anti-human IgM	Fcμ Fragment Specific	1:250	MDA	Jackson ImmunoResearch	109-006-129

Goat F(ab')$_2$ anti-mouse Igκ	(Antigen)	0.5-1µg/ml	MDA	Southern Biotech	1052-01
IgD-biotin	11-26c	1:100	CI	eBioScience	13-5993-82
IgG1-APC	X56	1:200	FC, MDA	BD Biosciences	550874
IgM-FITC	II/41	1:500	FC, MDA	eBioscience	23-5790-82
IgM-PE/Cy7	R6-60.2	1:400	FC	BD Biosciences	552867
Myosin IIA HC	(S1916)	5 µl/well	MDA	ECM Bioscience	MP5191
NF-κB1 p105/p50	D4P4D	5 µl/well or 1:50	MDA	Cell Signaling	13586S
NF-κB1 p65	D14E12	5 µl/well	MDA	Cell Signalling	8242P
p- p44/42-AlexaFluor488 (p-ERK)	D13.14.4E (T202/T204)	10 µl/well or 1:25	FC, MDA	Cell Signaling	4344S
p- SHIP-1	(Y1020)	5 µl/well or 1:50	FC, MDA	Cell Signaling	3941S
p- SYK-AlexaFluor488	C87C1 (Y525/526)	5 µl/well or 1:50	FC, MDA	Cell Signaling	4349S
p-AKT-AlexaFluor647	193H12 (S473)	10 µl/well or 1:25	FC, MDA	Cell Signaling	2337S
p-BLNK-AlexaFluor488	J117-1278	20 ul/well or 1:10	FC, MDA	BD Biosciences	558444
p-Myosin IIa	(S1943)	10 µl/well	MDA	Cell Signaling	5026S
p-Myosin Light Chain 2	(T18/S19)	5 µl/well or 1:50	FC, MDA	Cell Signaling	3674S
p-NF- κB1 p65-AlexFluor488	93H1 (S536)	5 µl/well	FC, MDA	Cell Signalling	4886S
p-PKC α/β II	(T638/641)	5 µl/well	MDA	Cell Signaling	9375S

p-PKC δ	Y52	1 µl/well	MDA	Abcam	ab74007
p-PKCα/β II	(T638/641)	10 µl/well or 1:25	MDA	Cell Signaling	9375P
p-SAPK/JNK	81E11 (T183/ Y185)	10 µl/well or 1:25	FC, MDA	Cell Signaling	4668S
PKC-β 1	EPR18512	1 µl/well	MDA	Abcam	ab195039
PKC-β II-AlexaFluor 647	(Y125)	2 µl/well	MDA	Abcam	ab195252
PKC-δ	EPR17075	1 µl/well	MDA	Abcam	ab182126
PKC-ε	EPR1482(2)	1 µl/well	MDA	Abcam	ab124806
pTyr-FITC	4G10	1:500	MDA	Merck Millipore	05-321
Rabbit anti-Goat IgG	$F(ab')_2$ Specific	n/a	MDA (ICs)	Jackson ImmunoResearch	111-005-006
α-Tubulin-AlexaFluor488	B-5-1-2	1:400	MDA	Invitrogen	322588

7.2 Table of inhibitors

Table 9 Inhibitor details

Name	Inhibits	Conc.	Buffer	Incubation Time
79-6	BCL-6	50 μM	Full RPMI	24 hr
BAY61- 3606	SYK	50 μM	HBSS/ lo BSA	15 min
BI 605906	IKK2	10 μM	Full RPMI	24 hr
Blebbistatin	Non-muscle myosin II	50 μM	HBSS/ lo BSA	15 min
Bosuitinib (SKI 606)	Abl and Src10 kinases	10 μM	HBSS/ lo BSA	15 min
CK-666	Arp 2/3	50 μM	HBSS/ lo BSA	15 min
Dynasore	Dynamin	80 μM	HBSS only	15 min
GDC-0941	PI3K	50 nM	Full RPMI	10 min
Gö 6976	PKC α/β	2 μM	HBSS/ lo BSA	30 min
Gö 6983	PKC (broad spectrum)	500 nM	HBSS/ lo BSA	30 min
LY294002	PI3K	20 μM	HBSS/ lo BSA	10 min
MK2206	AKT	2 μM	HBSS/ lo BSA	45 min

P505-15	SYK	10 μM	HBSS/ lo BSA	15 min
PD0325901	MEK/ERK	10 μM	HBSS/ lo BSA	15 min
PP2	Src (Lck)	50 μM	HBSS only	15 min
PRT062607	SYK	10 μM	HBSS/ lo BSA	15 min
SMFI	Formin	25 μM	HBSS/ lo BSA	15 min
Tofacitinib	JAK	100 nM	Full RPMI	24 hr
U-73122	PLC-γ	2 μM	HBSS/ lo BSA	45 min
VX745	P38-α	2 μM	Full RPMI	24 hr
Y-27632	ROCK	50 μM	HBSS/ lo BSA	15 min

7.3 Movie figure legends

Movie 1 Timelapse imaging of immune synapse formation in naive or germinal centre B cells

Antigen (anti-Igκ, grey) in naive (left) and GC (right) B cell synapses with PLBs observed using timelapse TIRF microscopy. Time is shown in minutes and seconds.

Movie 2 Timelapse imaging of germinal center calcium flux (Movie)

Cells loaded with the calcium indicator Fluo-4, which fluoresces when calcium is mobilised. Fluo-4 intensity depicted as a fire-scale where blue/purple indicates lower fluorescence intensity and red/white indicates higher fluorescence intensity. Movie running time represents 15 minutes total imaging.

Movie 3 Timelapse imaging capturing the effect of blebbistatin treatment on naive and germinal center immune synapse formation

Antigen (anti-Igκ, blue-yellow-white fire-scale) in naive and GC B cell synapses after pre-treatment with blebbistatin (separate movies, labelled accordingly). Cells were imaged on PLBs and observed using timelapse TIRF microscopy. Time is shown in minutes and seconds.

Movie 4 Pulling forces in naive and GC synapses observed using timelapse imaging

Synapses with anti-Igκ coupled to a 9 pN force sensor on PLBs in naive (upper panel) and GC (lower panel) B cell synapses. Signals from the force-insensitive label Atto550 (green) and the force-sensitive Atto647N (red) are overlaid on the left panels, and the red-to-green ratio defining opening of the sensor are shown on the right panels. Time is shown in minutes and seconds.

Movie 5 Z-stack acquisition of B cells interacting with antigen displayed on FDCs

B cells (B220, blue) interacting with immune-complex-loaded FDCs (anti-Igκ-Cy5, red). B cells interacted with live antigen-loaded FDCs for 30 minutes at 37°C before imaging. Movie cycles back and forth through 35 0.5 µm steps showing antigen clusters (red) up inside B cells (blue).

Reference List

Allan, L.L. et al., 2011. CD1d and CD1c expression in human B cells is regulated by activation and retinoic acid receptor signaling. *The Journal of Immunology*, 186(9), pp.5261–5272.

Allen, C.D.C. & Cyster, J.G., 2008. Follicular dendritic cell networks of primary follicles and germinal centers: Phenotype and function. *Seminars in Immunology*, 20(1), pp.14–25.

Allen, C.D.C. et al., 2004. Germinal center dark and light zone organization is mediated by CXCR4 and CXCR5. *Nature immunology*, 5(9), pp.943–952.

Allen, C.D.C., Okada, T. & Cyster, J.G., 2007. Germinal-center organization and cellular dynamics. *Immunity*, 27(2), pp.190–202.

Allen, C.D.C., Okada, T., Tang, H.L., et al., 2007. Imaging of germinal center selection events during affinity maturation. *Science*, 315(5811), pp.528–531.

Allman, D. & Pillai, S., 2008. Peripheral B cell subsets. *Current opinion in immunology*, 20(2), pp.149–157.

Allman, D., Li, J. & Hardy, R.R., 1999. Commitment to the B lymphoid lineage occurs before DH-JH recombination. *The Journal of experimental medicine*, 189(4), pp.735–740.

Andrian, von, U.H. & Mempel, T.R., 2003. Homing and cellular traffic in lymph nodes. *Nature Reviews: Immunology*, 3(11), pp.867–878.

Ansel, K.M. et al., 2000. A chemokine-driven positive feedback loop organizes lymphoid follicles. *Nature*, 406(6793), pp.309–314.

Apgar, J.R., 1991. Regulation of the antigen-induced F-actin response in rat basophilic leukemia cells by protein kinase C. *The Journal of cell biology*, 112(6), pp.1157–1163.

Arana, E. et al., 2008. Activation of the small GTPase Rac2 via the B cell receptor regulates B cell adhesion and immunological-synapse formation. *Immunity*, 28(1), pp.88–99.

Arnold, C.N. et al., 2007. The germinal center response is impaired in the absence of T cell-expressed CXCR5. *European journal of immunology*, 37(1), pp.100–109.

Attwood, S.J., Choi, Y. & Leonenko, Z., 2013. Preparation of DOPC and DPPC Supported Planar Lipid Bilayers for Atomic Force Microscopy and Atomic Force Spectroscopy. *International journal of molecular sciences*, 14(2), pp.3514–3539.

Avery, D.T. et al., 2008. IL-21-Induced Isotype Switching to IgG and IgA by Human Naive B Cells Is Differentially Regulated by IL-4. *Journal of immunology*,

181(3), pp.1767–1779.

Bachmann, M.F. et al., 1996. Induction of long-lived germinal centers associated with persisting antigen after viral infection. *The Journal of experimental medicine*, 183(5), pp.2259–2269.

Bannard, O. et al., 2013. Germinal center centroblasts transition to a centrocyte phenotype according to a timed program and depend on the dark zone for effective selection. *Immunity*, 39(5), pp.912–924.

Bannard, O. et al., 2016. Ubiquitin-mediated fluctuations in MHC class II facilitate efficient germinal center B cell responses. *The Journal of experimental medicine*, 162(6), pp.51682–1009.

Barberis, A. et al., 1990. A novel B-cell lineage-specific transcription factor present at early but not late stages of differentiation. *Genes & development*, 4(5), pp.849–859.

Barral, P. et al., 2008. B cell receptor-mediated uptake of CD1d-restricted antigen augments antibody responses by recruiting invariant NKT cell help in vivo. *Proceedings of the National Academy of Sciences of the United States of America*, 105(24), pp.8345–8350.

Basso, K. et al., 2010. Integrated biochemical and computational approach identifies BCL6 direct target genes controlling multiple pathways in normal germinal center B cells. *Blood*, 115(5), pp.975–984.

Basso, K. et al., 2004. Tracking CD40 signaling during germinal center development. *Blood*, 104(13), pp.4088–4096.

Basu, R. et al., 2016. Cytotoxic T Cells Use Mechanical Force to Potentiate Target Cell Killing. *Cell*, 165(1), pp.100–110.

Batista, F.D. & Harwood, N.E., 2009. The who, how and where of antigen presentation to B cells. *Nature Reviews: Immunology*, 9(1), pp.15–27.

Batista, F.D. & Neuberger, M.S., 1998. Affinity dependence of the B cell response to antigen: a threshold, a ceiling, and the importance of off-rate. *Immunity*, 8(6), pp.751–759.

Batista, F.D. & Neuberger, M.S., 2000. B cells extract and present immobilized antigen: implications for affinity discrimination. *The EMBO journal*, 19(4), pp.513–520.

Batista, F.D. et al., 2007. The role of integrins and coreceptors in refining thresholds for B-cell responses. *Immunological reviews*, 218, pp.197–213.

Batista, F.D., Iber, D. & Neuberger, M.S., 2001. B cells acquire antigen from target cells after synapse formation. *Nature*, 411(6836), pp.489–494.

Batista, F.D., Treanor, B. & Harwood, N.E., 2010. Visualizing a role for the actin

cytoskeleton in the regulation of B-cell activation. *Immunological reviews*, 237(1), pp.191–204.

Baumjohann, D., Okada, T. & Ansel, K.M., 2011. Cutting Edge: Distinct waves of BCL6 expression during T follicular helper cell development. *The Journal of Immunology*, 187(5), pp.2089–2092.

Bekeredjian Ding, I. & Jego, G., 2009. Toll-like receptors – sentries in the B-cell response. *Immunology*, 128(3), pp.311–323.

Bell, S.E. et al., 2004. PLCγ2 regulates Bcl-2 levels and is required for survival rather than differentiation of marginal zone and follicular B cells. *European journal of immunology*, 34(8), pp.2237–2247.

Benschop, R.J. et al., 1999. Distinct signal thresholds for the unique antigen receptor-linked gene expression programs in mature and immature B cells. *The Journal of experimental medicine*, 190(6), pp.749–756.

Berek, C., Berger, A. & Apel, M., 1991. Maturation of the immune response in germinal centers. *Cell*, 67(6), pp.1121–1129.

Bergqvist, P. et al., 2013. Re-utilization of germinal centers in multiple Peyer's patches results in highly synchronized, oligoclonal, and affinity-matured gut IgA responses. *Mucosal Immunology*, 6(1), pp.122–135.

Bergtold, A. et al., 2005. Cell surface recycling of internalized antigen permits dendritic cell priming of B cells. *Immunity*, 23(5), pp.503–514.

Bhan, A.K. et al., 1981. Stages of B cell differentiation in human lymphoid tissue. *The Journal of experimental medicine*, 154(3), pp.737–749.

Blakely, B.L. et al., 2014. A DNA-based molecular probe for optically reporting cellular traction forces. *Nature Methods*, 11(12), pp.1229–1232.

Blasioli, J. & Goodnow, C.C., 2002. Lyn/CD22/SHP-1 and their importance in autoimmunity. *Signal Transduction Pathways in Autoimmunity*, 5, pp.151–160.

Borst, J. Jacobs, H. & Brouns, G., 1996. Composition and function of T-cell receptor and B-cell receptor complexes on precursor lymphocytes. *Current opinion in immunology*, 8(2), pp.181–190.

Bossi, G. et al., 2002. The secretory synapse: the secrets of a serial killer. *Immunological reviews*, 189, pp.152–160.

Boulant, S. et al., 2011. Actin dynamics counteract membrane tension during clathrin-mediated endocytosis. *Nature cell biology*, 13(9), pp.1124–1131.

Breitfeld, D. et al., 2000. Follicular B helper T cells express CXC chemokine receptor 5, localize to B cell follicles, and support immunoglobulin production. *Journal of Experimental Medicine*, 192(11), pp.1545–1551.

Bresnick, A.R., 1999. Molecular mechanisms of nonmuscle myosin-II regulation. *Current opinion in cell biology*, 11(1), pp.26–33.

Brink, R. et al. 1992. Immunoglobulin M and D antigen receptors are both capable of mediating B lymphocyte activation, deletion, or anergy after interaction with specific antigen. *The Journal of experimental medicine*, 176(4), pp.991–1005.

Brink, R. Goodnow, C.C. & Basten, A., 1995. IgD expression on B cells is more efficient than IgM but both receptors are functionally equivalent in up-regulation CD80/CD86 co-stimulatory molecules. *European journal of immunology*, 25(7), pp.1980–1984.

Brossard, C. et al., 2005. Multifocal structure of the T cell - Dendritic cell synapse. *European journal of immunology*, 35(6), pp.1741–1753.

Brzeska, H. & Korn, E.D., 1996. Regulation of class I and class II myosins by heavy chain phosphorylation. *Journal of Biological Chemistry*, 271(29), pp.16983–16986.

Burton, D.R. et al., 2012. A Blueprint for HIV Vaccine Discovery. *Cell Host & Microbe*, 12(4), pp.396–407.

Busman-Sahay, K. et al., 2013. Cis and Trans Regulatory Mechanisms Control AP2-Mediated B Cell Receptor Endocytosis via Select Tyrosine-Based Motifs J. Keen, ed. *PloS one*, 8(1), p.e54938.

Calado, D.P. et al., 2012. The cell-cycle regulator c-Myc is essential for the formation and maintenance of germinal centers. *Nature immunology*, 13(11), pp.1092–1100.

Cambier, J.C. et al., 2007. B-cell anergy: from transgenic models to naturally occurring anergic B cells? *Nature Reviews: Immunology*, 7(8), pp.633–643.

Campi, G., Varma, R. & Dustin, M.L., 2005. Actin and agonist MHC-peptide complex-dependent T cell receptor microclusters as scaffolds for signaling. *The Journal of experimental medicine*, 202(8), pp.1031–1036.

Capolunghi, F. et al., 2008. CpG drives human transitional B cells to terminal differentiation and production of natural antibodies. *Journal of immunology*, 180(2), pp.800–808.

Cariappa, A. et al., 2007. Naive recirculating B cells mature simultaneously in the spleen and bone marrow. *Blood*, 109(6), pp.2339–2345.

Cariappa, A. et al., 2005. Perisinusoidal B cells in the bone marrow participate in T-independent responses to blood-borne microbes. *Immunity*, 23(4), pp.397–407.

Cariappa, A. et al., 2001. The follicular versus marginal zone B lymphocyte cell fate decision is regulated by Aiolos, Btk, and CD21. *Immunity*, 14(5), pp.603–615.

Carlin, L.M. et al., 2001. Intercellular transfer and supramolecular organization of

human leukocyte antigen C at inhibitory natural killer cell immune synapses. *The Journal of experimental medicine*, 194(10), pp.1507–1517.

Caron, G. et al., 2009. CXCR4 expression functionally discriminates centroblasts versus centrocytes within human germinal center B cells. *The Journal of Immunology*, 182(12), pp.7595–7602.

Carrasco, Y.R. & Batista, F.D. 2006a. B cell recognition of membrane-bound antigen: an exquisite way of sensing ligands. *Current opinion in immunology*, 18(3), pp.286–291.

Carrasco, Y.R. & Batista, F.D. 2006b. B-cell activation by membrane-bound antigens is facilitated by the interaction of VLA-4 with VCAM-1. *The EMBO journal*, 25(4), pp.889–899.

Carrasco, Y.R. & Batista, F.D., 2007. B cells acquire particulate antigen in a macrophage-rich area at the boundary between the follicle and the subcapsular sinus of the lymph node. *Immunity*, 27(1), pp.160–171.

Carrasco, Y.R. et al., 2004. LFA-1/ICAM-1 interaction lowers the threshold of B cell activation by facilitating B cell adhesion and synapse formation. *Immunity*, 20(5), pp.589–599.

Carter, R.H. & Fearon, D.T., 1992. CD19: lowering the threshold for antigen receptor stimulation of B lymphocytes. *Science*, 256(5053), pp.105–107.

Caswell, P.T., Vadrevu, S. & Norman, J.C., 2009. Integrins: masters and slaves of endocytic transport. *Nature Reviews Molecular Cell Biology*, 10(12), pp.843–853.

Cato, M.H., Yau, I.W. & Rickert, R.C., 2011. Magnetic-based purification of untouched mouse germinal center B cells for ex vivo manipulation and biochemical analysis. *Nature protocols*, 6(7), pp.953–960.

Catron, D.M. et al., 2010. A protease-dependent mechanism for initiating T-dependent B cell responses to large particulate antigens. *The Journal of Immunology*, 184(7), pp.3609–3617.

Chan, T.D. & Brink, R, 2012. Affinity-based selection and the germinal center response. *Immunological reviews*, 247(1), pp.11–23.

Chan, T.D. et al., 2009. Antigen affinity controls rapid T-dependent antibody production by driving the expansion rather than the differentiation or extrafollicular migration of early plasmablasts. *The Journal of Immunology*, 183(5), pp.3139–3149.

Chang, P.-P. et al., 2012. Identification of Bcl-6-dependent follicular helper NKT cells that provide cognate help for B cell responses. *Nature immunology*, 13(1), pp.35–43.

Chappell, C.P. et al., 2012. Extrafollicular B cell activation by marginal zone

dendritic cells drives T cell-dependent antibody responses. *The Journal of experimental medicine*, 209(10), pp.1825–1840.

Chatila, T. et al., 1989. Mechanisms of T cell activation by the calcium ionophore ionomycin. *Journal of immunology*, 143(4), pp.1283–1289.

Chatterjee, P. et al., 2012. Modulation of antigen presentation and B cell receptor signaling in B cells of beige mice. *Journal of Immunology*, 188(6), pp.2695–2702.

Chaturvedi, A. et al., 2011. Endocytosed BCRs sequentially regulate MAPK and Akt signaling pathways from intracellular compartments. *Nature immunology*, 12(11), pp.1119–1126.

Chaudhry, M.S. & Karadimitris, A. 2014. Role and regulation of CD1d in normal and pathological B cells. *The Journal of Immunology*, 193(10), pp.4761–4768.

Chen, L.L. et al., 1978. Distribution of horseradish peroxidase (HRP)-anti-HRP immune complexes in mouse spleen with special reference to follicular dendritic cells. *The Journal of cell biology*, 79(1), pp.184–199.

Chen, W. & Zhu, C, 2013. Mechanical regulation of T-cell functions. *Immunological reviews*, 256(1), pp.160–176.

Chen, Y. et al., 2015. Fluorescence Biomembrane Force Probe: Concurrent Quantitation of Receptor-ligand Kinetics and Binding-induced Intracellular Signaling on a Single Cell. *Journal of visualized experiments : JoVE*, (102), pp.e52975–e52975.

Cheng, P.C. et al., 1999. A role for lipid rafts in B cell antigen receptor signaling and antigen targeting. *The Journal of experimental medicine*, 190(11), pp.1549–1560.

Choudhuri, K. et al., 2014. Polarized release of T-cell-receptor-enriched microvesicles at the immunological synapse. *Nature*, 507(7490), pp.118–123.

Choudhuri, K. et al., 2005. T-cell receptor triggering is critically dependent on the dimensions of its peptide-MHC ligand. *Nature*, 436(7050), pp.578–582.

Chung, J.B. et al., 2003. Transitional B cells: step by step towards immune competence. *Trends in immunology*, 24(6), pp.342–348.

Ci, W. et al., 2009. The BCL6 transcriptional program features repression of multiple oncogenes in primary B cells and is deregulated in DLBCL. *Blood*,113(22), pp.5536–5548.

Cinamon, G. et al., 2008. Follicular shuttling of marginal zone B cells facilitates antigen transport. *Nature immunology*, 9(1), pp.54–62.

Cinamon, G. et al., 2004. Sphingosine 1-phosphate receptor 1 promotes B cell localization in the splenic marginal zone. *Nature immunology*, 5(7), pp.713–

720.

Clark, S.L., 1962. The reticulum of lymph nodes in mice studied with the electron microscope. *The American journal of anatomy*, 110, pp.217–257.

Comrie, W.A. & Burkhardt, J.K., 2016. Action and Traction: Cytoskeletal Control of Receptor Triggering at the Immunological Synapse. *Frontiers in Immunology*, 7(1), p.68.

Comrie, W.A., Babich, A. & Burkhardt, J.K., 2015. F-actin flow drives affinity maturation and spatial organization of LFA-1 at the immunological synapse. *The Journal of cell biology*, 208(4), pp.475–491.

Comrie, W.A., Li, S., et al., 2015. The dendritic cell cytoskeleton promotes T cell adhesion and activation by constraining ICAM-1 mobility. *The Journal of cell biology*, 208(4), pp.457–473.

Corti, D. et al., 2011. A neutralizing antibody selected from plasma cells that binds to group 1 and group 2 influenza A hemagglutinins. *Science*, 333(6044), pp.850–856.

Corti, D. et al., 2010. Heterosubtypic neutralizing antibodies are produced by individuals immunized with a seasonal influenza vaccine. *The Journal of clinical investigation*, 120(5), pp.1663–1673.

Crotty, S. Johnston, R.J. & Schoenberger, S.P., 2010. Effectors and memories: Bcl-6 and Blimp-1 in T and B lymphocyte differentiation. *Nature immunology*, 11(2), pp.114–120.

Cyster, J.G. 2010. B cell follicles and antigen encounters of the third kind. *Nature immunology*, 11(11), pp.989–996.

Cyster, J.G, 2015. Germinal Centers: Gaining Strength from the Dark Side. *Immunity*, 43(6), pp.1026–1028.

Cyster, J.G. et al. 2014. 25-Hydroxycholesterols in innate and adaptive immunity. *Nature Reviews: Immunology*, 14(11), pp.731–743.

Cyster, J.G. et al. 2000. Follicular stromal cells and lymphocyte homing to follicles. *Immunological reviews*, 176, pp.181–193.

Dal Porto, J.M. et al., 2004. B cell antigen receptor signaling 101. *Molecular immunology*, 41(6-7), pp.599–613.

Dal Porto, J.M. et al., 2002. Very low affinity B cells form germinal centers, become memory B cells, and participate in secondary immune responses when higher affinity competition is reduced. *Journal of Experimental Medicine*, 195(9), pp.1215–1221.

Davidson, A. Shefner, R. & Livneh, A., 1987. The role of somatic mutation of immunoglobulin genes in autoimmunity. *Annual review of ….*

Davis, M.M. et al., 2007. T Cells as a Self-Referential, Sensory Organ. *dx.doi.org*, 25(1), pp.681–695.

De Riva, A. et al., 2013. Accelerated turnover of MHC class II molecules in nonobese diabetic mice is developmentally and environmentally regulated in vivo and dispensable for autoimmunity. *The Journal of Immunology*, 190(12), pp.5961–5971.

de Vinuesa, C.G. et al., 2000. Germinal centers without T cells. *The Journal of experimental medicine*, 191(3), pp.485–494.

Depoil, D. et al., 2008. CD19 is essential for B cell activation by promoting B cell receptor-antigen microcluster formation in response to membrane-bound ligand. *Nature immunology*, 9(1), pp.63–72.

Depoil, D. et al., 2005. Immunological synapses are versatile structures enabling selective T cell polarization. *Immunity*, 22(2), pp.185–194.

Detre, C. et al., 2012. SAP expression in invariant NKT cells is required for cognate help to support B-cell responses. *Blood*, 120(1), pp.122–129.

Diamond, B. et al., 1992. The role of somatic mutation in the pathogenic anti-DNA response. *Annual Review of Immunology*, 10(1), pp.731–757.

Dogan, I. et al., 2009. Multiple layers of B cell memory with different effector functions. *Nature immunology*, 10(12), pp.1292–1299.

Dominguez-Sola, D. et al., 2015. The FOXO1 Transcription Factor Instructs the Germinal Center Dark Zone Program. *Immunity*, 43(6), pp.1064–1074.

Dominguez-Sola, D. et al., 2012. The proto-oncogene MYC is required for selection in the germinal center and cyclic reentry. *Nature immunology*, 13(11), pp.1083–1091.

Draghi, N.A. & Denzin, L.K., 2010. H2-O, a MHC class II-like protein, sets a threshold for B-cell entry into germinal centers. In Proceedings of the National Academy of Sciences of the United States of America. pp. 16607–16612.

Dudziak, D. et al., 2007. Differential antigen processing by dendritic cell subsets in vivo. *Science*, 315(5808), pp.107–111.

Dustin, M.L., 2005. A dynamic view of the immunological synapse. *Seminars in Immunology*, 17(6), pp.400–410.

Dustin, M.L., 2014a. How T cells lose their touch. *Immunity*, 40(2), pp.169–171.

Dustin, M.L., 2009. Supported bilayers at the vanguard of immune cell activation studies. *Journal of structural biology*, 168(1), pp.152–160.

Dustin, M.L., 2014b. What Counts in the Immunological Synapse? *Molecular cell*, 54(2), pp.255–262.

Dustin, M.L. & Groves, J.T., 2012. Receptor signaling clusters in the immune synapse. *Annual Review of Biophysics*, 41(1), pp.543–556.

Dykstra, M. et al., 2003. Location is everything: lipid rafts and immune cell signaling. *Annual Review of Immunology*, 21(1), pp.457–481.

Eisen, H.N., 2014. Affinity enhancement of antibodies: how low-affinity antibodies produced early in immune responses are followed by high-affinity antibodies later and in memory B-cell responses. *Cancer immunology research*, 2(5), pp.381–392.

Eisen, H.N. & Siskind, G.W., 1964. Variations in Affinities of Antibodies during the Immune Response. *Biochemistry*. 3(7) pp.996-1008

Elosegui-Artola, A. et al., 2016. Mechanical regulation of a molecular clutch defines force transmission and transduction in response to matrix rigidity. *Nature cell biology*, 18(5), pp.540–548.

Engels, N. et al., 2009. Recruitment of the cytoplasmic adaptor Grb2 to surface IgG and IgE provides antigen receptor-intrinsic costimulation to class-switched B cells. *Nature immunology*, 10(9), pp.1018–1025.

Ettinger, R. et al., 2005. IL-21 induces differentiation of human naive and memory B cells into antibody-secreting plasma cells. *Journal of immunology*, 175(12), pp.7867–7879.

Farr, A.G., Cho, Y. & De Bruyn, P.P., 1980. The structure of the sinus wall of the lymph node relative to its endocytic properties and transmural cell passage. *The American journal of anatomy*, 157(3), pp.265–284.

Fleire, S.J. et al., 2006. B cell ligand discrimination through a spreading and contraction response. *Science*, 312(5774), pp.738–741.

Fooksman, D.R. & Dustin, M.L., 2010. Affinity measured by microcluster. *Journal of Experimental Medicine*, 207(5), pp.907–909.

Fossum, S., 1980. The architecture of rat lymph nodes. IV. Distribution of ferritin and colloidal carbon in the draining lymph nodes after foot-pad injection. *Scandinavian journal of immunology*, 12(5), pp.433–441.

Gatto, D. & Brink, R., 2013. B cell localization: regulation by EBI2 and its oxysterol ligand. *Trends in immunology*, 34(7), pp.336–341.

Gatto, D. et al., 2009. Guidance of B cells by the orphan G protein-coupled receptor EBI2 shapes humoral immune responses. *Immunity*, 31(2), pp.259–269.

Gatto, D. et al., 2007. Regulation of memory antibody levels: the role of persisting antigen versus plasma cell life span. *Journal of immunology,* 178(1), pp.67–76.

Gauld, S.B. et al., 2005. Maintenance of B cell anergy requires constant antigen receptor occupancy and signaling. *Nature immunology*, 6(11), pp.1160–1167.

Gaya, M. et al., 2015. Host response. Inflammation-induced disruption of SCS macrophages impairs B cell responses to secondary infection. *Science*, 347(6222), pp.667–672.

Gazumyan, A., Reichlin, A. & Nussenzweig, M.C., 2006. Ig beta tyrosine residues contribute to the control of B cell receptor signaling by regulating receptor internalization. *The Journal of experimental medicine*, 203(7), pp.1785–1794.

Geahlen, R.L., 2009. Syk and pTyr'd: Signaling through the B cell antigen receptor. *Molecular Cell Research*, 1793(7), pp.1115–1127.

Gershon, R.K. & Kondo, K., 1970. Cell interactions in the induction of tolerance: the role of thymic lymphocytes. *Immunology*, 18(5), pp.723–737.

Getahun, A. et al., 2016. Continuous inhibitory signaling by both SHP-1 and SHIP-1 pathways is required to maintain unresponsiveness of anergic B cells. *The Journal of experimental medicine*, 213(5), pp.751–769.

Gitlin, A.D. et al., 2015. T cell help controls the speed of the cell cycle in germinal center B cells. *Science*, 349(6248), pp.643–646.

Gitlin, A.D. et al., 2016. Independent Roles of Switching and Hypermutation in the Development and Persistence of B Lymphocyte Memory. *Immunity*, 44(4), pp.769–781.

Gitlin, A.D., Shulman, Z. & Nussenzweig, M.C., 2014. Clonal selection in the germinal centre by regulated proliferation and hypermutation. *Nature*, 509(7502), pp.637–640.

Goidl, E.A. et al., 1968. The effect of antigen dose and time after immunization on the amount and affinity of anti-hapten antibody. *Journal of immunology*, 100(2), pp.371–375.

Golby, S.J., Dunn-Walters, D.K. & Spencer, J., 1999. Human tonsillar germinal center T cells are a diverse and widely disseminated population. *European journal of immunology*, 29(11), pp.3729–3736.

Gomez, T.S. et al., 2007. Formins Regulate the Actin-Related Protein 2/3 Complex-Independent Polarization of the Centrosome to the Immunological Synapse. *Immunity*, 26(2), pp.177–190.

Gonzalez, S.F. et al., 2010. Capture of influenza by medullary dendritic cells via SIGN-R1 is essential for humoral immunity in draining lymph nodes. 11(5), pp.427–434.

Good-Jacobson, K.L. et al., 2010. PD-1 regulates germinal center B cell survival and the formation and affinity of long-lived plasma cells. *Nature immunology*,

11(6), pp.535–542.

Goodnow, C.C., 1997. Chance encounters and organized rendezvous. *Immunological reviews*, 156, pp.5–10.

Goodnow, C.C. et al., 1988. Altered immunoglobulin expression and functional silencing of self-reactive B lymphocytes in transgenic mice. *Nature*, 334(6184), pp.676–682.

Grakoui, A. et al., 1999. The immunological synapse: a molecular machine controlling T cell activation. *Science*, 285(5425), pp.221–227.

Grawunder, U. et al., 1995. Down-regulation of RAG1 and RAG2 gene expression in PreB cells after functional immunoglobulin heavy chain rearrangement. *Immunity*, 3(5), pp.601–608.

Gray, D., 1993. Immunological memory. *Annual Review of Immunology*, 11, pp.49–77.

Green, J.A. et al., 2011. The sphingosine 1-phosphate receptor S1P2 maintains the homeostasis of germinal center B cells and promotes niche confinement. *Nature immunology*, 12(7), pp.672–680.

Gretz, J.E. et al., 2000. Lymph-borne chemokines and other low molecular weight molecules reach high endothelial venules via specialized conduits while a functional barrier limits access to the lymphocyte microenvironments in lymph node cortex. *The Journal of experimental medicine*, 192(10), pp.1425–1440.

Gretz, J.E., Anderson, A.O. & Shaw, S., 1997. Lymph node reticulum - Conduit facilitating immune surveillance. *FASEB Journal*, 11(3).

Griffiths, G.M., Tsun, A. & Stinchcombe, J.C., 2010. The immunological synapse: a focal point for endocytosis and exocytosis. *The Journal of cell biology*, 189(3), pp.399–406.

Gugasyan, R. et al., 2000. Rel/NF-kappaB transcription factors: key mediators of B-cell activation. *Immunological reviews*, 176, pp.134–140.

Guo, B., Su, T.T. & Rawlings, D.J., 2004. Protein kinase C family functions in B-cell activation. *Current opinion in immunology*, 16(3), pp.367–373.

Gupta, N. & DeFranco, A.L., 2007. Lipid rafts and B cell signaling. *Seminars in cell & developmental biology*, 18(5), pp.616–626.

Haberman, A.M. & Shlomchik, M.J., 2003. Reassessing the function of immune-complex retention by follicular dendritic cells. *Nature Reviews: Immunology*, 3(9), pp.757–764.

Hailman, E. et al., 2002. Immature CD4(+)CD8(+) thymocytes form a multifocal immunological synapse with sustained tyrosine phosphorylation. *Immunity*, 16(6), pp.839–848.

Han, S. et al., 1995. Cellular interaction in germinal centers. Roles of CD40 ligand and B7-2 in established germinal centers. *Journal of immunology*, 155(2), pp.556–567.

Hannum, L.G. et al., 2000. Germinal center initiation, variable gene region hypermutation, and mutant B cell selection without detectable immune complexes on follicular dendritic cells. *The Journal of experimental medicine*, 192(7), pp.931–942.

Hardy, R.R. & Hayakawa, K., 2001. B cell development pathways. *Annual Review of Immunology*, 19(1), pp.595–621.

Hardy, R.R. et al., 2000. B-cell commitment, development and selection. *Immunological reviews*, 175(1), pp.23–32.

Hardy, R.R. et al., 1983. Demonstration of B-cell maturation in X-linked immunodeficient mice by simultaneous three-colour immunofluorescence. *Nature*, 306(5940), pp.270–272.

Hartley, S.B. & Goodnow, C.C., 1994. Censoring of self-reactive b cells with a range of receptor affinities in transgenic mice expressing heavy chains for a lysozyme-specific antibody. *International Immunology*, 6(9), pp.1417–1425.

Hartley, S.B. et al., 1991. Elimination from peripheral lymphoid tissues of self-reactive B lymphocytes recognizing membrane-bound antigens. *Nature*, 353(6346), pp.765–769.

Hartley, S.B. et al., 1993. Elimination of self-reactive B lymphocytes proceeds in two stages: arrested development and cell death. *Cell*, 72(3), pp.325–335.

Harwood, N.E. & Batista, F.D., 2009. The Antigen Expressway: Follicular Conduits Carry Antigen to B Cells. *Immunity*, 30(2), pp.177–179.

Harwood, N.E. & Batista, F.D., 2011. The cytoskeleton coordinates the early events of B-cell activation. *Cold Spring Harbor perspectives in biology*, 3(2), pp.a002360–a002360.

Hauser, A.E. et al., 2007. Definition of germinal-center B cell migration in vivo reveals predominant intrazonal circulation patterns. *Immunity*, 26(5), pp.655–667.

He, J.-S. et al., 2013. The distinctive germinal center phase of IgE+ B lymphocytes limits their contribution to the classical memory response. *The Journal of experimental medicine*, 210(12), pp.2755–2771.

Heesters, B. et al., 2013. Endocytosis and Recycling of Immune Complexes by Follicular Dendritic Cells Enhances B Cell Antigen Binding and Activation. *Immunity*, 38(6), pp.1164–1175.

Heesters, B.A., Myers, R.C. & Carroll, M.C., 2014. Follicular dendritic cells:

dynamic antigen libraries. *Nature Reviews: Immunology*, 14(7), pp.495–504.

Heise, N. et al., 2014. Germinal center B cell maintenance and differentiation are controlled by distinct NF-κB transcription factor subunits. *The Journal of experimental medicine*, 211(10), pp.2103–2118.

Hemmi, H. et al., 2000. A Toll-like receptor recognizes bacterial DNA. *Nature*, 408(6813), pp.740–745.

Honda, T. et al., 2014. Tuning of antigen sensitivity by T cell receptor-dependent negative feedback controls T cell effector function in inflamed tissues. *Immunity*, 40(2), pp.235–247.

Hong, J. et al., 2015. Force-Regulated In Situ TCR-Peptide-Bound MHC Class II Kinetics Determine Functions of CD4+ T Cells. *The Journal of Immunology*, 195(8), pp.3557–3564.

Honjo, T., Kinoshita, K. & Muramatsu, M., 2002. Molecular mechanism of class switch recombination: linkage with somatic hypermutation. *Annual Review of Immunology*, 20, pp.165–196.

Hou, P. et al., 2006. B cell antigen receptor signaling and internalization are mutually exclusive events. D. Nemazee, ed. *PLoS biology*, 4(7), p.e200.

Huang, C. et al., 2014. The BCL6 RD2 domain governs commitment of activated B cells to form germinal centers. *Cell reports*, 8(5), pp.1497–1508.

Huang, N.-N. et al., 2005. B cells productively engage soluble antigen-pulsed dendritic cells: visualization of live-cell dynamics of B cell-dendritic cell interactions. *Journal of immunology*, 175(11), pp.7125–7134.

Huse, M., 2012. Microtubule-organizing center polarity and the immunological synapse: protein kinase C and beyond. *Frontiers in Immunology*, 3, p.235.

Huse, M., Le Floc'h, A. & Liu, X., 2013. From lipid second messengers to molecular motors: microtubule-organizing center reorientation in T cells. *Immunological reviews*, 256(1), pp.95–106.

Huse, M., Quann, E.J. & Davis, M.M., 2008. Shouts, whispers and the kiss of death: directional secretion in T cells. *Nature immunology*, 9(10), pp.1105–1111.

Ilani, T. et al., 2009. T cell antigen receptor signaling and immunological synapse stability require myosin IIA. *Nature immunology*, 10(5), pp.531–539.

Itano, A.A. et al., 2003. Distinct Dendritic Cell Populations Sequentially Present Antigen to CD4 T Cells and Stimulate Different Aspects of Cell-Mediated Immunity. *Immunity*, 19(1), pp.47–57.

Jacob, J. et al., 1993. In situ studies of the primary immune response to (4-hydroxy-3-nitrophenyl)acetyl. III. The kinetics of V region mutation and

selection in germinal center B cells. *The Journal of experimental medicine*, 178(4), pp.1293–1307.

Jacob, J. et al., 1991. Intraclonal generation of antibody mutants in germinal centres. *Nature*, 354(6352), pp.389–392.

Jacob, M. et al., 2008. Dual role of Cbl links critical events in BCR endocytosis. *International Immunology*, 20(4), pp.485–497.

Janeway, C.A. & Medzhitov, R., 2002. Innate immune recognition. *Annual Review of Immunology*, 20(1), pp.197–216.

Jiang, N. et al., 2013. Lineage Structure of the Human Antibody Repertoire in Response to Influenza Vaccination. *Science Translational Medicine*, 5(171), pp.171ra19–171ra19.

Junt, T. et al., 2007. Subcapsular sinus macrophages in lymph nodes clear lymph-borne viruses and present them to antiviral B cells. *Nature*, 450(7166), pp.110–114.

Kallewaard, N.L. et al., 2016. Structure and Function Analysis of an Antibody Recognizing All Influenza A Subtypes. *Cell*, 166(3), pp.596–608.

Kasaian, M.T. et al., 2002. IL-21 limits NK cell responses and promotes antigen-specific T cell activation: a mediator of the transition from innate to adaptive immunity. *Immunity*, 16(4), pp.559–569.

Kerfoot, S.M. et al., 2011. Germinal center B cell and T follicular helper cell development initiates in the interfollicular zone. *Immunity*, 34(6), pp.947–960.

Kessler, M.S., Samuel, R.L. & Gillmor, S.D., 2013. Polka-dotted vesicles: lipid bilayer dynamics and cross-linking effects. *Langmuir : the ACS journal of surfaces and colloids*, 29(9), pp.2982–2991.

Khalil, A.M., Cambier, J.C. & Shlomchik, M.J., 2012. B cell receptor signal transduction in the GC is short-circuited by high phosphatase activity. *Science*, 336(6085), pp.1178–1181.

Kim, H.-J. et al., 2010. Inhibition of follicular T-helper cells by CD8+ regulatory T cells is essential for self tolerance. *Nature*, 467(7313), pp.328–332.

King, I.L. et al., 2012. Invariant natural killer T cells direct B cell responses to cognate lipid antigen in an IL-21-dependent manner. *Nature immunology*, 13(1), pp.44–50.

Kitamura, D. et al., 1991. A B cell-deficient mouse by targeted disruption of the membrane exon of the immunoglobulin mu chain gene. *Nature*, 350(6317), pp.423–426.

Kitamura, D. et al., 1992. A critical role of λ5 protein in B cell development. *Cell*, 69(5), pp.823–831.

Kitano, M. et al., 2011. Bcl6 protein expression shapes pre-germinal center B cell dynamics and follicular helper T cell heterogeneity. *Immunity*, 34(6), pp.961–972.

Klein, F. et al., 2012. Broad neutralization by a combination of antibodies recognizing the CD4 binding site and a new conformational epitope on the HIV-1 envelope protein. *The Journal of experimental medicine*, 209(8), pp.1469–1479.

Klein, F., et al., 2013. Somatic mutations of the immunoglobulin framework are generally required for broad and potent HIV-1 neutralization. *Cell*, 153(1), pp.126–138.

Klein, F., et al., 2013. Antibodies in HIV-1 vaccine development and therapy. *Science*, 341(6151), pp.1199–1204.

Klein, U. & Dalla-Favera, R., 2008. Germinal centres: role in B-cell physiology and malignancy. *Nature Reviews: Immunology*, 8(1), pp.22–33.

Kondo, M., Weissman, I.L. & Akashi, K., 1997. Identification of clonogenic common lymphoid progenitors in mouse bone marrow. *Cell*, 91(5), pp.661–672.

Koppel, E.A. et al., 2005. Specific ICAM-3 grabbing nonintegrin-related 1 (SIGNR1) expressed by marginal zone macrophages is essential for defense against pulmonary Streptococcuspneumoniae infection. *European journal of immunology*, 35(10), pp.2962–2969.

Kosco-Vilbois, M.H., 2003. Are follicular dendritic cells really good for nothing? *Nature Reviews: Immunology*, 3(9), pp.764–769.

Krammer, F. & Palese, P., 2013. Influenza virus hemagglutinin stalk-based antibodies and vaccines. *Current opinion in virology*, 3(5), pp.521–530.

Krammer, F. & Palese, P., 2014. Universal influenza virus vaccines: need for clinical trials. *Nature immunology*, 15(1), pp.3–5.

Kraus, M. et al., 2001. Interference with immunoglobulin (Ig)alpha immunoreceptor tyrosine-based activation motif (ITAM) phosphorylation modulates or blocks B cell development, depending on the availability of an Igbeta cytoplasmic tail. *The Journal of experimental medicine*, 194(4), pp.455–469.

Kraus, M. et al., 2004. Survival of resting mature B lymphocytes depends on BCR signaling via the Igα/β heterodimer. *Cell*, 117(6), pp.787–800.

Krzewski, K. et al., 2006. Formation of a WIP-, WASp-, actin-, and myosin IIA-containing multiprotein complex in activated NK cells and its alteration by KIR inhibitory signaling. *The Journal of cell biology*, 173(1), pp.121–132.

Kuchen, S. et al., 2007. Essential role of IL-21 in B cell activation, expansion, and plasma cell generation during CD4+ T cell-B cell collaboration. *Journal*

of immunology, 179(9), pp.5886–5896.

Kumari, S. & Dustin, M.L., 2015. Immunology: Dendritic Cells Pull the T Cell's Strings. *Current Biology*, 25(10), pp.R413–R415.

Kumari, S. et al., 2014. T cell antigen receptor activation and actin cytoskeleton remodeling. *Biochimica et biophysica acta*, 1838(2), pp.546–556.

Kumari, S. et al., 2012. T lymphocyte myosin IIA is required for maturation of the immunological synapse. *Frontiers in Immunology*, 3(AUG), p.230.

Kuo, J.-C. et al., 2011. Analysis of the myosin-II-responsive focal adhesion proteome reveals a role for β-Pix in negative regulation of focal adhesion maturation. *Nature cell biology*, 13(4), pp.383–393.

Kurosaki, T., 2002. Regulation of B cell fates by BCR signaling components. *Current opinion in immunology*. 14(1) pp.341–347

Kwon, D.S. et al., 2002. DC-SIGN-Mediated Internalization of HIV Is Required for Trans-Enhancement of T Cell Infection. *Immunity*, 16(1), pp.135–144.

Lam, K.P., Kühn, R. & Rajewsky, K., 1997. In vivo ablation of surface immunoglobulin on mature B cells by inducible gene targeting results in rapid cell death. *Cell*, 90(6), pp.1073–1083.

Lanzavecchia, A., 1987. Antigen Uptake and Accumulation in Antigen-Specific B Cells. *Immunological reviews*, 99(1), pp.39–51.

Le Floc'H, A. & Huse, M., 2015. Molecular mechanisms and functional implications of polarized actin remodeling at the T cell immunological synapse. *Cellular and Molecular Life Sciences*, 72(3), pp.537–556.

Leadbetter, E.A. et al., 2008. NK T cells provide lipid antigen-specific cognate help for B cells. *Proceedings of the National Academy of Sciences of the United States of America*, 105(24), pp.8339–8344.

Lecuit, T., Lenne, P.-F. & Munro, E., 2011. Force generation, transmission, and integration during cell and tissue morphogenesis. *Annual review of cell and developmental biology*, 27(1), pp.157–184.

Leung, W.-H., Tarasenko, T. & Bolland, S., 2009. Differential roles for the inositol phosphatase SHIP in the regulation of macrophages and lymphocytes. *Immunologic research*, 43(1-3), pp.243–251.

Levayer, R., Pelissier-Monier, A. & Lecuit, T., 2011. Spatial regulation of Dia and Myosin-II by RhoGEF2 controls initiation of E-cadherin endocytosis during epithelial morphogenesis. *Nature cell biology*, 13(5), pp.529–540.

Li, H. et al., 2010. Cross talk between the bone and immune systems: osteoclasts function as antigen-presenting cells and activate CD4+ and CD8+ T cells.

Blood, 116(2), pp.210–217.

Li, Z.-W. et al., 2003. IKK beta is required for peripheral B cell survival and proliferation. *Journal of immunology (Baltimore, Md. : 1950)*, 170(9), pp.4630–4637.

Liao, H.-X. et al., 2013. Co-evolution of a broadly neutralizing HIV-1 antibody and founder virus. *Nature*, 496(7446), pp.469–476.

Lindquist, R.L. et al., 2004. Visualizing dendritic cell networks in vivo. *Nature immunology*, 5(12), pp.1243–1250.

Lingwood, D. et al., 2012. Structural and genetic basis for development of broadly neutralizing influenza antibodies. *Nature*, 489(7417), pp.566–570.

Linterman, M.A. et al., 2010. IL-21 acts directly on B cells to regulate Bcl-6 expression and germinal center responses. *The Journal of experimental medicine*, 207(2), pp.353–363.

Liu, C. et al., 2011. A Balance of Bruton's Tyrosine Kinase and SHIP Activation Regulates B Cell Receptor Cluster Formation by Controlling Actin Remodeling. *The Journal of Immunology*, 187(1), pp.230–239.

Liu, C., et al., 2013. N-wasp is essential for the negative regulation of B cell receptor signaling. D. Nemazee, ed. *PLoS biology*, 11(11), p.e1001704.

Liu, C., et al., 2013. The actin cytoskeleton coordinates the signal transduction and antigen processing functions of the B cell antigen receptor. *Frontiers in Biology*, pp.1–11.

Liu, W. et al., 2010. Antigen affinity discrimination is an intrinsic function of the B cell receptor. *The Journal of experimental medicine*, 207(5), pp.1095–1111.

Liu, W., et al., 2010. It's all about change: the antigen-driven initiation of B-cell receptor signaling. *Cold Spring Harbor perspectives in biology*, 2(7), p.a002295.

Liu, Y. et al., 2016. DNA-based nanoparticle tension sensors reveal that T-cell receptors transmit defined pN forces to their antigens for enhanced fidelity. *Proceedings of the National Academy of Sciences of the United States of America*, 113(20), pp.5610–5615.

Liu, Y.J. et al., 1991. Germinal center cells express bcl-2 protein after activation by signals which prevent their entry into apoptosis. *European journal of immunology*, 21(8), pp.1905–1910.

Liu, Y.J., Oldfield, S. & MacLennan, I.C.M., 1988. Memory B cells in T cell-dependent antibody responses colonize the splenic marginal zones. *European journal of immunology*, 18(3), pp.355–362.

Loder, F. et al., 1999. B cell development in the spleen takes place in discrete

steps and is determined by the quality of B cell receptor–derived signals. *Journal of Experimental Medicine*, 190(1), pp.75–89.

Ludowyke, R.I. et al., 2006. Phosphorylation of nonmuscle myosin heavy chain IIA on Ser1917 is mediated by protein kinase C beta II and coincides with the onset of stimulated degranulation of RBL-2H3 mast cells. *Journal of immunology*, 177(3), pp.1492–1499.

MacLennan, I.C., 1994. Germinal centers. *Annual Review of Immunology*, 12(1), pp.117–139.

MacLennan, I.C.M. et al., 2003. Extrafollicular antibody responses. *Immunological reviews*, 194(1), pp.8–18.

Malhotra, S. et al., 2009. B cell antigen receptor endocytosis and antigen presentation to T cells require Vav and dynamin. *Journal of Biological Chemistry*, 284(36), pp.24088–24097.

Malinova, D. et al., 2016. WASp-dependent actin cytoskeleton stability at the dendritic cell immunological synapse is required for extensive, functional T cell contacts. *Journal of leukocyte biology*, 99(5), pp.699–710.

Mandel, T.E. et al., 1980. The follicular dendritic cell: long term antigen retention during immunity. *Immunological reviews*, 53, pp.29–59.

Marston, D.J., Dickinson, S. & Nobes, C.D., 2003. Rac-dependent trans-endocytosis of ephrinBs regulates Eph|[ndash]|ephrin contact repulsion. *Nature cell biology*, 5(10), pp.879–888.

Martin, F. & Kearney, J.F., 2000. B-cell subsets and the mature preimmune repertoire. Marginal zone and B1 B cells as part of a “natural immune memory.” *Immunological reviews*.

Martinez-Pomares, L. et al., 1996. Fc chimeric protein containing the cysteine-rich domain of the murine mannose receptor binds to macrophages from splenic marginal zone and lymph node subcapsular sinus and to germinal centers. *Journal of Experimental Medicine*, 184(5), pp.1927–1937.

Mattila, P.K. et al., 2013. The actin and tetraspanin networks organize receptor nanoclusters to regulate B cell receptor-mediated signaling. *Immunity*, 38(3), pp.461–474.

Mauri, C. & Bosma, A., 2012. Immune regulatory function of B cells. *Annual Review of Immunology*, 30, pp.221–241.

Meffre, E. & Nussenzweig, M.C., 2002. Deletion of immunoglobulin β in developing B cells leads to cell death. In Proceedings of the National Academy of Sciences of the United States of America. pp. 11334–11339.

Melchers, F., 2005. The pre-B-cell receptor: selector of fitting immunoglobulin heavy chains for the B-cell repertoire. *Nature Reviews: Immunology*, 5(7),

pp.578–584.

Melchers, F. et al., 1999. The roles of preB and B cell receptors in the stepwise allelic exclusion of mouse IgH and L chain gene loci. *Seminars in Immunology*, 11(5), pp.307–317.

Merrell, K.T. et al., 2006. Identification of Anergic B Cells within a Wild-Type Repertoire. *Immunity*, 25(6), pp.953–962.

Meyer-Hermann, M. et al., 2012. A theory of germinal center B cell selection, division, and exit. *Cell reports*, 2(1), pp.162–174.

Miner, C.A. et al., 2015. Acquisition of activation receptor ligand by trogocytosis renders NK cells hyporesponsive. *The Journal of Immunology*, 194(4), pp.1945–1953.

Mombaerts, P. et al., 1992. RAG-1-deficient mice have no mature B and T lymphocytes. *Cell*, 68(5), pp.869–877.

Monks, C.R. et al., 1998. Three-dimensional segregation of supramolecular activation clusters in T cells. *Nature*, 395(6697), pp.82–86.

Morita, S., Kojima, T. & Kitamura, T., 2000. Plat-E: an efficient and stable system for transient packaging of retroviruses. *Gene therapy*, 7(12), pp.1063–1066.

Moseman, E.A. et al., 2012. B Cell Maintenance of Subcapsular Sinus Macrophages Protects against a Fatal Viral Infection Independent of Adaptive Immunity. *Immunity*, 36(3), pp.415–426.

Mowen, K.A. & David, M., 2014. Unconventional post-translational modifications in immunological signaling. *Nature immunology*, 15(6), pp.512–520.

Mueller, C.G. et al., 2001. Mannose receptor ligand-positive cells express the metalloprotease decysin in the B cell follicle. *Journal of immunology*, 167(9), pp.5052–5060.

Mueller, J., Matloubian, M. & Zikherman, J., 2015. Cutting edge: An in vivo reporter reveals active B cell receptor signaling in the germinal center. *The Journal of Immunology*, 194(7), pp.2993–2997.

Muramatsu, M. et al., 2000. Class Switch Recombination and Hypermutation Require Activation-Induced Cytidine Deaminase (AID), a Potential RNA Editing Enzyme. *Cell*, 102(5), pp.553–563.

Nagata, K. et al., 1997. The Ig alpha/Igbeta heterodimer on mu-negative proB cells is competent for transducing signals to induce early B cell differentiation. *Immunity*, 7(4), pp.559–570.

Natkanski, E. et al., 2013. B Cells Use Mechanical Energy to Discriminate Antigen

Affinities. *Science*, 340(6140), pp.1587–1590.

Neuberger, M.S. et al., 1999. Antibody diversification and selection in the mature B-cell compartment. *Cold Spring Harbor symposia on quantitative biology*, 64(0), pp.211–216.

Nieuwenhuis, P. & Opstelten, D., 1984. Functional anatomy of germinal centers. *American journal of anatomy*, (170), pp.421–435.

Niiro, H. & Clark, E.A., 2002. Regulation of B-cell fate by antigen-receptor signals. *Nature Reviews: Immunology*, 2(12), pp.945–956.

Nishizuka, Y., 1992. Intracellular signaling by hydrolysis of phospholipids and activation of protein kinase C. *Science*, 258(5082), pp.607–614.

Nitschke, L., 2005. The role of CD22 and other inhibitory co-receptors in B-cell activation. *Current opinion in immunology*, 17(3), pp.290–297.

Nitschke, L. et al., 1997. CD22 is a negative regulator of B-cell receptor signalling. *Current Biology*, 7(2), pp.133–143.

Nurieva, R.I. et al., 2009. Bcl6 Mediates the Development of T Follicular Helper Cells. *Science*, 325(5943), pp.1001–1005.

Nussenzweig, A. & Nussenzweig, M.C., 2010. Origin of Chromosomal Translocations in Lymphoid Cancer. *Cell*, 141(1), pp.27–38.

Nussenzweig, V. & Benacerraf, B., 1967. ANTIHAPTEN ANTIBODY SPECIFICITY AND L CHAIN TYPE. *The Journal of experimental medicine*, 126(4), pp.727–743.

Nutt, S.L. et al., 1999. Commitment to the B-lymphoid lineage depends on the transcription factor Pax5. *Nature*, 401(6753), pp.556–562.

Obino, D. & Lennon-Duménil, A.-M., 2014. A critical role for cell polarity in antigen extraction, processing, and presentation by B lymphocytes. *Advances in immunology*, 123, pp.51–67.

Oettinger, M.A. et al., 1990. RAG-1 and RAG-2, adjacent genes that synergistically activate V(D)J recombination. *Science*, 248(4962), pp.1517–1523.

Ohnishi, K. & Melchers, F., 2003. The nonimmunoglobulin portion of lambda5 mediates cell-autonomous pre-B cell receptor signaling. *Nature immunology*, 4(9), pp.849–856.

Okada, T. & Cyster, J.G., 2006. B cell migration and interactions in the early phase of antibody responses. *Current opinion in immunology*, 18(3), pp.278–285.

Okada, T. et al., 2005. Antigen-engaged B cells undergo chemotaxis toward the T zone and form motile conjugates with helper T cells. *PLoS biology*, 3(6), pp.1047–1061.

Ozaki, K. et al., 2002. A critical role for IL-21 in regulating immunoglobulin production. *Science,* 5598, pp.1630-1635

Ozaki, K. et al., 2004. Regulation of B cell differentiation and plasma cell generation by IL-21, a novel inducer of Blimp-1 and Bcl-6. *Journal of immunology*, 173(9), pp.5361–5371.

O'Connor, B.P. et al., 2006. Imprinting the fate of antigen-reactive B cells through the affinity of the B cell receptor. *Journal of immunology*, 177(11), pp.7723–7732.

Pani, G., Siminovitch, K.A. & Paige, C.J., 1997. The motheaten mutation rescues B cell signaling and development in CD45-deficient mice. *The Journal of experimental medicine*, 186(4), pp.581–588.

Pao, L.I., Famiglietti, S.J. & Cambier, J.C., 1998. Asymmetrical phosphorylation and function of immunoreceptor tyrosine-based activation motif tyrosines in B cell antigen receptor signal transduction. *Journal of immunology*, 160(7), pp.3305–3314.

Pape, K.A. et al., 2011. Different B cell populations mediate early and late memory during an endogenous immune response. *Science*, 331(6021), pp.1203–1207.

Pape, K.A. et al., 2007. The humoral immune response is initiated in lymph nodes by B cells that acquire soluble antigen directly in the follicles. *Immunity*, 26(4), pp.491–502.

Paus, D. et al., 2006. Antigen recognition strength regulates the choice between extrafollicular plasma cell and germinal center B cell differentiation. *The Journal of experimental medicine*, 203(4), pp.1081–1091.

Peperzak, V. et al., 2013. Mcl-1 is essential for the survival of plasma cells. *Nature immunology*, 14(3), pp.290–297.

Pereira, J.P. et al., 2009. EBI2 mediates B cell segregation between the outer and centre follicle. *Nature*, 460(7259), pp.1122–1126.

Pereira, J.P., Kelly, L.M. & Cyster, J.G., 2010. Finding the right niche: B-cell migration in the early phases of T-dependent antibody responses. *International Immunology*, 22(6), pp.413–419.

Pène, J. et al., 2004. Cutting edge: IL-21 is a switch factor for the production of IgG1 and IgG3 by human B cells. *Journal of immunology*, 172(9), pp.5154–5157.

Phan, T.G. et al., 2005. Altered migration, recruitment, and somatic hypermutation in the early response of marginal zone B cells to T cell-dependent antigen. *Journal of immunology*, 174(8), pp.4567–4578.

Phan, T.G. et al., 2007. Subcapsular encounter and complement-dependent

transport of immune complexes by lymph node B cells. *Nature immunology*, 8(9), pp.992–1000.

Phan, T.G., Gray, E.E. & Cyster, J.G., 2009. The microanatomy of B cell activation. 21(3), pp.258–265.

Phan, T.G., et al., 2009. Immune complex relay by subcapsular sinus macrophages and noncognate B cells drives antibody affinity maturation. *Nature immunology*, 10(7), pp.786–793.

Pierce, S.K.S. et al., 2010. The tipping points in the initiation of B cell signalling: how small changes make big differences. *Nature Reviews: Immunology*, 10(11), pp.767–777.

Pillai, S. & Cariappa, A., 2009. The follicular versus marginal zone B lymphocyte cell fate decision. *Nature Reviews: Immunology*, 9(11), pp.767–777.

Pillai, S., Cariappa, A. & Moran, S.T., 2004. Positive selection and lineage commitment during peripheral B-lymphocyte development. *Immunological reviews*, 197, pp.206–218.

Pogue, S.L. & Goodnow, C.C., 2000. Gene dose-dependent maturation and receptor editing of B cells expressing immunoglobulin (Ig)G1 or IgM/IgG1 tail antigen receptors. *The Journal of experimental medicine*, 191(6), pp.1031–1044.

Poo, W.J., Conrad, L. & Janeway, C.A., 1988. Receptor-directed focusing of lymphokine release by helper T cells. *Nature*, 332(6162), pp.378–380.

Purbhoo, M.A., 2013. The function of sub-synaptic vesicles during T-cell activation. *Immunological reviews*, 251(1), pp.36–48.

Qi, H. et al., 2006. Extrafollicular activation of lymph node B cells by antigen-bearing dendritic cells. *Science*, 312(5780), pp.1672–1676.

Quann, E.J. et al., 2011. A cascade of protein kinase C isozymes promotes cytoskeletal polarization in T cells. *Nature immunology*, 12(7), pp.647–654.

Quann, E.J. et al., 2009. Localized diacylglycerol drives the polarization of the microtubule-organizing center in T cells. *Nature immunology*, 10(6), pp.627–635.

Qureshi, O.S. et al., 2011. Trans-Endocytosis of CD80 and CD86: A Molecular Basis for the Cell-Extrinsic Function of CTLA-4. *Science*, 332(6029), pp.600–603.

Rahman, Z.S.M. et al., 2003. Normal induction but attenuated progression of germinal center responses in BAFF and BAFF-R signaling-deficient mice. *The Journal of experimental medicine*, 198(8), pp.1157–1169.

Rajewsky, K., 1996. Clonal selection and learning in the antibody system. *Nature*,

381(6585), pp.751–758.

Reichlin, A. et al., 2001. B cell development is arrested at the immature B cell stage in mice carrying a mutation in the cytoplasmic domain of immunoglobulin beta. *The Journal of experimental medicine*, 193(1), pp.13–23.

Reinhardt, R.L., Liang, H.-E. & Locksley, R.M., 2009. Cytokine-secreting follicular T cells shape the antibody repertoire. *Nature immunology*, 10(4), pp.385–393.

Reth, M., 1989. Antigen receptor tail clue. *Nature*, 338(6214), pp.383–384.

Reth, M. & Wienands, J., 1997. Initiation and processing of signals from the B cell antigen receptor. *Annual Review of Immunology*, 15, pp.453–479.

Reth, M. et al., 1987. Activation of V kappa gene rearrangement in pre-B cells follows the expression of membrane-bound immunoglobulin heavy chains. *The EMBO journal*, 6(11), pp.3299–3305.

Richie, L.I. et al., 2002. Imaging Synapse Formation during Thymocyte Selection Inability of CD3ζ to Form a Stable Central Accumulation during Negative Selection. *Immunity*, 16(4), pp.595–606.

Rickert, R.C., 2013. New insights into pre-BCR and BCR signalling with relevance to B cell malignancies. *Nature Reviews: Immunology*, 13(8), pp.578–591.

Ritter, A.T. et al., 2015. Actin depletion initiates events leading to granule secretion at the immunological synapse. *Immunity*, 42(5), pp.864–876.

Roers, A. et al., 2000. Single-cell PCR analysis of T helper cells in human lymph node germinal centers. *The American journal of pathology*, 156(3), pp.1067–1071.

Roes, J. & Rajewsky, K., 1993. Immunoglobulin D (IgD)-deficient mice reveal an auxiliary receptor function for IgD in antigen-mediated recruitment of B cells. *The Journal of experimental medicine*, 177(1), pp.45–55.

Roozendaal, R. et al., 2009. Conduits mediate transport of low-molecular-weight antigen to lymph node follicles. *Immunity*, 30(2), pp.264–276.

Roozendaal, R., Mebius, R.E. & Kraal, G., 2008. The conduit system of the lymph node. *International Immunology*, 20(12), pp.1483–1487.

Röhlich, K., 1930. *Beitrag zur Cytologie der Keimzentren der Lymphknoten*, *Z*. Mikrosk. Anat. Forsch.

Saito, M. et al., 2009. BCL6 suppression of BCL2 via Miz1 and its disruption in diffuse large B cell lymphoma. In Proceedings of the National Academy of Sciences of the United States of America. pp. 11294–11299.

Saito, T. et al., 2003. Notch2 is preferentially expressed in mature B cells and indispensable for marginal zone B lineage development. *Immunity*, 18(5),

pp.675–685.

Samardzic, T. et al., 2002. Reduction of marginal zone B cells in CD22-deficient mice. *European journal of immunology*, 32(2), pp.561–567.

Sander, S. et al., 2015. PI3 Kinase and FOXO1 Transcription Factor Activity Differentially Control B Cells in the Germinal Center Light and Dark Zones. *Immunity*, 43(6), pp.1075–1086.

Satpathy, S. et al., 2015. Systems-wide analysis of BCR signalosomes and downstream phosphorylation and ubiquitylation. *Molecular systems biology*, 11(6), pp.810–810.

Scandella, E. et al., 2008. Restoration of lymphoid organ integrity through the interaction of lymphoid tissue-inducer cells with stroma of the T cell zone. *Nature immunology*, 9(6), pp.667–675.

Schaerli, P. et al., 2000. CXC chemokine receptor 5 expression defines follicular homing T cells with B cell helper function. *Journal of Experimental Medicine*, 192(11), pp.1553–1562.

Schamel, W.W.A. et al., 2005. Coexistence of multivalent and monovalent TCRs explains high sensitivity and wide range of response. *The Journal of experimental medicine*, 202(4), pp.493–503.

Schatz, D.G., Oettinger, M.A. & Baltimore, D., 1989. The V(D)J recombination activating gene, RAG-1. *Cell*, 59(6), pp.1035–1048.

Scheid, J.F. et al., 2009. Broad diversity of neutralizing antibodies isolated from memory B cells in HIV-infected individuals. *Nature*, 458(7238), pp.636–640.

Scheid, J.F. et al., 2011. Sequence and Structural Convergence of Broad and Potent HIV Antibodies That Mimic CD4 Binding. *Science*, 333(6049), pp.1633–1637.

Schnyder, T. et al., 2011. B cell receptor-mediated antigen gathering requires ubiquitin ligase Cbl and adaptors Grb2 and Dok-3 to recruit dynein to the signaling microcluster. *Immunity*, 34(6), pp.905–918.

Schweighoffer, E. et al., 2013. The BAFF receptor transduces survival signals by co-opting the B cell receptor signaling pathway. *Immunity*, 38(3), pp.475–488.

Schwickert, T.A. et al., 2011. A dynamic T cell-limited checkpoint regulates affinity-dependent B cell entry into the germinal center. *The Journal of experimental medicine*, 208(6), pp.1243–1252.

Schwickert, T.A. et al., 2009. Germinal center reutilization by newly activated B cells. *The Journal of experimental medicine*, 206(13), pp.2907–2914.

Schwickert, T.A. et al., 2007. In vivo imaging of germinal centres reveals a dynamic open structure. *Nature*, 446(7131), pp.83–87.

Seeley-Fallen, M.K. et al., 2014. Actin-binding protein 1 links B-cell antigen receptors to negative signaling pathways. *Proceedings of the National Academy of Sciences of the United States of America*, 111(27), pp.9881–9886.

Sharma, S., Orlowski, G. & Song, W., 2009. Btk regulates B cell receptor-mediated antigen processing and presentation by controlling actin cytoskeleton dynamics in B cells. *The Journal of Immunology*, 182(1), pp.329–339.

Shih, T.-A.Y. et al., 2002. Role of BCR affinity in T cell dependent antibody responses in vivo. *Nature immunology*, 3(6), pp.570–575.

Shikh, El, M.E. et al., 2006. Follicular dendritic cell (FDC)-FcγRIIB engagement via immune complexes induces the activated FDC phenotype associated with secondary follicle development. *European journal of immunology*, 36(10), pp.2715–2724.

Shlomchik, M.J. & Weisel, F., 2012a. Germinal center selection and the development of memory B and plasma cells. 247(1), pp.52–63.

Shlomchik, M.J. & Weisel, F., 2012b. Germinal centers. *Immunological reviews*, 247(1), pp.5–10.

Shokat, K.M. & Goodnow, C.C., 1995. Antigen-induced B-cell death and elimination during germinal-centre immune responses. *Nature*, 375(6529), pp.334–338.

Shulman, Z. et al., 2013. T follicular helper cell dynamics in germinal centers. *Science*, 341(6146), pp.673–677.

Siemasko, K. & Clark, M.R., 2001. The control and facilitation of MHC class II antigen processing by the BCR. *Current opinion in immunology*.

Siemasko, K. et al., 1999. Ig alpha and Ig beta are required for efficient trafficking to late endosomes and to enhance antigen presentation. *Journal of immunology*, 162(11), pp.6518–6525.

Sims, T.N. et al., 2007. Opposing Effects of PKCθ and WASp on Symmetry Breaking and Relocation of the Immunological Synapse. *Cell*, 129(4), pp.773–785.

Sixt, M. et al., 2005. The conduit system transports soluble antigens from the afferent lymph to resident dendritic cells in the T cell area of the lymph node. *Immunity*, 22(1), pp.19–29.

Sohn, H.W., Gu, H. & Pierce, S.K., 2003. Cbl-b negatively regulates B cell antigen receptor signaling in mature B cells through ubiquitination of the tyrosine kinase Syk. *The Journal of experimental medicine*, 197(11), pp.1511–1524.

Sohn, H.W., Tolar, P. & Pierce, S.K., 2008. Membrane heterogeneities in the formation of B cell receptor-Lyn kinase microclusters and the immune synapse.

The Journal of cell biology, 182(2), pp.367–379.

Song, H. & Cerny, J., 2003. Functional heterogeneity of marginal zone B cells revealed by their ability to generate both early antibody-forming cells and germinal centers with hypermutation and memory in response to a T-dependent antigen. *The Journal of experimental medicine*, 198(12), pp.1923–1935.

Song, W. et al., 2013. Actin-mediated feedback loops in B-cell receptor signaling. *Immunological reviews*, 256(1), pp.177–189.

Spitaler, M. et al., 2006. Diacylglycerol and protein kinase D localization during T lymphocyte activation. *Immunity*, 24(5), pp.535–546.

Srinivasan, L. et al., 2009. PI3 kinase signals BCR-dependent mature B cell survival. *Cell*, 139(3), pp.573–586.

Steele, S. et al., 2016. Trogocytosis-associated cell to cell spread of intracellular bacterial pathogens. *eLife*, 5, p.e1000211.

Stinchcombe, J.C. et al., 2011. Centriole polarisation to the immunological synapse directs secretion from cytolytic cells of both the innate and adaptive immune systems. *BMC biology*, 9(1), p.45.

Stinchcombe, J.C. et al., 2006. Centrosome polarization delivers secretory granules to the immunological synapse. *Nature*, 443(7110), pp.462–465.

Stinchcombe, J.C. et al., 2001. The immunological synapse of CTL contains a secretory domain and membrane bridges. *Immunity*, 15(5), pp.751–761.

Stoddart, A. et al., 2002. Lipid Rafts Unite Signaling Cascades with Clathrin to Regulate BCR Internalization. *Immunity*, 17(4), pp.451–462.

Stoddart, A., Jackson, A.P. & Brodsky, F.M., 2005. Plasticity of B cell receptor internalization upon conditional depletion of clathrin. *Molecular biology of the cell*, 16(5), pp.2339–2348.

Su, T.T., Guo, B. & Rawlings, D.J., 2002. Emerging roles for PKC isoforms in immune cell function. *Mol Interv*, 2(3), pp.141–144.

Su, T.T., Guo, B., Kawakami, Y., et al., 2002. PKC-beta controls I kappa B kinase lipid raft recruitment and activation in response to BCR signaling. *Nature immunology*, 3(8), pp.780–786.

Sui, J. et al., 2009. Structural and functional bases for broad-spectrum neutralization of avian and human influenza A viruses. *Nature structural & molecular biology*, 16(3), pp.265–273.

Sukumar, S., Szakal, A.K. & Tew, J.G., 2006. Isolation of functionally active murine follicular dendritic cells. *Journal of immunological methods*, 313(1-2), pp.81–95.

Suzuki, K. et al., 2009. Visualizing B cell capture of cognate antigen from follicular dendritic cells. *Journal of Experimental Medicine*, 206(7), pp.1485–1493.

Szakal, A.K., Holmes, K.L. & Tew, J.G., 1983. Transport of immune complexes from the subcapsular sinus to lymph node follicles on the surface of nonphagocytic cells, including cells with dendritic morphology. *Journal of immunology*, 131(4), pp.1714–1727.

Talay, O. et al., 2012. IgE+ memory B cells and plasma cells generated through a germinal-center pathway. *Nature immunology*, 13(4), pp.396–404.

Tarlinton, D.M. & Smith, K.G.C., 2000. Dissecting affinity maturation: a model explaining selection of antibody-forming cells and memory B cells in the germinal centre. *Immunology today*, 21(9), pp.436–441.

Tas, J.M.J. et al., 2016. Visualizing antibody affinity maturation in germinal centers. *Science*, 351(6277), pp.1048–1054.

Taylor, J.J. et al., 2015. Apoptosis and antigen affinity limit effector cell differentiation of a single naïve B cell. *Science*, 347(6223), pp.784–787.

Taylor, P.R. et al., 2005. Macrophage receptors and immune recognition. *Annual Review of Immunology*, 23, pp.901–944.

Tew, J.G., 1993. Follicular dendritic cells and dendritic cell nomenclature. In Advances in Experimental Medicine and Biology. Boston, MA: Springer US, pp. 467–468.

Tew, J.G. & Mandel, T.E., 1979. Prolonged antigen half-life in the lymphoid follicles of specifically immunized mice. *Immunology*, 37(1), pp.69–76.

Tew, J.G. et al., 1997. Follicular dendritic cells and presentation of antigen and costimulatory signals to B cells. *Immunological reviews*, 156, pp.39–52.

Tew, J.G. et al., 1993. Follicular dendritic cells in germinal center reactions. *Advances in experimental medicine and biology*, 329, pp.461–465.

Tew, J.G., Phipps, R.P. & Mandel, T.E., 1980. The Maintenance and Regulation of the Humoral Immune Response: Persisting Antigen and the Role of Follicular Antigen-Binding Dendritic Cells as Accessory Cells. *Immunological reviews*, 53(1), pp.175–201.

Thome, M. et al., 2010. Antigen receptor signaling to NF-kappaB via CARMA1, BCL10, and MALT1. *Cold Spring Harbor perspectives in biology*, 2(9), pp.a003004–a003004.

Throsby, M. et al., 2008. Heterosubtypic neutralizing monoclonal antibodies cross-protective against H5N1 and H1N1 recovered from human IgM+ memory B cells. D. Unutmaz, ed. *PloS one*, 3(12), p.e3942.

Tolar, P., 2011. Inside the microcluster: antigen receptor signalling viewed with

molecular imaging tools. *Immunology*, 133(3), pp.271–277.

Tolar, P. & Meckel, T., 2009. Imaging B-cell receptor signaling by single-molecule techniques. *Methods in molecular biology (Clifton, N.J.)*, 571, pp.437–453.

Tolar, P. & Pierce, S.K., 2010. A conformation-induced oligomerization model for B cell receptor microclustering and signaling. *Current topics in microbiology and immunology*, 340, pp.155–169.

Tolar, P. & Spillane, K.M., 2014. Force generation in B-cell synapses: mechanisms coupling B-cell receptor binding to antigen internalization and affinity discrimination. *Advances in immunology*, 123, pp.69–100.

Tolar, P. et al., 2009. The constant region of the membrane immunoglobulin mediates B cell-receptor clustering and signaling in response to membrane antigens. *Immunity*, 30(1), pp.44–55.

Tolar, P., Sohn, H.W. & Pierce, S.K., 2005. The initiation of antigen-induced B cell antigen receptor signaling viewed in living cells by fluorescence resonance energy transfer. *Nature immunology*, 6(11), pp.1168–1176.

Tolar, P. et al., 2009. The molecular assembly and organization of signaling active B-cell receptor oligomers. *Immunological reviews*, 232(1), pp.34–41.

Treanor, B. et al., 2010. The Membrane Skeleton Controls Diffusion Dynamics and Signaling through the B Cell Receptor. *Immunity*, 32(2), pp.187–199.

Trinh, D.L. et al., 2013. Analysis of FOXO1 mutations in diffuse large B-cell lymphoma. *Blood*, 121(18), pp.3666–3674.

Varma, R. et al., 2006. T Cell Receptor-Proximal Signals Are Sustained in Peripheral Microclusters and Terminated in the Central Supramolecular Activation Cluster. *Immunity*, 25(1), pp.117–127.

Vascotto, F. et al., 2007. Antigen presentation by B lymphocytes: how receptor signaling directs membrane trafficking. *Current opinion in immunology*, 19(1), pp.93–98.

Venkataswamy, M.M. & Porcelli, S.A., 2010. Lipid and glycolipid antigens of CD1d-restricted natural killer T cells. *Seminars in Immunology*, 22(2), pp.68–78.

Victora, G.D. & Nussenzweig, M.C., 2012. Germinal centers. *Annual Review of Immunology*, 30(1), pp.429–457.

Victora, G.D. et al., 2010. Germinal center dynamics revealed by multiphoton microscopy with a photoactivatable fluorescent reporter. *Cell*, 143(4), pp.592–605.

Victora, G.D. et al., 2012. Identification of human germinal center light and dark zone cells and their relationship to human B-cell lymphomas. *Blood*, 120(11), pp.2240–2248.

Vikström, I. et al., 2010. Mcl-1 Is Essential for Germinal Center Formation and B Cell Memory. *Science*, 330(6007), pp.1095–1099.

Vinuesa, C.G. & Chang, P.-P., 2013. Innate B cell helpers reveal novel types of antibody responses. *Nature immunology*, 14(2), pp.119–126.

Vinuesa, C.G. et al., 2005. A RING-type ubiquitin ligase family member required to repress follicular helper T cells and autoimmunity. *Nature*, 435(7041), pp.452–458.

Vinuesa, C.G., Sanz, I. & Cook, M.C., 2009. Dysregulation of germinal centres in autoimmune disease. *Nature Reviews: Immunology*, 9(12), pp.845–857.

Vinuesa, C.G., Toellner, K.-M. & Papa, I., 2016. *Extrafollicular Antibody Responses*, Elsevier.

Vogelzang, A. et al., 2008. A fundamental role for interleukin-21 in the generation of T follicular helper cells. *Immunity*.

Wan, Z. et al., 2013. B cell activation is regulated by the stiffness properties of the substrate presenting the antigens. *The Journal of Immunology*, 190(9), pp.4661–4675.

Wang, J. et al., 2016. Utilization of a photoactivatable antigen system to examine B-cell probing termination and the B-cell receptor sorting mechanisms during B-cell activation. *Proceedings of the National Academy of Sciences of the United States of America*, 113(5), pp.201517612–67.

Wang, X. et al., 2011. Follicular dendritic cells help establish follicle identity and promote B cell retention in germinal centers. *The Journal of experimental medicine*, 208(12), pp.2497–2510.

Wang, X & Ha, T., 2013. Defining Single Molecular Forces Required to Activate Integrin and Notch Signaling. *Science*, 340(6135), pp.991–994.

Wang, Y. & Carter, R.H., 2005. CD19 regulates B cell maturation, proliferation, and positive selection in the FDC zone of murine splenic germinal centers. *Immunity*, 22(6), pp.749–761.

Wardemann, H. et al., 2003. Predominant autoantibody production by early human B cell precursors. *Science*, 301(5638), pp.1374–1377.

Weber, M. et al., 2008. Phospholipase C-gamma2 and Vav cooperate within signaling microclusters to propagate B cell spreading in response to membrane-bound antigen. *The Journal of experimental medicine*, 205(4), pp.853–868.

Weller, S. et al., 2004. Human blood IgM “memory” B cells are circulating splenic marginal zone B cells harboring a prediversified immunoglobulin repertoire. *Blood*, 104(12), pp.3647–3654.

Wen, L. et al., 2005. Evidence of marginal-zone B cell-positive selection in spleen. *Immunity*, 23(3), pp.297–308.

Wen, R. et al., 2003. Phospholipase Cgamma2 provides survival signals via Bcl2 and A1 in different subpopulations of B cells. *Journal of Biological Chemistry*, 278(44), pp.43654–43662.

Wilkinson, D.G., 2015. Balancing cell behavior at boundaries. *The Journal of cell biology*, 208(6), pp.659–660.

Woodside, M.T. et al., 2006. Nanomechanical measurements of the sequence-dependent folding landscapes of single nucleic acid hairpins. *Proceedings of the National Academy of Sciences of the United States of America*, 103(16), pp.6190–6195.

Wrammert, J. et al., 2011. Broadly cross-reactive antibodies dominate the human B cell response against 2009 pandemic H1N1 influenza virus infection. *Journal of Experimental Medicine*, 208(2), pp.411–411.

Wykes, M. et al., 1998. Dendritic cells interact directly with naive B lymphocytes to transfer antigen and initiate class switching in a primary T-dependent response. *Journal of immunology*, 161(3), pp.1313–1319.

Yang, J. & Reth, M., 2010. The dissociation activation model of B cell antigen receptor triggering. *FEBS letters*, 584(24), pp.4872–4877.

Yang, Z., Sullivan, B.M. & Allen, C.D.C., 2012. Fluorescent In Vivo Detection Reveals that IgE+ B Cells Are Restrained by an Intrinsic Cell Fate Predisposition. *Immunity*, 36(5), pp.857–872.

Yasuda, M. et al., 1998. A comparative study of germinal center: fowls and mammals. *Comparative Immunology, Microbiology and Infectious Diseases*, 21(3), pp.179–189.

Yu, D. et al., 2009. The Transcriptional Repressor Bcl-6 Directs T Follicular Helper Cell Lineage Commitment. *Immunity*, 31(3), pp.457–468.

Yuseff, M.-I. et al., 2011. Polarized secretion of lysosomes at the B cell synapse couples antigen extraction to processing and presentation. *Immunity*, 35(3), pp.361–374.

Zhang, M. et al., 2007. Ubiquitinylation of Ig beta dictates the endocytic fate of the B cell antigen receptor. *Journal of immunology*, 179(7), pp.4435–4443.

Zhang, Y. et al., 2013. Germinal center B cells govern their own fate via antibody feedback. *The Journal of experimental medicine*, 210(3), pp.457–464.

Zhang, Y. Garcia-Ibanez, L. & Toellner, K.-M., 2016. Regulation of germinal center B-cell differentiation. *Immunological reviews*, 270(1), pp.8–19.

Zhang, Y. et al., 2014. DNA-based digital tension probes reveal integrin forces

during early cell adhesion. *Nature communications*, 5, p.5167.

Zheng, B., Han, S. & Kelsoe, G., 1996. T helper cells in murine germinal centers are antigen-specific emigrants that downregulate Thy-1. *The Journal of experimental medicine*, 184(3), pp.1083–1091.

Zotos, D. et al., 2010. IL-21 regulates germinal center B cell differentiation and proliferation through a B cell-intrinsic mechanism. *The Journal of experimental medicine*, 207(2), pp.365–378.

Zouali, M. & Richard, Y., 2011. Marginal zone B-cells, a gatekeeper of innate immunity. *Frontiers in Immunology*, 2, p.63.